LAWRENCE
LIVERMORE
NATIONAL
LABORATORY

LLNL-PROC-430824-PT-2

JOWOG 32Mat: Conference Proceedings Part 2

daniel orlikowski, John Heidrich

May 11, 2010

JOWOG 32 Mat
Livermore, CA, United States
January 25, 2010 through January 29, 2010

Disclaimer

JOWOG 32MAT

January 25-29, 2010
Conference Proceedings Part 2 of 2
Monday-Wednesday

Bld. 132 Auditorium
Livermore, CA

LLNL • LANL • SNL • AWE

This work performed under the auspices of the U.S. Department of Energy by Lawrence Livermore National Laboratory under Contract DE-AC52-07NA27344.

JOWOG 32MAT Conference Agenda January 25-29, 2010

MONDAY, January 25

07:45 Formalities — Visitor Badges, etc. West Badge Office

08:15 M. Dunning, J. Heidrich — Welcome, Bldg 132 Auditorium

Session 1: EOS I

Session Chairman: Chris Robinson

09.30 Geoff Cox — UK.01
EOS for Titanium

10:00 BREAK

Session 2: EOS II & Model Assessment I

Session Chairman: Lorin Benedict

10:30 Steven McGuire — UK.02
EOS for Vanadium

11:00 Michael Prime — LA.02
Comparison of Beryllium EOS & Constitutive Models with Recent Shock D

12:00 LUNCH

16:30 CLOSE

TUESDAY, January 26

08:20 Formalities

Session 4: EOS IV

Session Chairman: Carl Greeff

09:30 Eric Chisolm — LA.04
Recent Advances In Vibration-Transit Theory of Liquids

10:00 BREAK

Session 5: EOS V & Dynamic Experiments I

Session Chairman: Eric Chisolm

11.00 Jim Belak — LL.06
Phase-Field Modeling of Coring in Pu Alloys

11:30 Jeremy Millett — UK.05
On the Behavior of Body Centered Cubic Metals During One-Dimensional Shock Loading

12:00 LUNCH

Session 6: Dynamic Experiments II

Session Chairman: Jean-Paul Davis

13:30 Jon Eggert — LL.07
Laser-Induced Ramp Compression of Tantalum and Iron to Over 300 Gpa: EOS & X-Ray Diffraction

14:00 Matthew Cotton — UK.06
EOS & Spall Data for Ta-2.5% W

14:30 Jeremy Millett — UK.07
Response of Aluminum Alloys to Shock Loading

15:00 BREAK

15:30 Discussion Session
EOS Test Problem: Comparison of Lab's EOSs (30 min.)
(Discussion Leader: Chris Robinson)
EOS Theory: Phases, Future Directions (60 min.)
(Discussion Leader: Lorin Benedict))

17:00 CLOSE

WEDNESDAY, January 27

08:20 Formalities

Session 7: Dynamic Experiments III

Session Chairman: Frank Cherne

09:00 Jean-Paul Davis — SN.01
Update on Multi-Megabar Ramp Compression at Z

10:00 BREAK

Session 8: Strength & Damage I

Session Chairman: Brian Jensen

11:00 Scott Alexander — SN.02
New Strength Data on Aluminum to 160 GPa

11:30 LUNCH

15:00 Discussion Sessions
MaRIE: (Discussion Leaders: Curt Bronkhorst & Franz Freibert)
2007 Strength & Damage Test Problems
(Discussion Leader: James Turner)

16:30 CLOSE

18:30 Conference Banquet - Zyphyr Grill & Bar*

19:00 Dinner Served

***Directions:**

- Exit South-East Gate/Go straight on East Avenue/Turn right onto South Livermore/Turn left onto First Street/Zephyr Grill & Bar located on right hand side next to Vine Cinema

• LLNL Presentations • LANL Presentations • SNL Presentations • AWE Presentations

JOWOG 32MAT Conference Agenda January 25-29, 2010

THURSDAY, January 28

08:50 Formalities

Session 10: STRENGTH & DAMAGE III
Session Chairman: Davis Tonks

09:00 Gareth Owen UK.09
Assessment of the Self Consistent Technique on the Determination of the Shear Strength of Shocked Metal Targets

09:303Bryan Reed LL.11
Extracting Plastic Flow Properties from Shock Velocity

10:00 BREAK

Session 11: STRENGTH & DAMAGE IV
Session Chairman: Bryan Reed

12:00 LUNCH

Session 12: STRENGTH & MULTISCALE MODELING I
Session Chairman: Curt Bronkhorst

13:30 Thomas Canfield LA.09
Damage Modeling with Void Evolution

14:00 Roger Minich LL.13
Spall & Melt Kinetics

14:30 Ellen Cerreta LA.10
Influence of Microstructure on Materials Modeling

15:00 BREAK

Session 13: STRENGTH & MULTISCALE MODELING II
Session Chairman: Bill Blumenthal

15:30 Curt Bronkhorst LA.11
Modeling the Grain Scale Micostructural Evolution of Metallic Polycrystals

16:00 Tom Arsenlis LL.14
Multiscale Models for the Dynamic Strength of Ta and V

16:30 CLOSE

FRIDAY, January 29

08:20 Formalities

Session 14: MULTISCALE MODELING & FRICTION I
Session Chairman: Jeremy Millett

08:30 Franz Freibert LA.12
Pu Microstructures & Thermal Physical Properties

09:00 Stewart Stirk UK.10
Investigations of Dynamic Dry Friction at Obliquely Shocked Metal Interfaces

10:00 BREAK

10:30 Discussion Session
Multiscale Models & Anisotropic Models
(Discussion Leader: Nigel Park)

11:30 LUNCH

12:30 Summary of Discussion Sessions
DAC
Bruce Baer (10 min.)
EOS Test Problem
Chris Robinson (10 min.)
EOS Theory Phases & Future Direction
Lorin Benedict (10 min.)
MaRIE
Curt Bronkhorst & Franz Freibert (10 min.)
Strength & Damage Test Problems
James Turner (10 min.)
Multiscale Models & Anisotropic Model
Nigel Park (10 min.)

13:30 Final Remarks

13:45 Executive Meeting
Chris Robinson, James Hammerberg, Tracy Vogler, John Heidrich, Daniel Orlikowski

• LLNL Presentations • LANL Presentations • SNL Presentations • AWE Presentations

JOWOG 32MAT

January 25-29, 2010
(Conference Agenda)
Bld. 132 Auditorium

Conference Banquet
Wednesday, 6:30 PM
Zephyr Grill & Bar
1736 First Street
Livermore, CA
(925) 961-1000

LLNL • LANL • SNL • AWE

JOWOG 32MAT

January 28, 2010
Thursday

Assessment of the Self Consistent Technique

Gareth Owen
Dynamic Material Response Group, Hydrodynamics Department
Ex. 25294

Summary

- Introduction to Self Consistent Method
- Initial computational analysis
- Initial views of the technique and reasoning
- Preliminary experimental results and analysis
- Investigation using external results
- Assessment of technique
- Computational code issues
- Conclusions

The Self consistent Technique

- What

  A technique used to calculate the strength of a material at a shocked state.
- Principals of Technique

  After initially shocking a material, the shocked material may strengthen over time. This strengthening can only be seen by a second shock pulse, whereby the new elastic limit of the material is then reached. Using wave profile analysis the new strength of the shocked state can be calculated.
- Paper Authors

  J. R. Asay, L.C. Chhabildas, J. Lipkin, H. Huang, T.J.Vogler ……
- Why

  Widely used technique in many laboratories.
- Requirement and Objectives of AWE

  Assess the validity of the technique

Self consistent Technique (SCT)

Basic Experimental set up

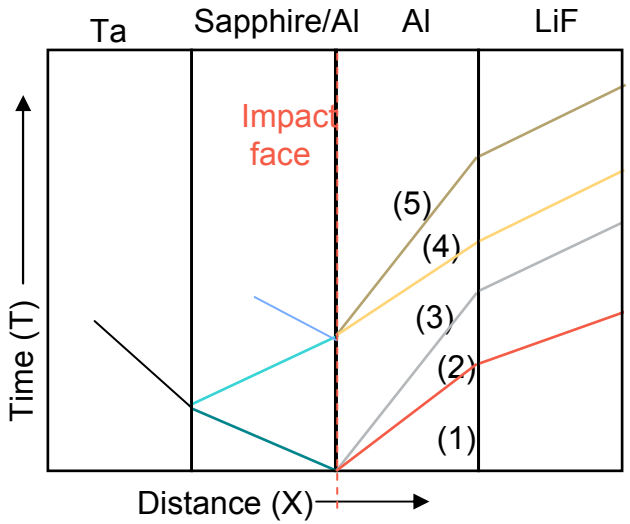

Illustration of states

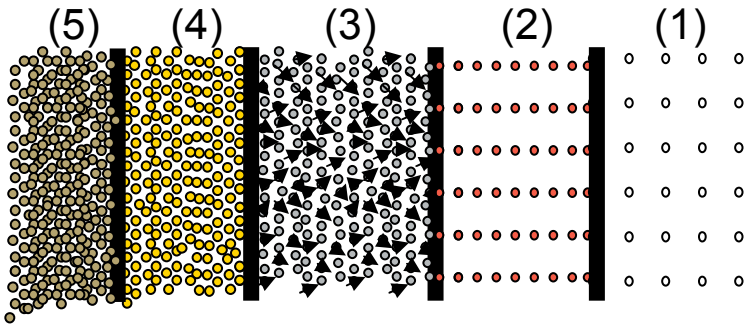

State (3)
Molecular movements behind shock wave result in material strength effects. This new elastic strengthening can only be seen by another shock wave, producing another elastic wave followed by a second plastic wave.

Schematic Experimental Result

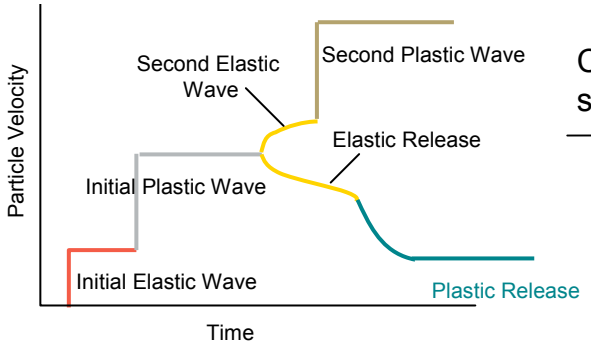

Converted to stress strain

Stress Strain plot (from Experimental Results)

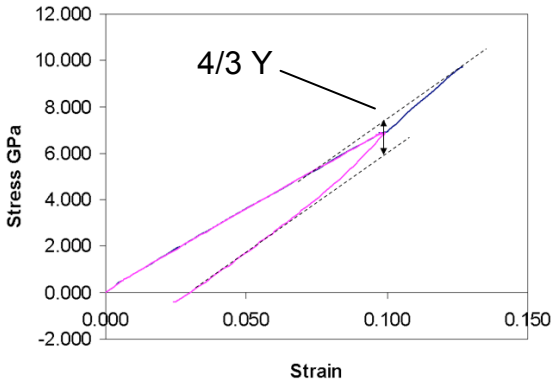

Huang H. and Asay J. R. – Compressive strength measurements in aluminium for shock compression over the stress range of 4-22 GPa

Initial Computational Analysis

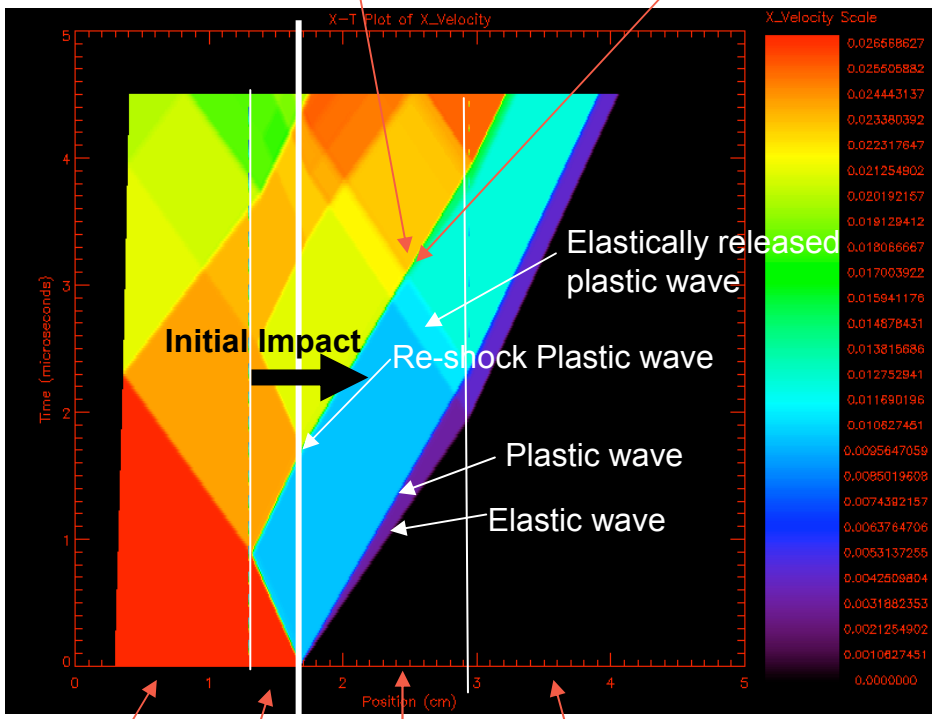

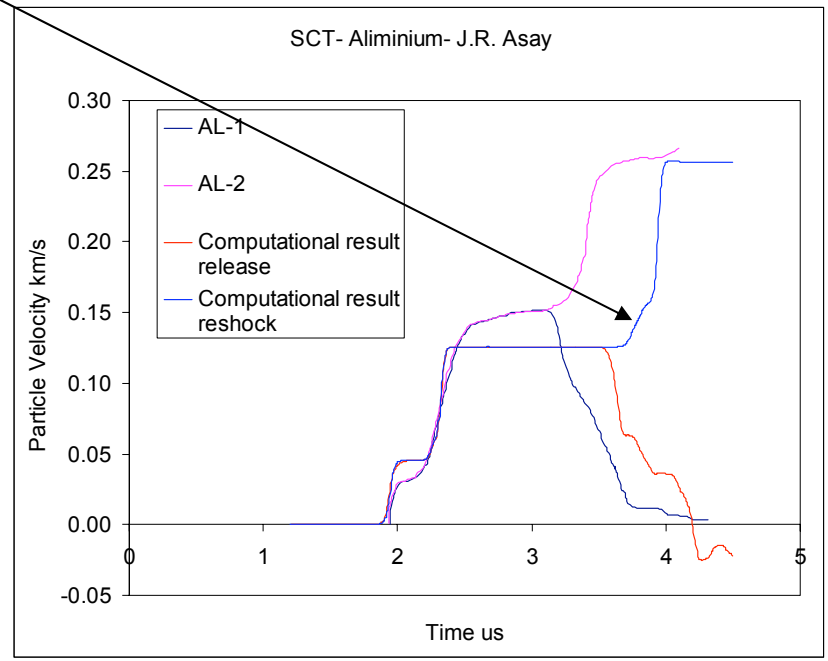

J.R. Asay and J. Lipkin
A self-consistent technique for estimating the dynamic yield strength of a shock-loaded material

X-T plot and computation simulations produced by E. Harris
X-T Plot Process developed by J. Turner

In-situ/Window computational Comparison

Illustrates how after wave profile analysis, the release produced by the window leads to incorrect in-situ values.

Aluminum "Window"

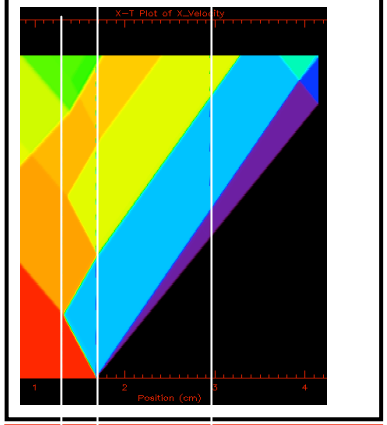

Silica Window

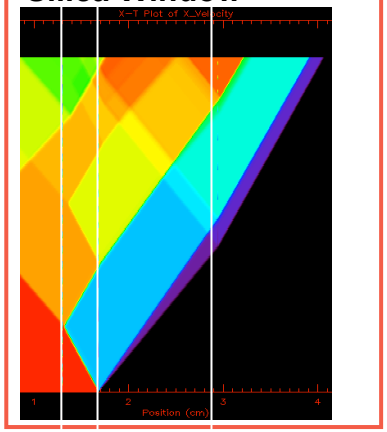

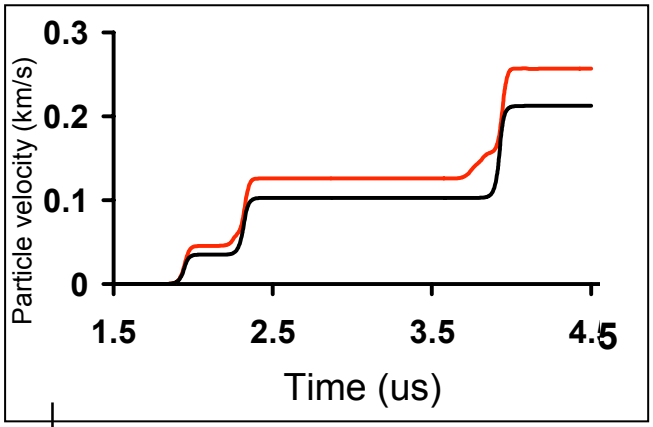

Converted to in-situ stress

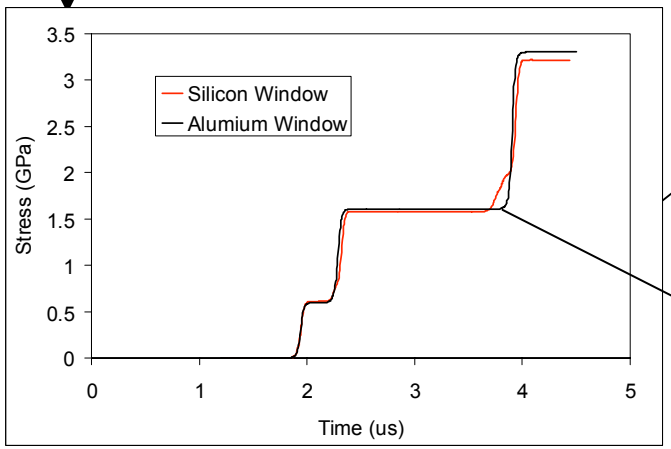

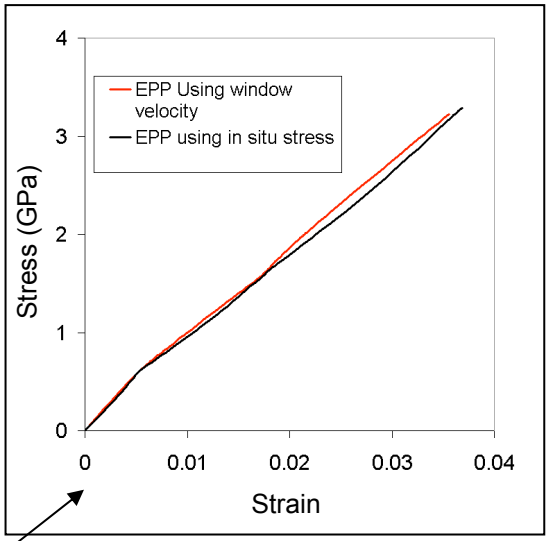

Aluminium window provides the in-situ stress in the target

Self consistent Technique (SCT)

From Computation and Analytical study, it can be seen that position and value of the second elastic wave dictates all the strengthening conclusions of the self-consistent method.

HOWEVER this bump can be caused by impedance mismatch of the window and target material.

Hardening Effect- Reloading

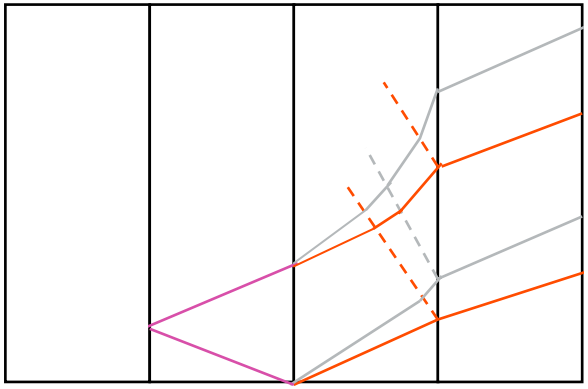

Wave Perturbation Only

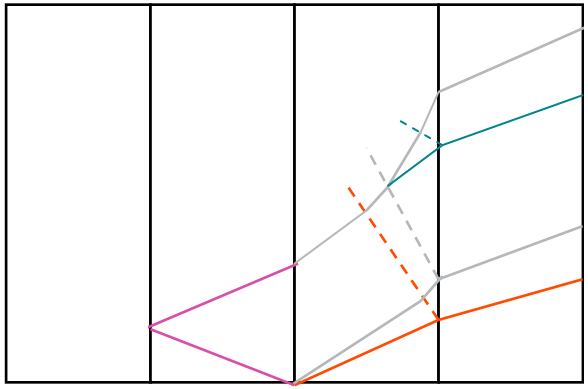

Combination of Material Hardening and Wave interaction

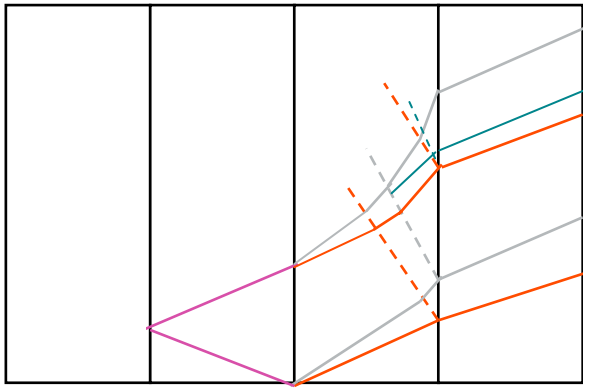

Previous investigation into perturbation

Huang H. and Asay J. R. – Compressive strength measurements in aluminium for shock compression over the stress range of 4-22 GPa

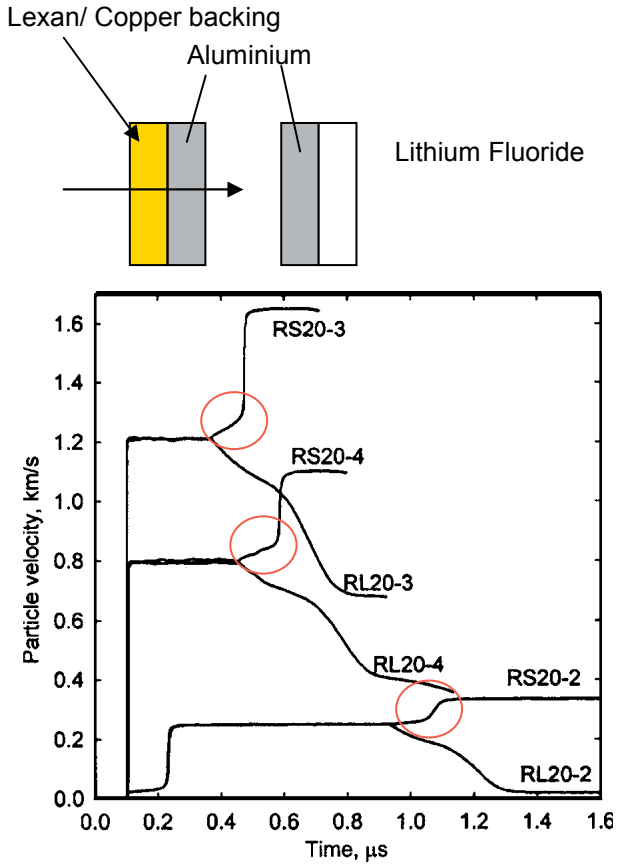

(Comments taken from papers)

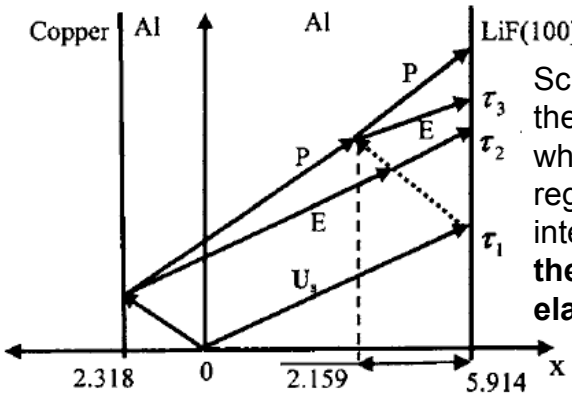

Schematic x-t diagram for wave interaction in the target for reshock experiment RS20-3, where the reshock wave was disturbed in the region of 2.159mm to the target/window interface. This causes a **slight perturbation to the following plastic wave since a new elastic wave is formed at the interaction**.

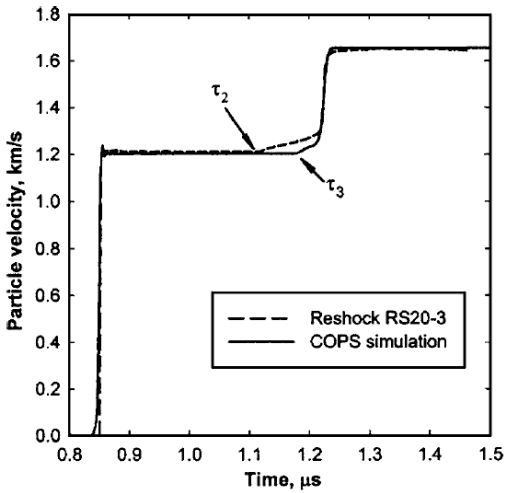

A relative small apparent quasielastic response arises from a target/window impedance mismatch when the window has a lower impedance than the target. The **dashed profile shows the actual measured profile** for the experiment RS20-3 and the **solid line corresponds to a 1D simulation** with an elastic-plastic model. The perturbation results from the wave interaction in Fig 12, **forming a new elastic wave by the interaction of the reflected elastic unloading and the plastic reloading.**

Initial Analysis Conclusions

Initial Computational Analysis has illustrated the same problem mentioned by Huang and Asay, however the perturbation from our codes appeared to be larger than that concluded in their studies.

After interaction with the lower impedance window, the material releases elastically.

The re-shock therefore initially re-stresses elastically, producing another elastic wave, before producing a second plastic wave.

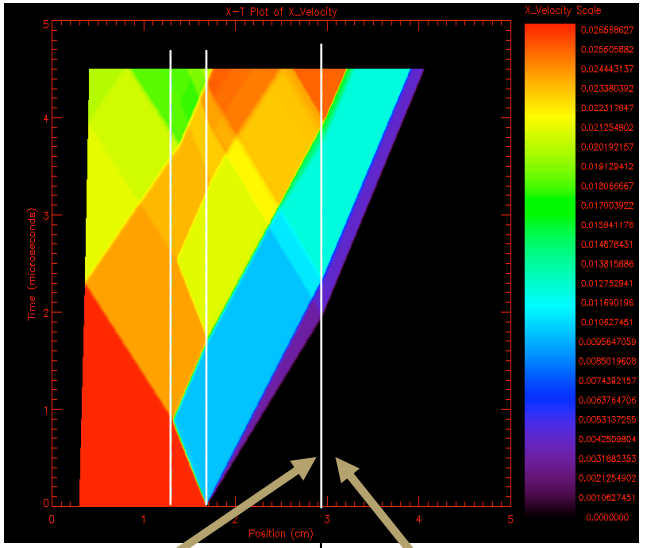

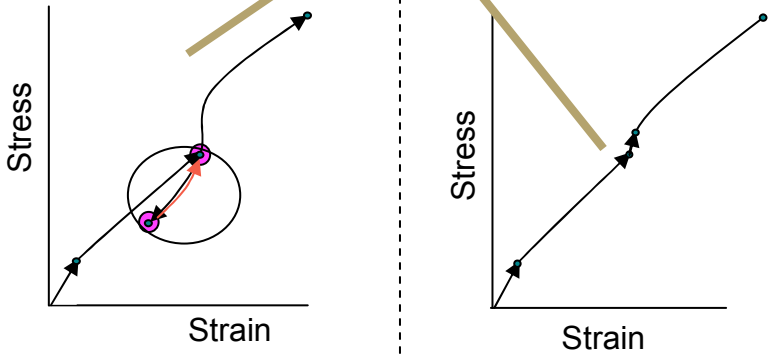

Schematic Stress Strain plot illustrating the history of the Aluminium sample near the window

Schematic Stress Strain plot illustrating the history of the Lithium Fluoride window near the interface

Preliminary Experiments –Copying Huang/Asay

Additionally longitudinal gauges were used in order to have a separate diagnostic to verify the effects of the Lithium Fluoride window, comparing it against an Aluminium backed gauge.

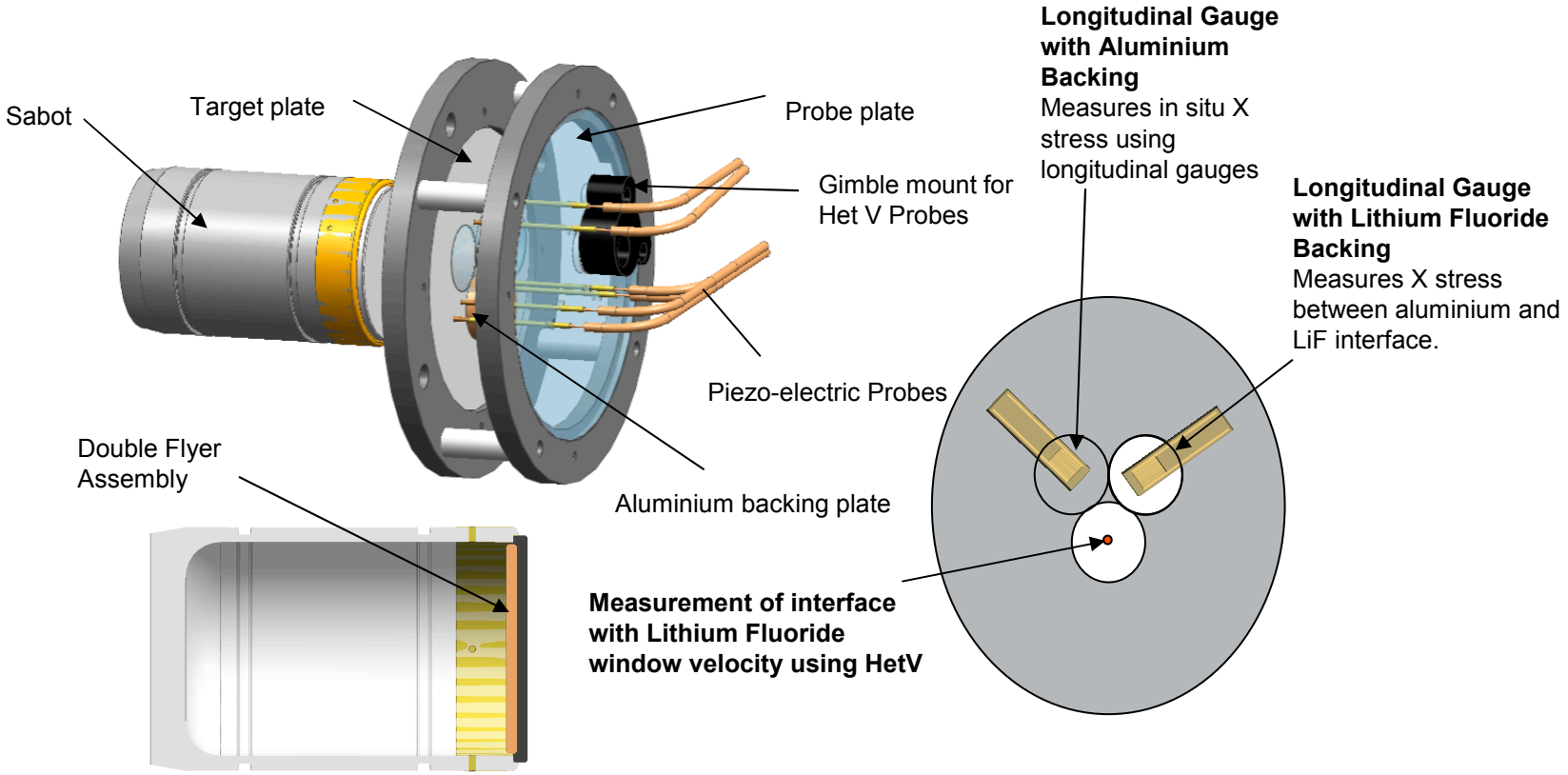

Velocity Interferometry Results

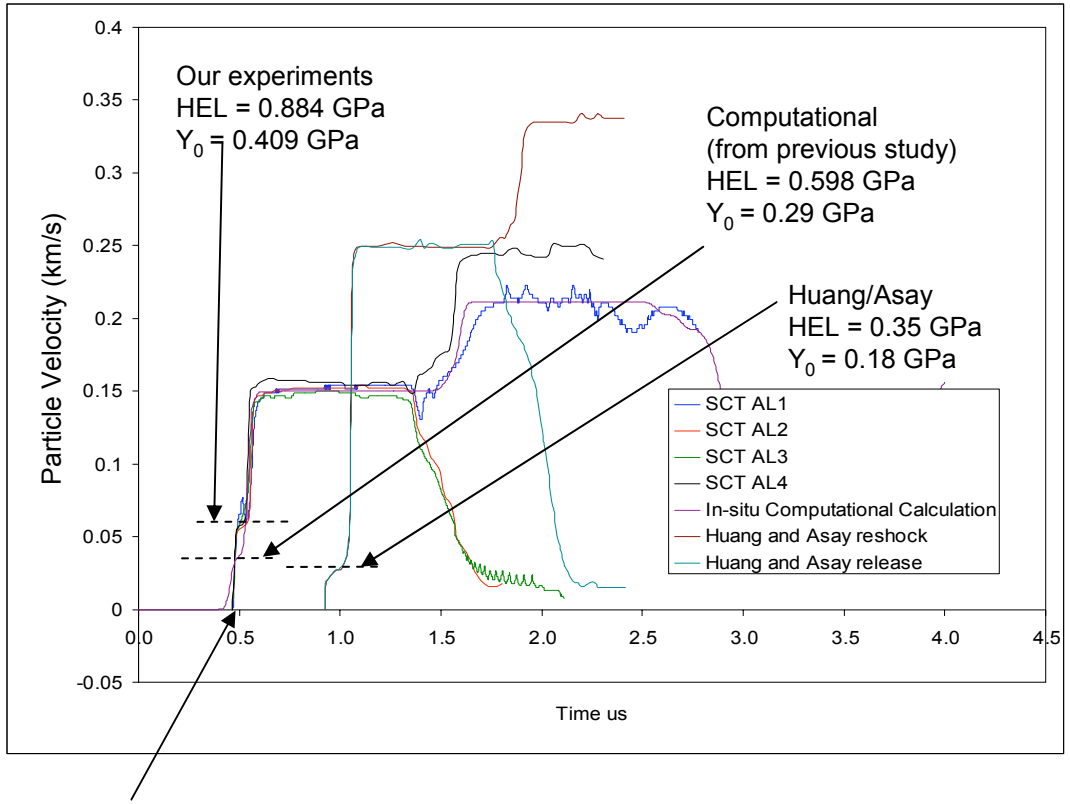

Elastic wave arrival time of traces use C_L from Ultra-Sonics.
Time derived using piezo-electric probes was found to have too much variation to supply useful results.

Electron Backscatter Diffraction Analysis of an Extruded AL 6061 T6

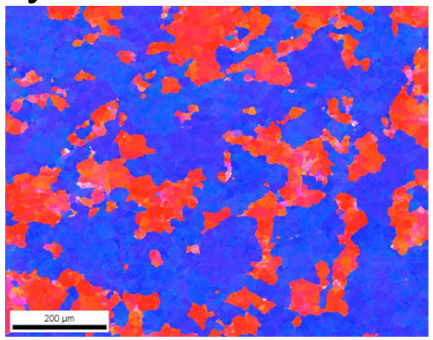

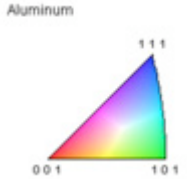

Longitudinal axis

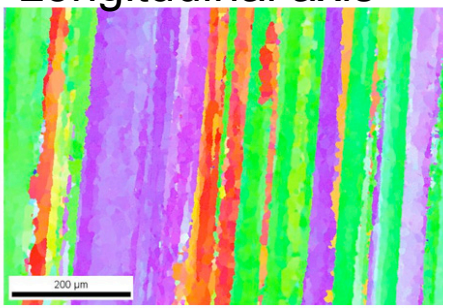

Radial axis

The grains are long and narrow, elongated in the axial direction.

Detailed Assessment of Traces

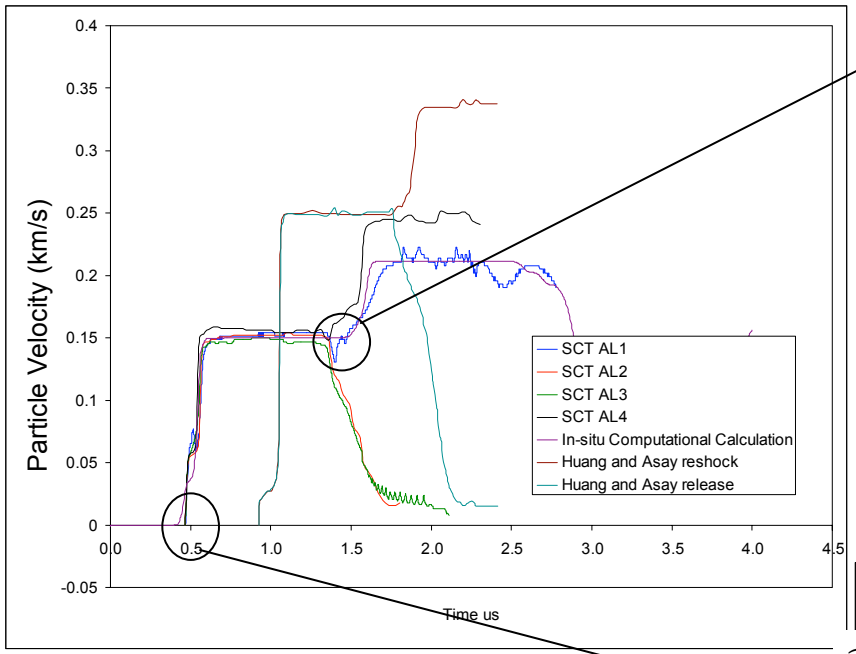

Drop caused by glue layer between front flyer and second flyer.

This drop incidentally produces a larger elastic release, and therefore a larger elastic re-shock wave.

This is being addressed in future trials by decreased roughness tolerance of flyers and then bolting the plates together.

Other experimentalist use a thin indium interlayer to make sure there are no gaps, however this interlayer (higher impedance than Aluminium) will lead to an additional shock, producing another slight step.

Jump off shape altered

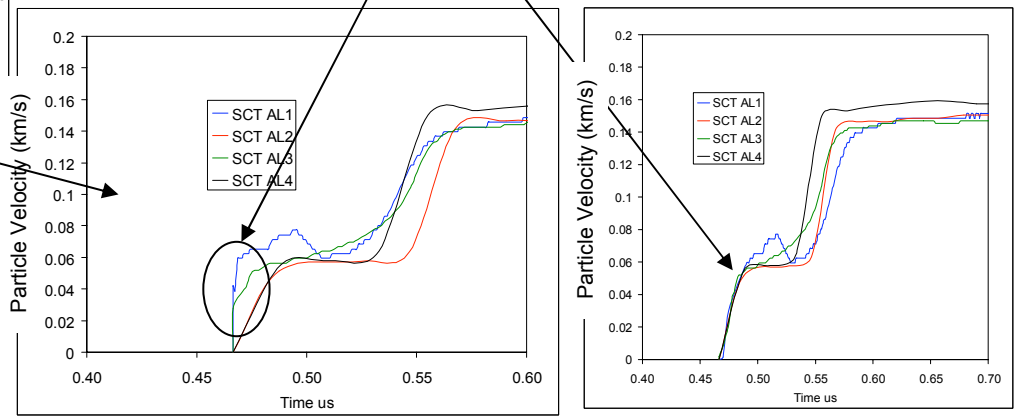

Het V is not known to have good accuracy when measuring initial jump offs (hence alteration)
It is possible that the flatness and surface finish of the target were not sufficient.

Strength Calculations

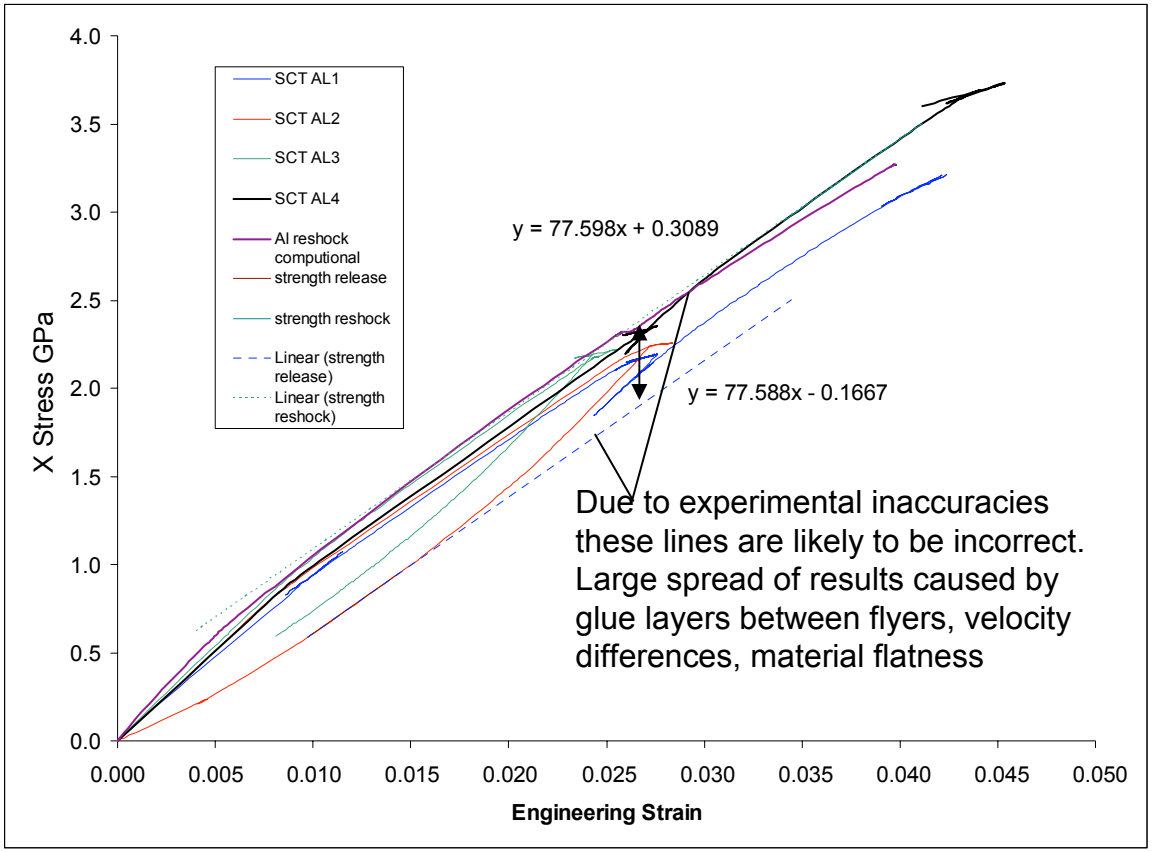

	x	y
Re-shock	0.26668768	21.00333
Release	0.26668768	20.52506
	8/3 tor	0.478267
	tor	0.17935

Longitudinal stress = 2.2 GPa
Tau = 0.17935 GPa (at 300m/s)

From Asay and Huang
Tau c^c = 0.121 GPa (at 500m/s)

Using the Method employed by J. Asay et al. a similar strength was attained.
The differences were probably down to the inaccuracies created by the experiment

Longitudinal Stress Results compared to in-situ computational calculation-Raw Data

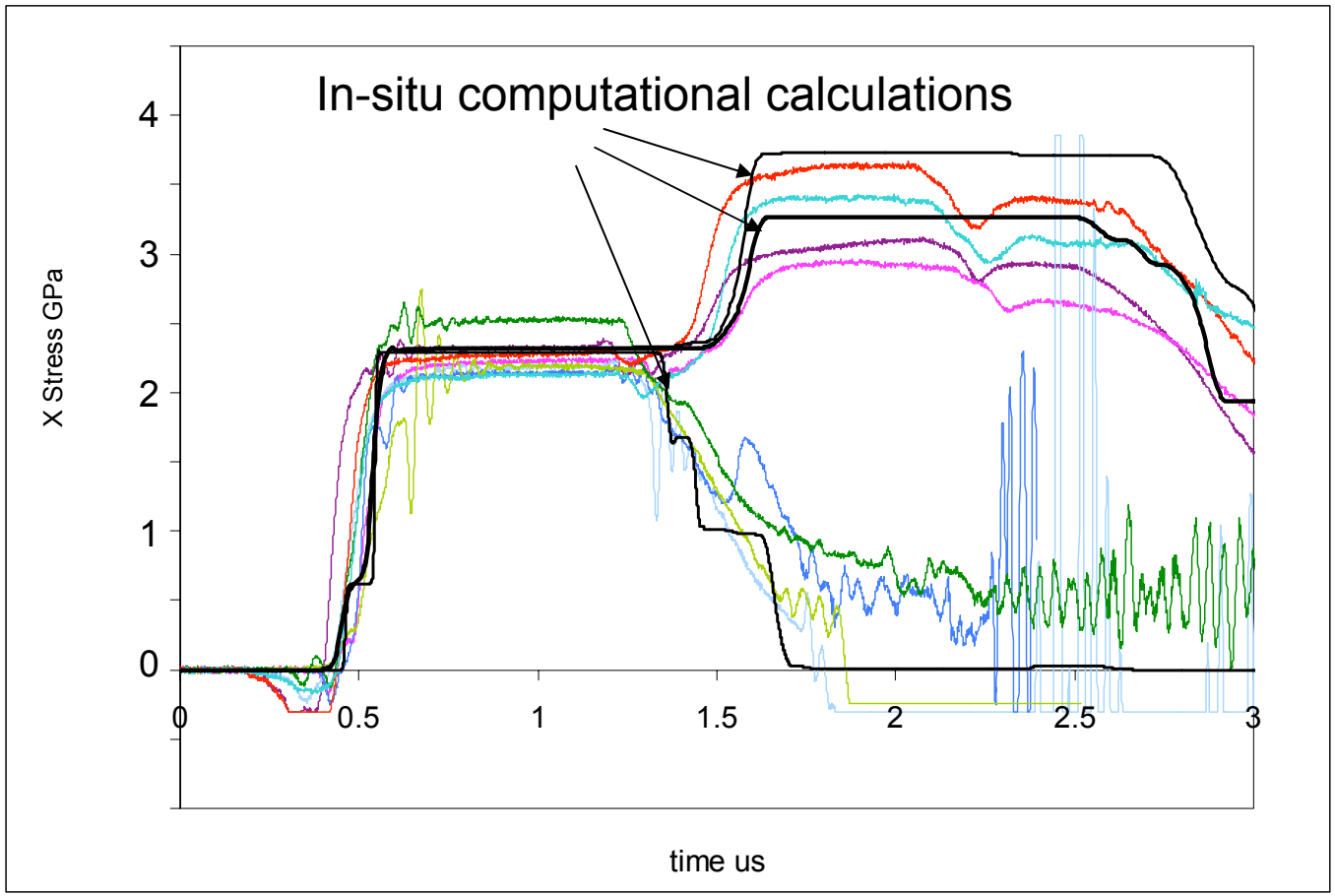

Gauges were used in order to have an additional diagnostic to verify the effects of the Lithium Fluoride window, comparing it to an Aluminium backed gauge.

However it was not possible to assess the effects of the window because of the ring up times related to longitudinal gauge because of their construction.

Provided an initial check for the x stress of the first plastic wave.

From investigation the second pressure wave proved to be inaccurate caused by hysteresis (the gauge is not calibrated for two shocks).

Re-shock results
Converting all results into X stress using wave profile analysis

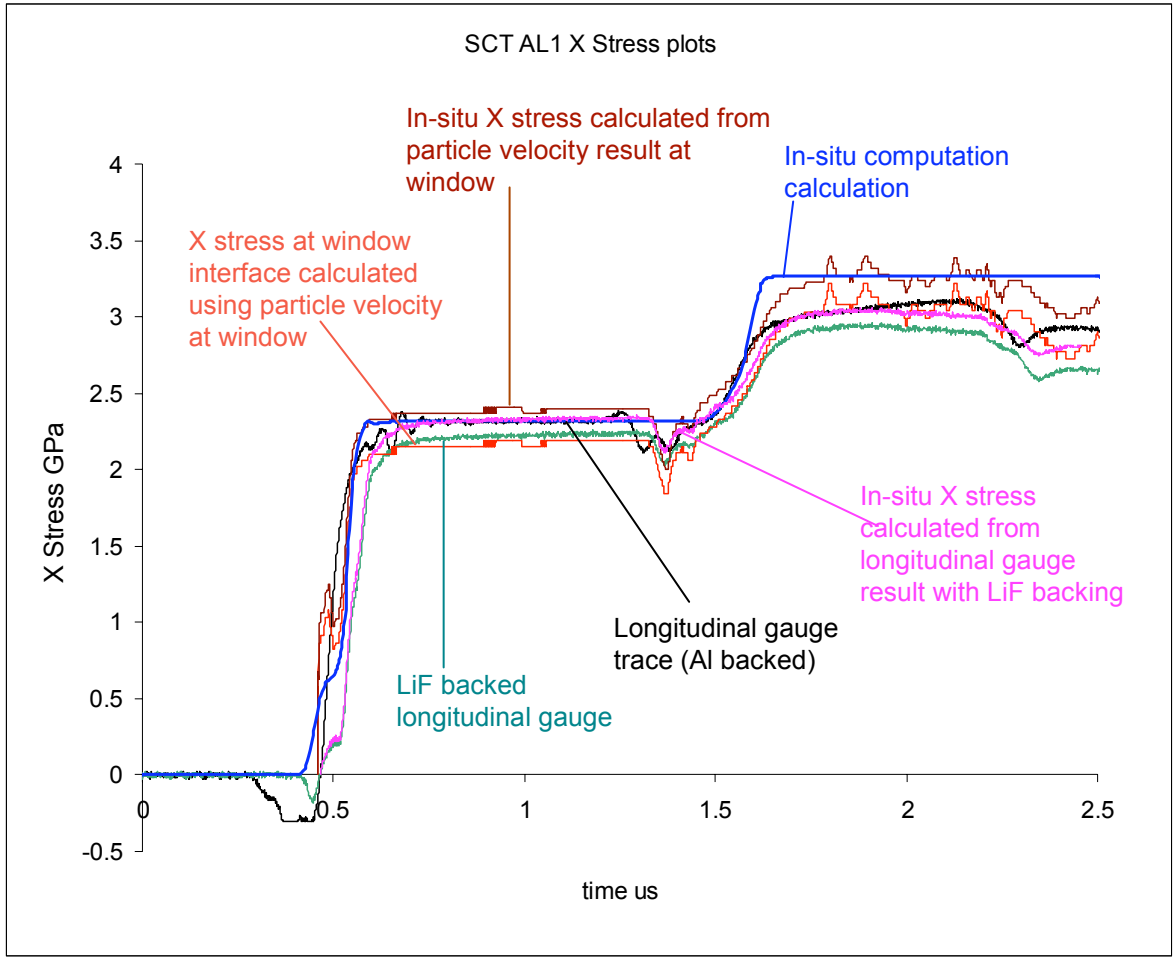

Using the wave profile analysis it is possible to convert all results into stress plane.

Comparisons have illustrated that the gauge traces produce a reduced stress at the second shock.

The initial stress acquired by the gauge trace is correct.

Because of the associated ring up requirements of the gauges the shapes of the longitudinal gauges cannot be used evaluate the effects of the lower impedance window.

SCT AL1 – 299.64m/s +/- 3.67m/s

Release results
Converting all results into X stress using wave profile analysis

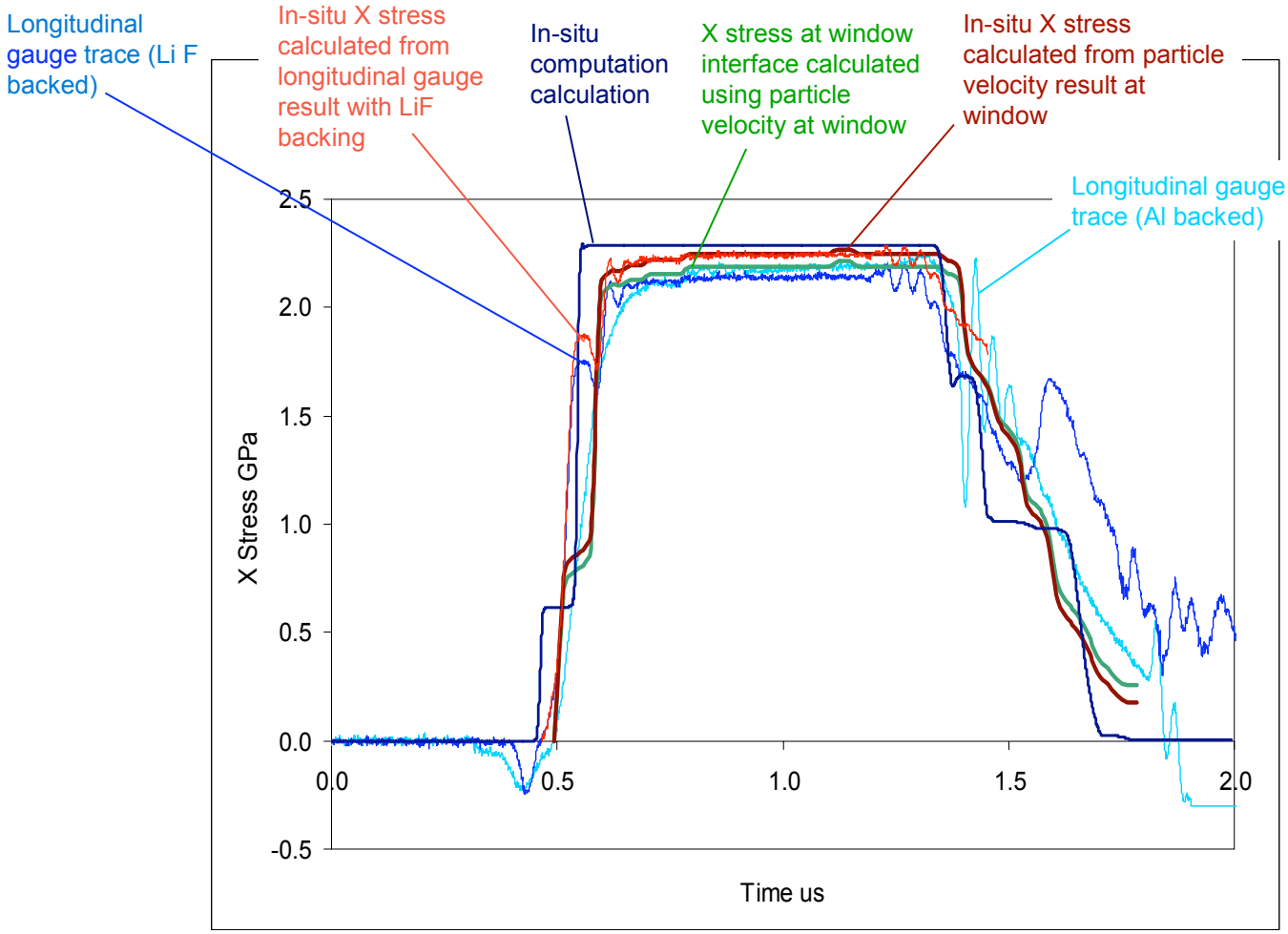

It can be seen that the release shape of the trace is similar to the computational code.

SCT 2- 296.89m/s+/-1.687m/s

Comparison between experimental and computational result for the second elastic wave

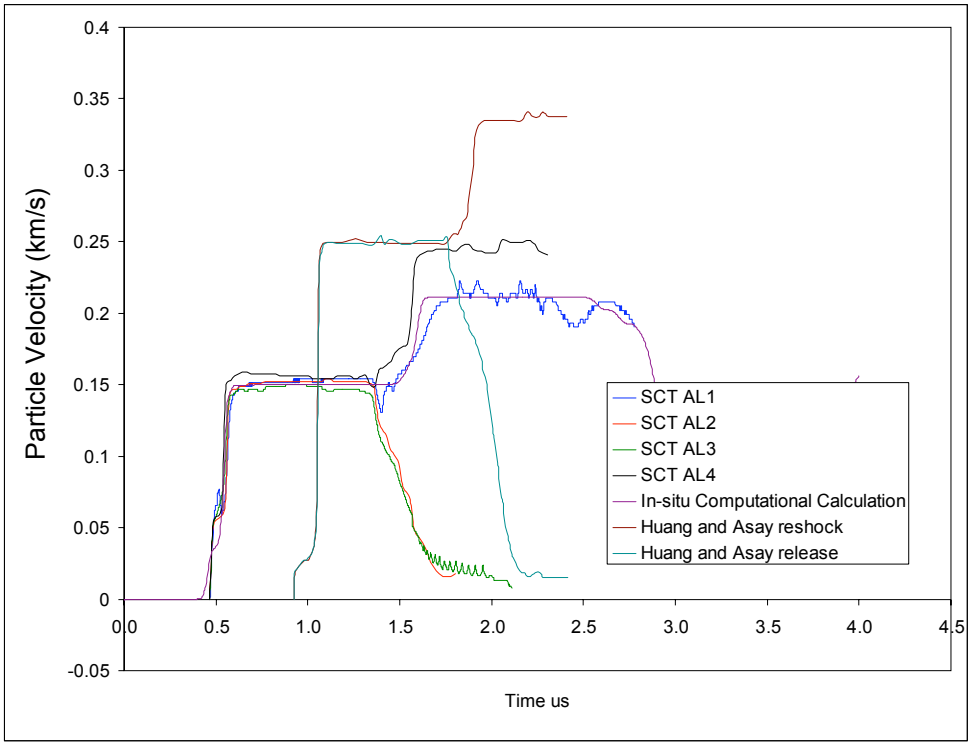

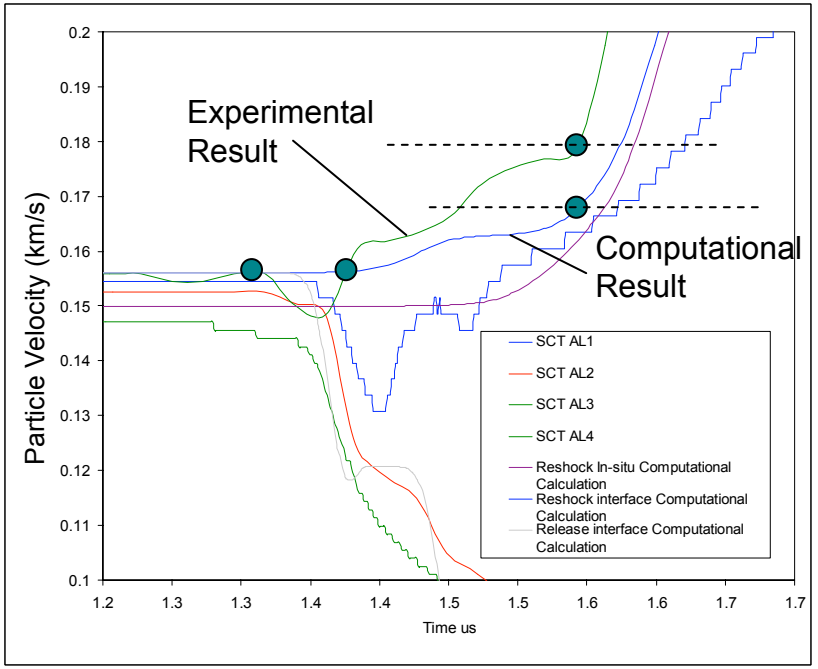

The Computation result (treating Lithium Fluoride window as a fluid), produces a similar bump that occurs at a similar time to the experimental result.
Leading to conclusion that it is caused by the impedance mis-match of the window, rather than another elastic wave.

Comparison between Huang/Asay results and AWE computational result

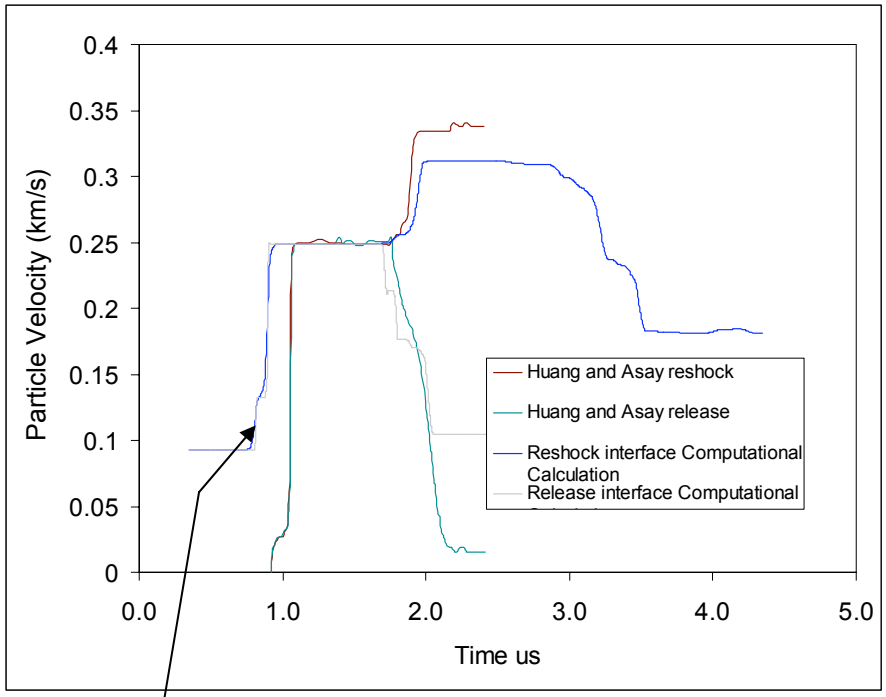

Computational results moved for comparison

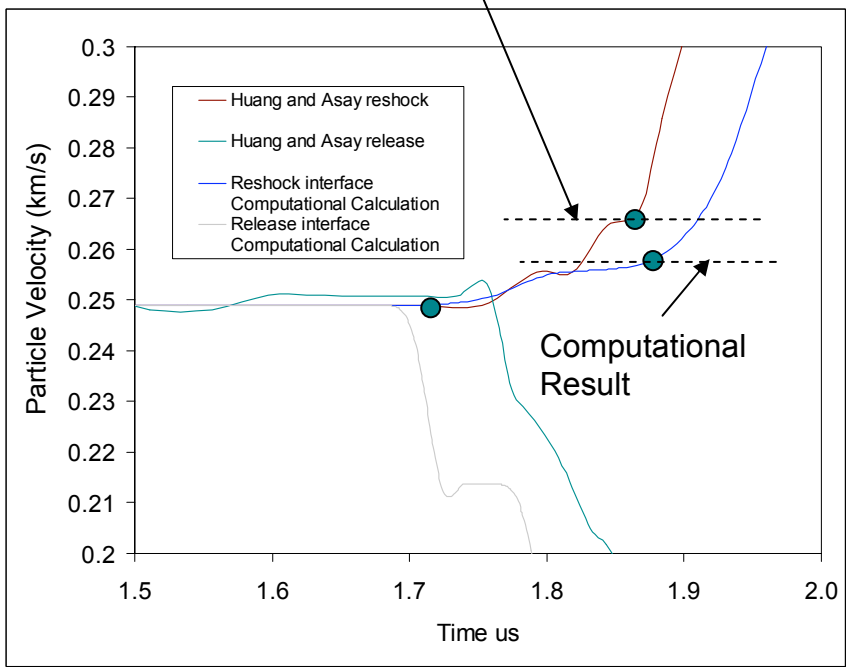

It can be seen that the bump is of a similar scale for the computation and experiment. Illustrating that it is likely that it is created by the lower impedance window.

Hydrodyamic investigation

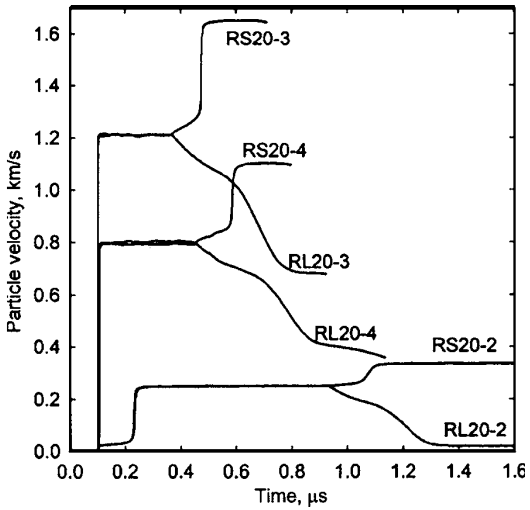

Huang H. and Asay J. R. – Compressive strength measurements in aluminium for shock compression over the stress range of 4-22 GPa

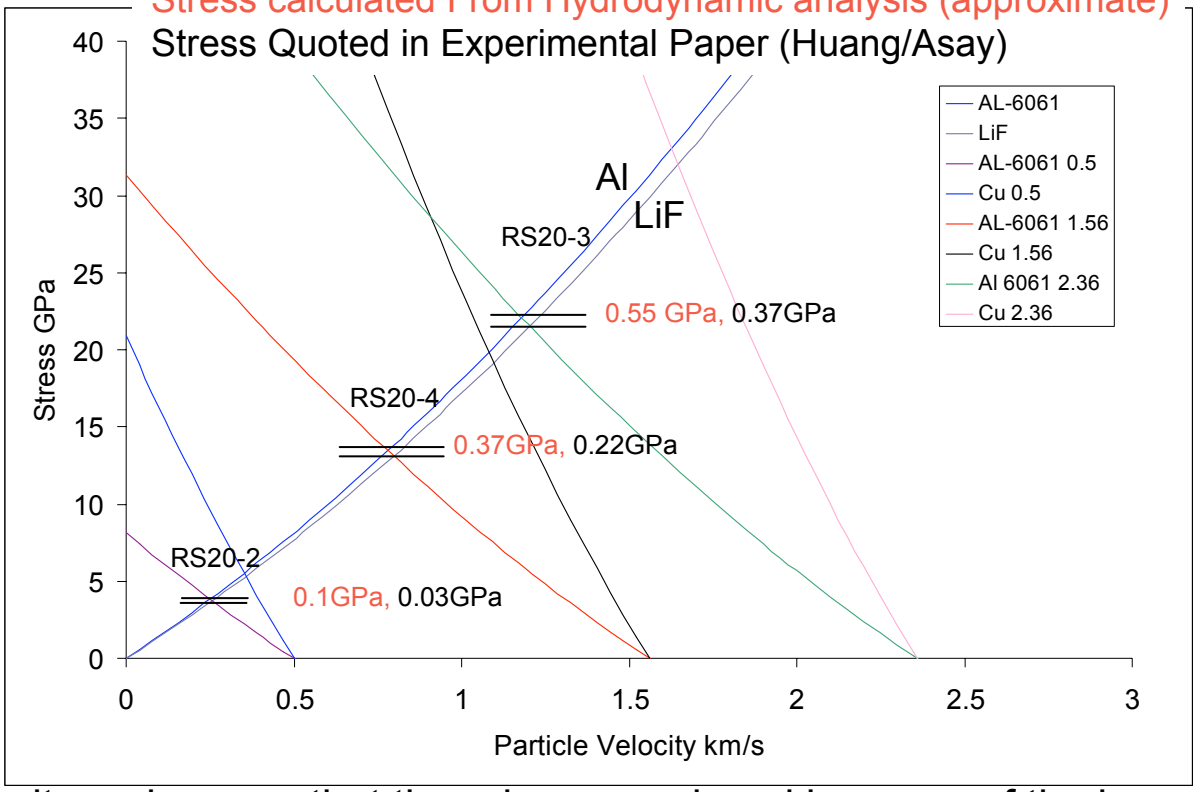

By using simple hydrodynamics it can be seen that the release produced because of the lower impedance window, would increase as the initial impact stress increases, leading to a larger elastic re-shock bump, and the conclusion that the material strengthens with increased pressure.

Hydrodynamic investigation

Further investigations using additional elastic release Hugoniots reveals approximate increases in pressure and particle velocity which are comparable to those measured in experiments

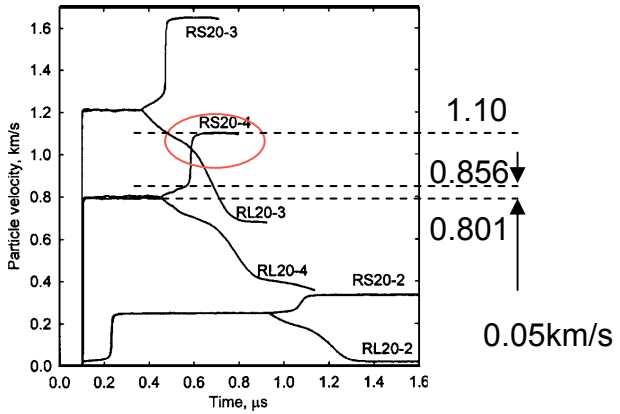

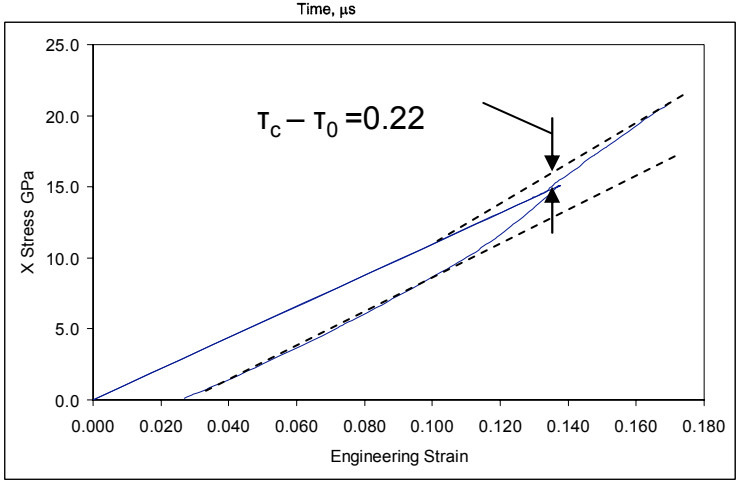

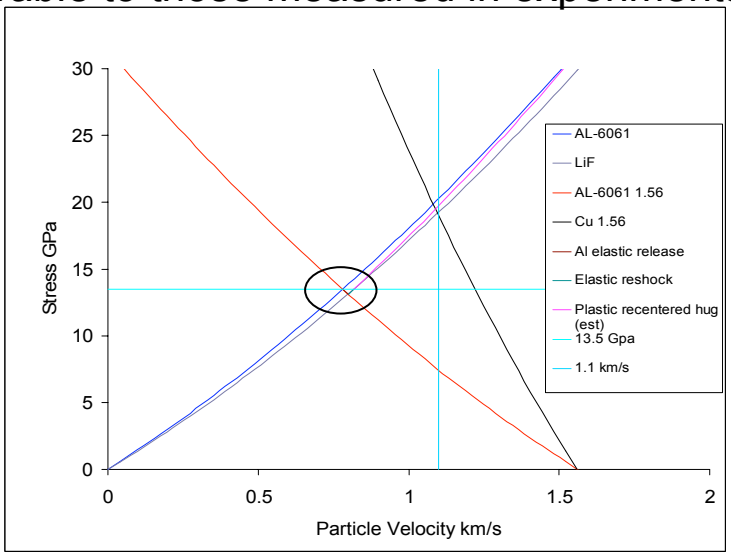

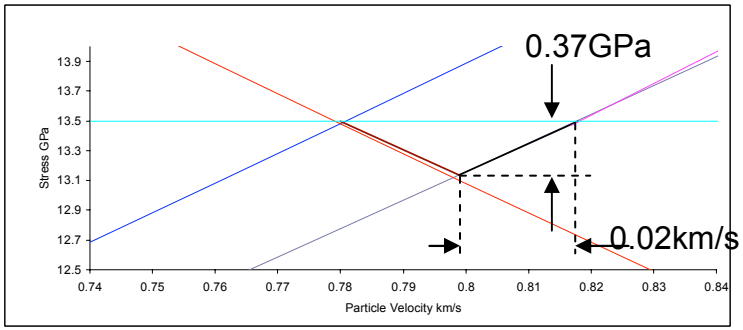

Hydrodynamic investigation

Additional reflections could also occur in the experiment, which would lead to an increased bump size, coupled with this is the fact that these waves have a rarefaction associated with them producing a ramped affect.

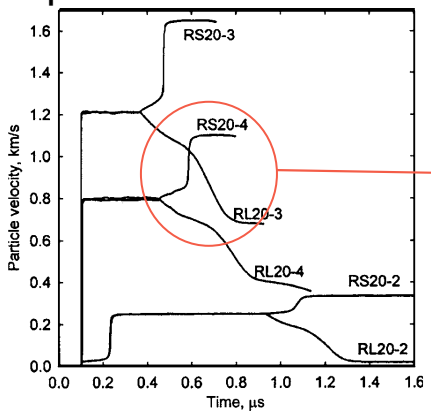

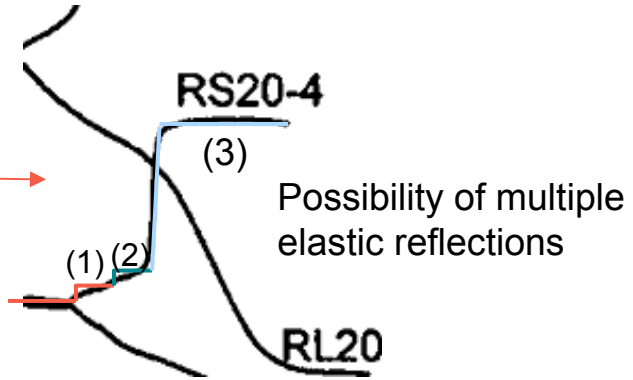

Possibility of multiple elastic reflections

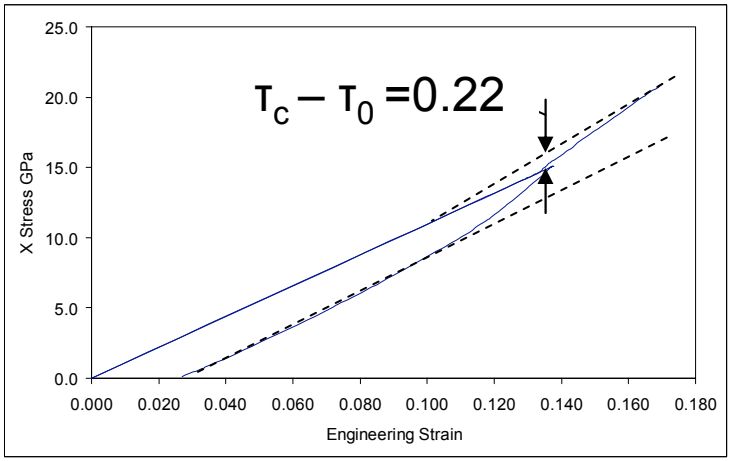

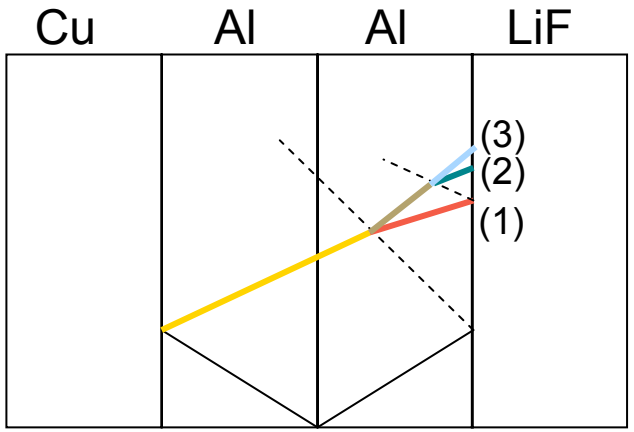

Computation Code issues

The elastic perfectly plastic model used in these calculations doesn’t incorporate any strain, strain rate, or time dependant hardening, however it has qualitatively reproduced the effects seen in the experiments. i.e. the EPP model provides an explanation for what happens without the need for additional physics.

Summary of work

- The Self Consistent Technique is widely used in many laboratories, in order to measure strength of a material at a shocked state.
- As customers of this technique we need to make sure that the strength values obtained from this technique are correct.
- Four trials were carried out using both velocity interferometry and longitudinal gauges, unfortunately a glue layer between the two flyers have led to a drop at a critical point in the experiment, however it was still possible to illustrate the use of the technique.
- Longitudinal gauges were used in order to have an additional method of evaluating the effect of the lower impedance window. However as the gauges have an associated ring up time, this led to them not being able to differentiate a between the traces produced with different windows.
- Though the gauges gave a credible result for the initial shock, from the investigation the second pressure wave proved to be inaccurate, mainly due to hysteresis, and that the gauges are not designed to be used in multiple shocks.
- Three further experiments are planned on Aluminium using mechanical processes and high tolerance faces to produce more accurate results.

Conclusions

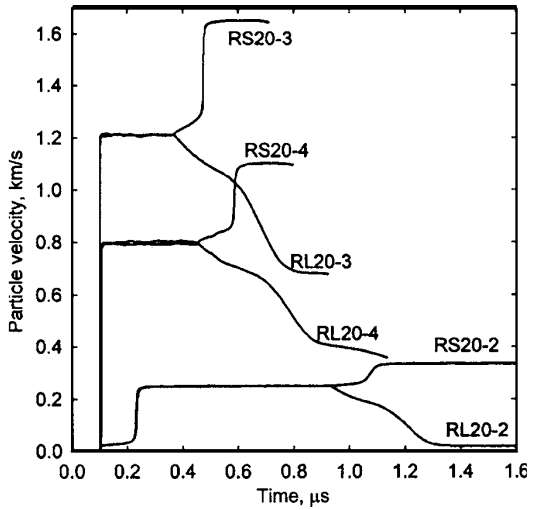

Current Process

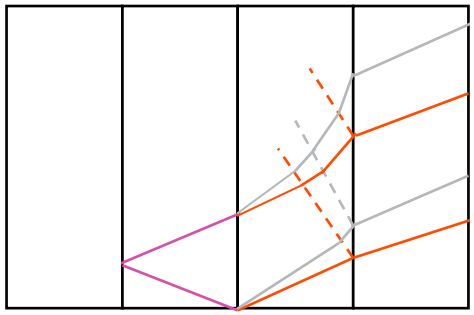

Strengthening effects

Alternative Process

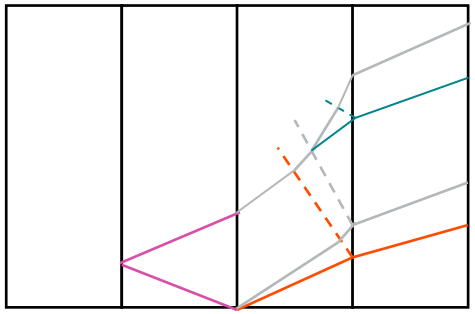

Perturbation effects

- In my opinion the investigation has revealed that the current process of acquiring the strength of the material at a shocked state may have problems, and the effects seen are most likely caused by the difference in impedance between the window and the target.
- However, the shock and re-shock/release process does provide a lot of information about multiple shock systems, and is therefore a great vehicle for improving the validity of the computational codes, using forward analysis to attain correct material properties.
- Further experiments will be designed taken into account the lessons learnt in the pilot series.

Additional Comments

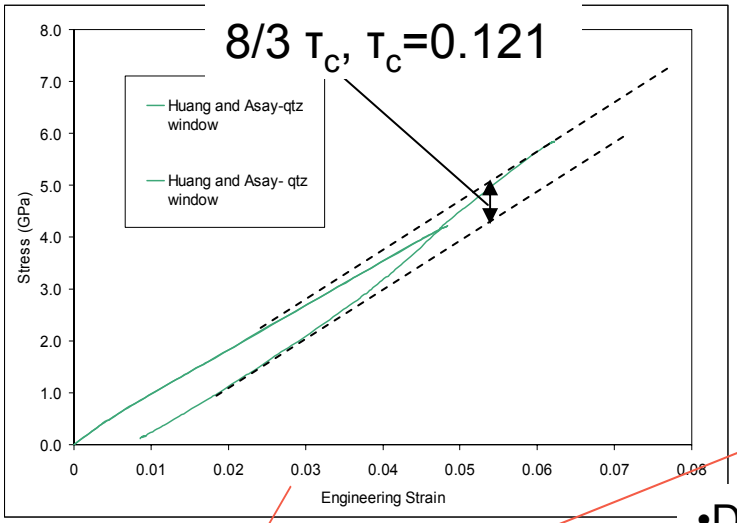

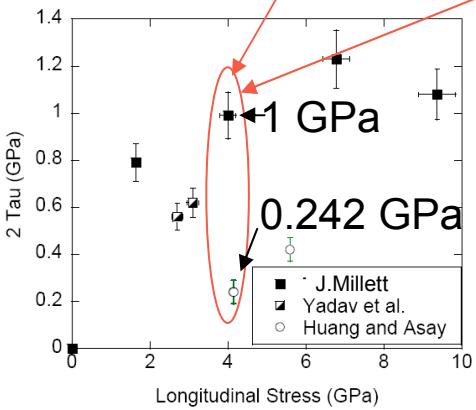

Lateral gauge trace Al 6061 T6 (J.Millett)

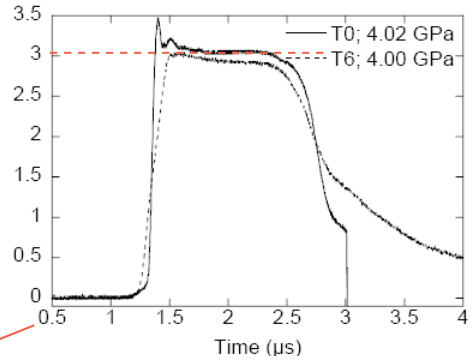

Longitudinal stress = 4GPa

- Direct comparison between a longitudinal gauge trace and a lateral gauge trace (assuming the lateral trace has reached equilibrium) would provide the strength of the material during compression.
- The SCT calculates the strength of the material at a given shock pressure by measuring the distance between the two sides of the yield surface.
- Alternatively this could illustrate that the SCT method merely records an effect produced by the lower impedance window.

Lawrence Livermore National Laboratory

Extracting Plastic Flow Properties from Shock Velocimetry

Bryan W. Reed, Roger W. Minich, James S. Stolken, and Mukul Kumar

Lawrence Livermore National Laboratory, P. O. Box 808, Livermore, CA 94551

This work performed under the auspices of the U.S. Department of Energy by Lawrence Livermore National Laboratory under Contract DE-AC52-07NA27344

LLNL-PRES-422522

We are developing a coherent array of analysis tools for compression wave data

Noise-tolerant PDV velocity extraction with uncertainties

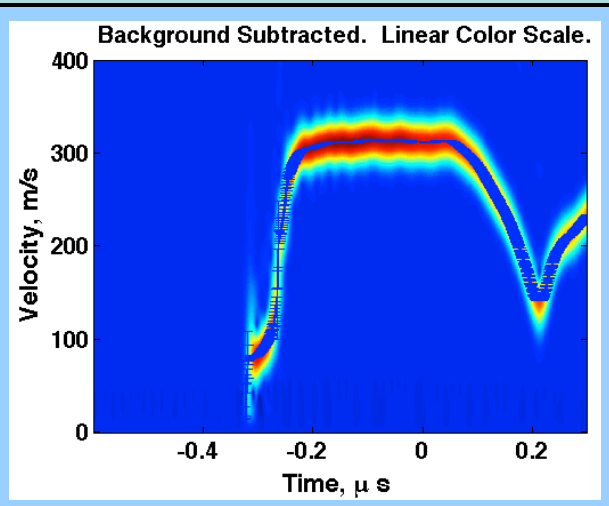

Full error propagation (sensitivity analysis) of all parameters

Same code can be used in conjunction with hydro simulations for optimizing experimental design

Second-order interpolation function with free surface corrections

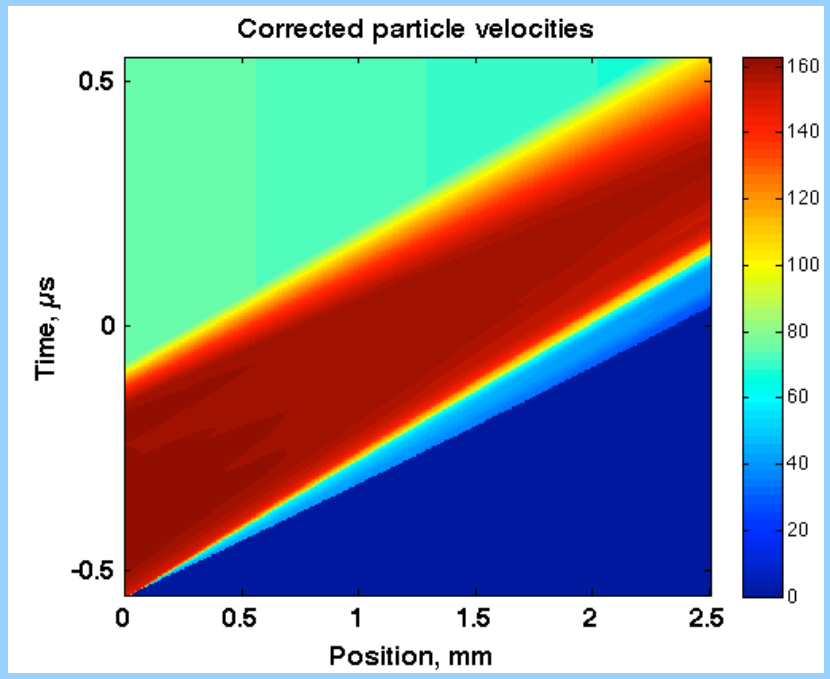

Can handle nonsteady waves, ramps, weak shocks, strong shocks

The methods aim to pull out as much information as possible while keeping the physics completely general

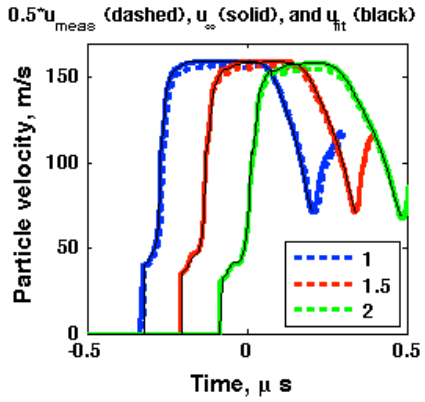

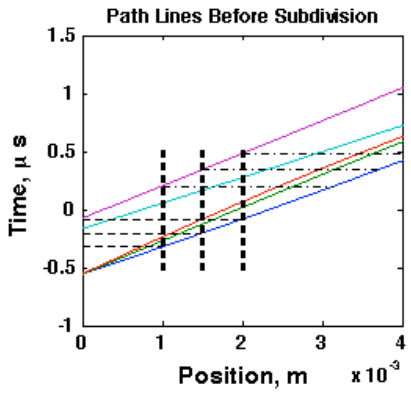

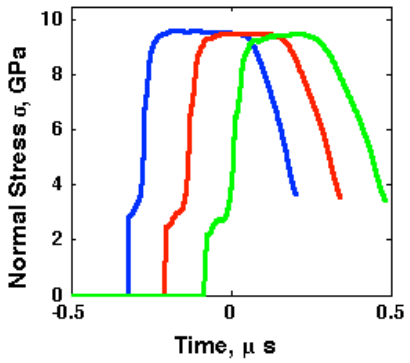

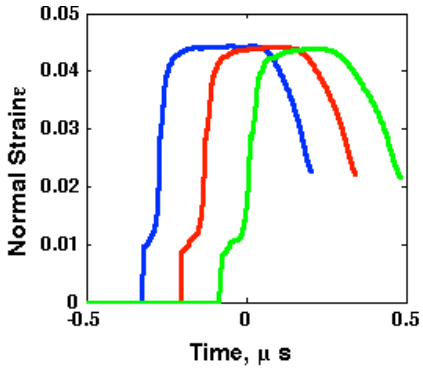

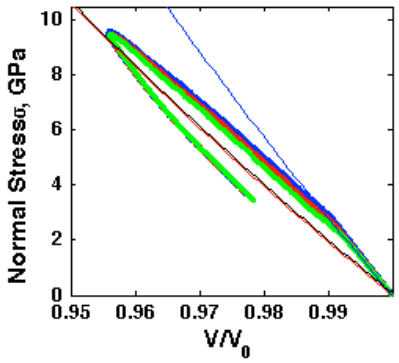

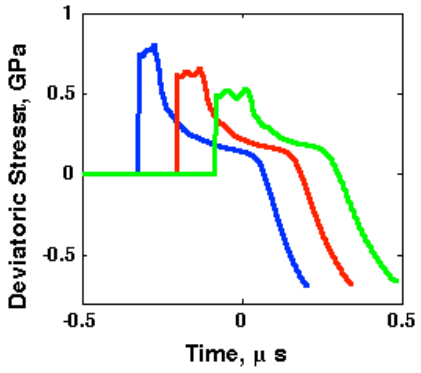

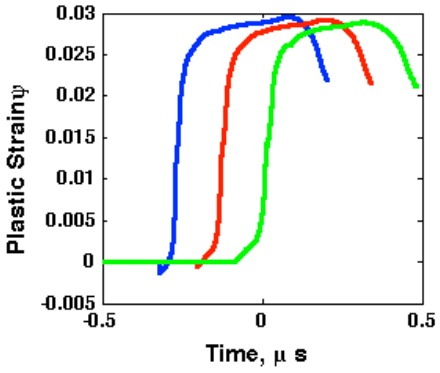

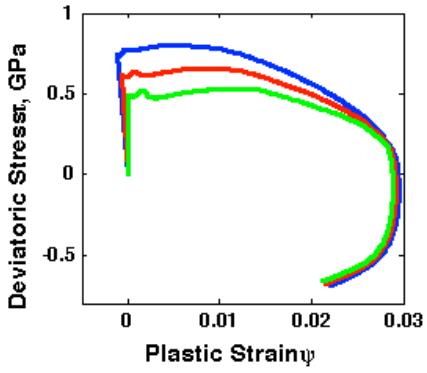

Data-driven analysis allows extraction of important parameters with minimal assumptions about the material

Lagrangian analysis <u>and strength extraction</u> are in a unified framework. Full in situ tensor stresses and elastic/plastic strains are calculated.

The methods were developed on data from gas gun shots on three-step Ta targets

Ta-on-Ta and Ta-on-LiF gas gun shots to 10, 25, 45, and 60 GPa

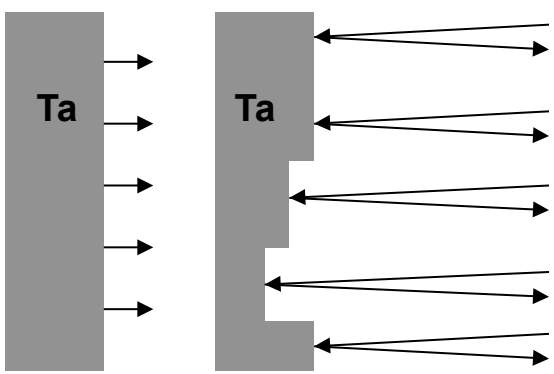

PDV 2.0 mm thickness

PDV 1.5 mm thickness

PDV 1.0 mm thickness

7 extra PDV channels for tilt/flatness correction

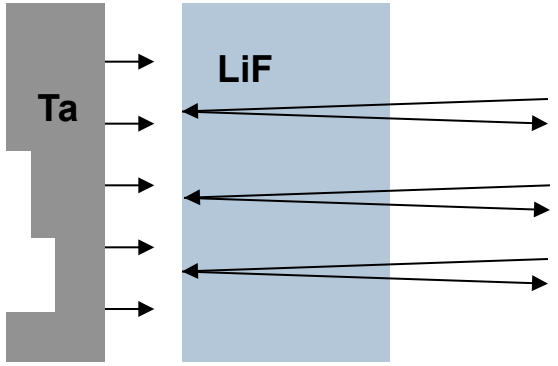

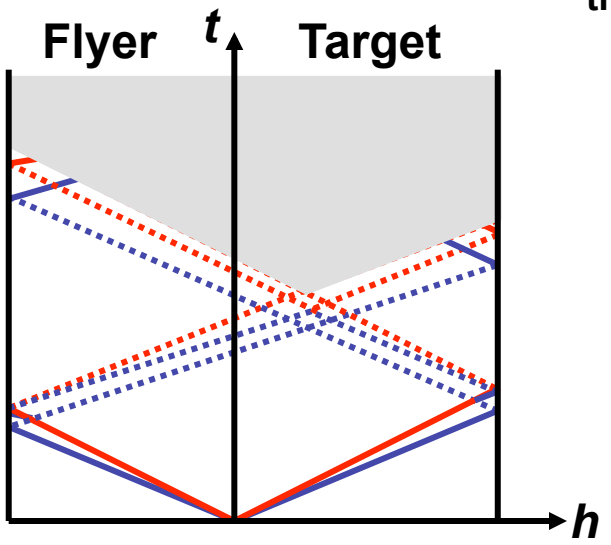

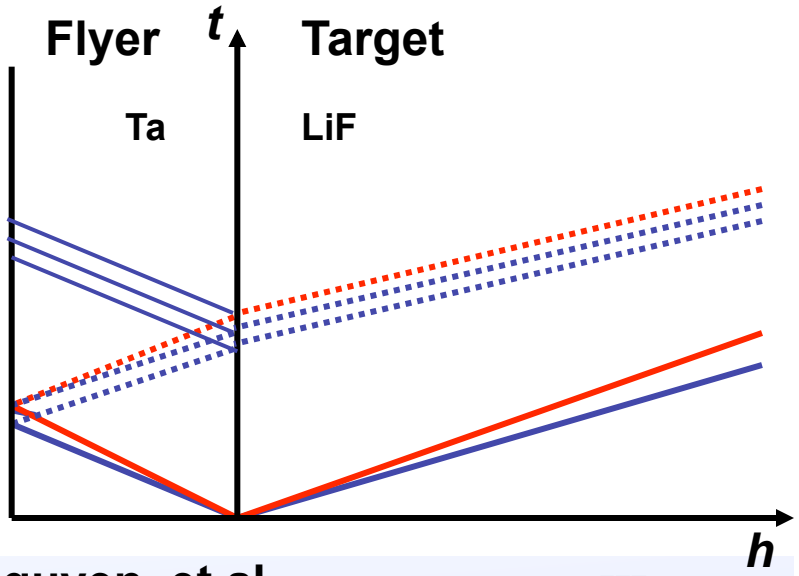

Collaboration with R. Patterson, J. H. Nguyen, et al.

The tools include noise-tolerant PDV velocity extraction

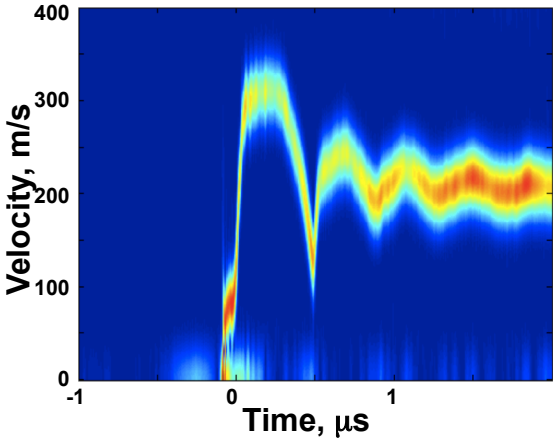

Raw windowed Fourier transform

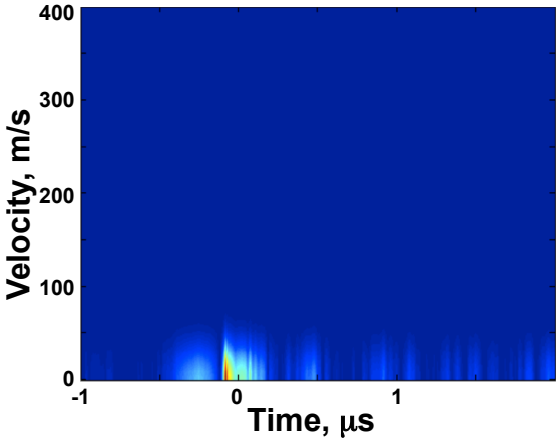

Extracted noise component

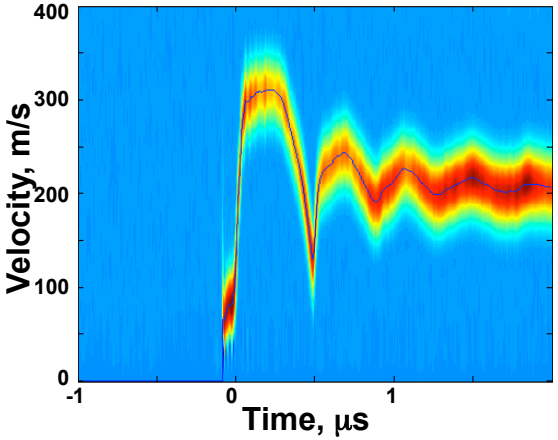

Remove noise and track the peak as a function of time.

Resolution is:
5 ns temporal
1 m/s velocity

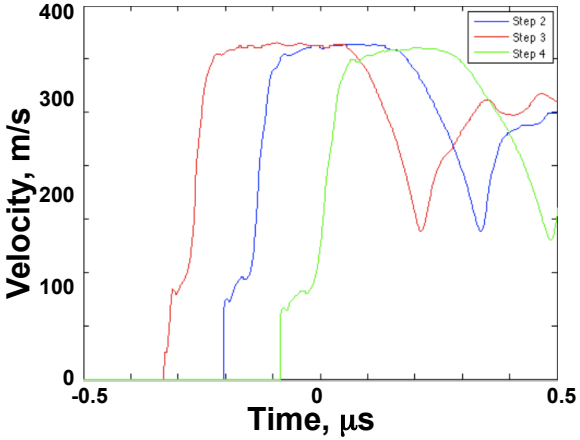

Combine data from all the step heights to get a sense of the wave propagation

Background removal and optimized noise thresholding and window size selection result in a very robust velocity extraction

Normal stress and strain are derived from the particle velocities using integrals in space and time

Conserve Momentum: $\frac{\partial \sigma}{\partial h} = -\rho_0 \frac{\partial u}{\partial t}$

Conserve Mass: $\frac{\partial \varepsilon}{\partial t} = -\frac{\partial u}{\partial h}$

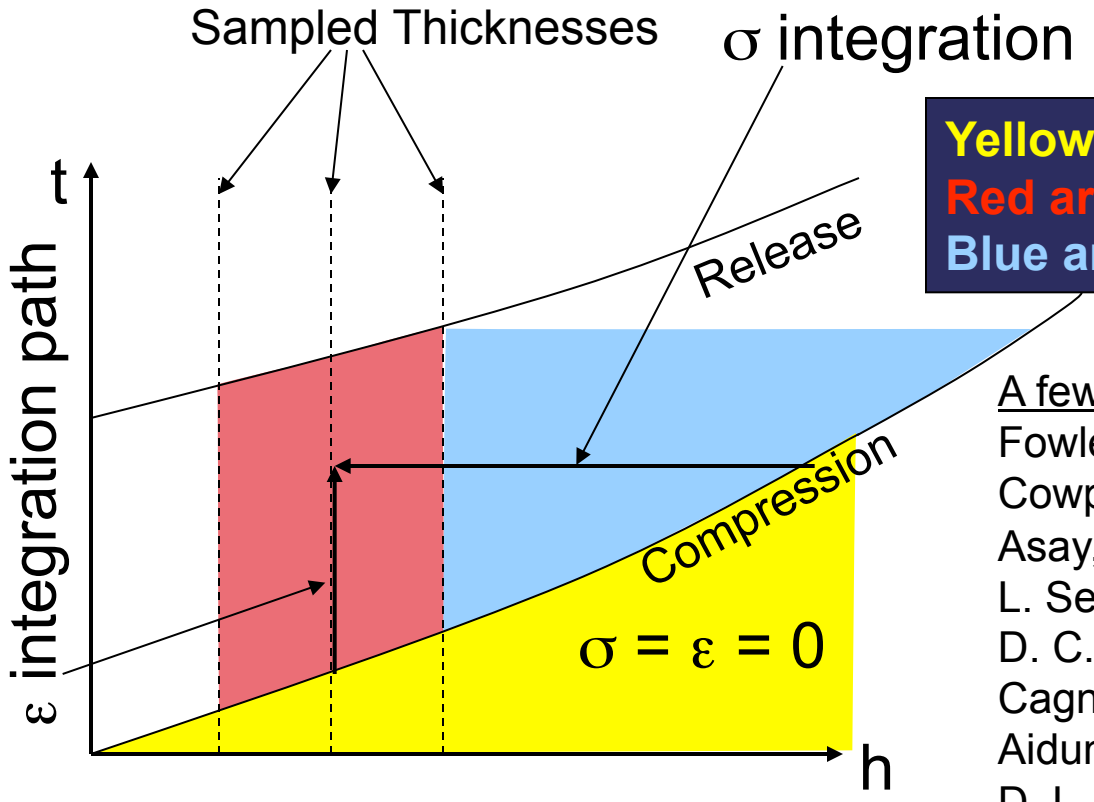

Yellow areas have known conditions
Red areas are interpolated
Blue areas are extrapolated

A few of *many* references:
Fowles & Williams, JAP 41, 360 (1970)
Cowperthwaite & Williams, JAP 42, 456 (1971)
Asay, Fowles, & Gupta, JAP 43, 744 (1972)
L. Seaman, JAP 45, 4303 (1974)
D. C. Wallace, PRB 22, 1487 (1980)
Cagnoux et al., Ann. Phys. Fr. 12, 451 (1987)
Aidun & Gupta, JAP 69, 6998 (1991)
D. L. Tonks, "DataShoP," LA-12068-MS
D. Hayes et al., LA-13830-MS

The integrals are performed piecewise analytically using a second order interpolation/extrapolation function

$$u = \frac{(t_{i+1} - t)u_i^+ + (t - t_i)u_{i+1}^-}{t_{i+1} - t_i} + 4\beta_i \frac{(t - t_i)(t_{i+1} - t)}{(t_{i+1} - t_i)^2}, t_i < t < t_{i+1}$$

linear interpolation of u on each time segment

parabolic term

sections are in temporal order for the relevant h range

$t_i(h) = t_{i,2}h^2 + t_{i,1}h + t_{i,0}$ Paths need not travel with constant speed.

$u_i^{\pm}(h) = u_{i,1}^{\pm}h + u_{i,0}^{\pm}$ Linear velocity decay is allowed. Velocity jumps are allowed.

$\beta_i(h) = \beta_{i,0}$ β is held constant for each section (already a higher order term).

This produces substantial gains in precision and smoothness for a given number of fit parameters.

It also allows nonsteady wave behavior to come in naturally.

Once rough path lines are defined by the user, the computer can automatically refine the "mesh."

The resulting differential equations are analytically integrable.

Deviatoric stress and plastic strain can be deduced from symmetry and known elastic response

- Assume uniaxial strain in a symmetric impact
- Assume EOS is known. Two contributions:
  - Isentropic compression curve $P_0(\varepsilon)$
  - Gruneisen term for irreversible heating
- Assume plastic deformation is isochoric and completely dissipated as heat
- Shear response is pressure-dependent but assumed linear in deviatoric stress
- Combines and generalizes several methods found in the literature

$$\sigma_{ij} = \begin{bmatrix} -\sigma & 0 & 0 \\ 0 & -\sigma + 2\tau & 0 \\ 0 & 0 & -\sigma + 2\tau \end{bmatrix} \qquad \varepsilon_{ij}^{elastic} = \begin{bmatrix} \ln(1-\varepsilon) + \psi & 0 & 0 \\ 0 & -\psi/2 & 0 \\ 0 & 0 & -\psi/2 \end{bmatrix}$$

Definitions:

ψ = plastic strain

τ = deviatoric stress

Governing Equations (solve by iteration):

$$P = P_0(\varepsilon) + 2\gamma \int \tau d\psi = \sigma - 4\tau/3$$

$$\psi = -\frac{2}{3}\left(\frac{\tau}{\mu(P)} + \ln(1-\varepsilon)\right)$$

Summarizing the logic so far

IF we know

- The in situ particle velocity u(h,t)
- The elastic response

THEN we can calculate, for all (h,t),

- The full stress tensor
- The full elastic strain tensor
- The plastic strain
- The equivalent plastic strain $\int |d\psi|$
- The irreversible work

This scheme generalizes previous methods to include in a single formalism:

Nonsteady waves

Full extraction of tensor stresses and elastic/plastic strains

Improved convergence at higher pressures

So in essence, the problem is reduced to determining u(h,t).

To calibrate, we simulated shocks and analyzed the simulated velocimetry using the same techniques used for experimental data

- **Comparisons are from the surface reflection region in initial loading**
- **Black ovals show regions of significant discrepancy**
- **Results are good up to the arrival of the plastic compression wave**
- **This shows us where we need to correct systematic errors, and where the basic analysis is reliable**

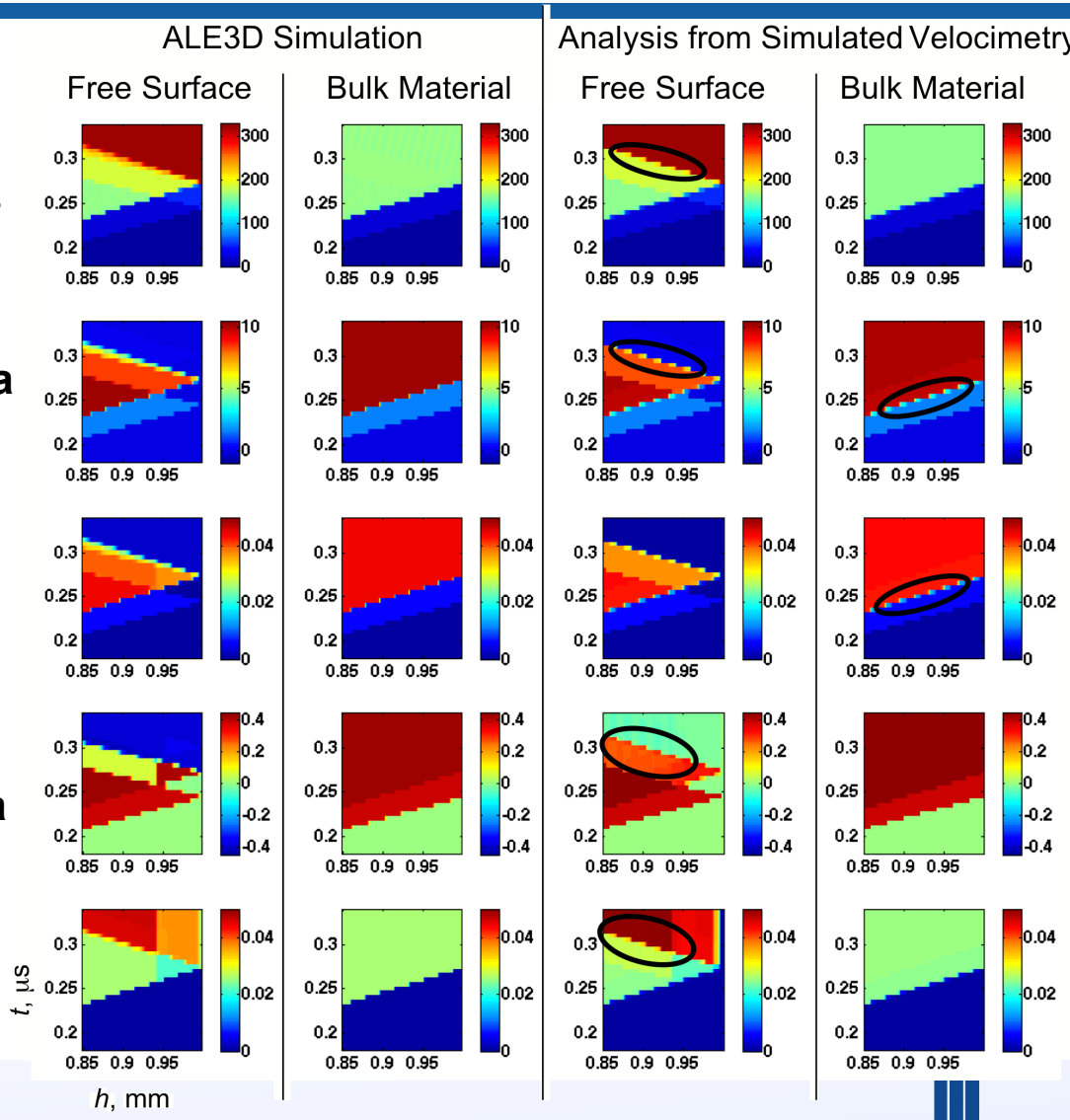

The lack of an impedance-matched window adds complications in the plastic compression measurement

The Idealized Experiment

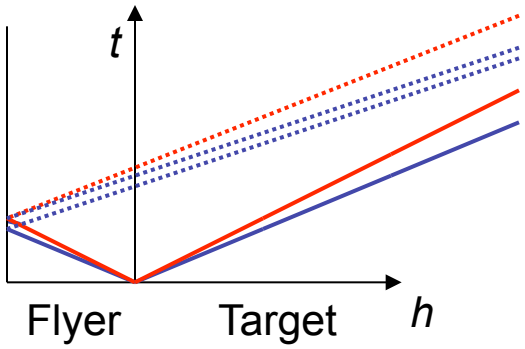

The Actual Experiment

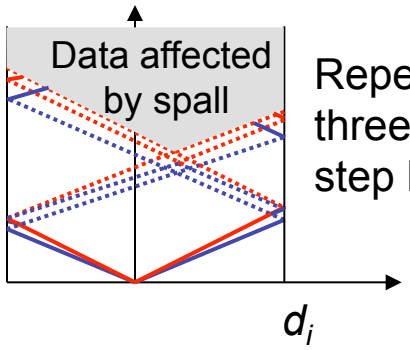

Repeat with three different step heights d_i

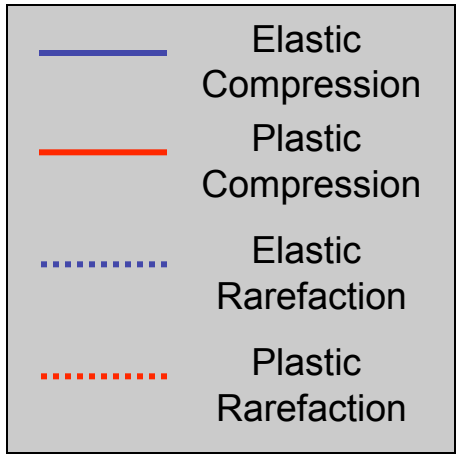

The Free-Surface Velocity Interpolation Function

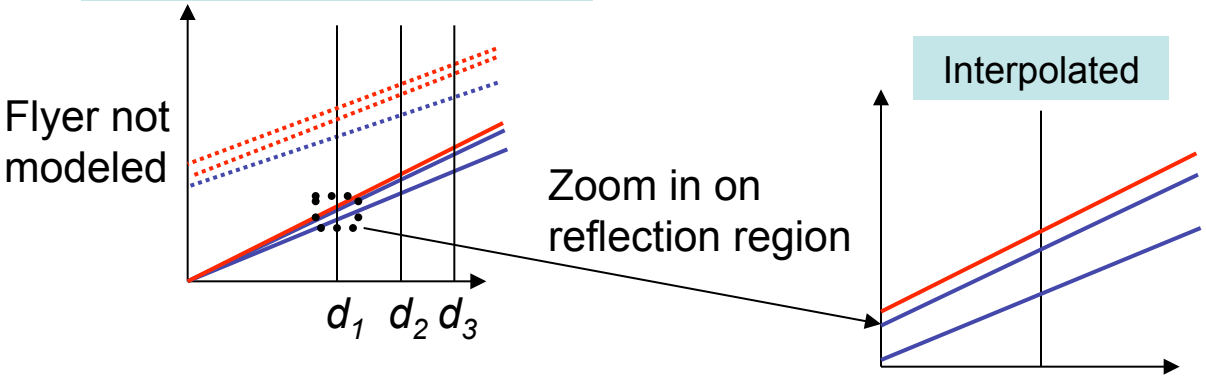

The free surface effects can be identified and corrected

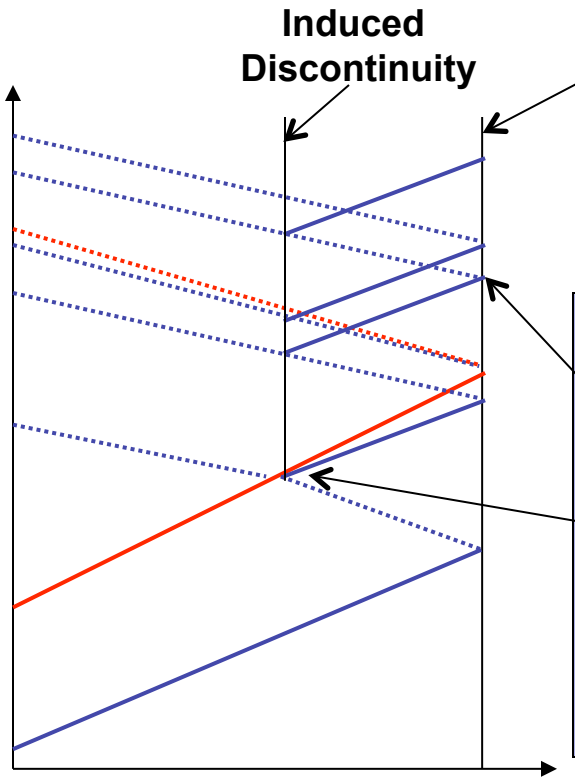

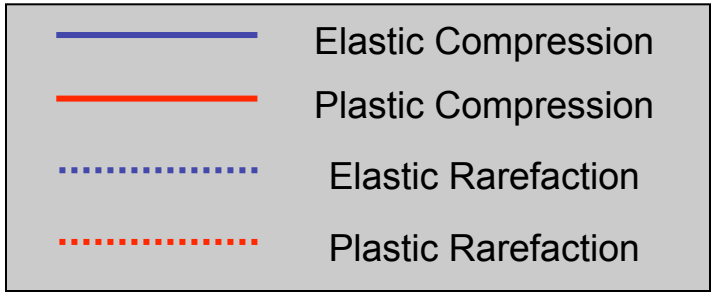

Effects to correct for:

- Reverberations are artificial; would not have happened in infinite material
- Plastic load is split, partially reflected, and slightly delayed
- Thermodynamic path hysteresis means velocity doubling is not exact

These are all few-percent systematic errors for shocks ~10-30 GPa.

Even a rough estimate is enough to reduce residual systematic error to less than 1% (as validated through simulation including rate-dependent effects).

Our code includes auxiliary functions to estimate and correct for all of these free surface effects

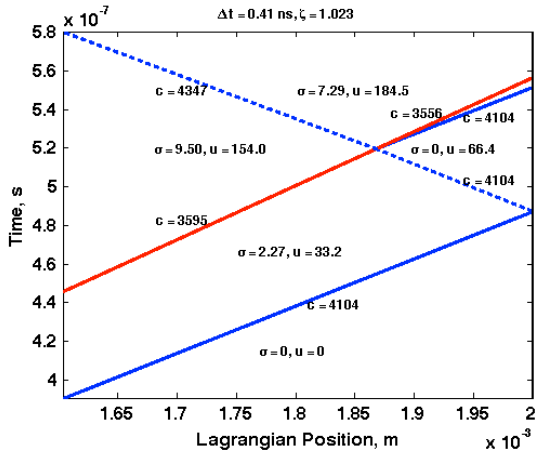

Nonlinear characteristics-crossing calculation gives partial-reflection factor ζ and time shift Δt

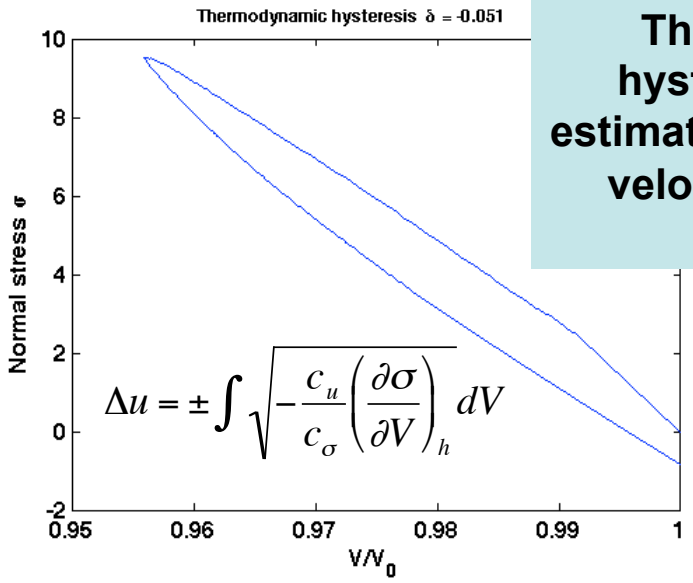

Thermodynamic hysteresis integral estimates plateau particle velocity deep in the material

The actual correction is a simple transformation

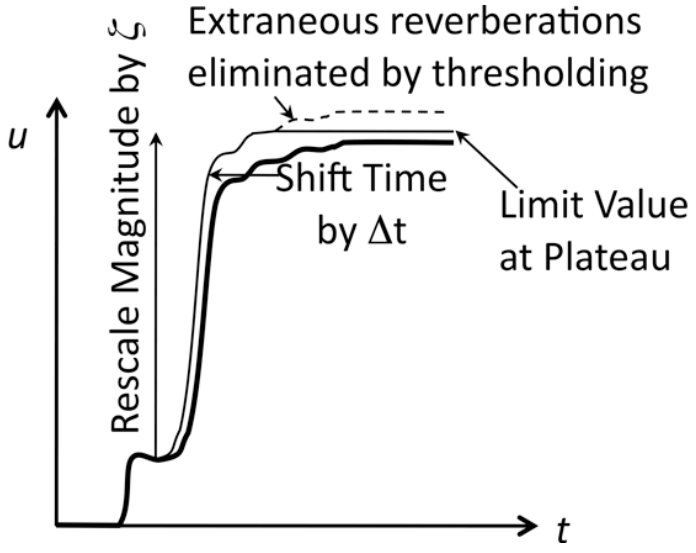

Analysis example: Ta 3-step shock experiment
Part 1: Velocity modeling with reliability diagnostics

Free surface corrections and curve fits

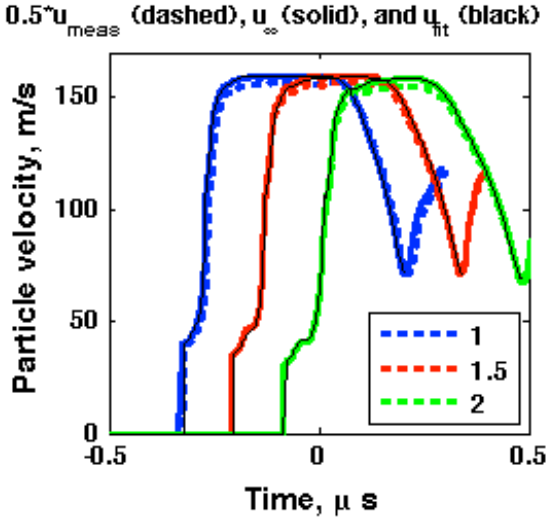

User-defined interpolation zones

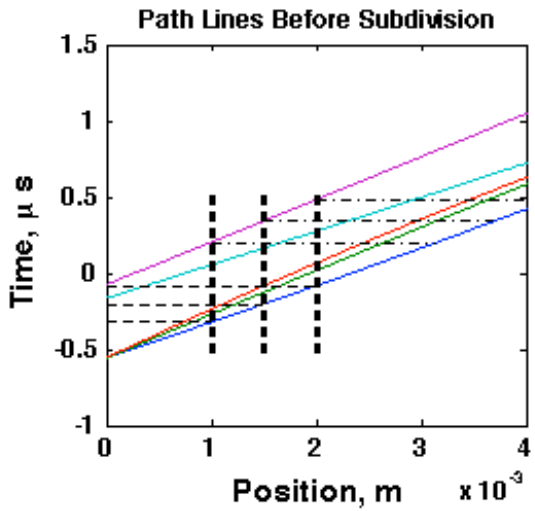

Extrapolation to drive surface

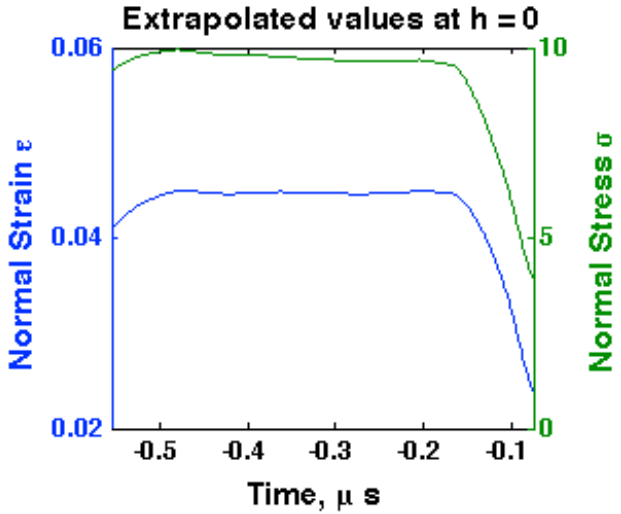

While adjusting all analysis parameters, user sees in real time:

- If curve fits follow the data precisely enough
- If path lines originate from expected spacetime points
- Which regions are calculated from interpolation and which need extrapolation
- Whether the calculated drive is consistent with experimental design

Analysis example: Ta 3-step shock experiment
Part 2: Lagrangian analysis with plastic work iteration

Calculated normal stress for all steps

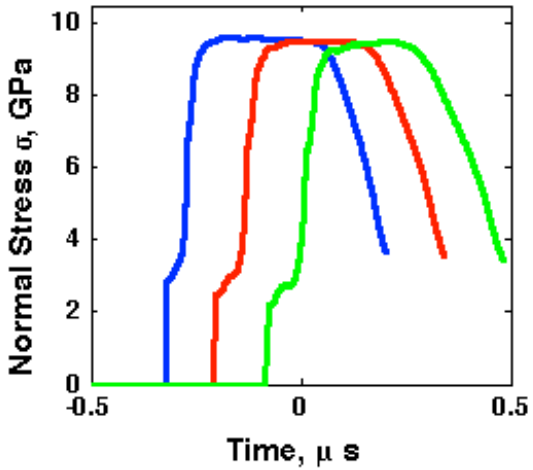

Calculated normal strain for all steps

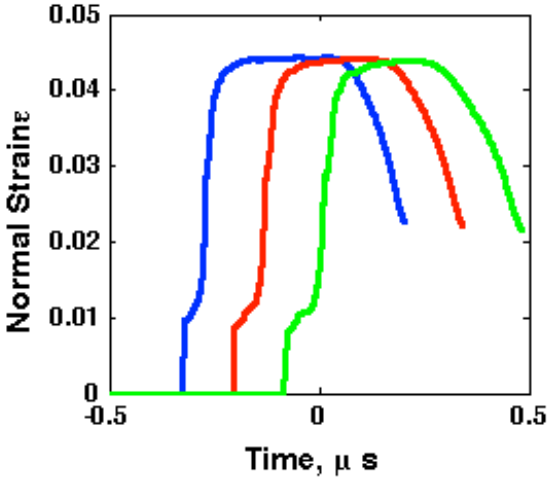

Thermodynamic path, with superposed EOS

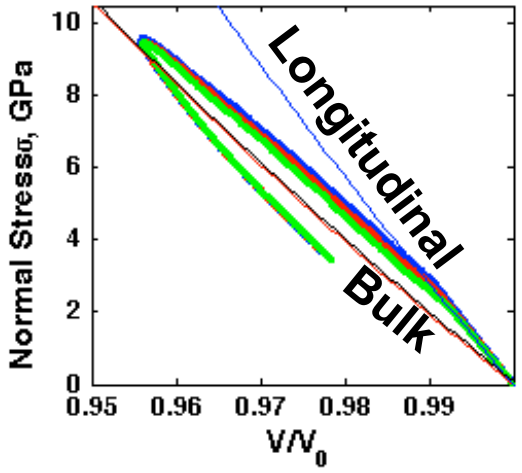

These are updated in real time as well. Diagnostics:

- Are rate dependence and wave decay of roughly the expected magnitude?
- Does the elastic loading follow the known uniaxial compression curve?
- Does the plastic loading parallel the known bulk compression curve?
- Is the calculation stable as we make small changes in parameters?
- How large is the plastic work correction? Is the iteration stable?

Analysis example: Ta 3-step shock experiment Part 3: Deviatoric stress and plastic strain

Calculated deviatoric stress for all steps

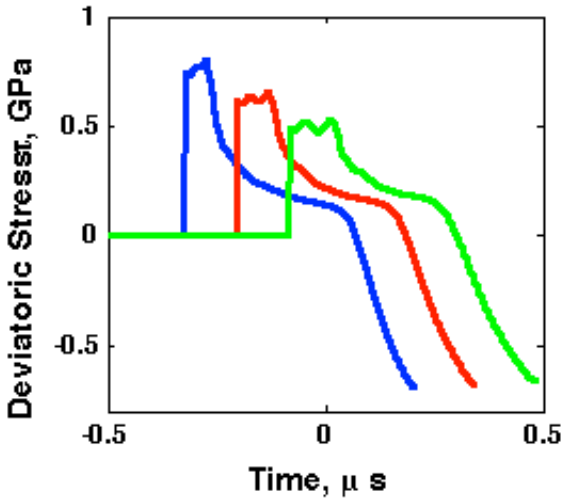

Calculated plastic strain for all steps

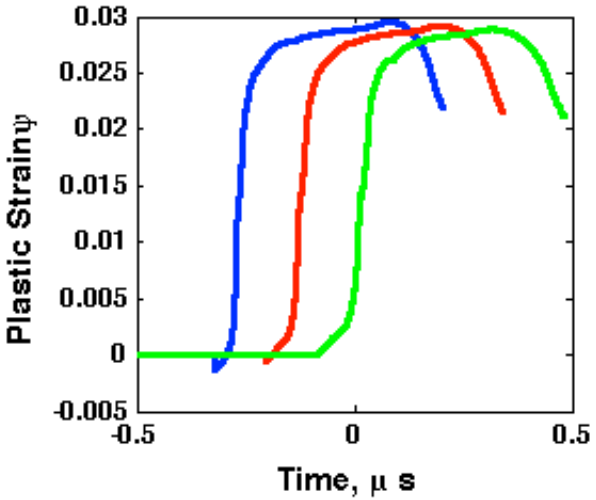

Plastic part of the stress-strain relation

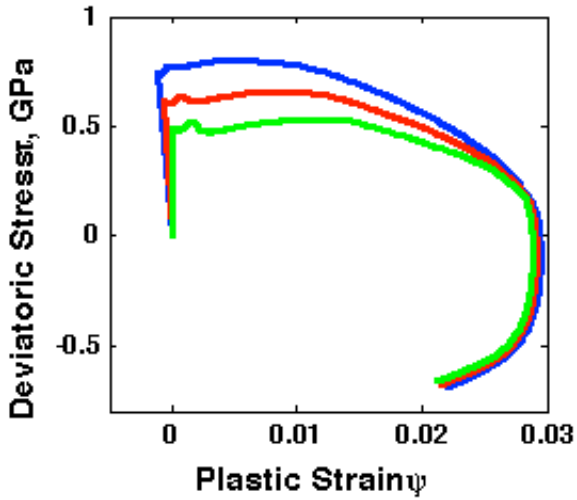

Real time diagnostics:

- Are rate dependence and wave decay of roughly the expected magnitude?
- Do plastic strain rate and deviatoric stress have the same sign at all times?
- Is calculated plasticity negligible during the elastic parts of the wave?
- Not shown: To what extent is τ/μ a single valued function of $\left(\psi_{equiv}, \dot{\psi}\right)$?

Once the analysis is done, we can plot the data any way we like, e.g. looking at strain rate and history effects on strength

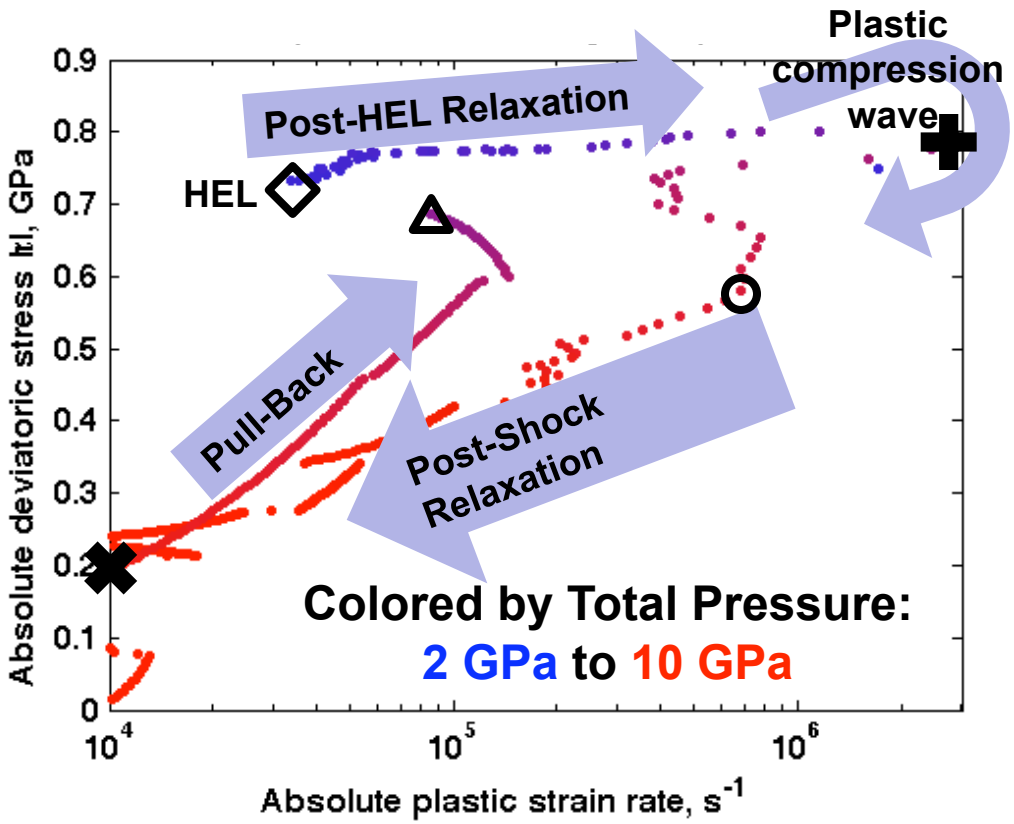

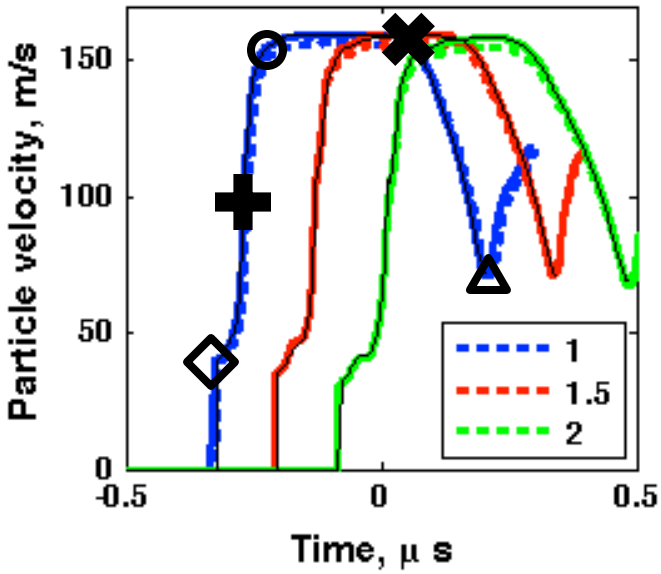

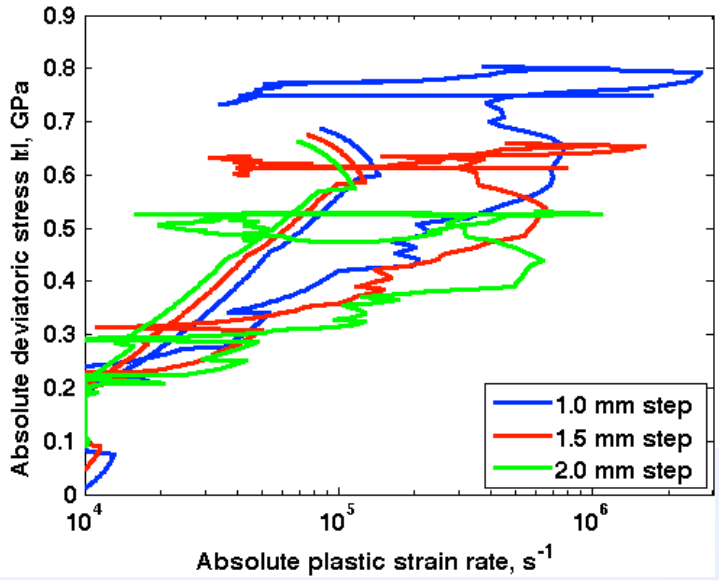

Additional features and work in progress

- We calculate the full parameter sensitivity matrix linking *all* input parameters to *all* calculated values
  - ~25000 x ~5000 matrix
  - Facilitates full error propagation
  - Also facilitates experimental design

- Preliminary tests on ramp waves are very promising
  - Drive was estimated based on surface velocities
  - Very close match even with rate-dependent plasticity

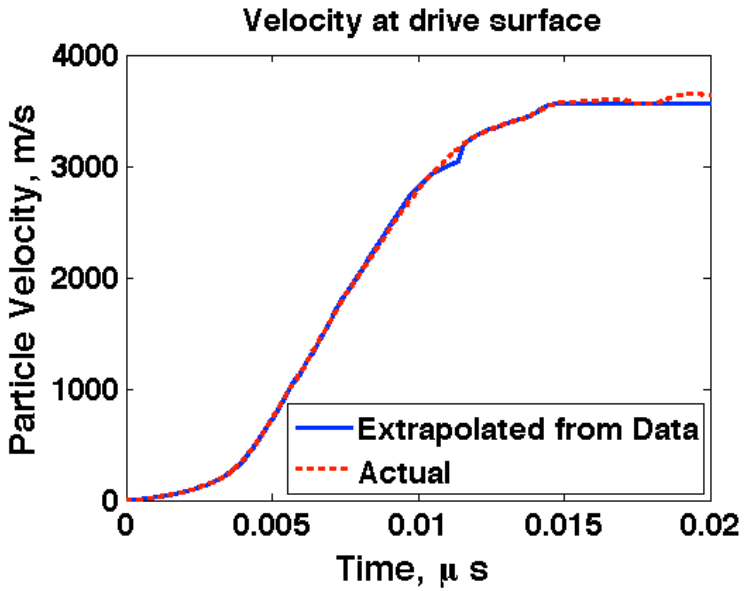

Damage Modeling with Void Evolution (U)

LA-UR-10-00291

Thomas R. Canfield

T-3, Theoretical Division

Los Alamos National Laboratory

Los Alamos, New Mexico

January 28, 2010

Damage Modeling with Void Evolution (U)
Outline

- Motivation
- Models of Damage Evolution and Failure
- Void Evolution
- Void Material Creation
- Internal Constraints
- Summary and Conclusions
- Future Directions

Damage Modeling with Void Evolution (U)
Motivation

Late Time X-Ray Image of Ta-Hemi

- The evolution of damage in metals
  - Stress localization
  - Development of micro-cracks
  - Eventually coalesce to form inclusions or pores
- Eventually the material fails when it is damaged to the extent that it can no longer support a load.
- Classical *corn flakes*
- Modeling challenge
  - 3D phenomenon
  - 2 Phase (Chunks and Void)

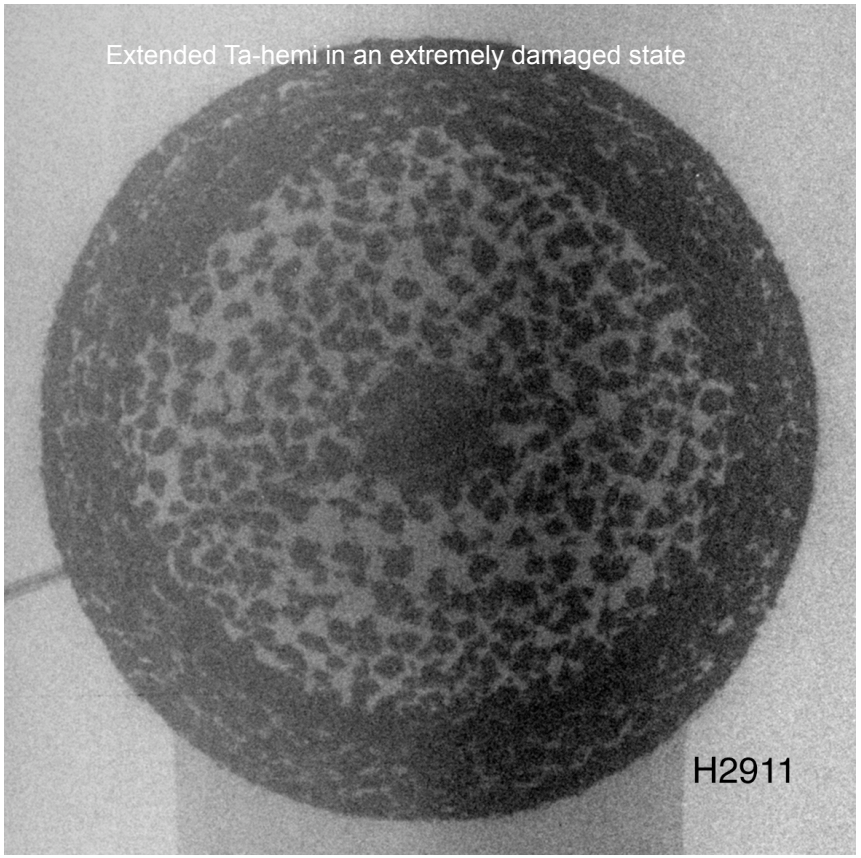

Damage Modeling with Void Evolution (U)
Motivation

- Damage:

$$D = \begin{Bmatrix} \phi & F < 1 \\ 1 & F \geq 1 \end{Bmatrix}$$

- Effect:

$$\bar{T}_{ij} = (1 - D)T_{ij}$$
$$\bar{S}_{ij} = (1 - D)S_{ij}$$
$$\bar{p} = (1 - D)p$$

Damage Modeling with Void Evolution (U)
Motivation

- ϕ - Porosity (void volume fraction)

$$V = V_0 + V_S$$

$$\phi = \frac{V_0}{V}$$

- If $\phi < \phi_f$ the voids are entrained in the material.

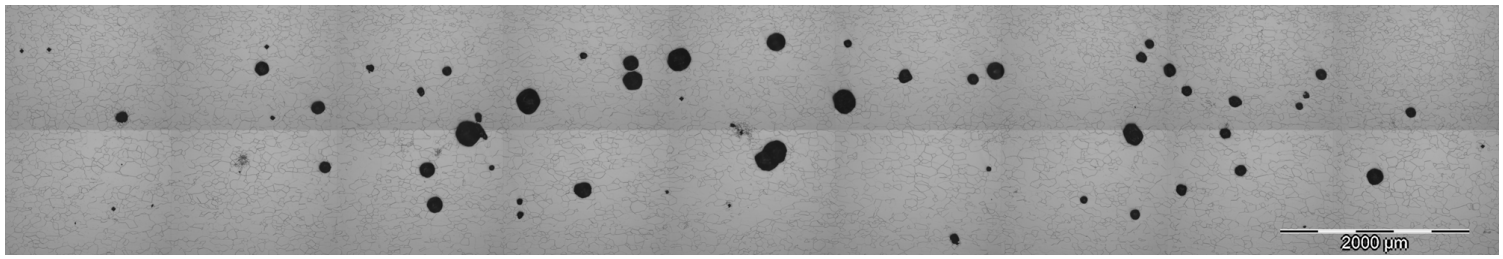

Section of a soft recovered Ta target from a gas gun experiment: 5.6 GPa 1.1 µs Pulse – Only Voids

Thissell, WR, Zurek, AK, Tonks, DL, and Hixson, RS AIP Conference Proceeding; 2000; v.505, p.451-454

Damage Modeling with Void Evolution (U)
Models of Damage Evolution and Failure

- Damage Models (entrained void: porosity)
  - Johnson-Spall
    - Damage: pressure driven void evolution
    - Failure: critical porosity
  - TEPla
    - Damage: void evolution coupled with strength
    - Failure: Modified Hancock-Mackenzie stress triaxiality
- Other Failure Models
  - P_{min} Spall
  - Maximum Tensile Stress
  - Johnson-Cook Brittle Fracture Model
    - Includes Hancock-Mackenzie stress triaxiality
- Finite Rotation
- Where do we go from here? What do you do with failed zones/elements?

Damage Modeling with Void Evolution (U)

Void Evolution: Johnson-Spall

- *P*-α form where

$$\bar{p} = \frac{1}{\alpha} p_s(\alpha\bar{\rho}, e) \qquad \alpha = \frac{V}{V_s} = \frac{1}{1-\phi}$$

- Evolution Equations

$$\dot{\alpha} = -\frac{\alpha}{\eta}(\alpha-1)^{1/3}(\alpha_0-1)^{2/3}\Delta\bar{p}$$

$$\Delta\bar{p} = \begin{cases} \text{sign}[\bar{p}]\left(|\bar{p}| - |p_C|\right) & |\bar{p}| \geq |p_C| \\ 0 & |\bar{p}| < |p_C| \end{cases}$$

$$p_C(\alpha, T) = \begin{cases} a_C\left[1 - a_T\left(T - T_{Melt}\right)\right]\frac{1}{\alpha}\ln\frac{\alpha}{\alpha-1} & 0 < T < T_M \\ 0 & T \geq T_M \end{cases}$$

Damage Modeling with Void Evolution (U)

Void Evolution: Johnson-Spall

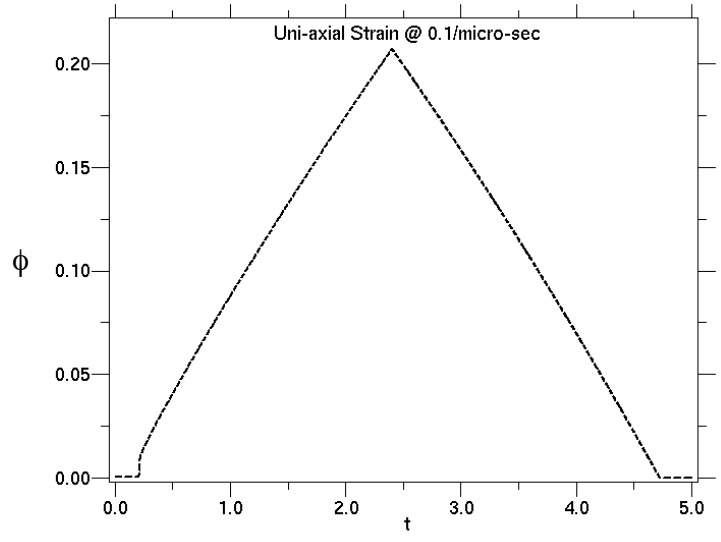

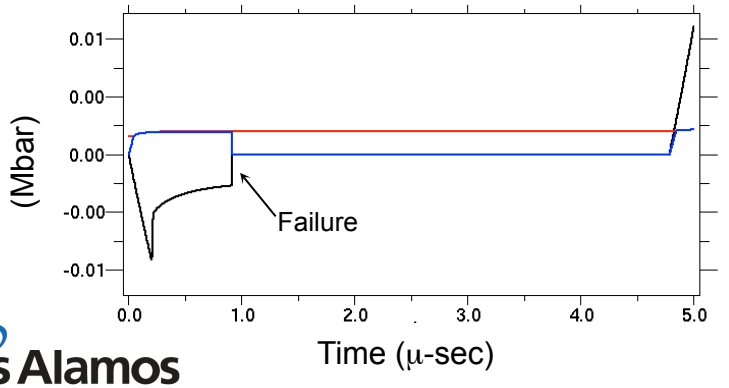

- Material: Sn
- Uni-axial Strain - numerical test
  - Constant strain rate
  - Reversed at t = 2.3μ-sec
  - Similar to Gas-Gun Test
  - SG-Ko Strength Model
  - JS Parameters
    - a_c=750 bar
    - a_T=2.12e-3 / °K
    - η=1.0e-6 bar/sec
    - α_f=1.087
- Failure due to porosity growth

p - pressure
τ - effective stress
σ_f - flow stress
ϕ - porosity

Damage Modeling with Void Evolution (U)
Void Evolution: TEPla (Tensile Elastic-Plastic)

- Void Evolution

$$\dot{\phi} = (1-\phi)\left[\frac{\dot{V}}{V} - \frac{\dot{V}_S}{V_S}\right]$$
$$= (1-\phi)\dot{\varepsilon}^p_{kk}$$

- Gurson Surface

$$\tau^2 - \sigma_f^2\left[1 + q_3\phi^2 - 2q_1\cosh\delta\right] \le 0$$

$$\delta = -\frac{3q_2\bar{p}}{2\sigma_s}$$

$$\tau = \sqrt{3/2\,\bar{S}_{ij}\bar{S}_{ij}}$$

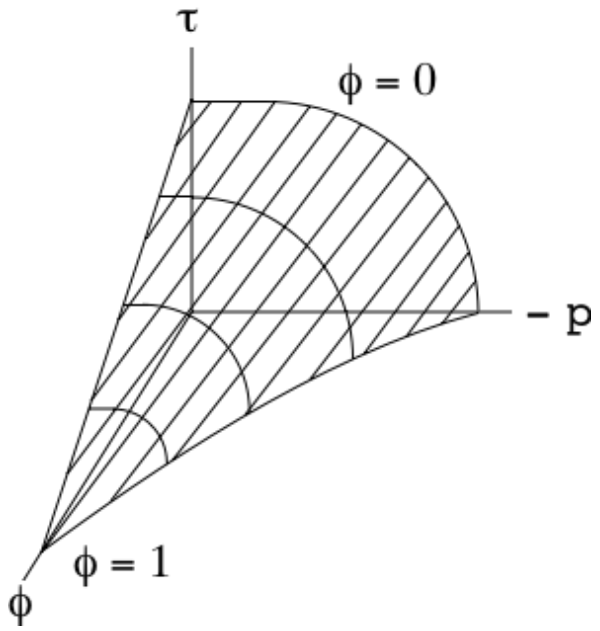

Damage Modeling with Void Evolution (U)
Void Evolution: TEPla (Tensile Elastic-Plastic)

- Residual equations

$$\left(1+\frac{6\bar{G}}{\sigma_f}\frac{\lambda}{\sigma_f}\right)\frac{\tau}{\sigma_f}-\frac{\tau_t}{\sigma_f}=0$$

$$\delta-\delta_t+\frac{3q_2}{2}\left(\frac{\sigma_f}{\sigma_s}\right)\frac{\lambda}{\sigma_f}\left[3q_1q_2\frac{\alpha}{\sigma_s}\phi\sinh\delta+2\Gamma\left(\frac{\tau}{\sigma_f}\right)^2\right]=0$$

$$\phi-\phi_t-3q_1q_2\left(\frac{\sigma_f}{\sigma_s}\right)\frac{\lambda}{\sigma_f}(1-\phi)\phi\sinh\delta=0$$

$$\left(\frac{\tau}{\sigma_f}\right)^2-\left[1+q_3\phi^2-2q_1\phi\cosh\delta\right]=0$$

Solve for

$$\frac{\tau}{\sigma_f},\frac{\lambda}{\sigma_f},\delta,\phi$$

Damage Modeling with Void Evolution (U)

Void Evolution: TEPla (Tensile Elastic-Plastic)

where

$$\alpha = (1-\phi)\left[\bar{B} - (1+2\Gamma)\bar{p}\right]$$

$$B = \rho \left.\frac{\partial p}{\partial \rho}\right|_e + \Gamma p$$

$$\bar{B} = (1-\phi)B$$

$$\bar{G} = (1-\phi)G$$

Damage Modeling with Void Evolution (U)

Void Evolution: TEPla (Tensile Elastic-Plastic)

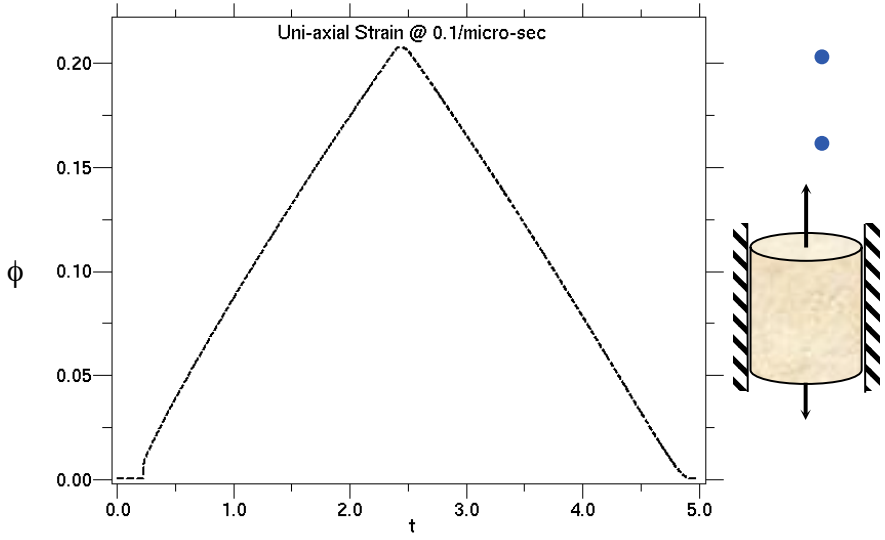

- Material: Cu
- Uni-axial Strain - numerical test
  - Constant strain rate
  - Reversed at t = 2.3μ-sec
  - Similar to Gas-Gun Test
  - PTW Strength Model
  - TEPla Parameters

    q_1=1.5

    q_2=1.0

    q_3=2.25

    η =1.0e-6

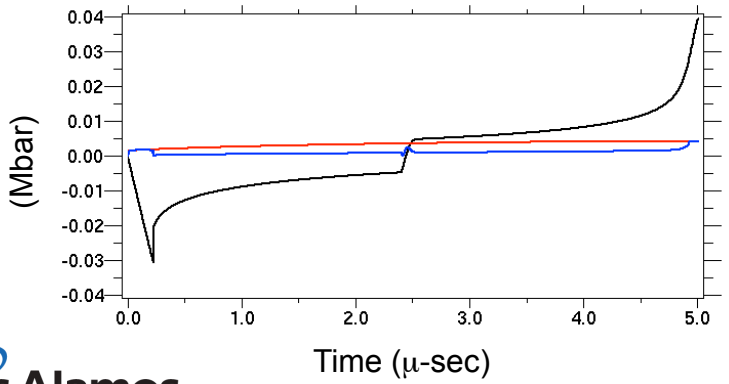

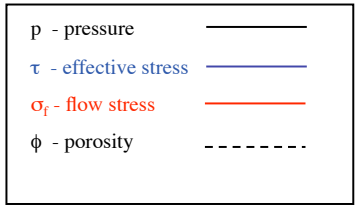

Damage Modeling with Void Evolution (U)

Failure: P_{min} Spall

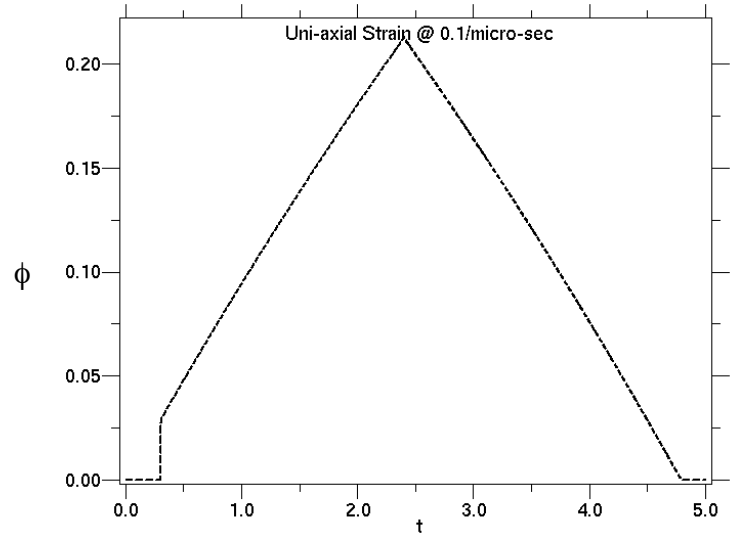

- Material: Cu
- Uni-axial Strain - numerical test
  - Constant strain rate
  - Reversed at t = 2.3μ-sec
  - Similar to Gas-Gun Test
  - PTW Strength Model
- Failure

$$F = \begin{cases} 0 & p > p_{min} \\ 1 & p \le p_{min} \end{cases}$$

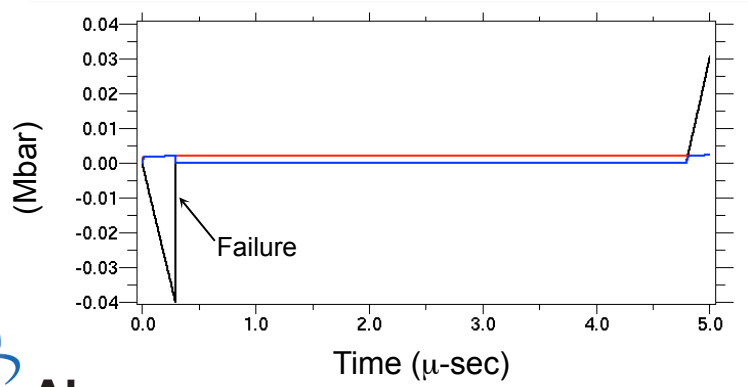

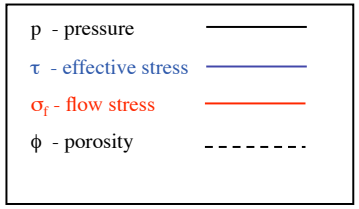

Damage Modeling with Void Evolution (U)
Failure: Modified Johnson-Cook Brittle Fracture

- Failure:

$$F = \begin{cases} 1 & \text{if } \left(\frac{\phi}{\phi_f}\right)^2 + \left(\frac{\varepsilon^p}{\varepsilon_f}\right)^2 \geq 1 \\ 0 & \text{if } \left(\frac{\phi}{\phi_f}\right)^2 + \left(\frac{\varepsilon^p}{\varepsilon_f}\right)^2 < 1 \end{cases}$$

$$\varepsilon^p = \sqrt{\frac{2}{3}\left(\varepsilon'^p_{ij}\varepsilon'^p_{ij}\right)}$$

$$\varepsilon_f = \left[\gamma_1 + \gamma_2 \exp\left\{\gamma_3 \frac{\bar{p}}{\tau}\right\}\right]\left[1 + \gamma_4 \ln \dot{\varepsilon}^*\right]\left[1 + \gamma_5 T^*\right]$$

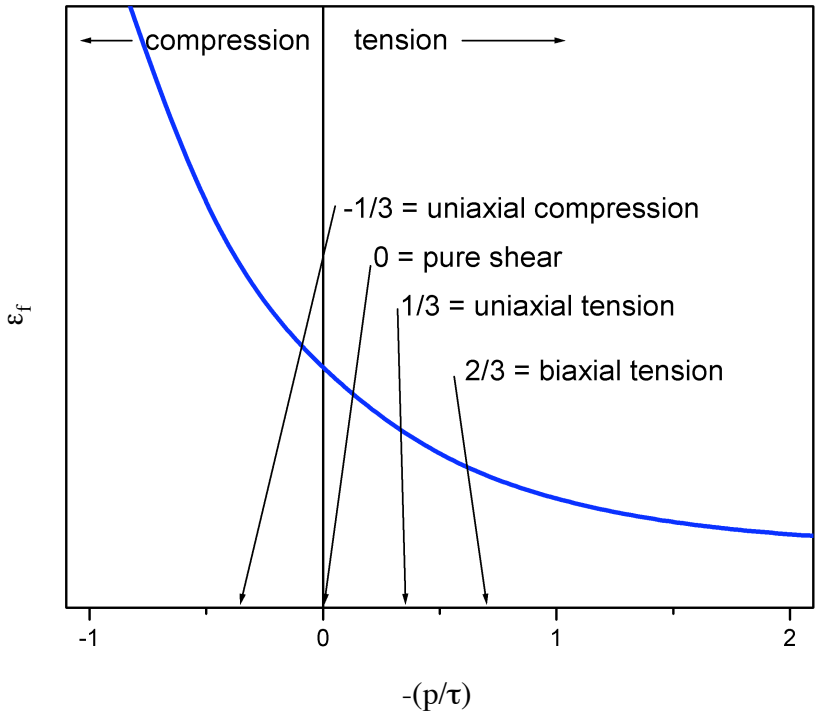

Damage Modeling with Void Evolution (U)
Failure: Maximum Tensile Stress

- Test the principal stresses (Eigen values) for failure:

$$\left(\sigma_{ij} - \lambda\delta_{ij}\right)u_j = 0 \quad \Rightarrow \quad \sigma_1 \geq \sigma_2 \geq \sigma_3$$

$$F = \begin{cases} 1 & \text{if} \quad \sigma_1 \geq \sigma_f \\ 0 & \text{if} \quad \sigma_1 < \sigma_f \end{cases}$$

- Have unit vectors (Eigen vectors) in the direction of failure in the material frame

Damage Modeling with Void Evolution (U)
Void Material Creation

- In the previous examples the void was evolved after failure
  - You could think of this as book keeping
    - Enables the material to reengage in compression
    - Avoids non-physical evaluations of the Material and EOS
- In Lagrangian mode the void is entrained and impenetrable
- In Full ALE mode materials are allowed to mix
- Creation of void material in failed zones/elements provides a potential space for movement of adjacent materials

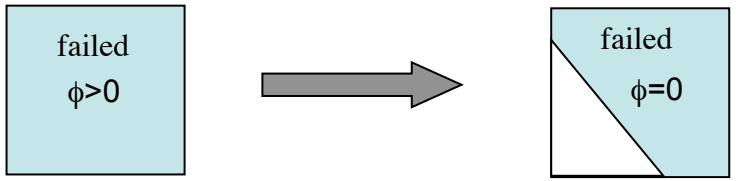

Damage Modeling with Void Evolution (U)
Internal Constraints

- Since void is always at zero pressure cannot equilibrate.
- Compliance averaging scheme has been modified equilibrate the pressure of non-void material.
- The average pressure in the non-void materials is relaxed toward zero or until the void space vanishes.

Damage Modeling with Void Evolution (U)

Internal Constraints: Two Solutions for Zone with Void

- Since void is always at zero pressure,
  the pressure in the material should always be zero!

- Since void is always at zero pressure,
  the pressure in the material may not always be zero!

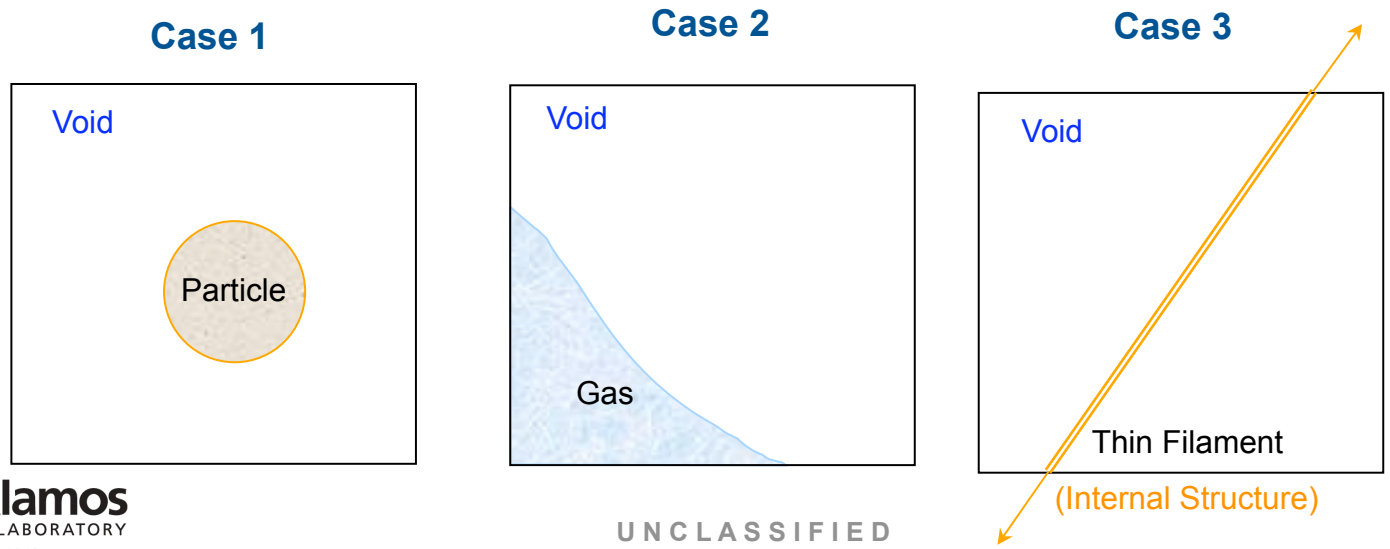

Test: HE Driven Hemi with ALE

- 1 mm thick Cu hemispherical shell
  - TEPla damage model (slightly juiced)
  - Void material evolution on failure
- 20mm HE hemisphere
  - PBX9501
  - Slight detonation asymmetry
- 3mm exterior layer of air
  - Free to expand outward
- Updated Mixed Tipton
  - Default parameters:
    - No pressure Relaxation
    - α = 0.5
- ALE turned on at t = 2.5μs

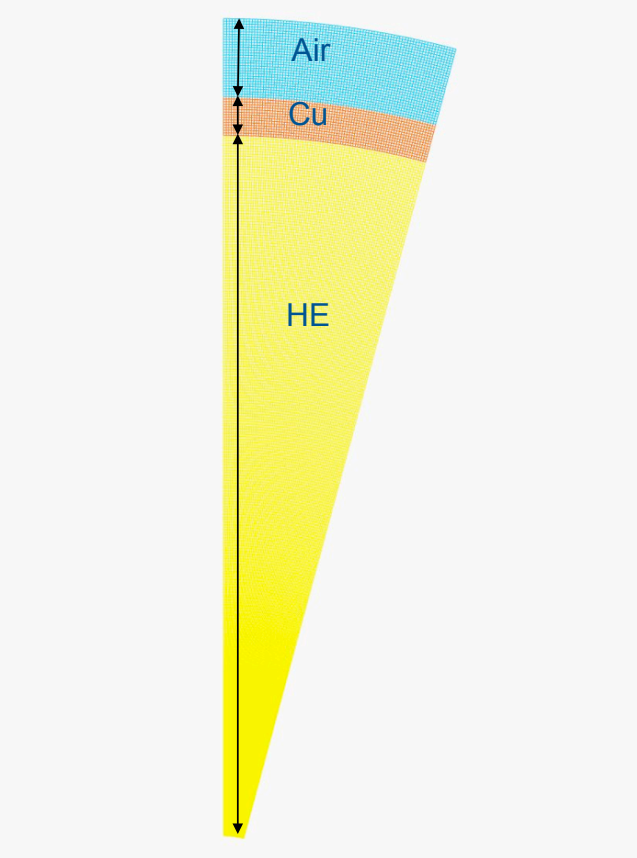

Void Evolution in a Damaged Material

HE Driven Cu Hemi

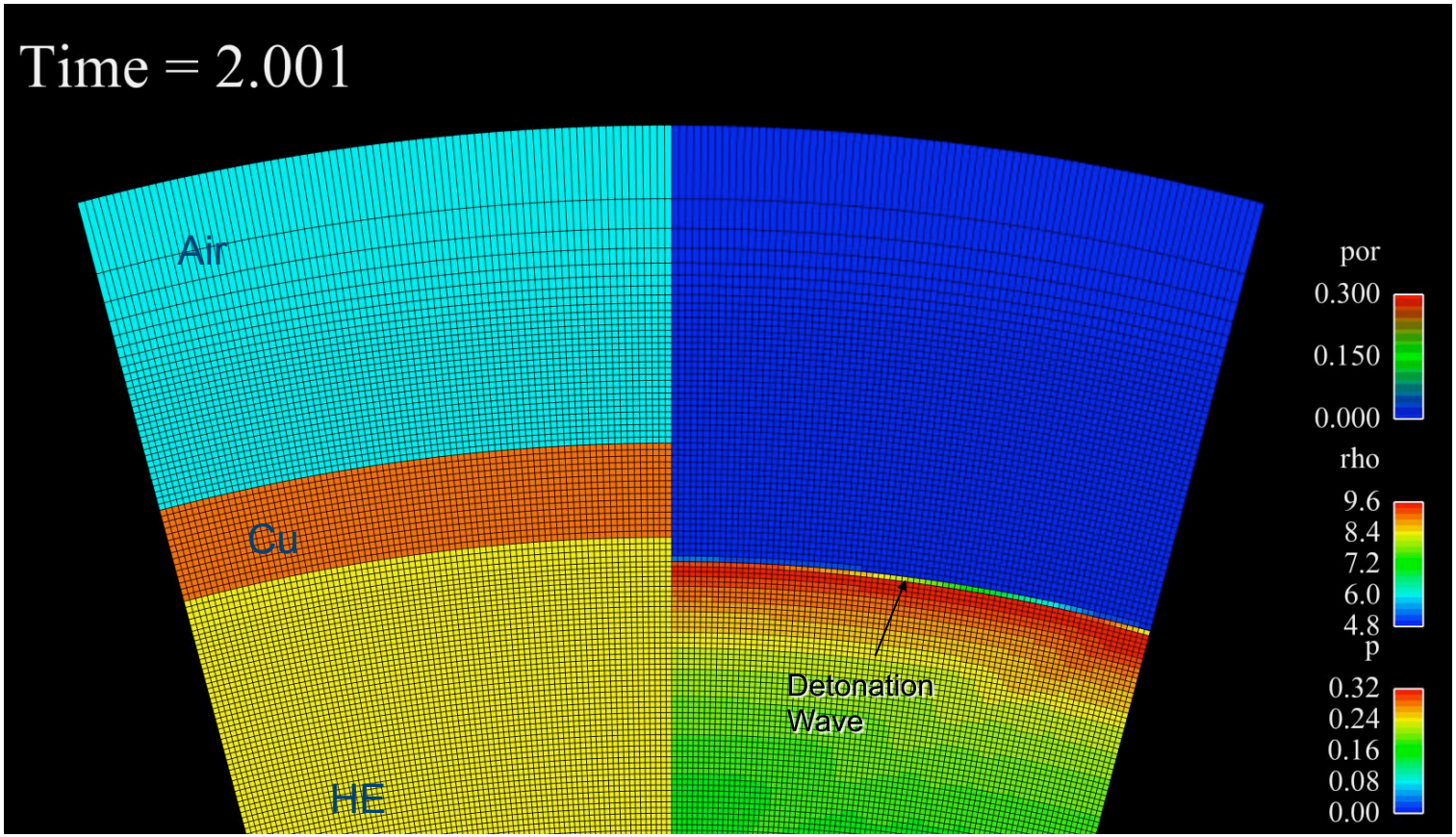

Density Cu-Porosity/HE-Pressure

Void Evolution in a Damaged Material

HE Driven Cu Hemi

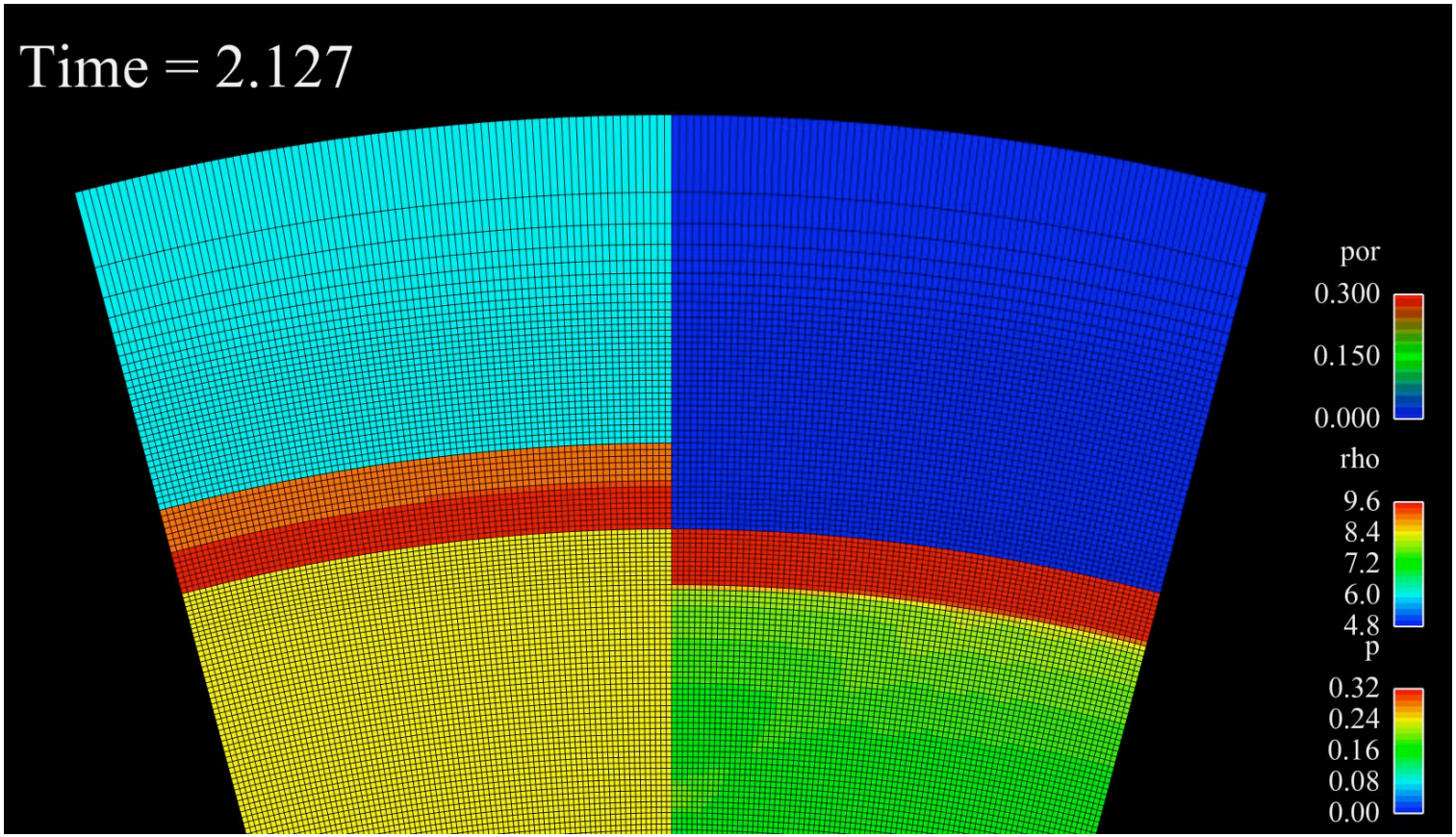

Void Evolution in a Damaged Material

HE Driven Cu Hemi

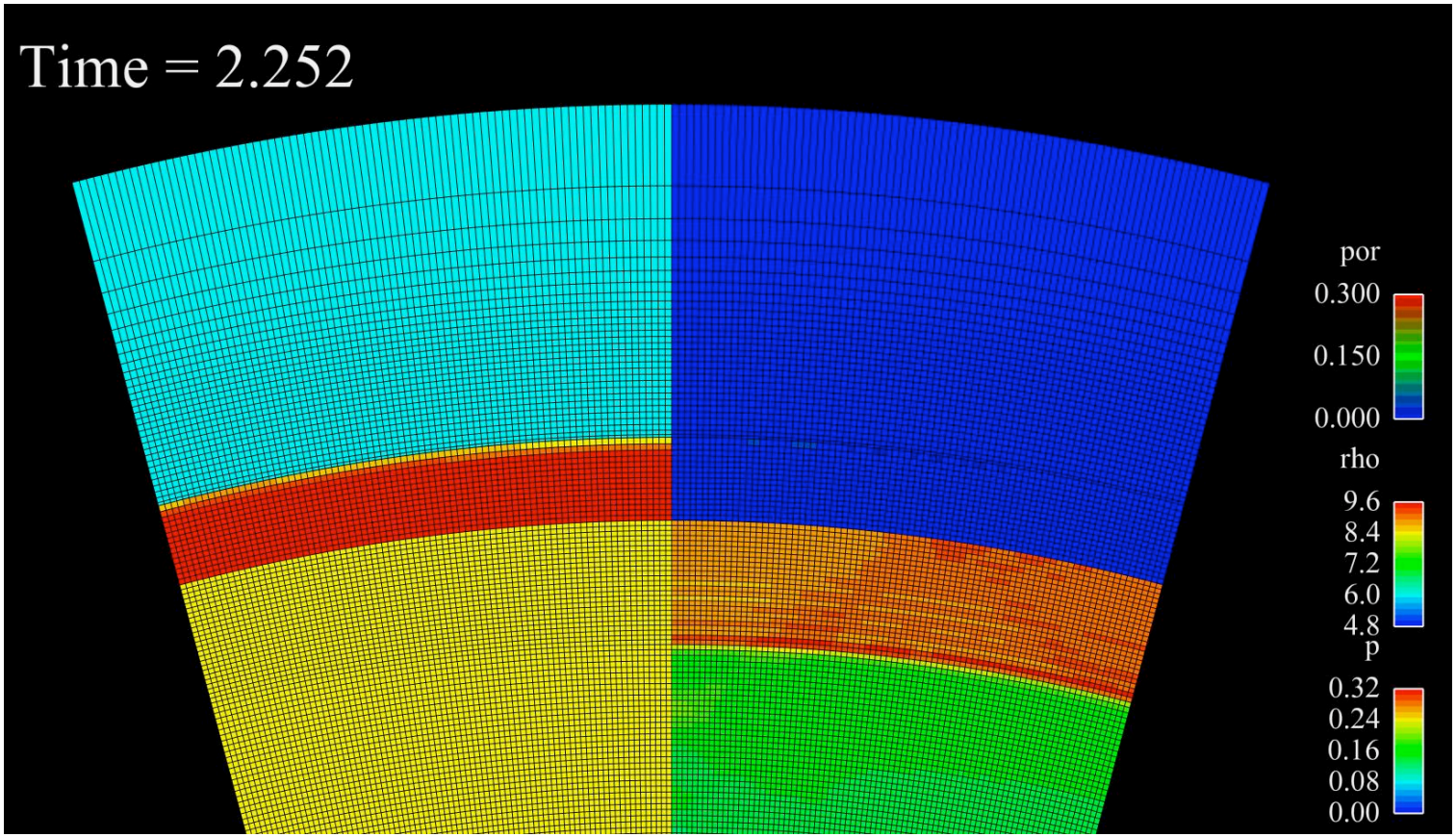

Void Evolution in a Damaged Material

HE Driven Cu Hemi

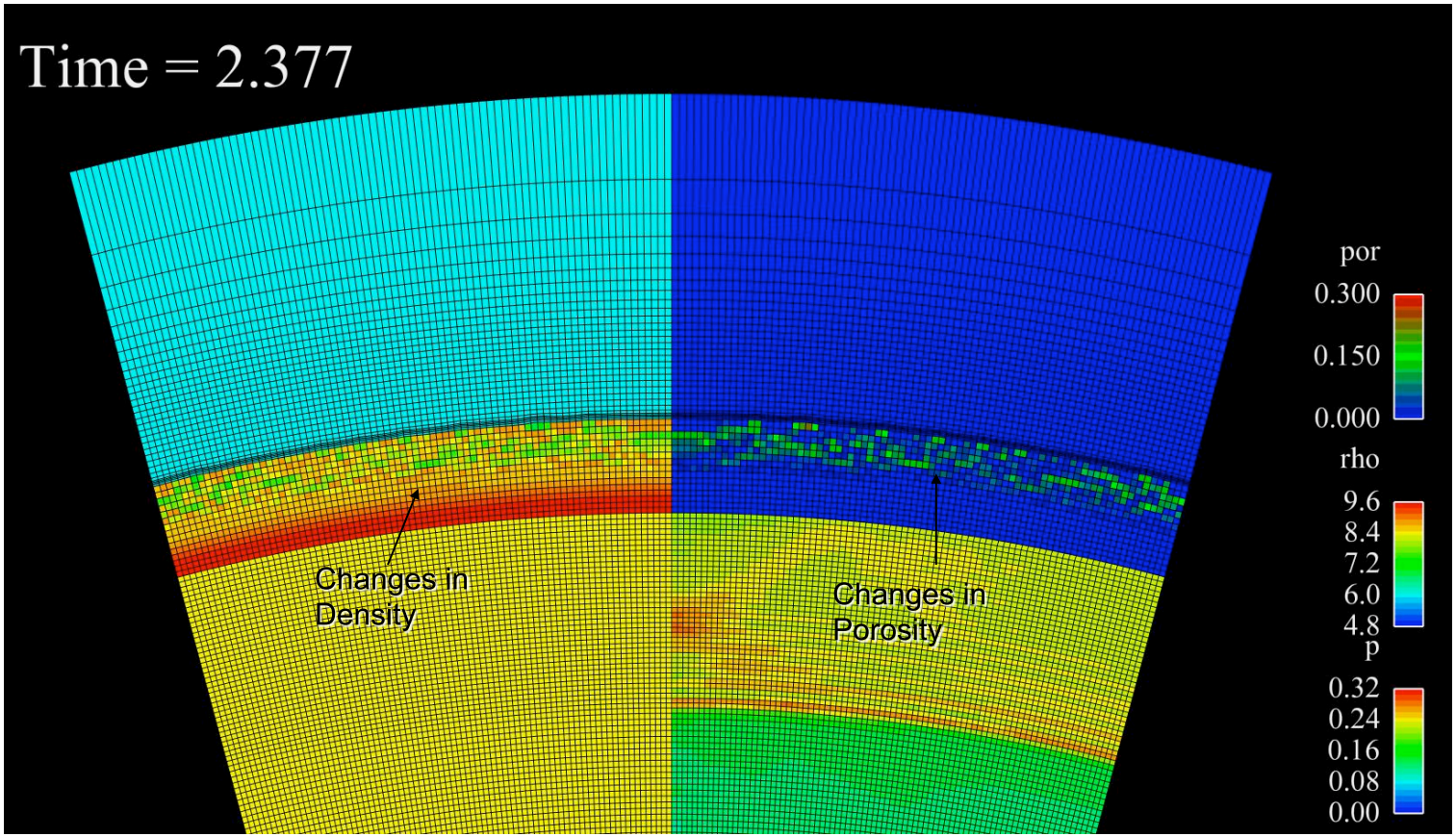

Void Evolution in a Damaged Material

HE Driven Cu Hemi (ALE Turned On)

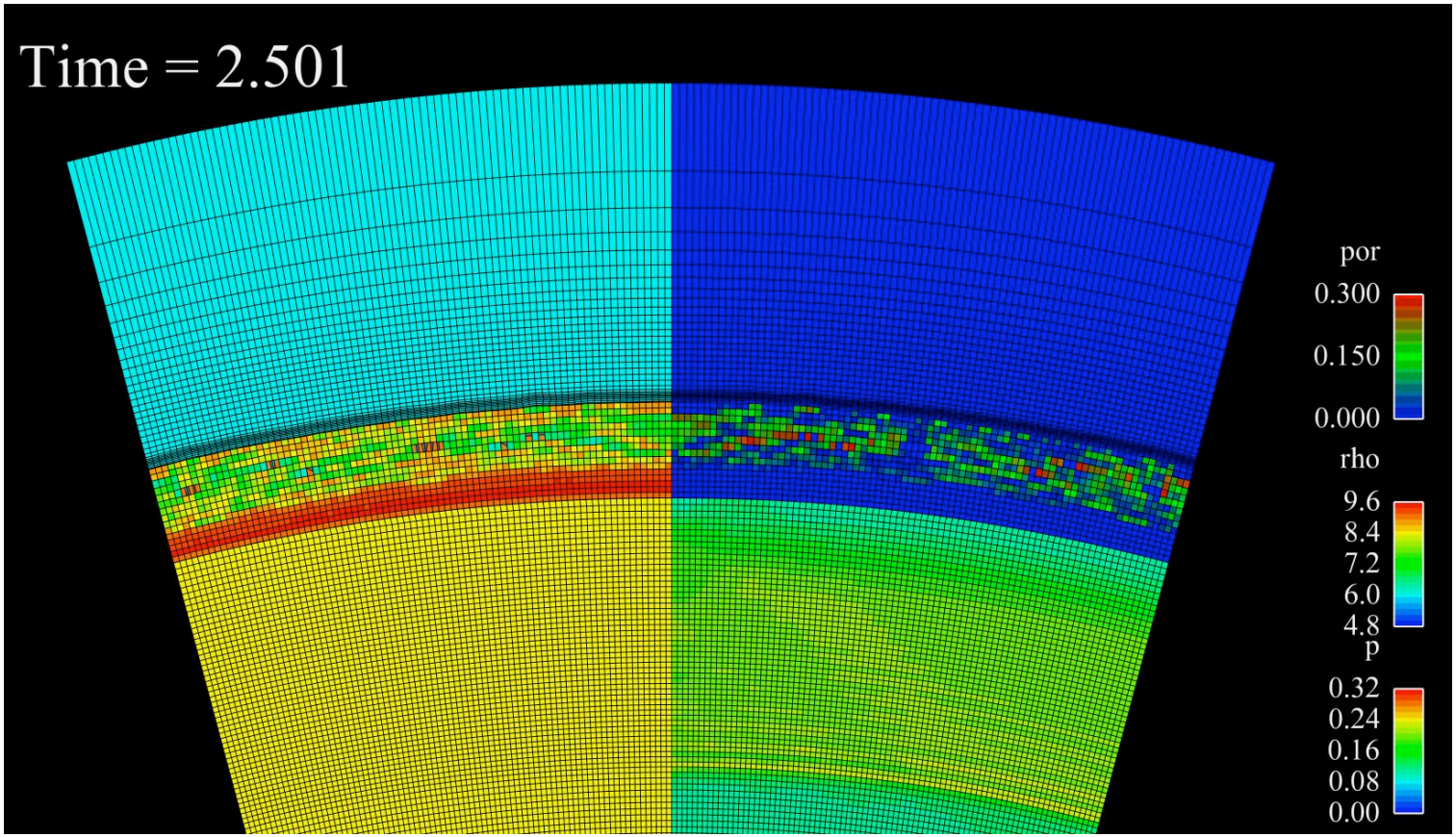

Void Evolution in a Damaged Material

HE Driven Cu Hemi

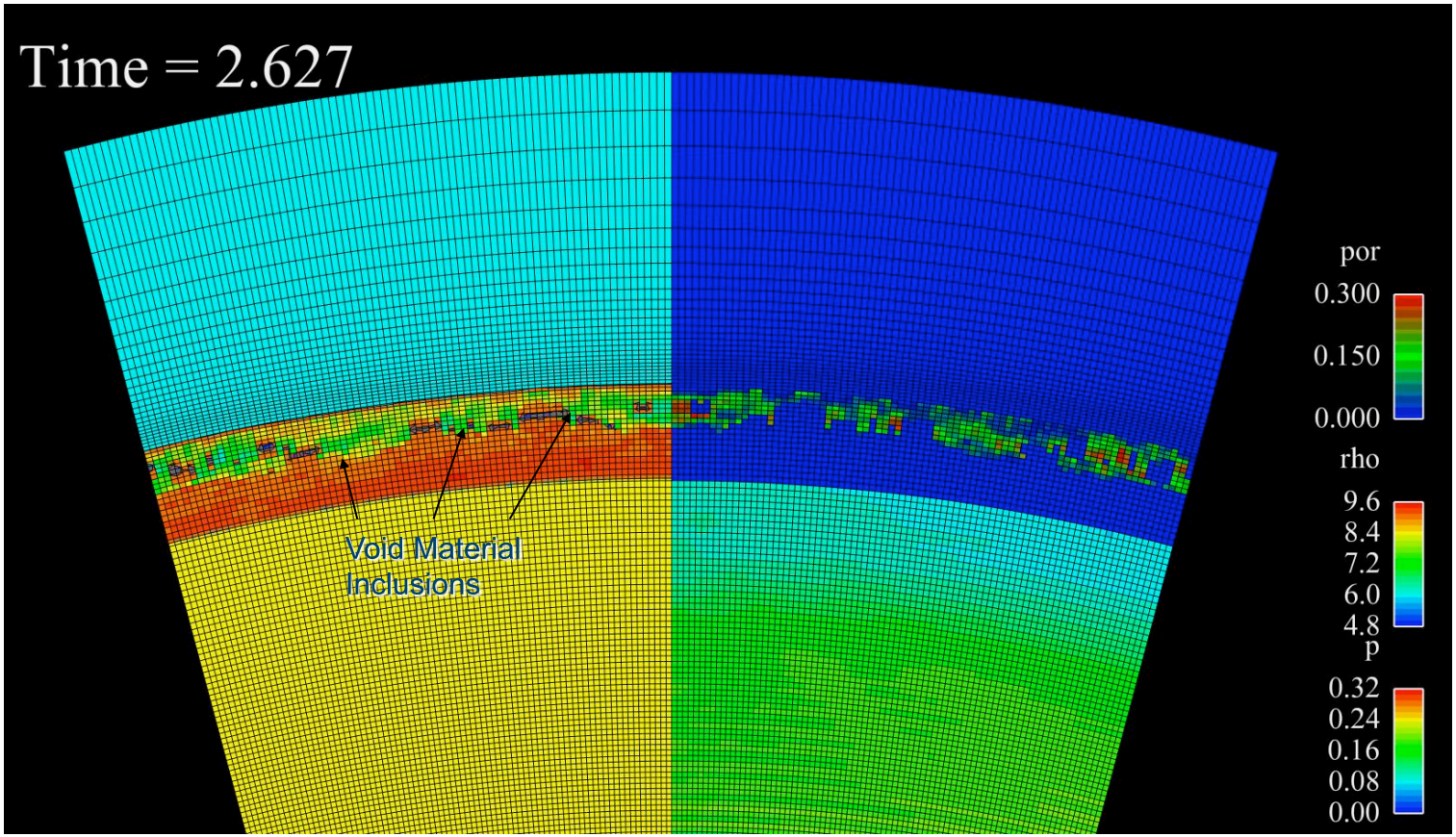

Void Evolution in a Damaged Material

HE Driven Cu Hemi

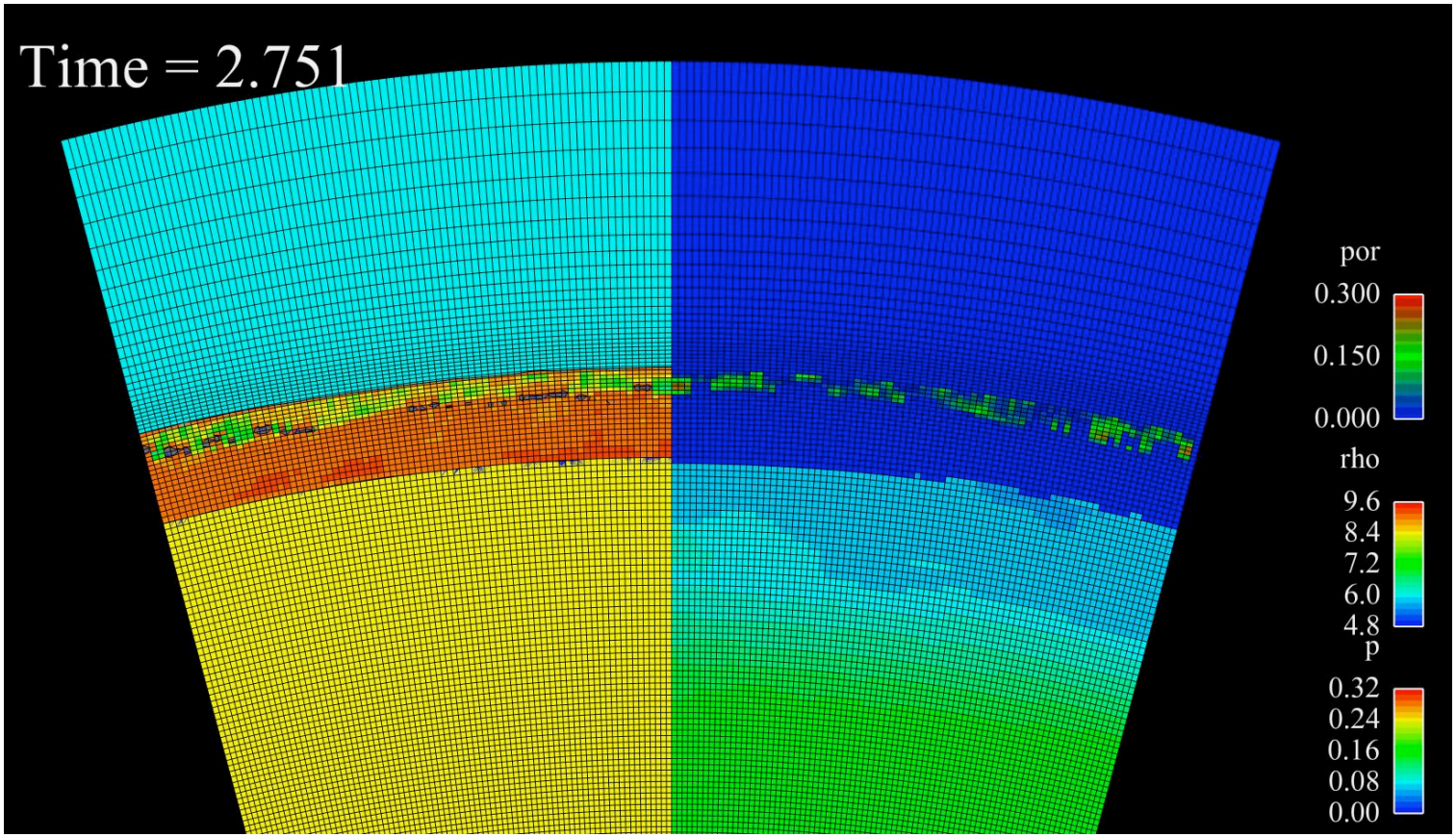

Void Evolution in a Damaged Material

HE Driven Cu Hemi

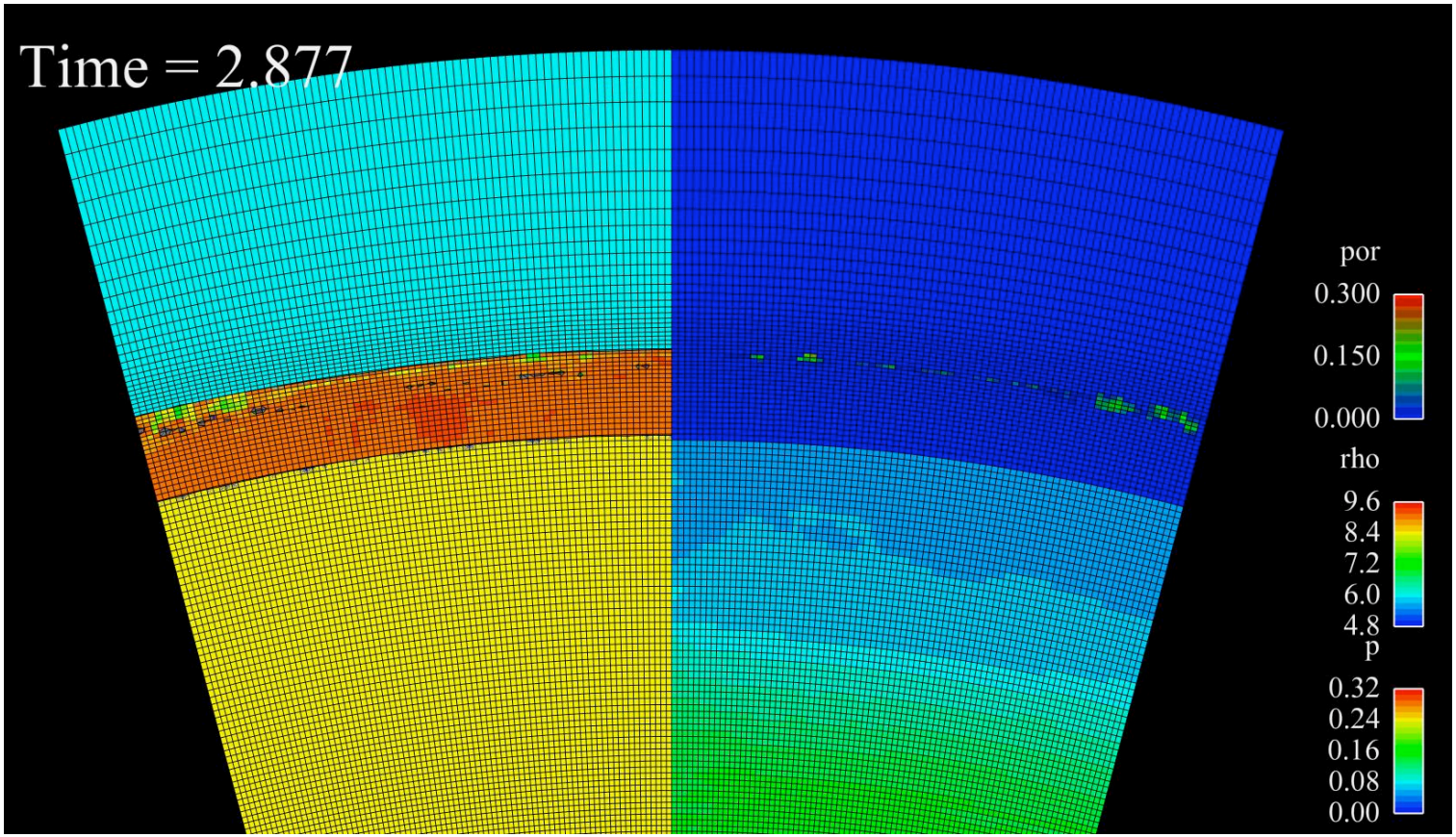

Void Evolution in a Damaged Material

HE Driven Cu Hemi

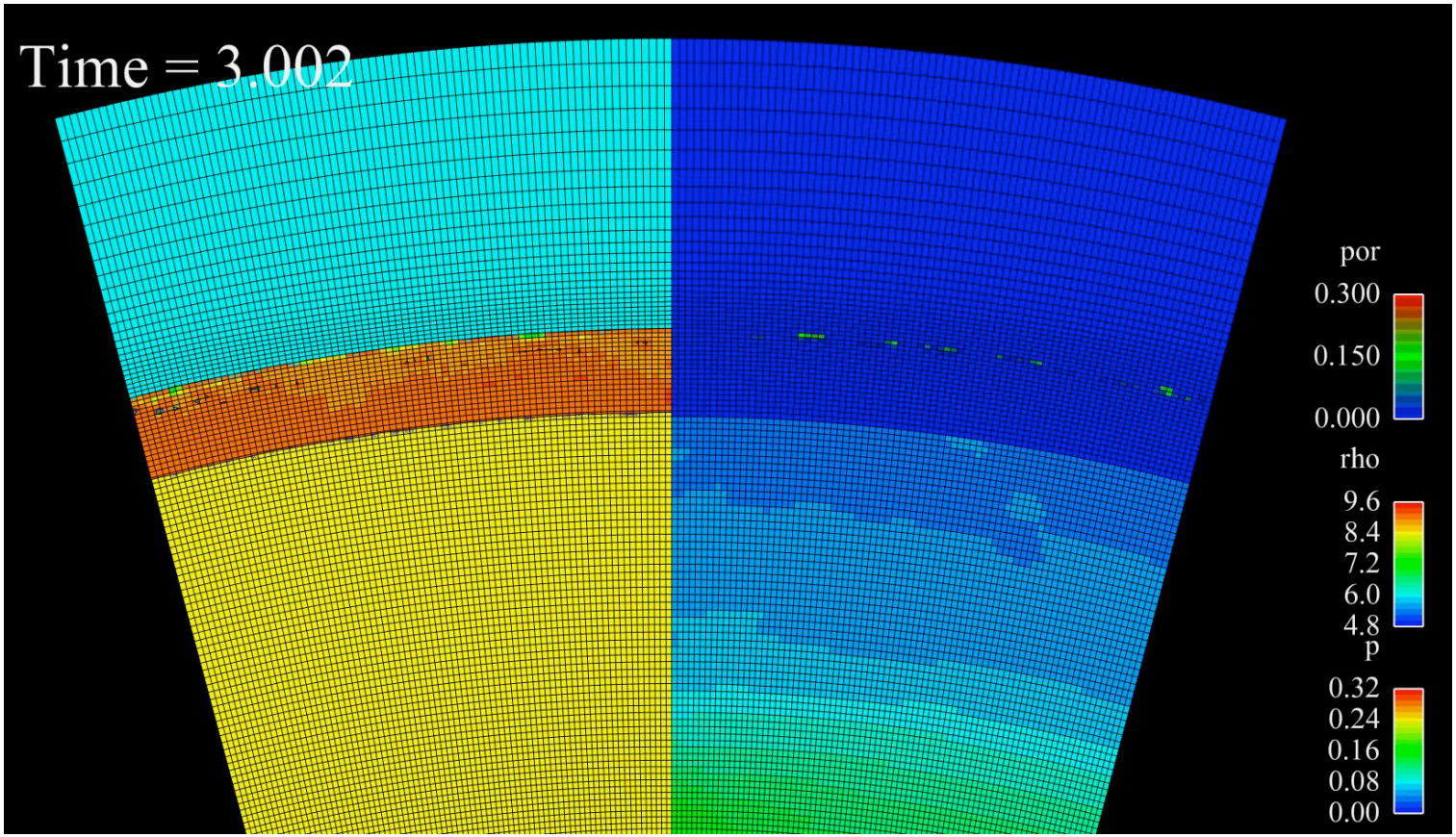

Void Evolution in a Damaged Material

HE Driven Cu Hemi (Void Crushed Out)

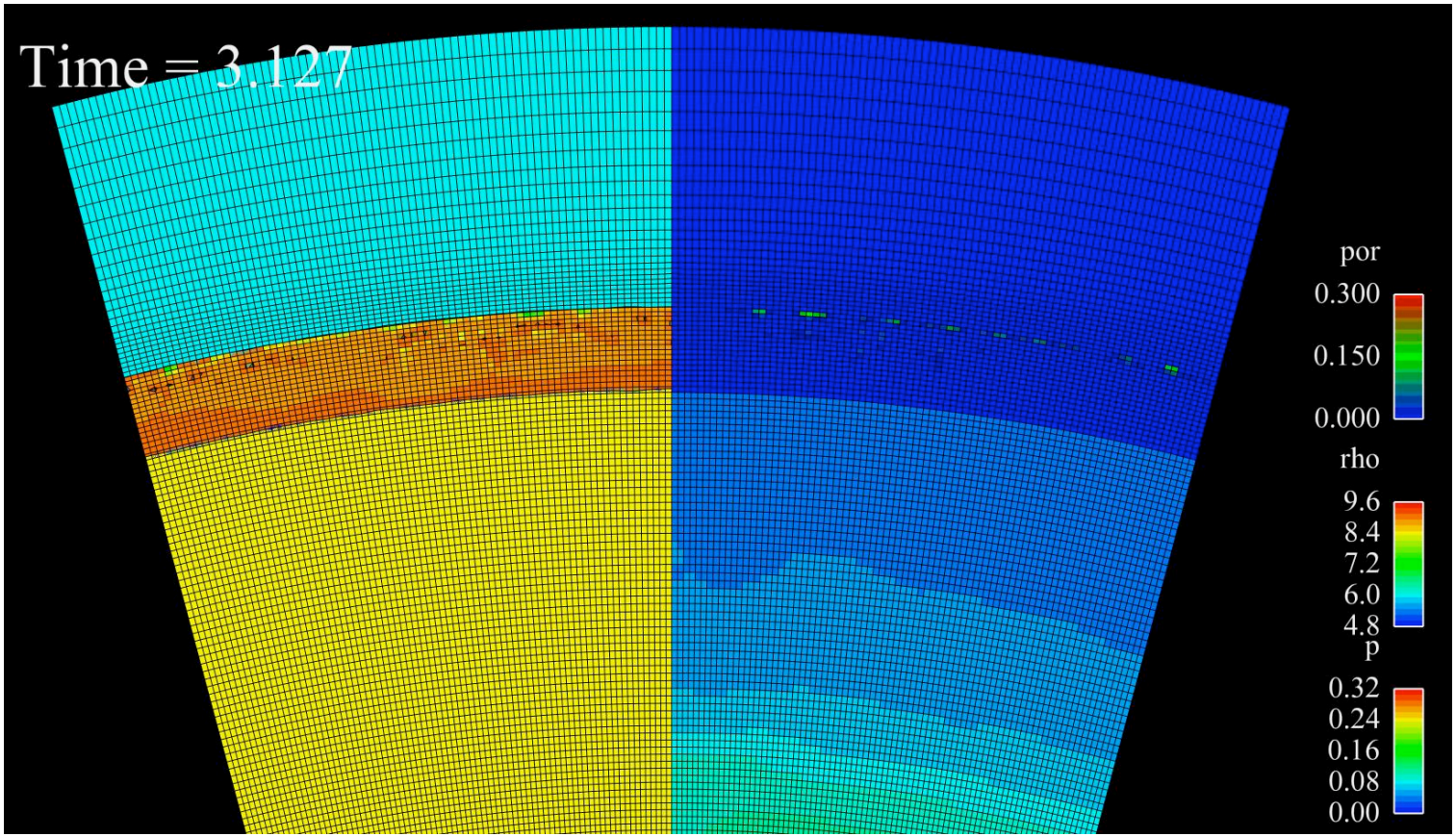

Void Evolution in a Damaged Material

HE Driven Cu Hemi

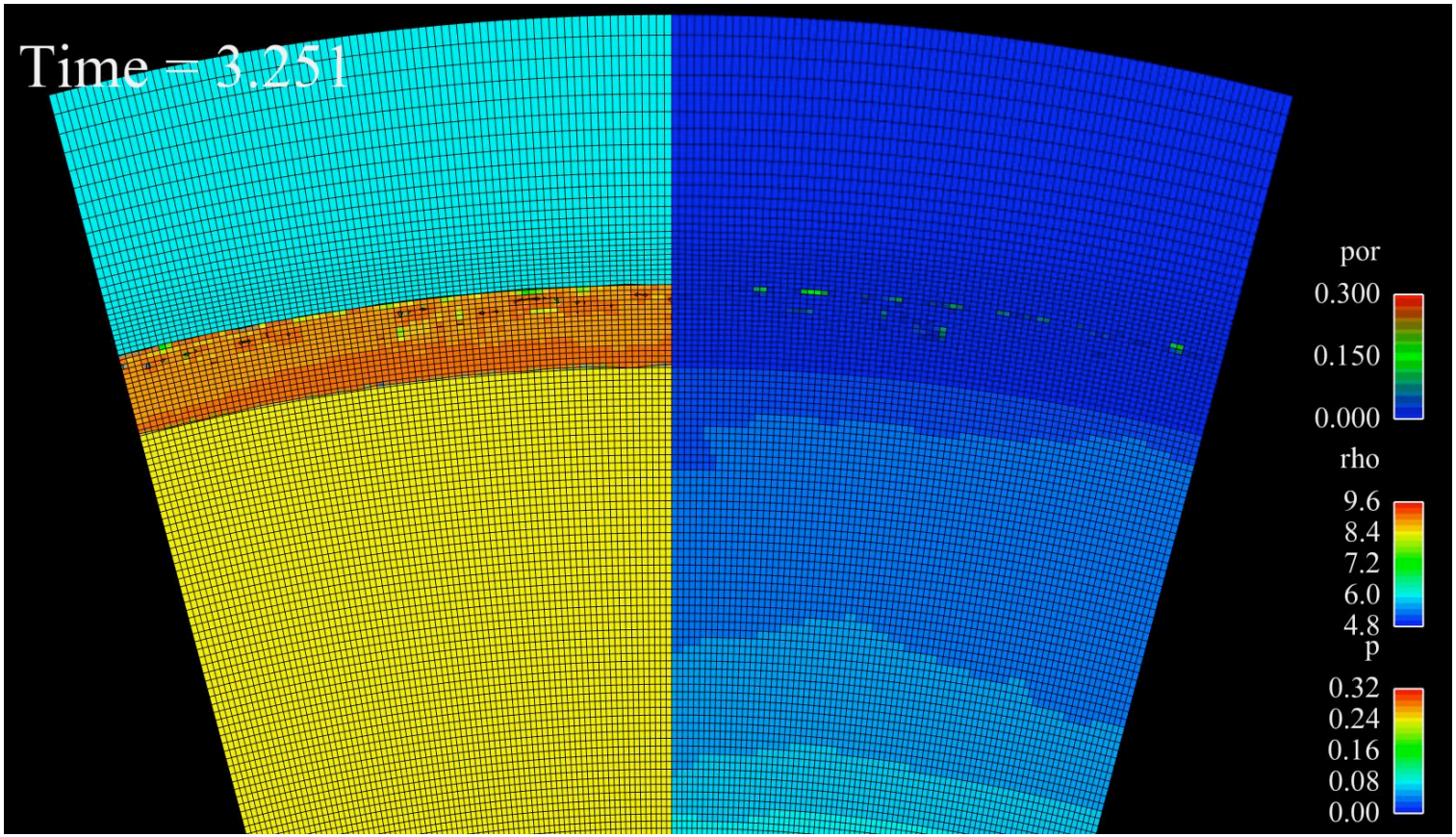

Void Evolution in a Damaged Material
HE Driven Cu Hemi

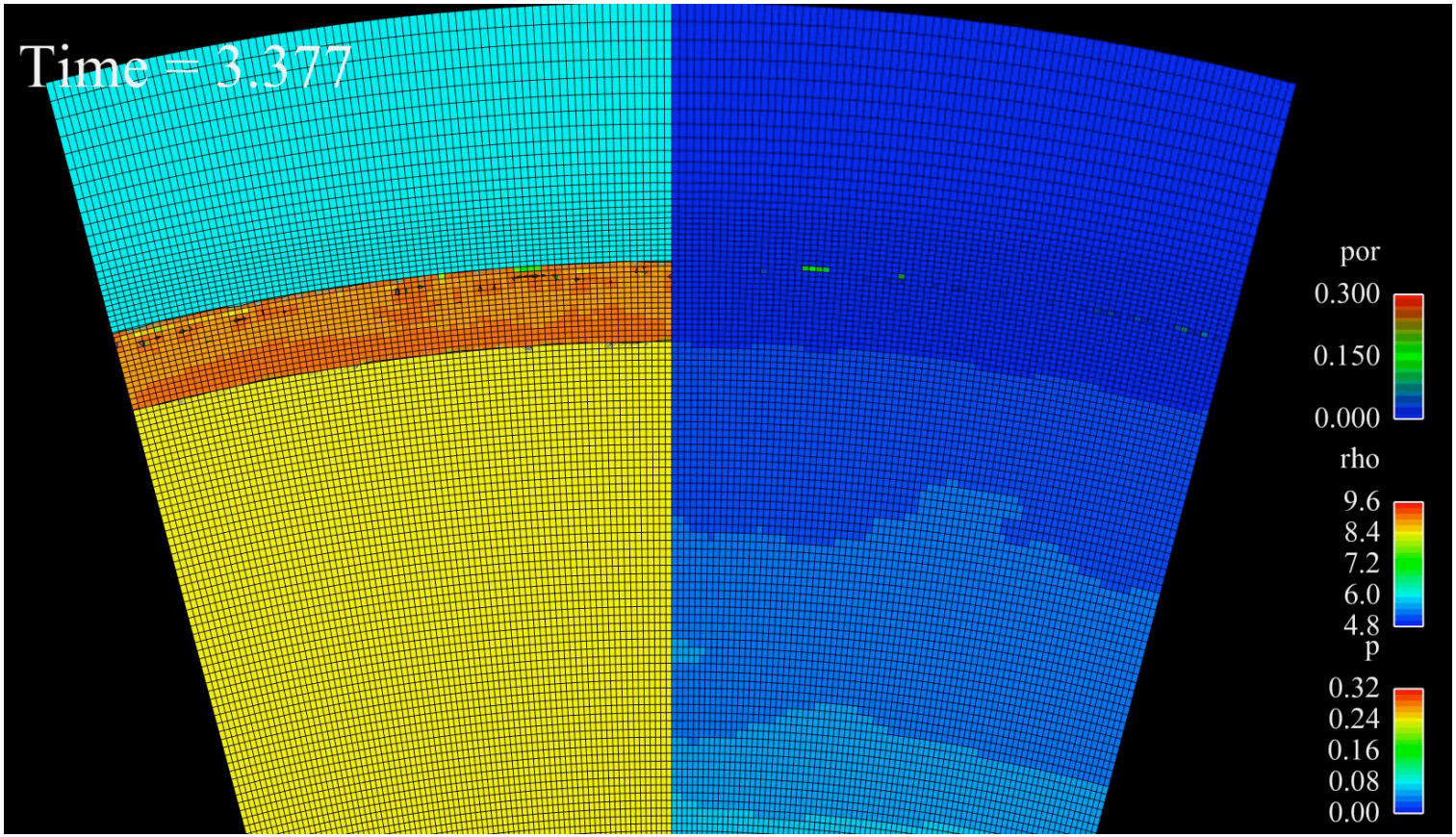

Void Evolution in a Damaged Material

HE Driven Cu Hemi

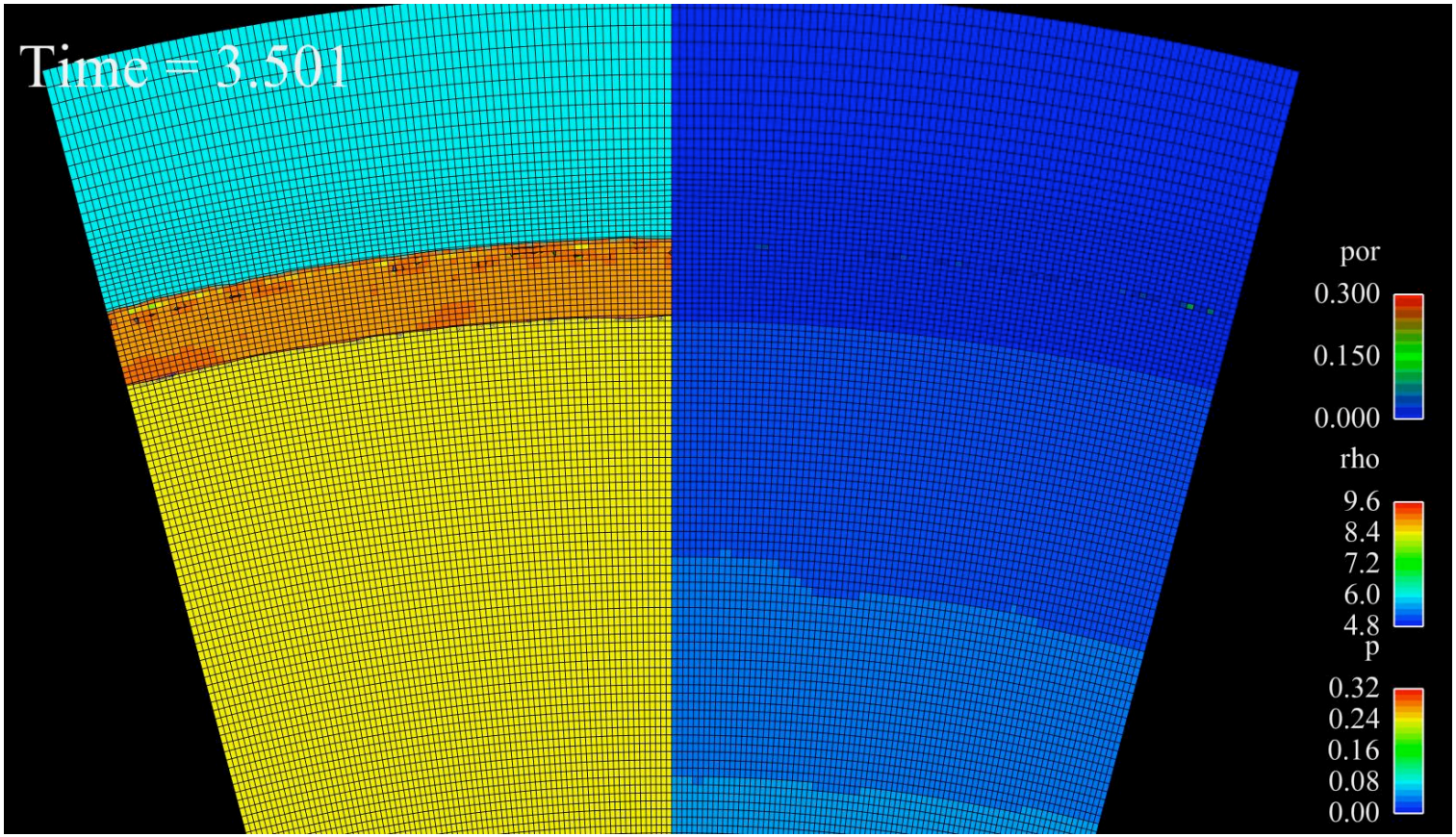

Void Evolution in a Damaged Material

HE Driven Cu Hemi

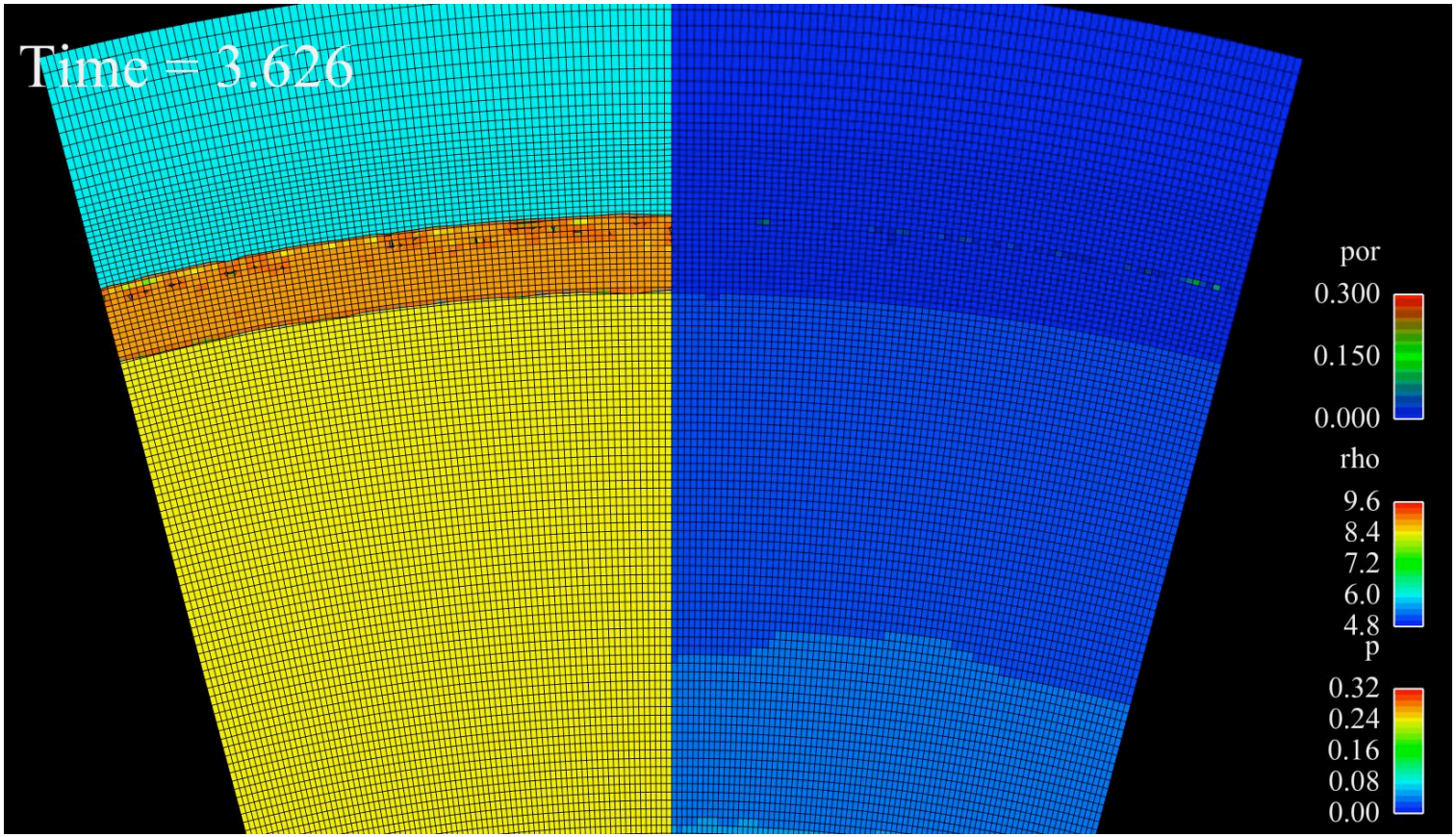

Void Evolution in a Damaged Material
HE Driven Cu Hemi

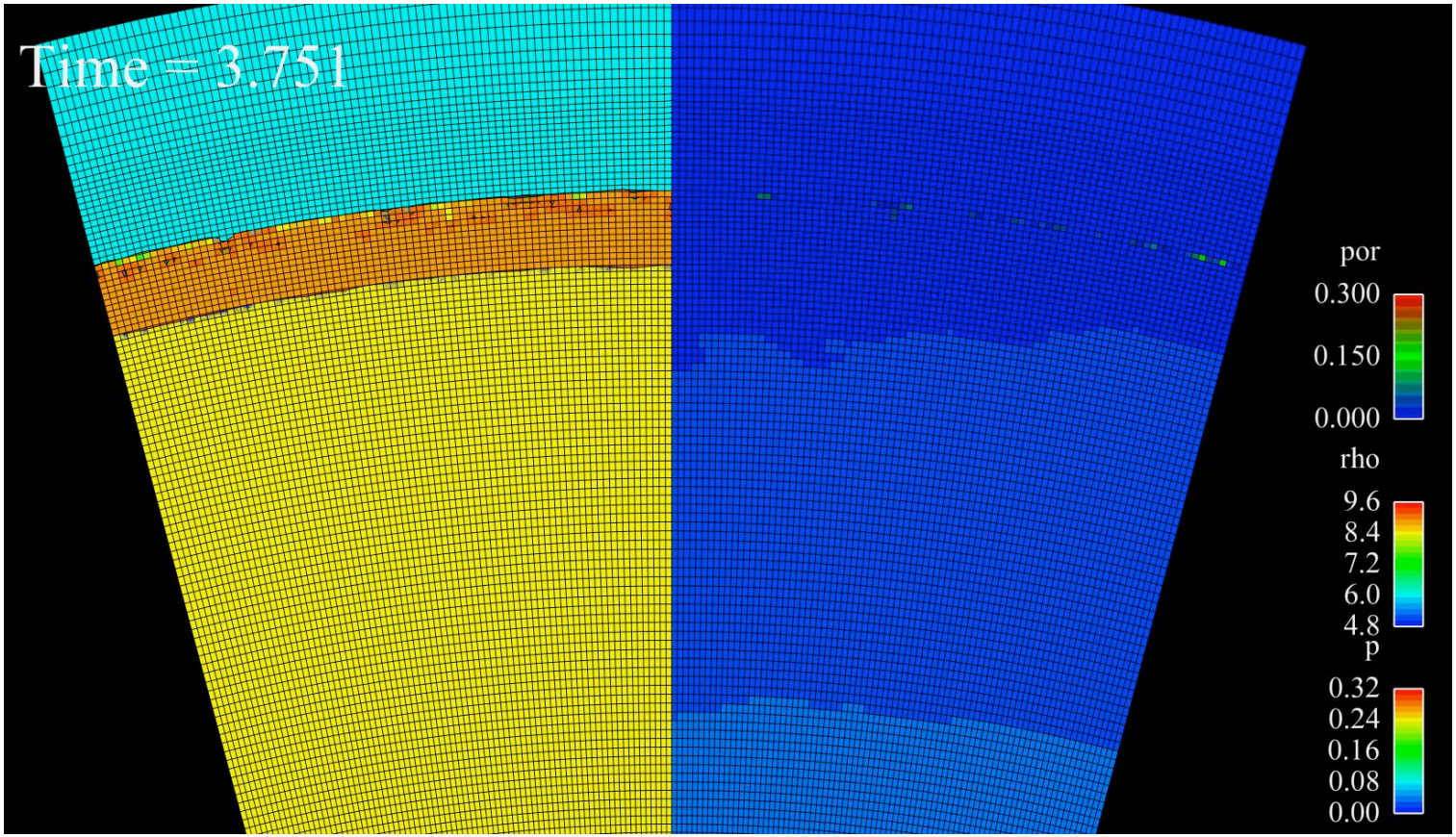

Void Evolution in a Damaged Material

HE Driven Cu Hemi

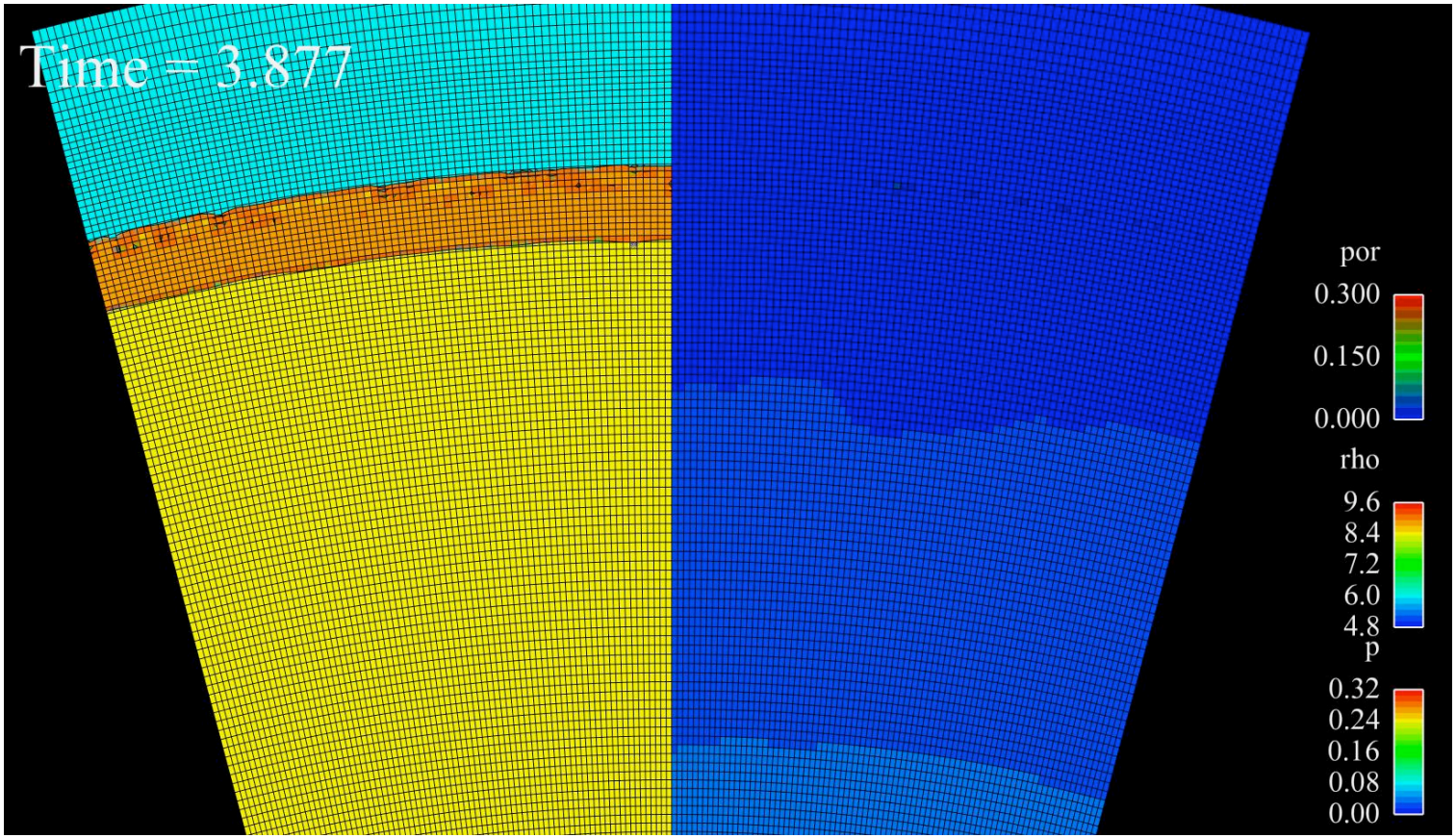

Void Evolution in a Damaged Material

HE Driven Cu Hemi (Air Filling Surface Voids … Arrows)

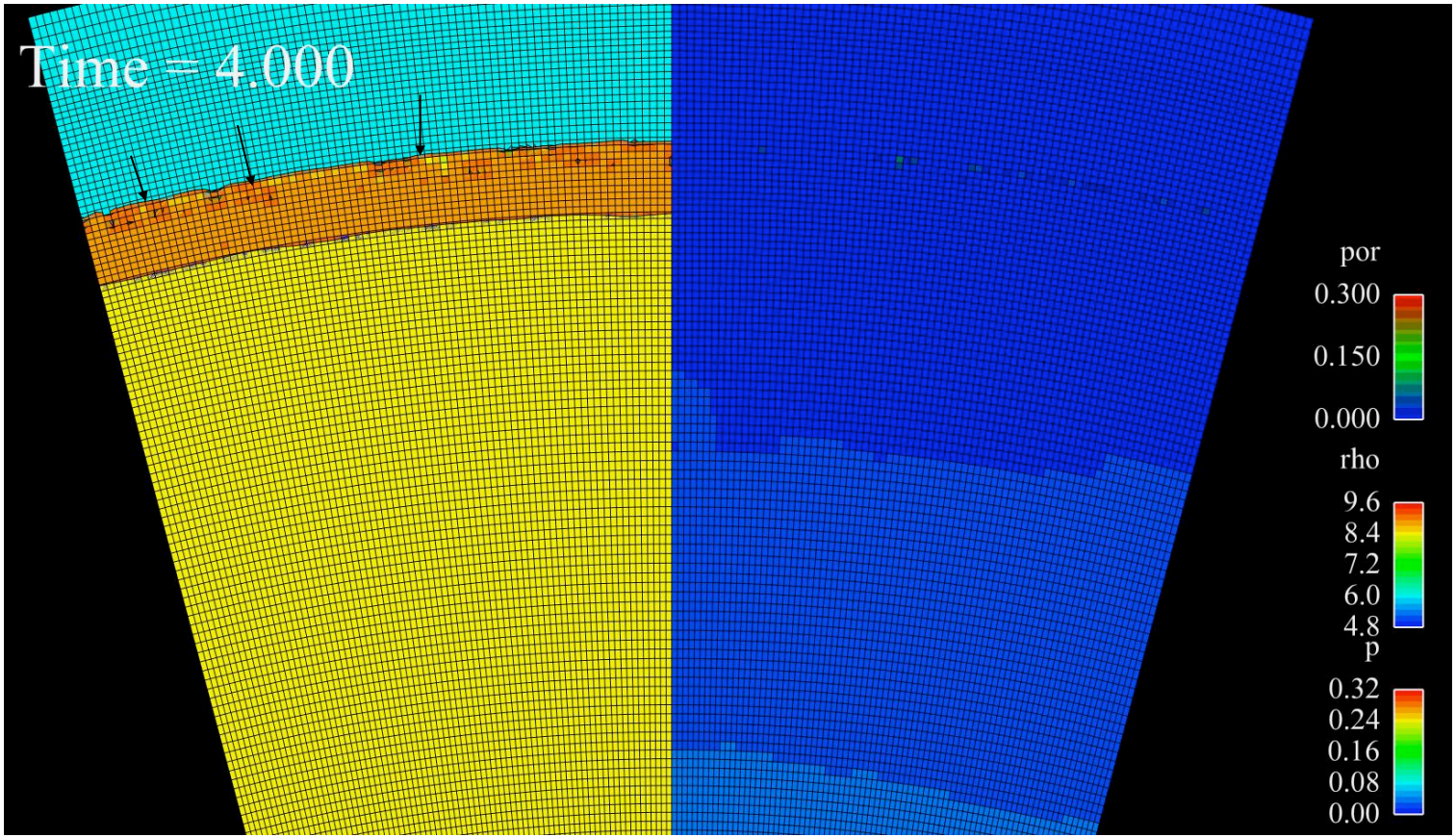

Damage Modeling with Void Evolution (U)
Summary and Conclusions

- Damage models such as TEPla evolve void until failure.
- Multiple failure criteria can be combined in one material
- Void material is created at failure
- When ALE is turned on the adjacent materials fill the void spaces

Damage Modeling with Void Evolution (U)
Next Step: Anisotropic Failure and Internal Constraints

- Isotropic Failure - Failure in all directions (atomized particles)
  - A 3D stress state in tension is reduced to 0D state
    - $S_{ij}=0$ and $p=0$
- Anisotropic Failure - Has direction
  - Mode 1 failure reduces the stress state to 2D plane stress
  - Mode 2 failure reduces the stress state to 1D uniaxial stress
  - Mode 3 failure is isotropic failure
- Apply internal constraints to the stress tensor based upon the failure modes

Lawrence Livermore National Laboratory

Spall and Melt Kinetics:
Scaling of Spall Strength with Pressure and Temperature

Roger W. Minich, Mukul Kumar, James Cazamias and Adam Schwartz

January 25 – January 29, 2010, LLNL
JOWOG 32-Mat

Lawrence Livermore National Laboratory, P. O. Box 808, Livermore, CA 94551
This work performed under the auspices of the U.S. Department of Energy by
Lawrence Livermore National Laboratory under Contract DE-AC52-07NA27344

LLNL-PRES-424897

Spall Strength: Scaling with impact pressure and initial temperature

- A review of pressure scaling studies in Cu on Cu gas-gun experiments.
- Introduction of a statistical spall model connecting void nucleation and growth, flow stress and spall strength.
- Application of statistical spall model to study temperature scaling near melt.

Dissecting a spall signal (Cu)

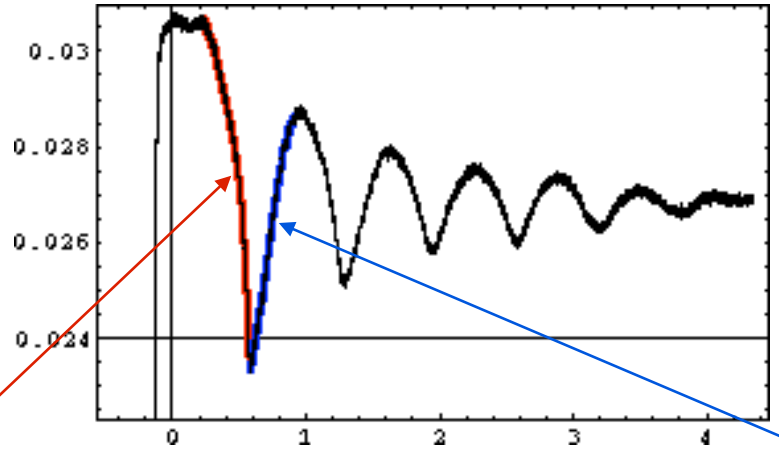

$$\Delta v_{pb} \propto v_{impactor}^{\ \alpha}$$

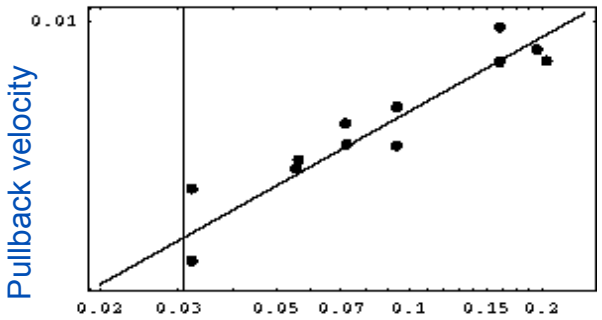

$$\Delta v_{growth} \propto v_{impactor}\left(1 - b v_{impactor}\right)$$

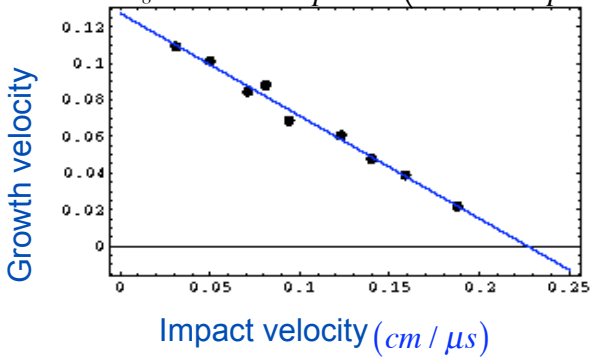

Scaling of pullback velocity with impact velocity (Cu) suggest relationship to void nucleation

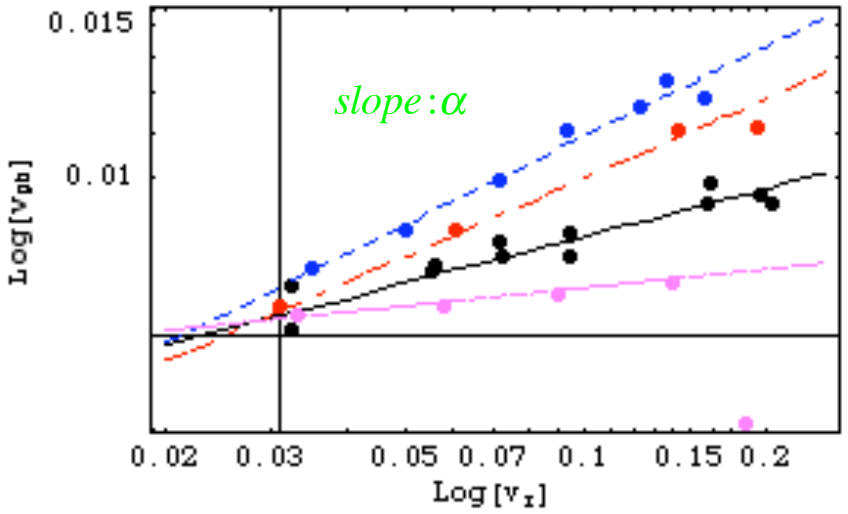

Monocrystal: 100

Polycrystal: 50 microns

Polycrystal: 8.6 microns

Cu monocrystal w/0.15% wt. Si

$$slope:\alpha = \frac{1-\Gamma}{1+\lambda}$$

Γ ← Nucleation exponent

λ ← Growth exponent

The dependence of α exponent on grain size follows Hall-Petch relationship for flow stress.

Grain size: λ_G **Noise parameter:** $\langle\tau\rangle Q = \dfrac{\langle\delta\tau^2\rangle}{\langle\tau\rangle}$

$$\frac{\alpha'}{\alpha} = \frac{\langle\tau\rangle Q}{\langle\tau'\rangle Q'} = \frac{\hat{\tau}_{flow}}{\hat{\tau}'_{flow}} = \frac{\hat{\tau}_0 + \hat{\tau}_1\sqrt{\dfrac{l_0}{\lambda_G}}}{\hat{\tau}_0 + \hat{\tau}_1\sqrt{\dfrac{l_0}{\lambda'_G}}} = \frac{1+\dfrac{\gamma}{\sqrt{\lambda_G}}}{1+\dfrac{\gamma}{\sqrt{\lambda'_G}}} \qquad \gamma \equiv \frac{\hat{\tau}_0\sqrt{l_0}}{\hat{\tau}_1} \approx 7.5\mu m^{1/2}$$

Saturation of α consistent with trend in flow stress.

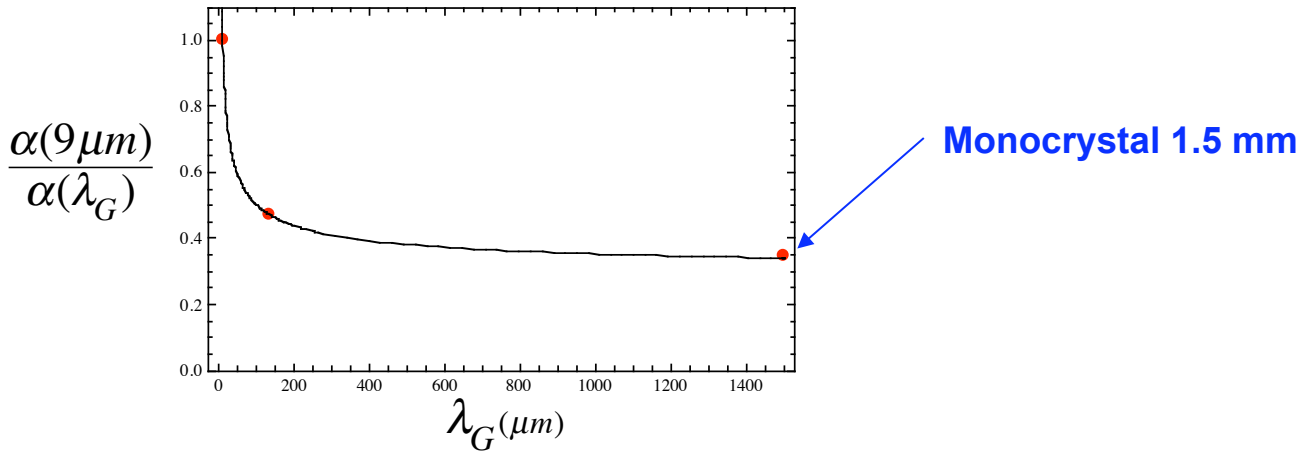

Spall Model (Minich) Reproduces Experimental Pressure Scaling of Pullback Signal with No Adjustable Parameters

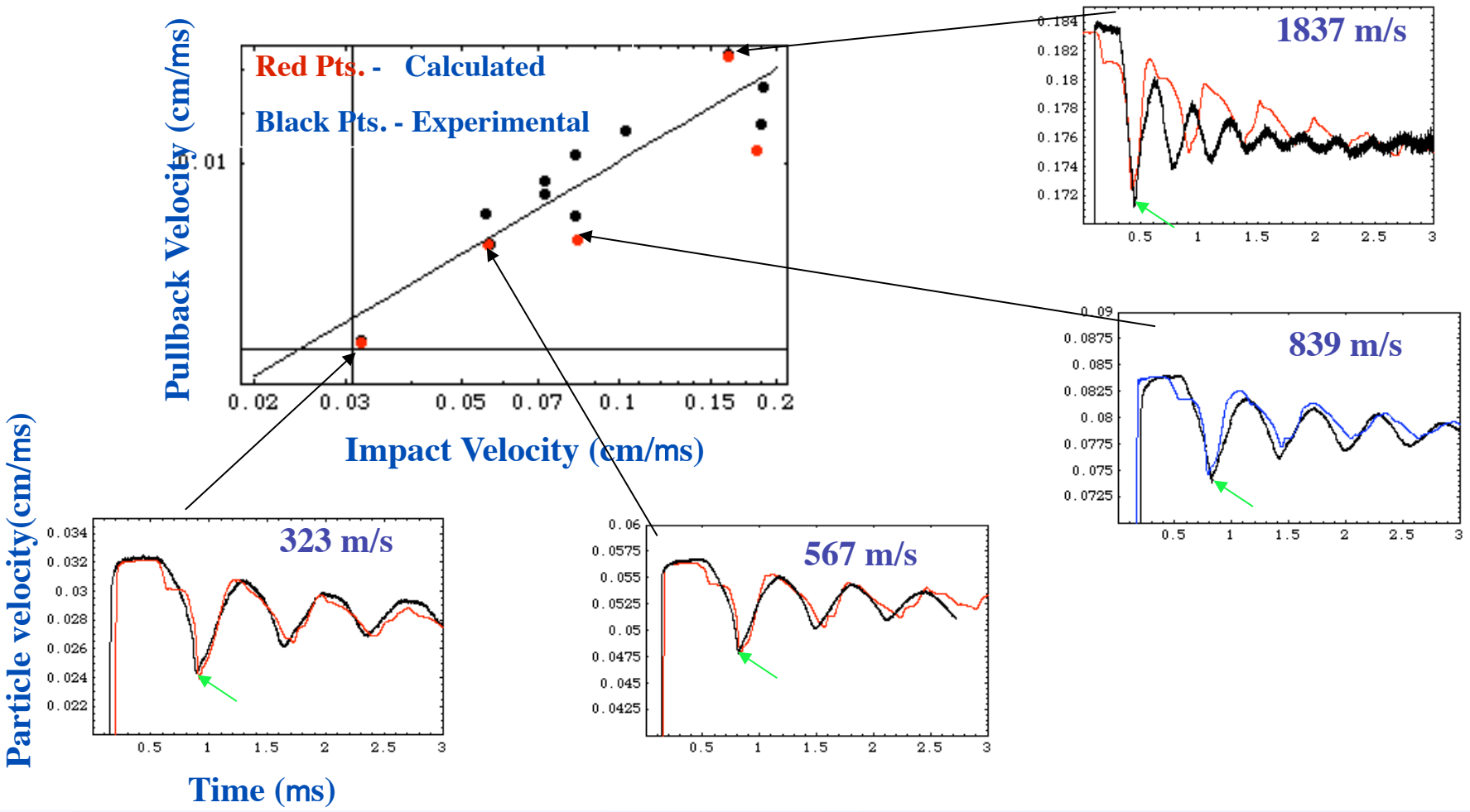

Spall Strength: Spall strength and temperature scaling - calculation

$$v_{pb} \sim \left[1 - \frac{T}{T_m}\right]^{x/(1+\lambda)} \qquad x = 1 \qquad \lambda = 1$$

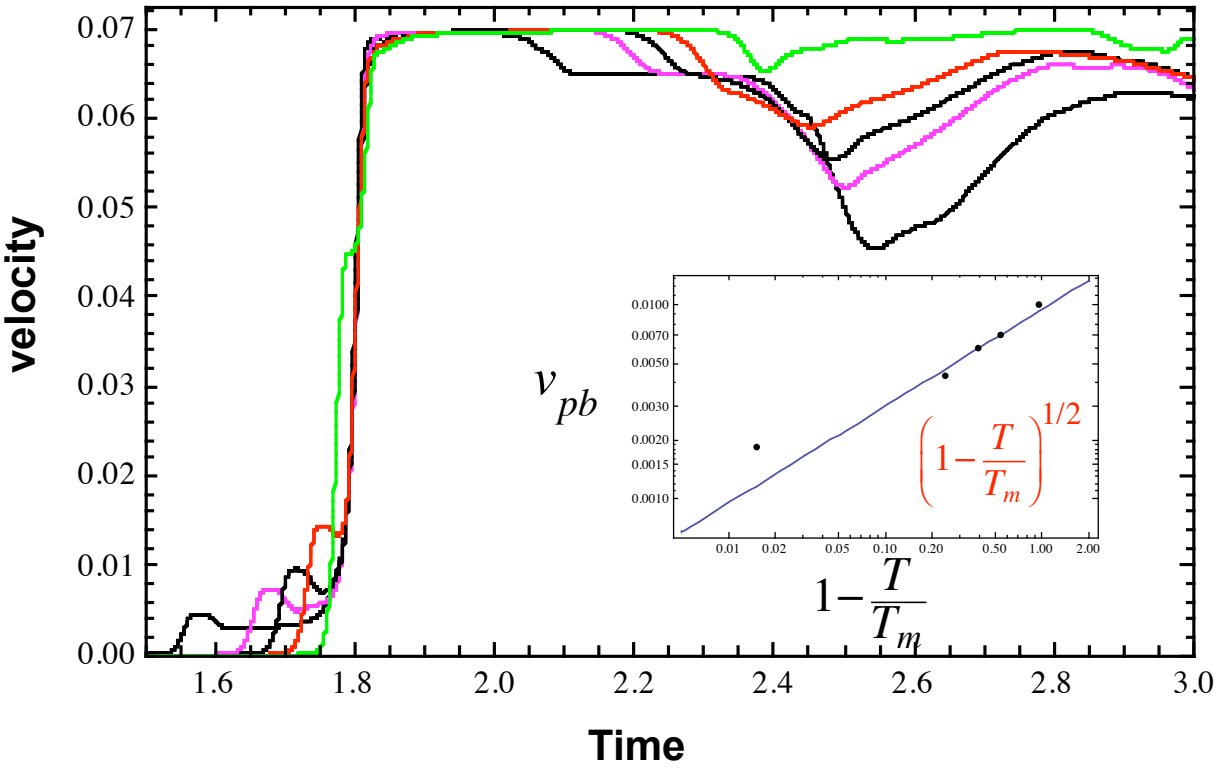

Spall Strength: Spall strength and temperature scaling –experiment (Al)

Kanel Al Gas-gun experiments:

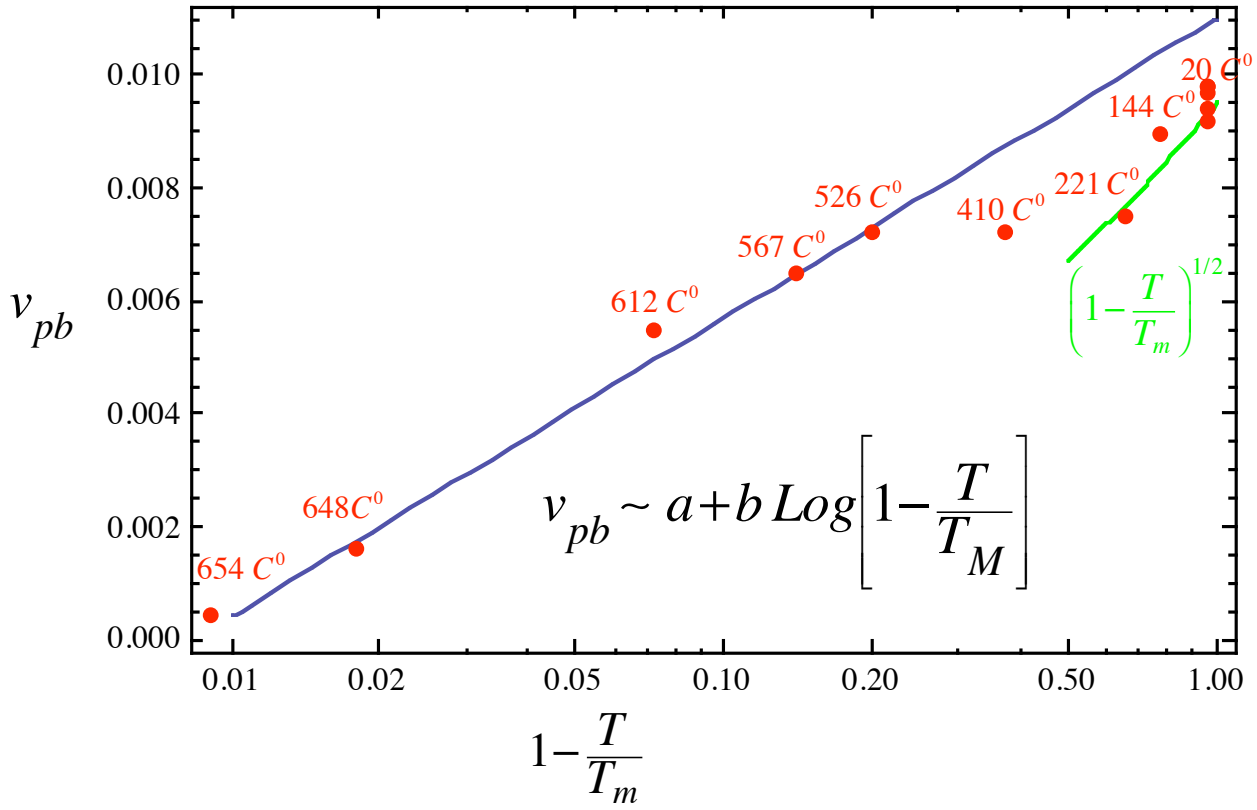

Observed logarithmic scaling may be due to large scale fluctuations near noise driven phase transition

Size distribution:

$$P(\xi)=\gamma\left[\frac{1+\kappa}{\gamma}\frac{\tau_c}{\langle\tau\rangle}\right]^{\frac{1+\kappa}{\gamma}}\Gamma^{-1}\left(\frac{1+\kappa}{\gamma}\right)\xi^{\alpha}\,e^{-\frac{1+\kappa}{\gamma}\frac{\tau_c}{\langle\tau\rangle}\xi^{\gamma}} \qquad \kappa=\frac{2}{Q\,\Omega\langle\tau\rangle}-1$$

Large scale fluctuations: $\kappa\ll 1$ $\quad\frac{\tau_c}{\langle\tau\rangle}\ll 1$ $\quad P(\xi)\approx a+b\,Log[\xi]$

$$v_{pb}\approx a+b'\frac{x}{1+\lambda}Log\left[1-\frac{T}{T_m}\right] \qquad \xi\sim\left[1-\frac{T}{T_m}\right]^{-x}$$

Summary and Conclusions

- Pressure scaling of spall strength can relate spall strength and flow stress.
- Temperature scaling of spall strength is naively predicted to be a power law $\left(1-\frac{T}{T_m}\right)^{\frac{x}{1+\lambda}}$ in disagreement with experiment
- Theory can exhibit correct experimental logarithmic scaling $a+b\,Log\left(1-\frac{T}{T_m}\right)$ near a critical point.

Influence of Microstructure on Materials Modeling: DU and U6Nb

E.K. Cerreta, D.D. Koller, G.T. Gray III, A. Kelly, R. Forsythe, R. McCabe, C.A. Bronkhorst, R. Lebensohn, F. Addessio, and J. Plohr

Failure and Fragmentation of U-alloys is frequently linked to shear and void nucleation processes

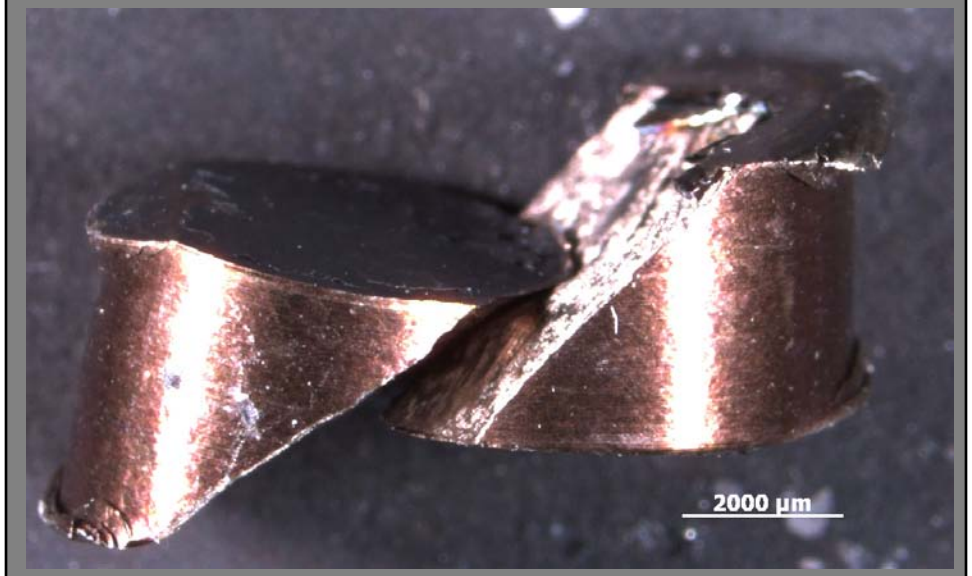

Cold Rolled U6Nb tested quasi-statically at -100°C

During quasi-static and dynamic tests, shear failure occurs abruptly in specimens

Competing shear localizations develop and ultimately lead to failure in explosively shocked U6Nb

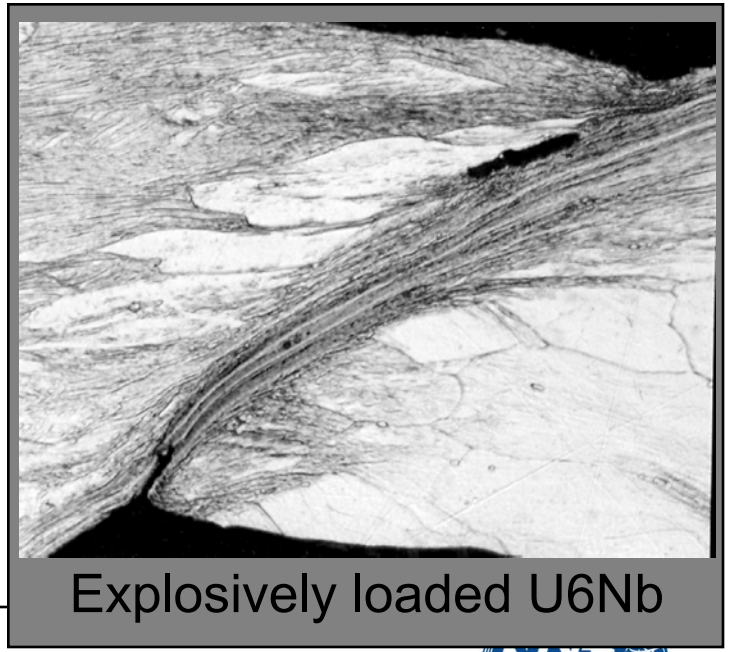

Explosively loaded U6Nb

Accurate prediction of the damage evolution in these alloys drives characterization

- Damage evolution and failure of U6Nb and DU has been linked to shear localization during dynamic loading
- Details of porosity, shear banding, and cracking during deformation are not well understood
- These processes must be understood physically for accurate prediction of damage

Dynamic damage results from/influenced by a collection of processes occurring during loading, prior to fragmentation

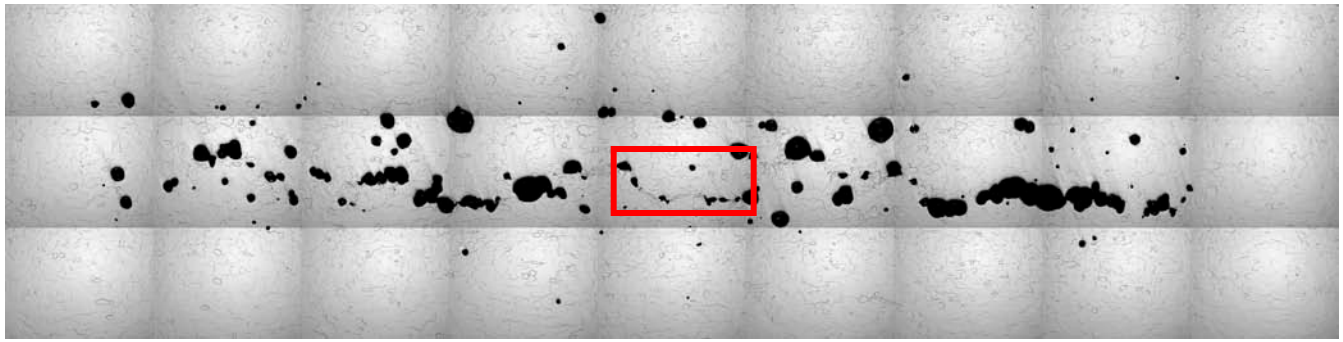

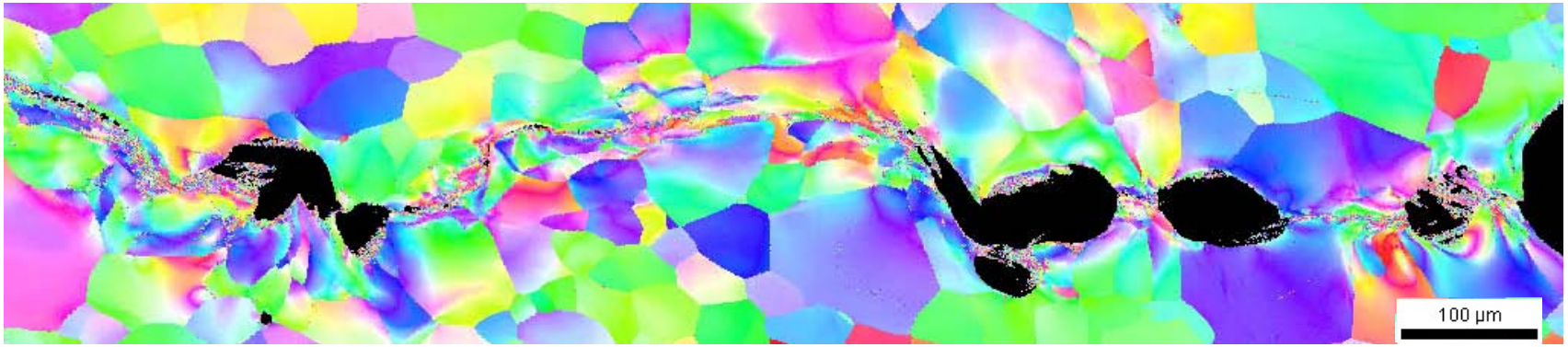

- This response is altered by shock wave shape – rise time, pulse duration, release kinetics, volume sampled, etc.
- Understanding the influence of stress history on microstructure evolution key to predicting damage

Current ability to predict this type of ductile damage is limited

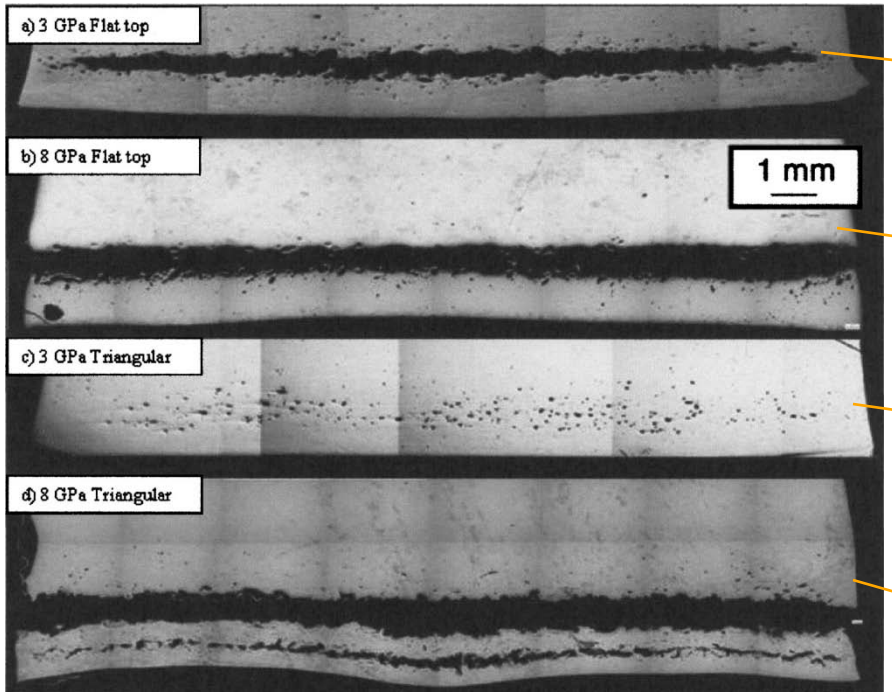

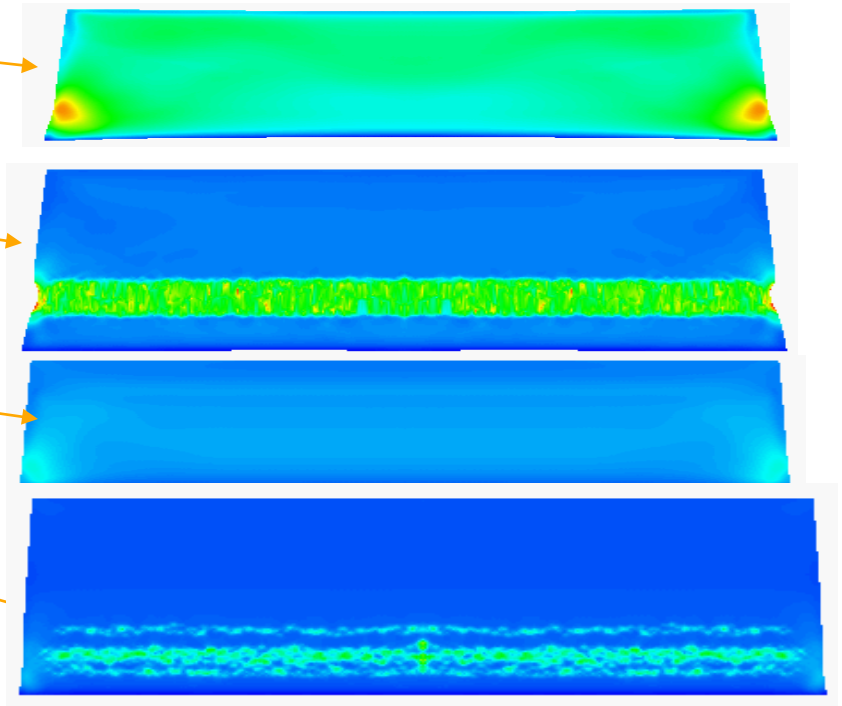

- Koller and Cerreta, *J. Appl. Phys*, Nov. 2003
- Harstad et. al, *Plasticity Proceedings*, Jan 2009.

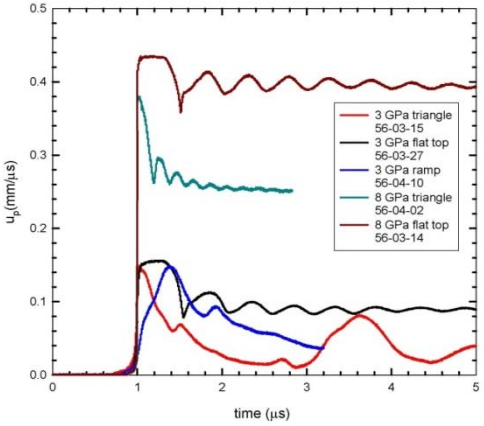

Current Modeling Techniques are Mesh Size Dependent

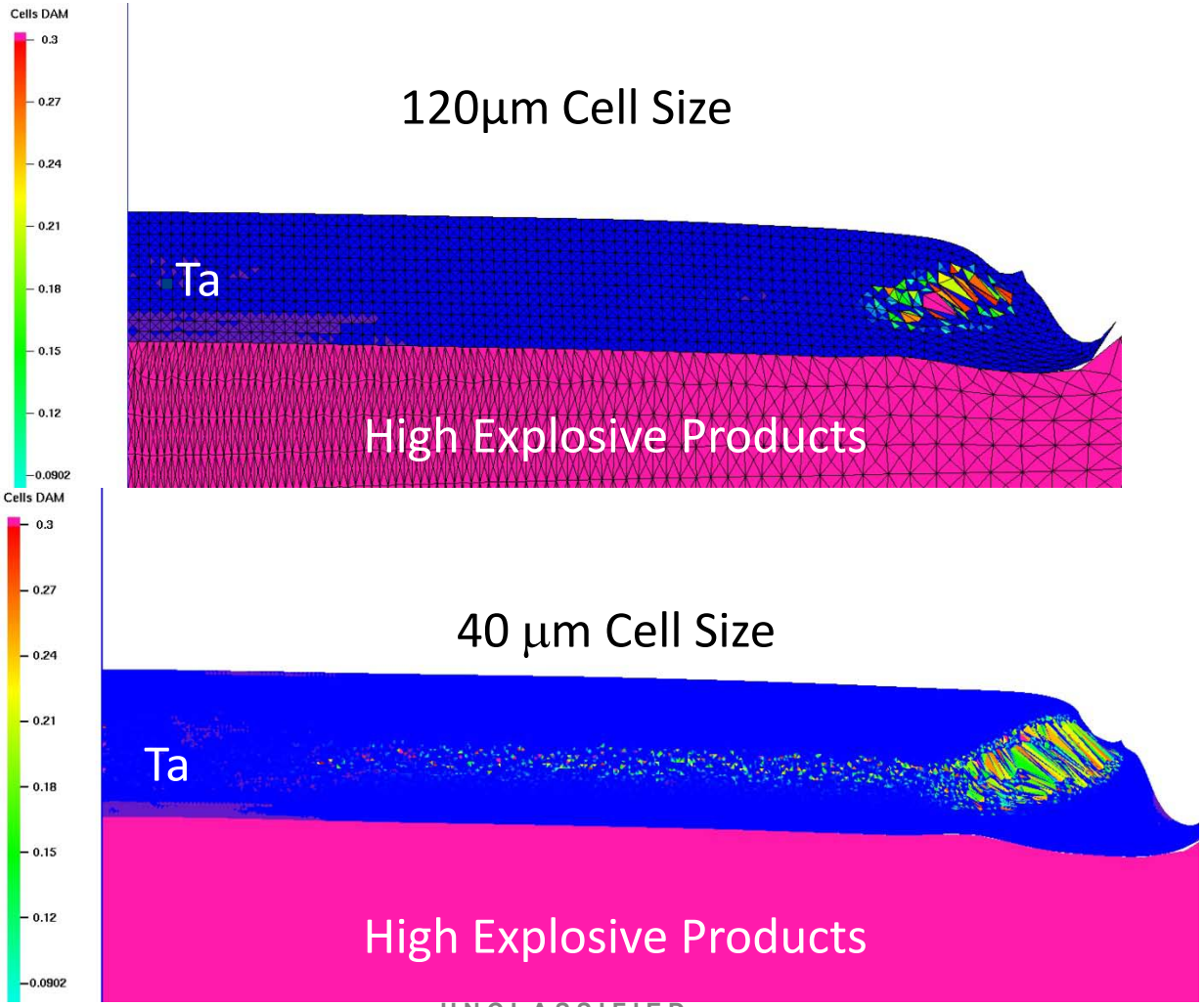

Goals of developing models that track small length scale phenomena

- Within an element, physics associated with small length scales could be tracked in the background

- A mesoscale understanding of length scale and kinetic effects on damage would be used to statistically understand damage and failure

- Then accounting for this damage within a cell could be done at the subgrid level

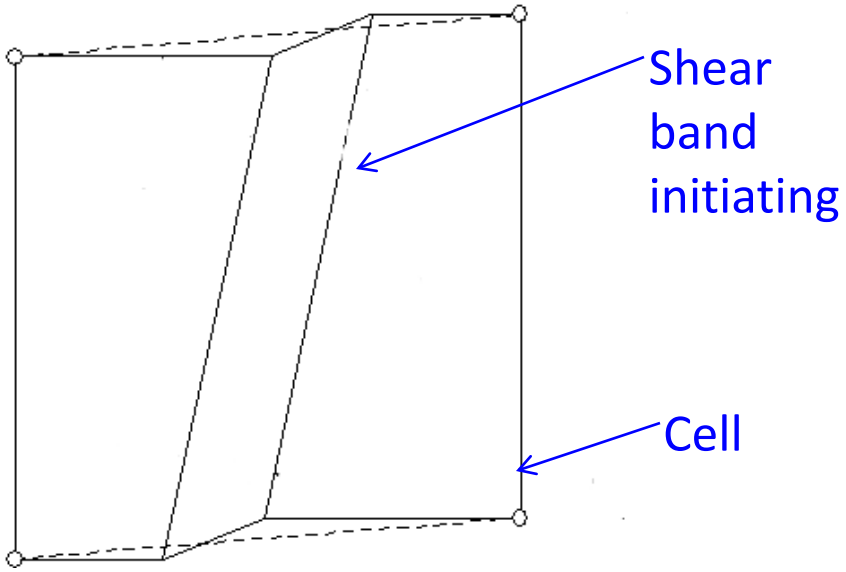

Representation of the initial stages of shear localization within a cell

Haghi, J. Mech. Phys. Solids, 1995.

Void Coalescence is an Example of a Small Scale Process that can be Tracked

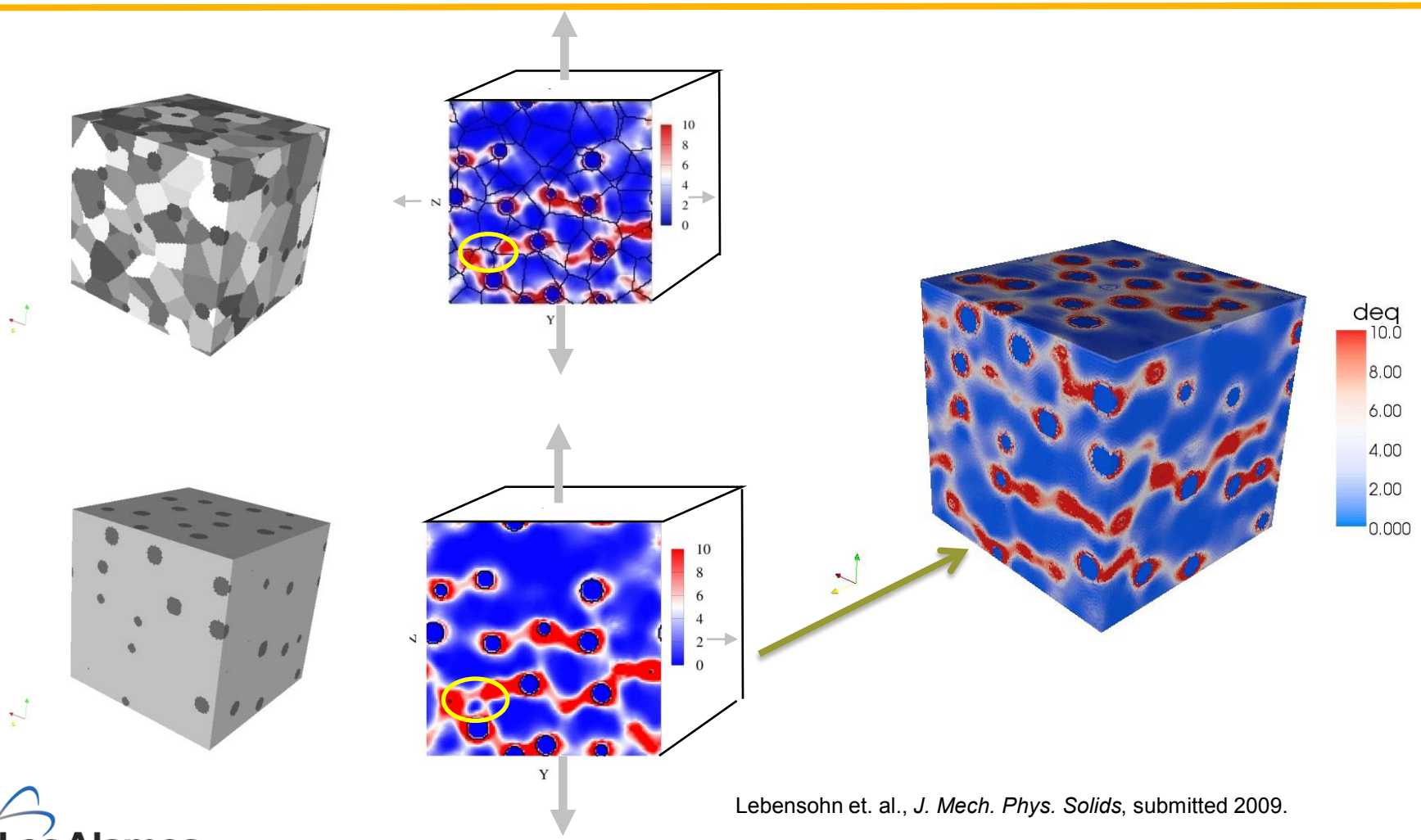

Lebensohn et. al., *J. Mech. Phys. Solids*, submitted 2009.

There are a number of important considerations in doing this for U-alloys

- While for high purity cubic metals, many incipient damage experiments have been performed and characterized, not the case for the uranium and its alloys
- We know length scales are important to ductile damage, multiple length scales in uranium alloys
  - Grain size
  - Inclusion Distribution
  - Chemical Banding, Etc.
- Under uni-axial stress, mechanical response is rate dependent

Frequently a dynamic damage experiment is characterized through spall strength measurements

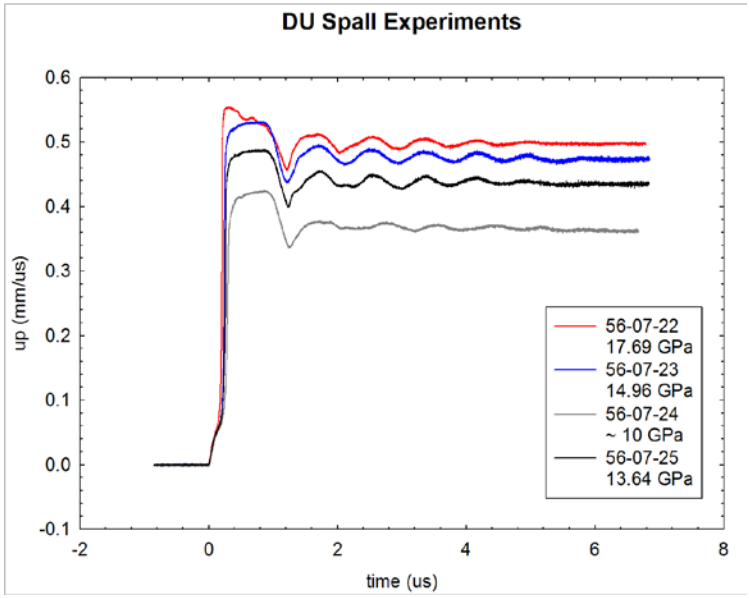

Spall Strength is one parameter that results from a complex set of elastic and plastic processes

Shot number	*Us (mm/us)*	*Up (mm/us)*	*P (GPa)*	*Spall layer thickness (mm)*	*Spall strength (GPa)*
56-07-22	2.750 +/- 0.018	0.331 +/- 0.001	17.69 +/- 0.06	1.057 +/- 0.11	2.25 +/- 0.115
56-07-23	2.719 +/- 0.010	0.282 +/- 0.001	14.96 +/- 0.03	1.13 +/- 0.11	2.20 +/- 0.118
56-07-24	Not calculated	Not calculated	≈ 10	Not calculated	2.02 +/- 0.118
56-07-25	2.681 +/- 0.010	0.260 +/- 0.0005	13.64 +/- 0.023	0.944+/- 0.09	2.06 +/- 0.118

Dynamic experiments performed to characterize low pressure behavior – Refinement of Marsh Compendium

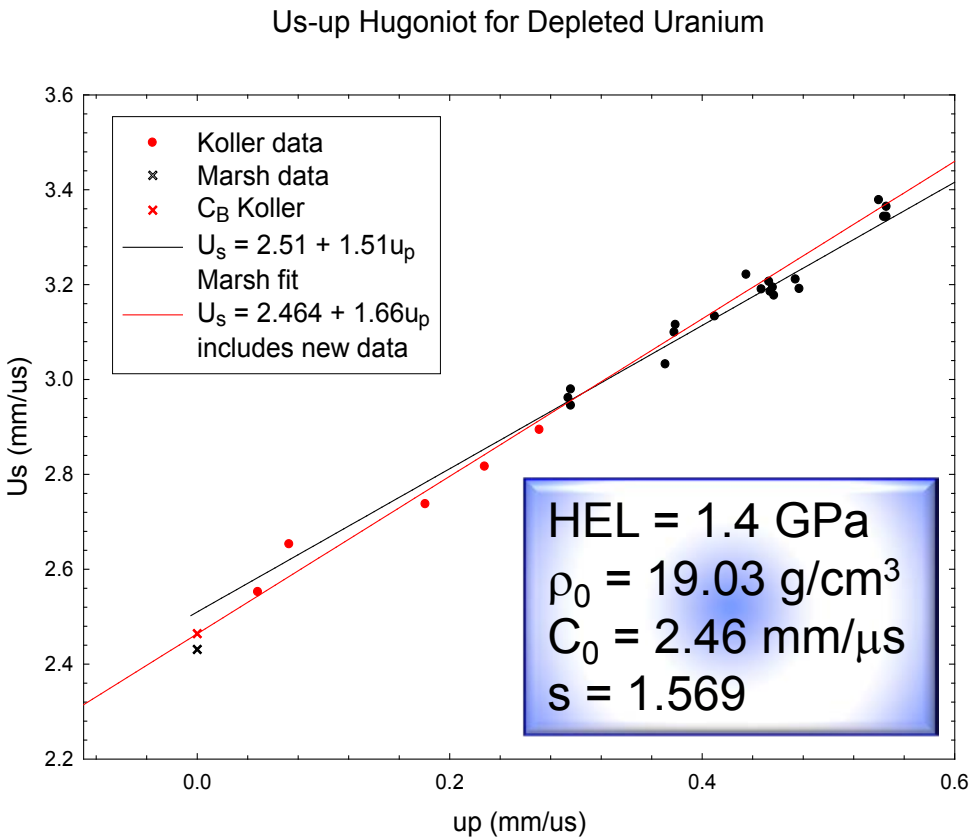

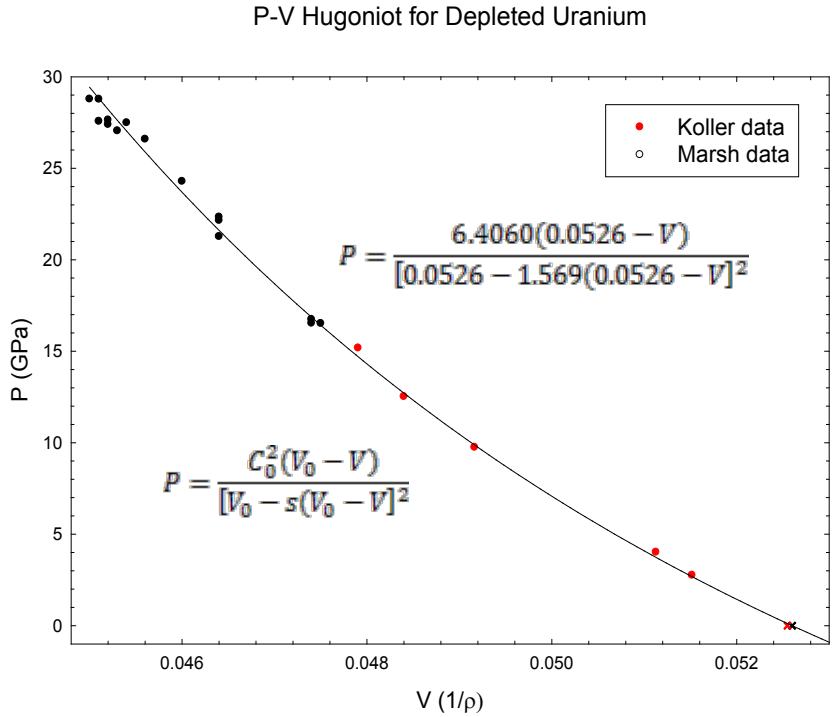

New fit gives values for C_o and s

New results for low pressure DU Hugnoniot give a more refined U_s-u_p and P-V relationship

Shot	C_L mm/μs	C_s mm/μs	ρ_0 g/cm^3	ρ_1 g/cm^3	P_2 GPa	U_{s2} mm/μs	u_{p2} mm/μs	ρ_2 g/cm^3
56-06-37	3.426	2.089	19.0396	19.1516	9.7563	2.7372	0.1808	20.34
56-07-01	3.499	2.164	19.055	19.1422	2.7605	2.5519	0.0481	19.4122
56-07-02	3.503	2.162	19.06	19.1767	4.0208	2.6527	0.0729	19.5594
56-07-14	3.497	2.15	18.954	19.0703	15.1826	2.894	0.2712	20.8748
56-07-15	3.500	2.15	19.028	19.1446	12.5288	2.8165	0.2278	20.6615

HEL = 1.4 GPa
ρ_0 = 19.03 g/cm^3
C_0 = 2.46 mm/μs
s = 1.569

Complex combinations of the elastic and plastic processes during dynamic loading directly influence in-situ measurements but are difficult to isolate

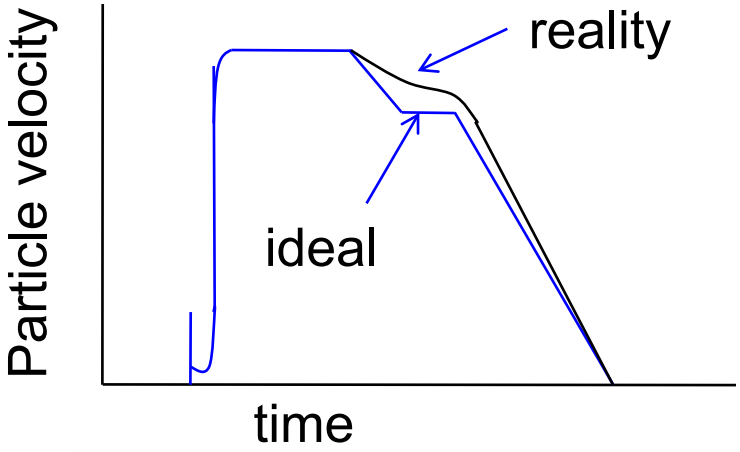

Ideal elastic-plastic release behavior :

- Material releases elastically until the tensile yield strength is reached
- Then plastic release continues until stress returns to zero

In reality, the process of plastic deformation during compression involves defect generation (dislocations, slip, & twinning) which smears out the release.

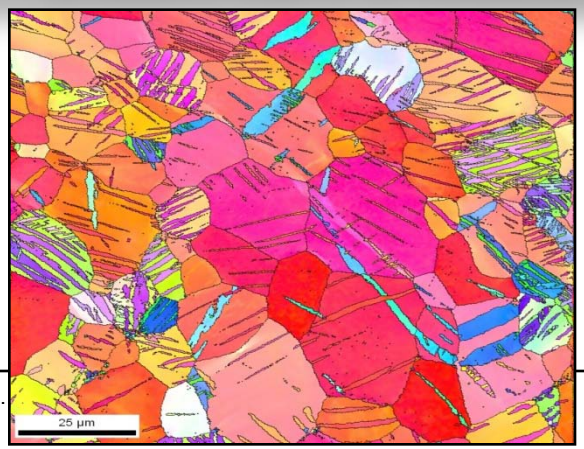

Twinning in shock loaded DU

In DU, a quasi-elastic notch is observed in the shock experiments and no enhanced hardening upon reload

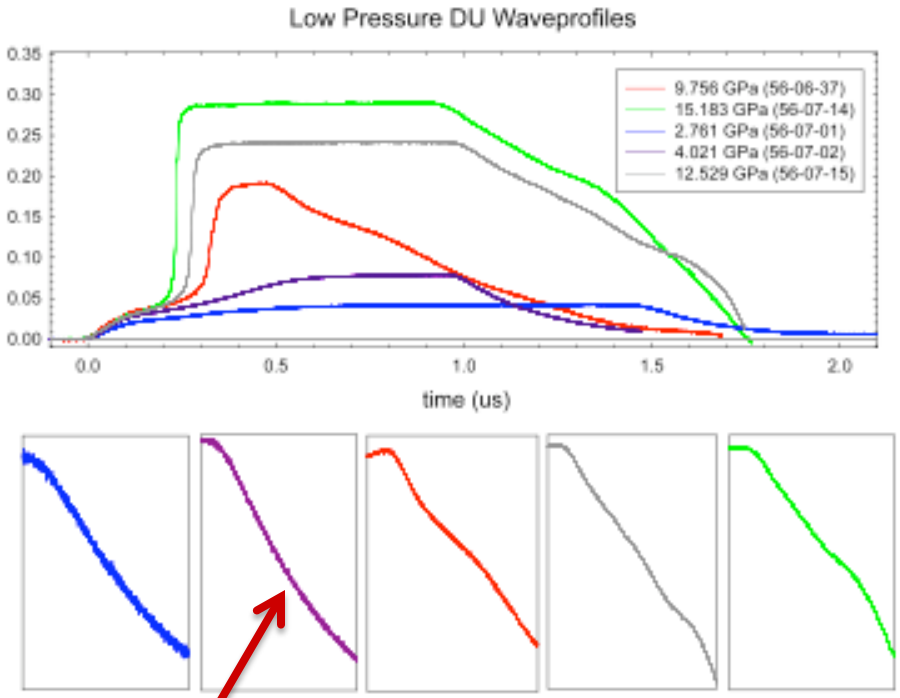

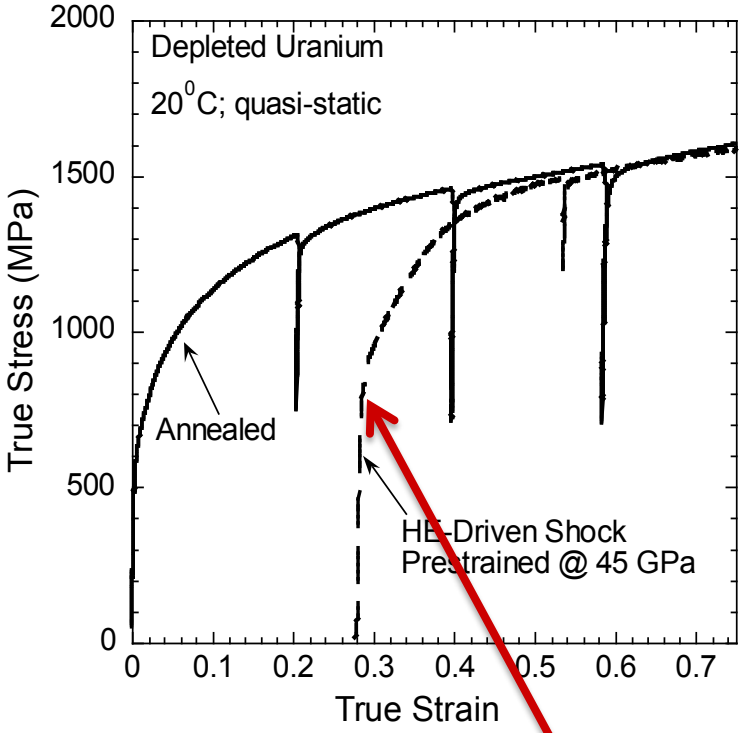

Non-ideal, quasi-elastic notch

Twinning may contribute to Bauschinger effect

Low yield

Recovery experiments were also performed to examine the dynamic failure in DU

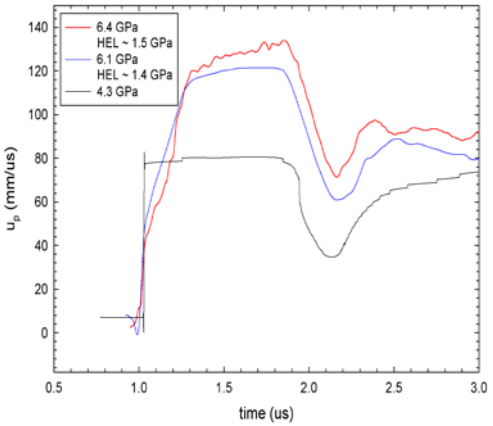

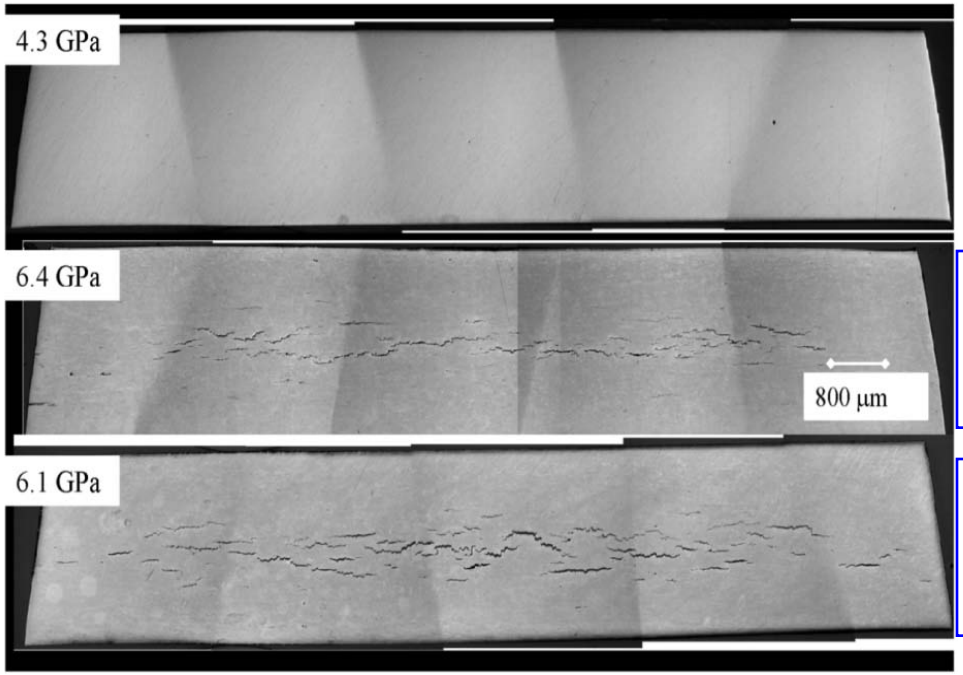

- Crack area= 0.331 mm^2
- Avg. crack = 0.004 mm^2
- Area fraction of cracks = 0.97%

- Crack Area = 0.151 mm^2
- Avg crack = 0.003 mm^2
- Area fraction of cracks = 0.45%

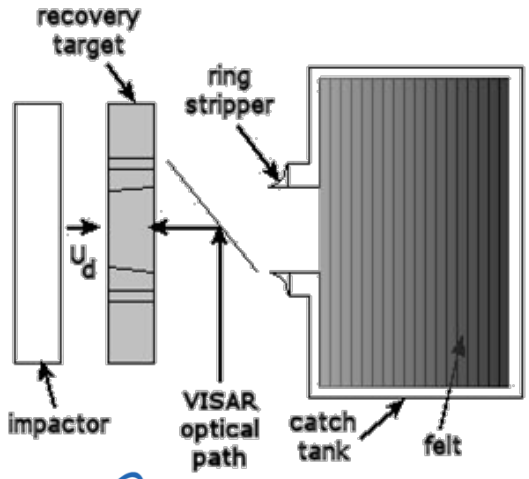

Enhanced damage with increasing peak shock pressure

Metallography reveals that damage included cracks and flow localizations

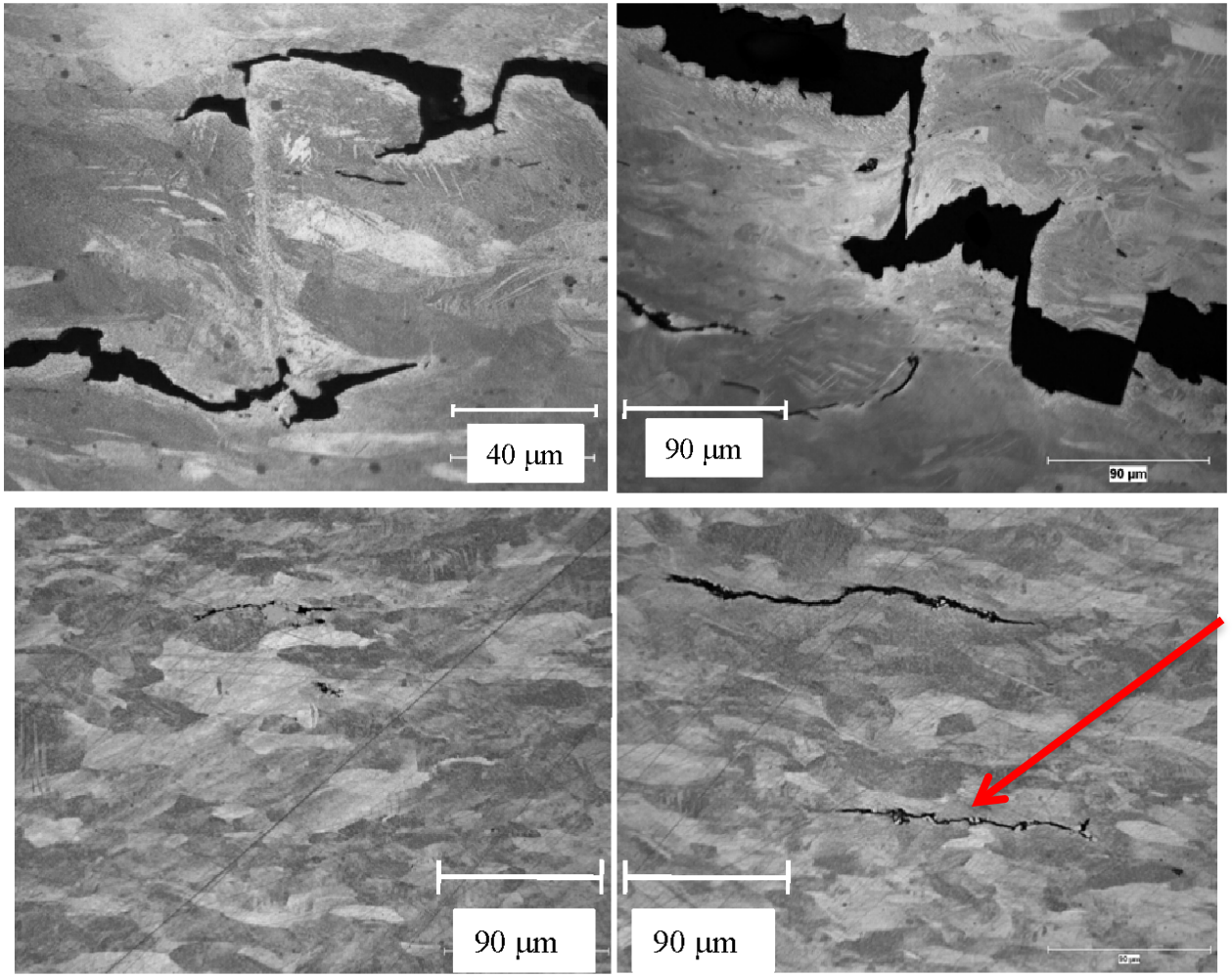

Many times damage is linked with inclusions

EBSD used to examine extent of deformation twinning

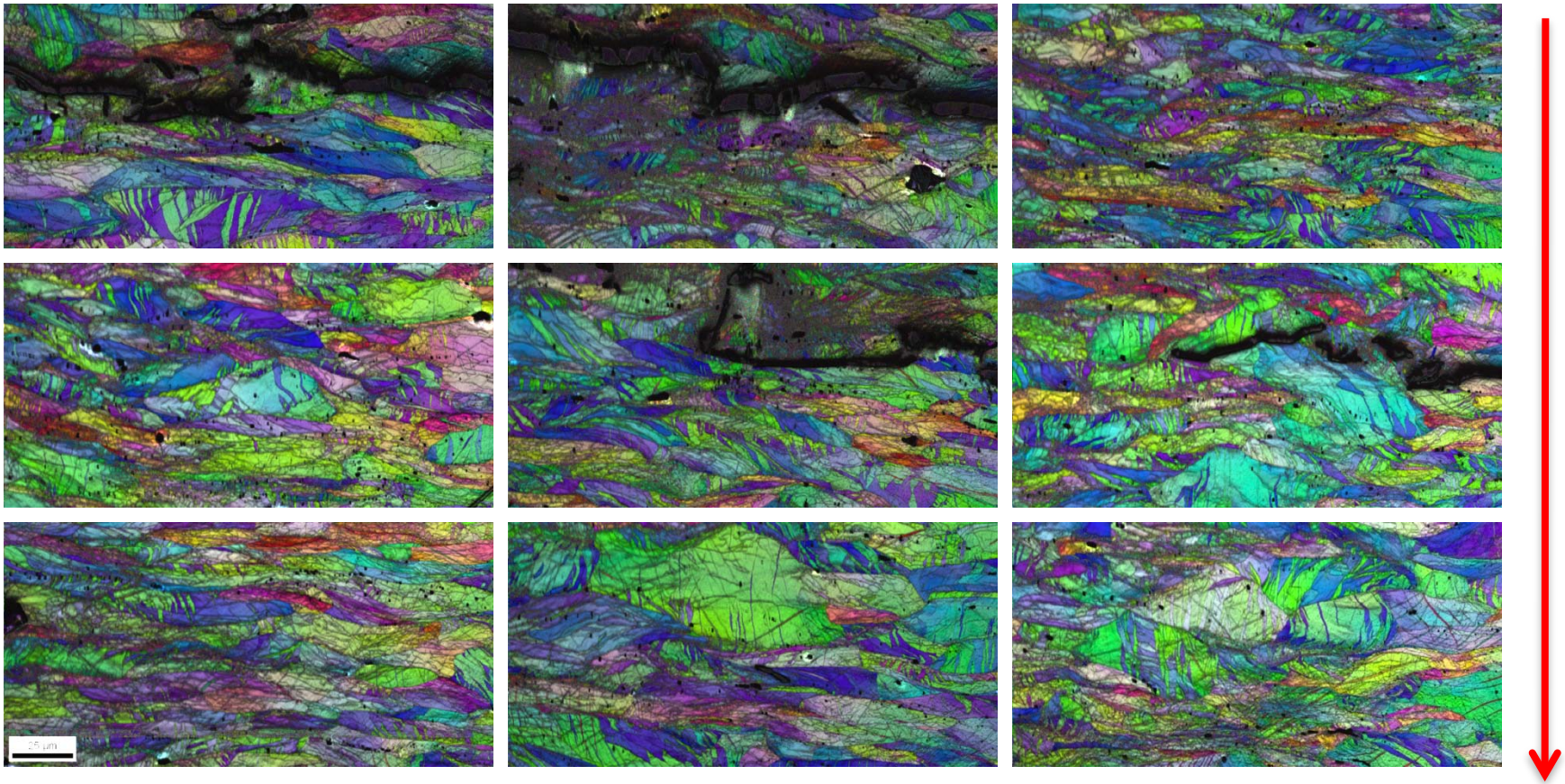

U-Nb alloys have complicated phase diagrams

U6Nb displays a range of metastable phases

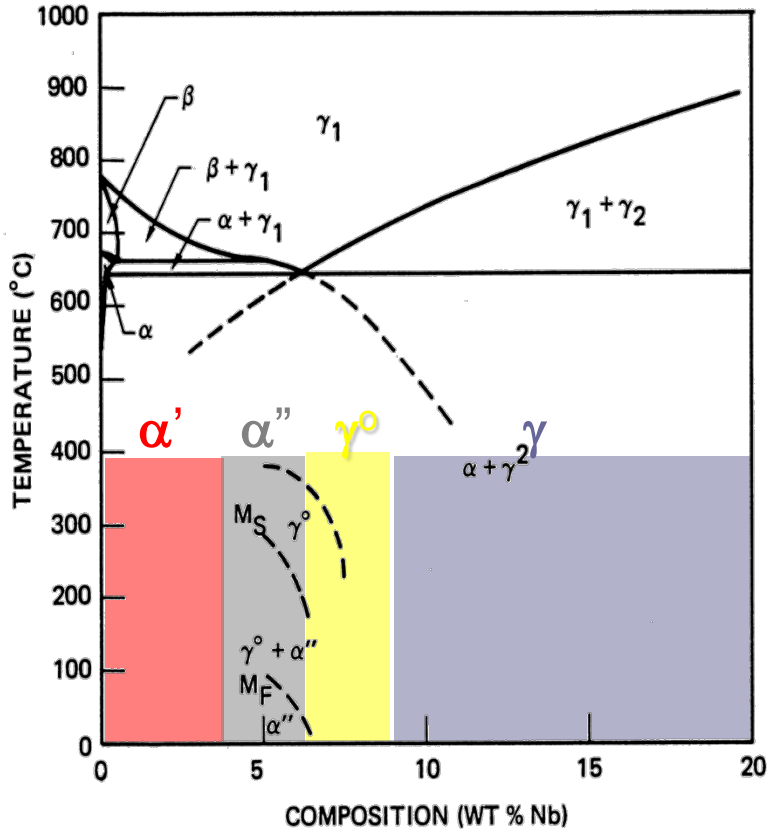

For U-6wt.%Nb

Equilibrium

- $\gamma_1 \rightarrow \alpha + \gamma_2$ (diffusion controlled)

Metastable

- $\gamma_1 \rightarrow \gamma^o \rightarrow \alpha''$ (diffusionless)

	G (GPa)	E (GPa)	B(GPa)	ν
DU	84	120	110	0.20
U-6Nb	19	52	66	0.37

R.A. Vandermeer, Report Y/DV-207, (Y-12, Oak Ridge, TN, 1982), Thoma, unpublished data

Low pressure experiments show a lack of a well defined HEL in U6Nb

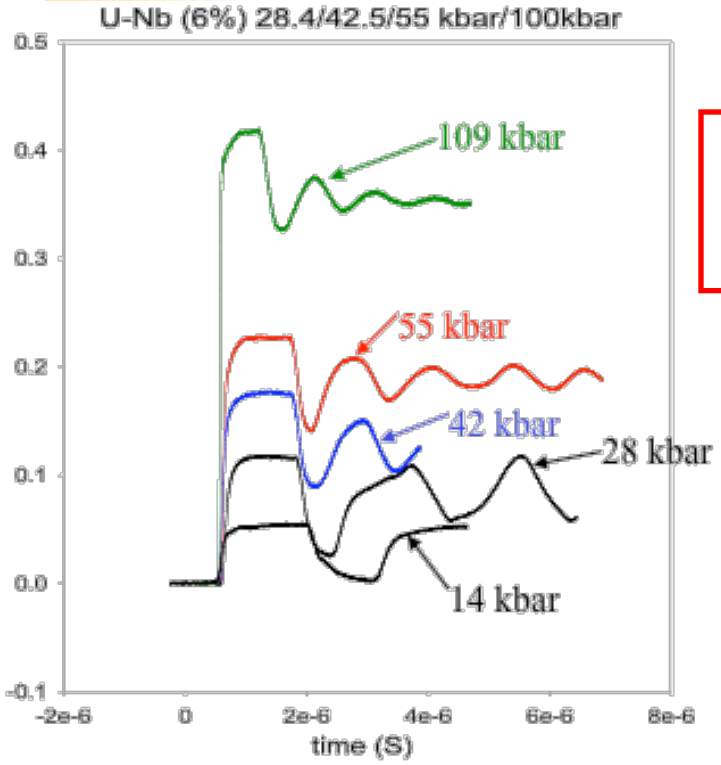

D. B. Hayes, et al: Shock Compression of Condensed Matter-2003,

α" starts to convert to γ° with a hydrostatic pressure of 2 kbar!!

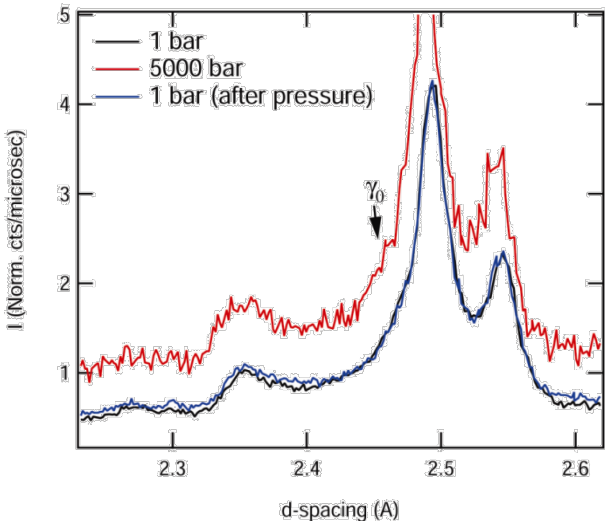

- U-6Nb does not display an HEL (plastic wave overrides the elastic wave)
- Twin alignment has been used to describe the event – profuse twinning observed
- A pressure induced phase change starting at ~2 kbar would be consistent – we see γ^0, γ', and γ like phases in shocked specimens
- Shear strength goes towards zero, consistent with EOS modeling.

Low Pressure Hugoniot Data Leaves the Previously Reported Quadratic U_s-u_p trend

- Could be the result of this material entering a plastic deformation mode in a non-linear way
- Could be that the two wave structure is masked

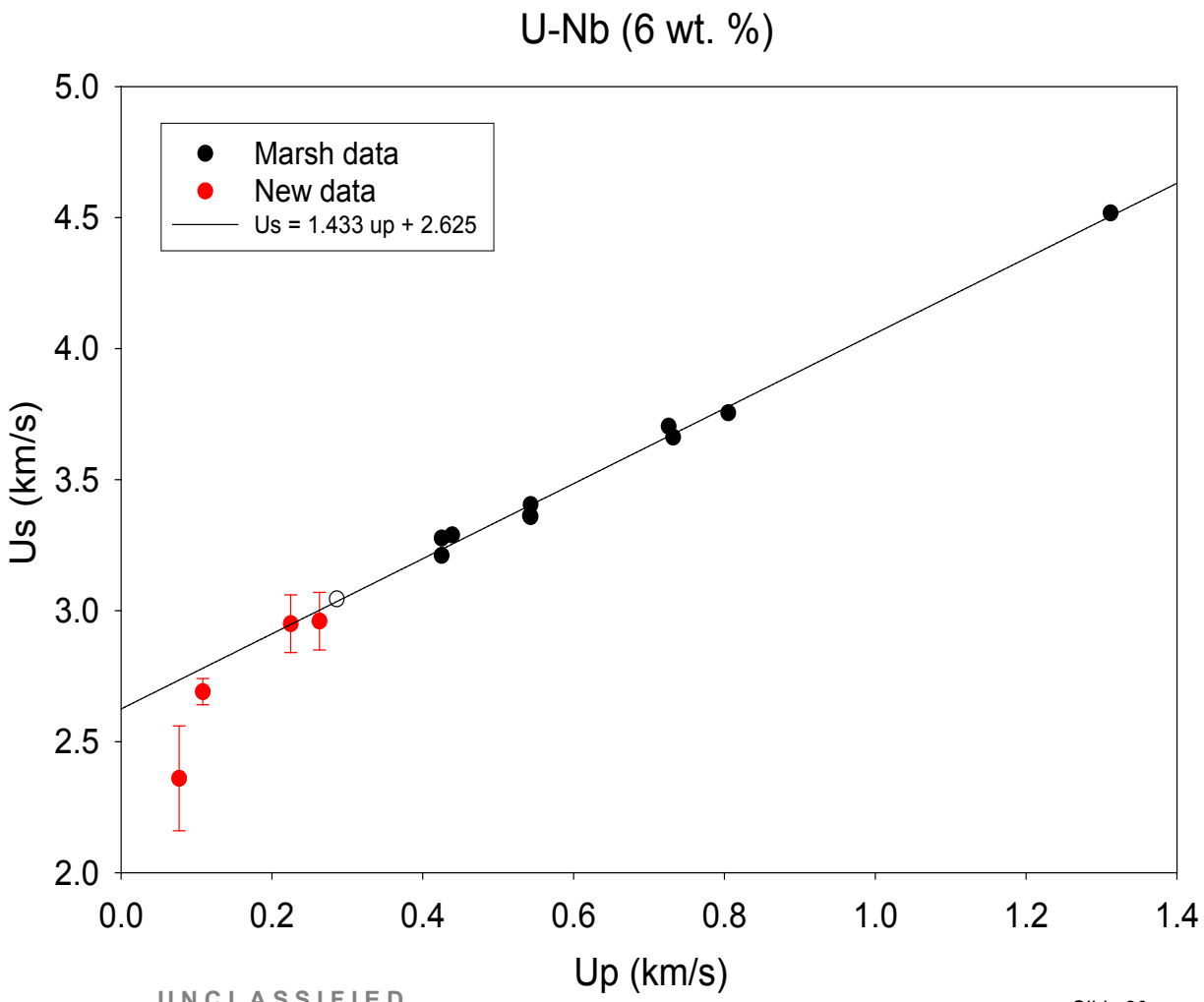

Dynamic experiments on U6Nb indicates a low temperature heat treatment may cause phase stabilization

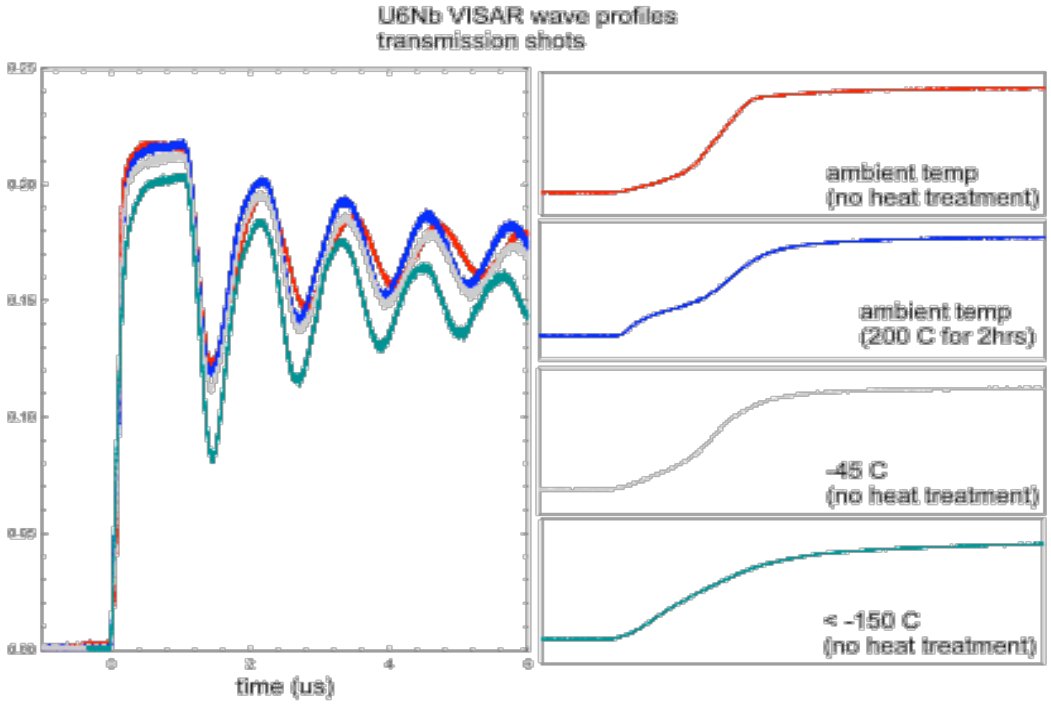

- As quenched and fired at ambient temperature.
  - smeared two wave structure.
  - 1st wave peak pressure at 0.611 GPa.
- As quenched and fired at – 45 ºC.
  - Smeared two wave structure
  - 1st wave peak pressure at 1.16 GPa.
- As quenched and fired at < – 100 ºC.
  - Clear single wave structure.

- As quenched and heat treated at 200 ºC for 2 hours fired at ambient temperature.
  - Shows clear 2 wave structure.
  - 1st wave peak pressure at 2.86 GPa.

Recovery experiments with post experiment metallurgical analysis reveals the ductile failure of U6Nb

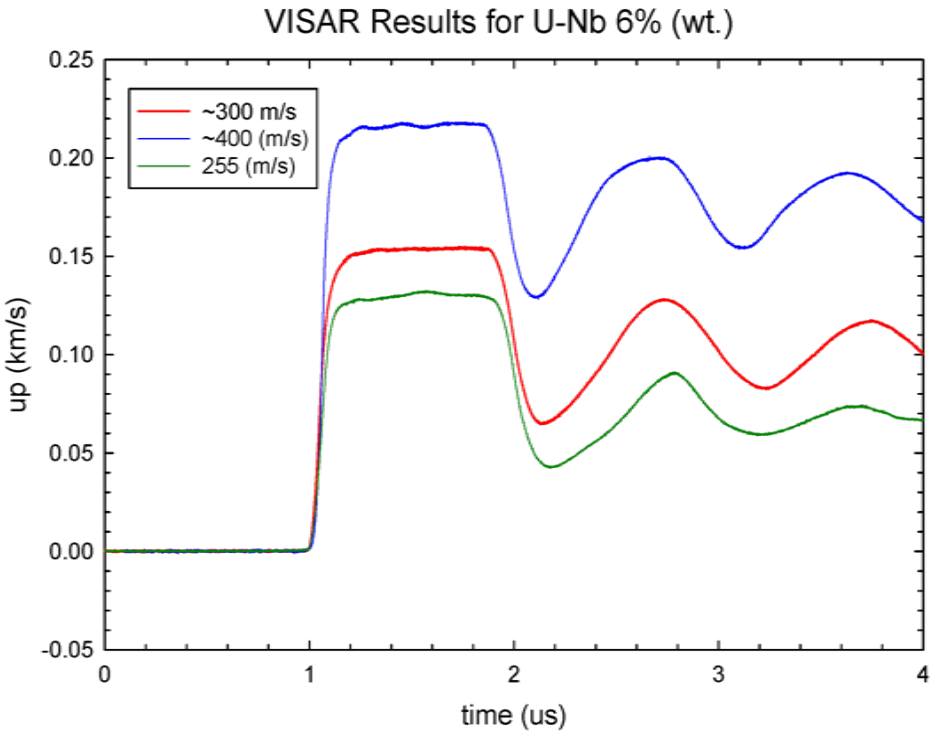

- Area of voids = 0.504 mm^2
- Avg void size = 0.006 mm^2
- Area fraction of voids = 2.4%

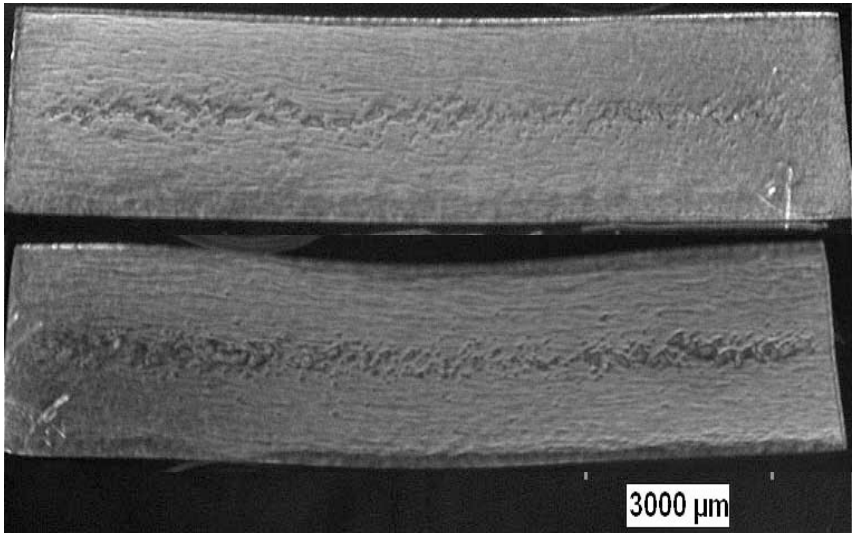

- Area of voids = 0.907 mm^2
- Avg void size = 0.016 mm^2
- Area fraction of voids = 5.2%

U6Nb shows classic ductile damage and coalescence

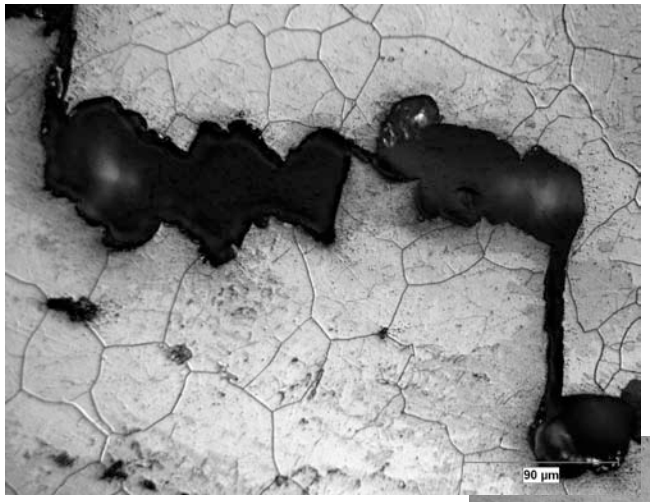

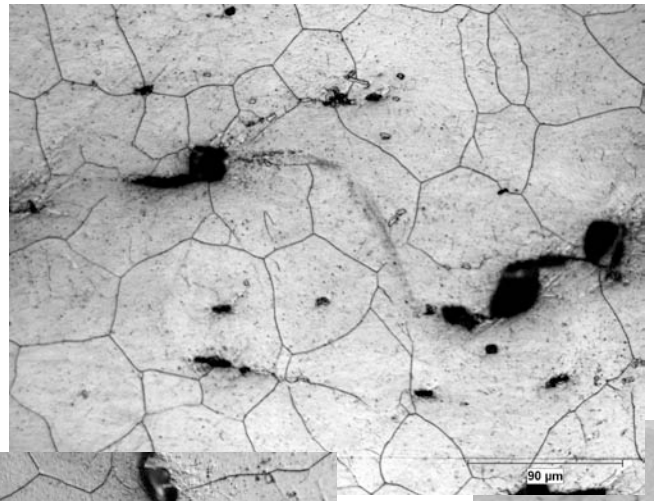

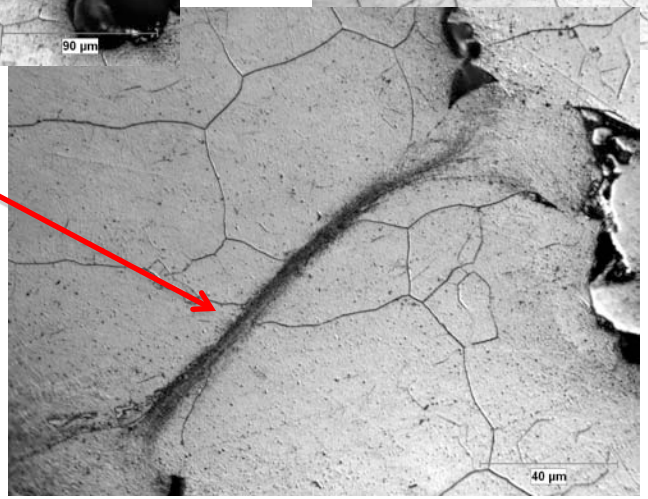

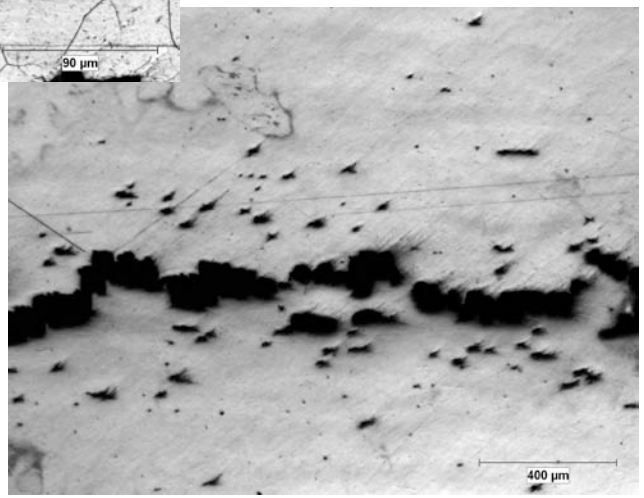

Shear localization and cracking along localizations

SEM of fully spalled U6Nb shows that in many ductile dimples is an inclusion

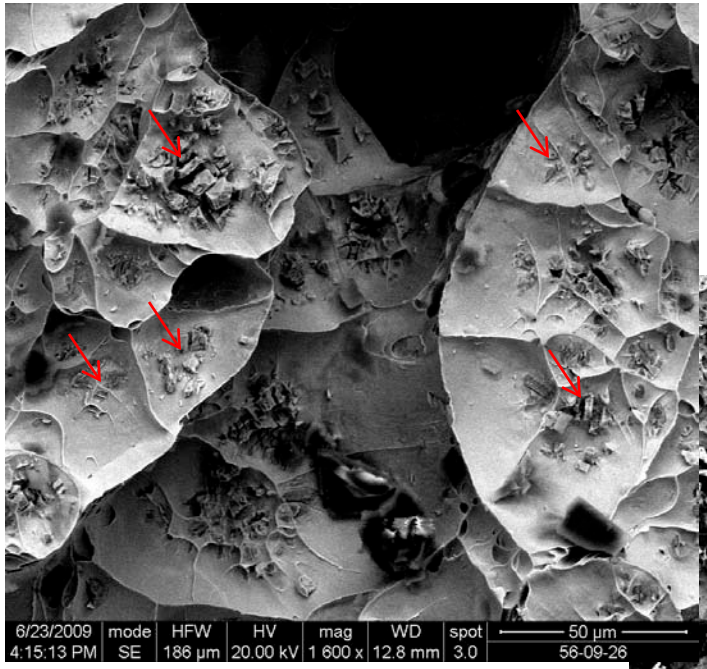

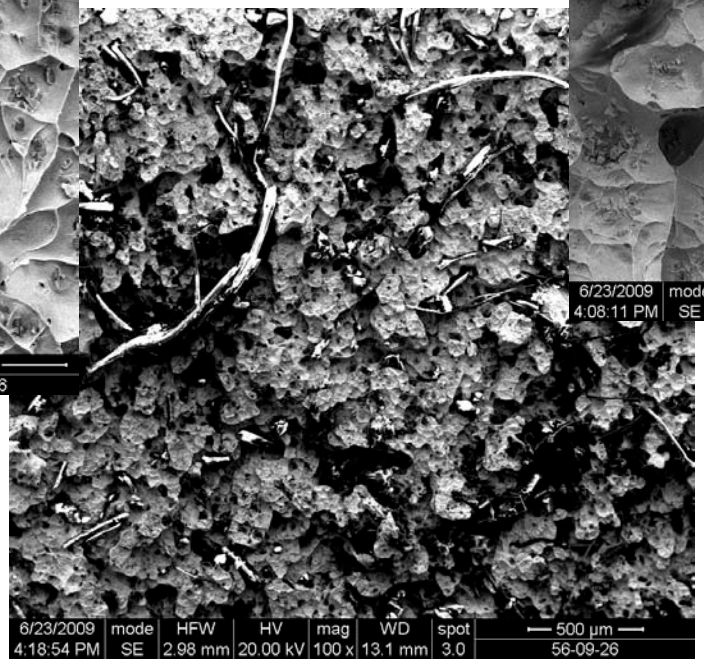

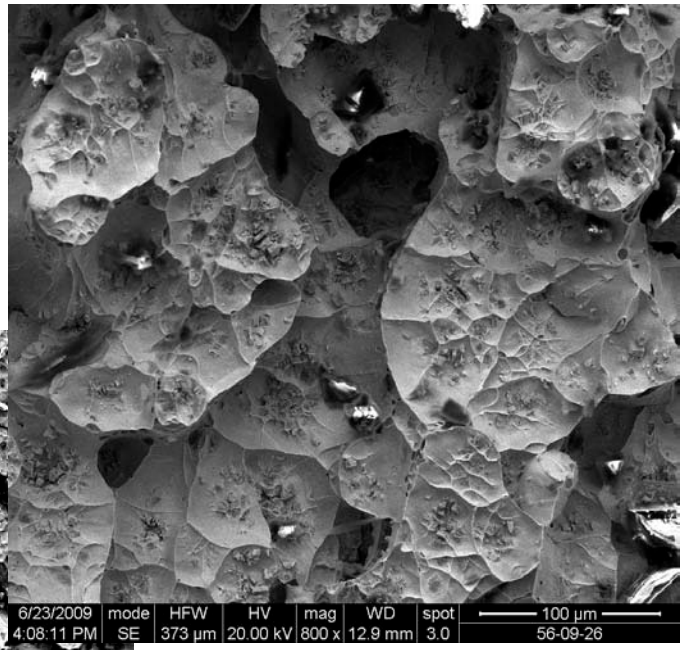

Recovered HE loaded U6Nb was examined metallographically

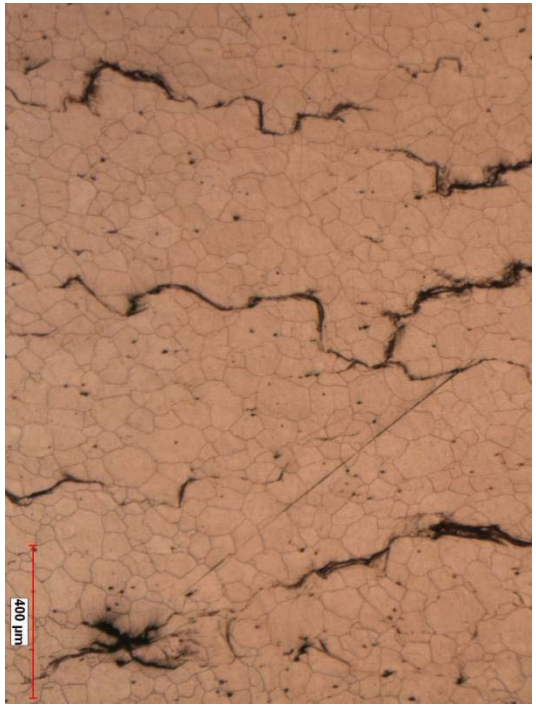

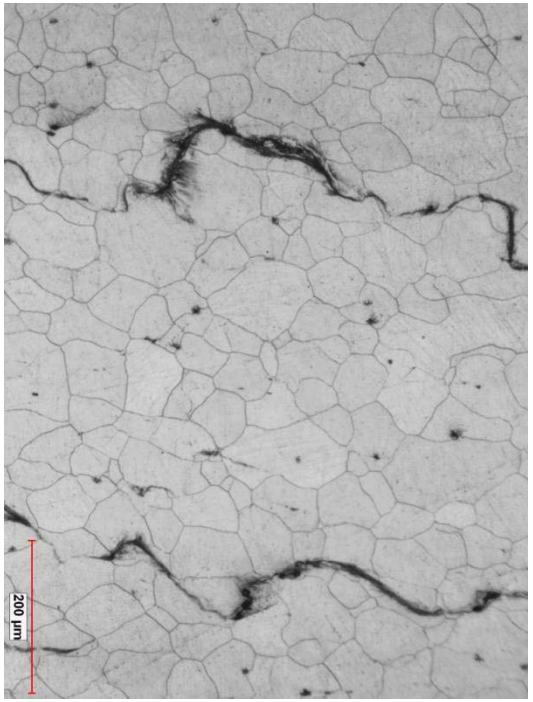

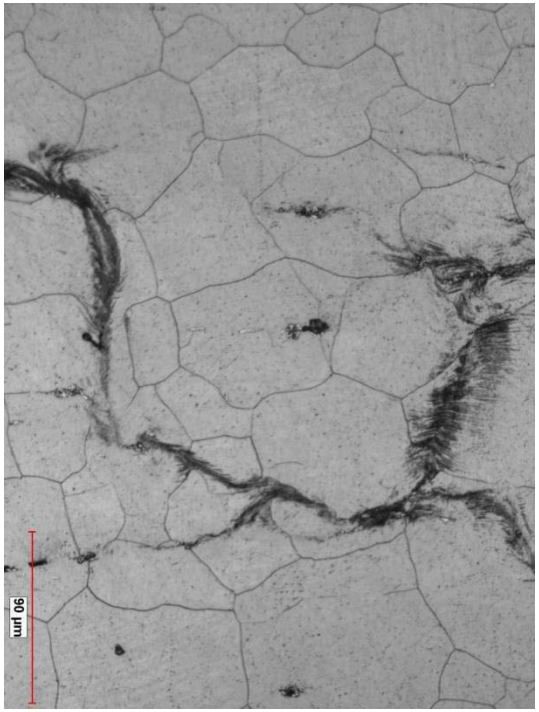

- Multiple incipient spall planes, concentrated toward the back half, free surface of specimen
- Inclusion delamination within the bulk is apparent
- Few obvious voids
- Instead shear localization and cracking along shear localizations between delaminated inclusions

Recovered HE loaded DU was examined metallographically

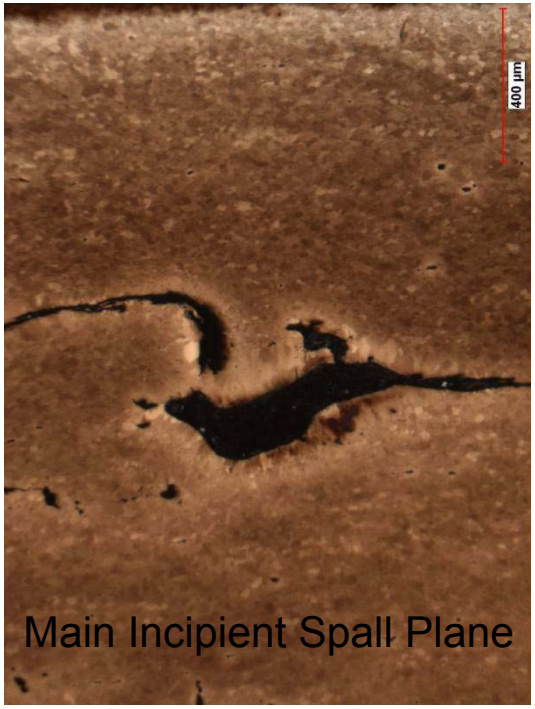

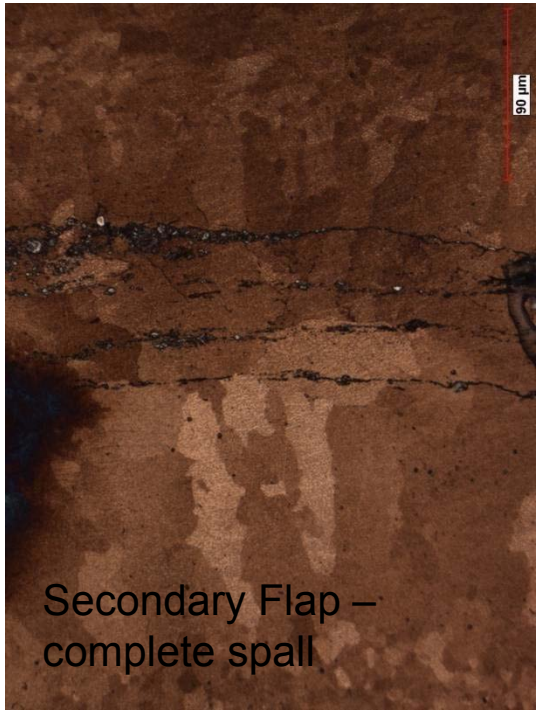

- Significant grain coarsening around cracks in the incipient spall plane
- Significant twinning observed far from incipient spall plane

There are multiple differences between damage in the gas gun and HE drive experiments

- **U6Nb**
  - Gas Gun: clear void nucleation, growth coalescence of voids, some shear localization between voids, 1 spall plane
  - HE Drive: no clear void nucleation, multiple spall planes, of shear localizations linking up delaminated inclusions
- **DU**
  - Gas Gun: as received, mostly brittle failure
  - HE Drive: as-annealed, multiple spall planes, cracking followed by significant grain coarsening around cracks

Summary

- **Shock recovery and reload experiments provide a view to the mechanisms leading to damage in materials subjected to uniaxial shock loading.**
- **A better understanding of material strength and the role of defect kinetics controlling that strength requires further examination.**
  - Defect generation and storage (twinning) leads to Bauschinger effect and quasi-elastic release in DU.
- **New low pressure Hugoniot data provide refinement to the previously reported fits for DU .**
- **DU displays multi-mode damage in shock recovery.**
  - Cracking is intergranular with extremely localized plastic flow connecting crack tips.
  - Connected to inclusions

Summary, Cont.

U-6Nb does not display a HEL at room temperature

- Easy plastic deformation affected by low relative stability of the martensite
  - Deviation of low pressure Hugoniot points supports this.
- Heat-treatment changes the martensite matrix to be consistent with a Nb lean α", raising the austenite start temperature over 125°C, increasing the relative stability – HEL observed
- Lowering the test temperature to liquid nitrogen does not affect twin mobility but does increase relative stability – HEL not observed

The high temperature phase is stabilized after shock loading

- With the temperature-pressure excursion, the martensitic transition back to ambient conditions does not occur
- Retention of the high temperature phase implies a pressure and temperature pathway dependence, possibly involving retained strains

U-Nb 6% (wt.) displays ductile damage in shock recovery.

- SEM of fully spalled sample indicates that void formation is strongly linked to nitride and carbide inclusions.

Microstructural Evolution of Polycrystalline Tantalum Exposed to Large Deformation Shear

C. A. Bronkhorst, B. L. Hansen,
Theoretical Division

A. R. Ross, E. K. Cerreta, J. F. Bingert
Materials Science & Technology Division

Los Alamos National Laboratory

JOWOG 32Mat
LLNL
25-29 January 2010

Official Use Only

Outline

- Motivation and challenge
- Macro-scale experiments
- Continuum isotropic constitutive model
  - Anisotropic MTS
- Thermo-viscoplastic single crystal model
  - Thermally activated slip
- Embedded polycrystal forced shear simulations
- Comparison to experimental results
- Summary & comments

Challenge of linking microstructure to performance

Ta Plate Impact

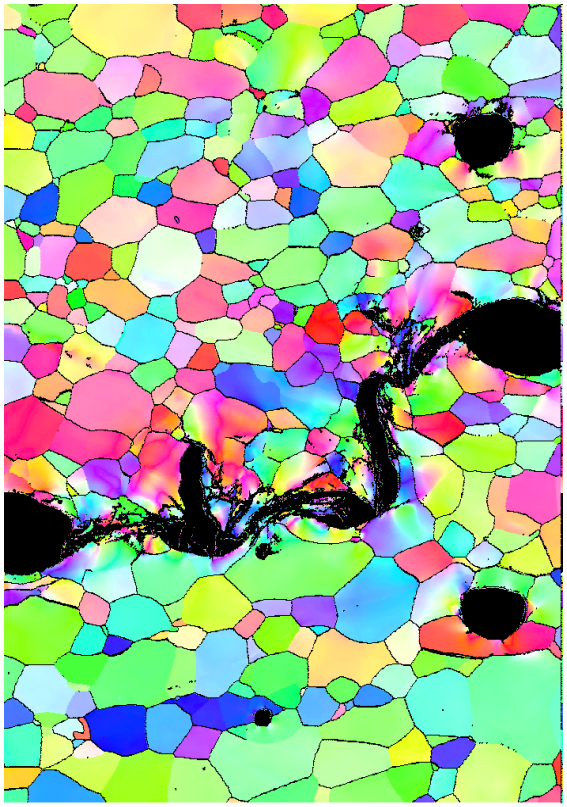

B. Henrie

Cu Plane Strain Compression

Undeformed

ε = -1.5

- The ductile failure process generally involves localization, porosity initiation, porosity growth, and coalescence dominated by localized deformation.
- These events occur at the length scale of the single crystal.

Forced shear experiments

- Axisymmetric, Split-Hopkinson
- Top-to-bottom loading, 10-25 m/s
- Tantalum plate, residual texture (Chen & Gray, 1996; Maudlin et al., 1999), grain size 42 μm
- -100 °C and 25 °C

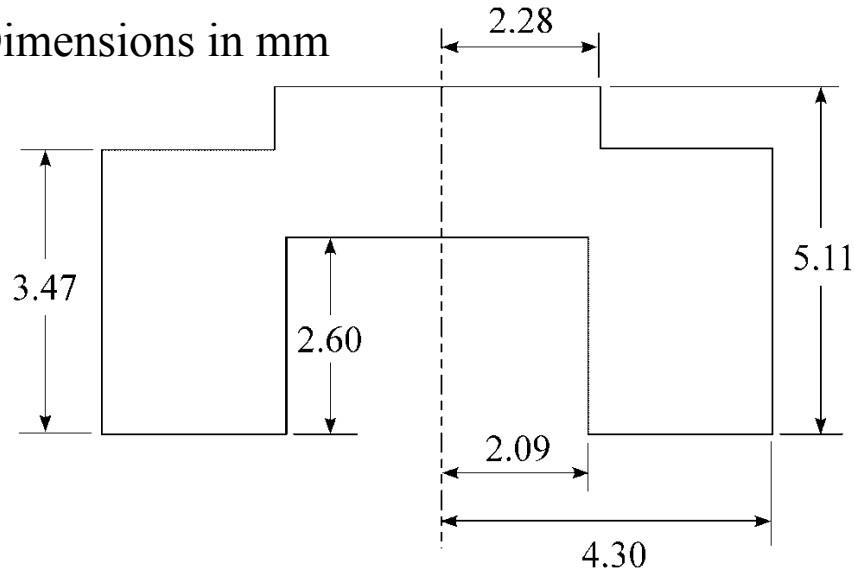

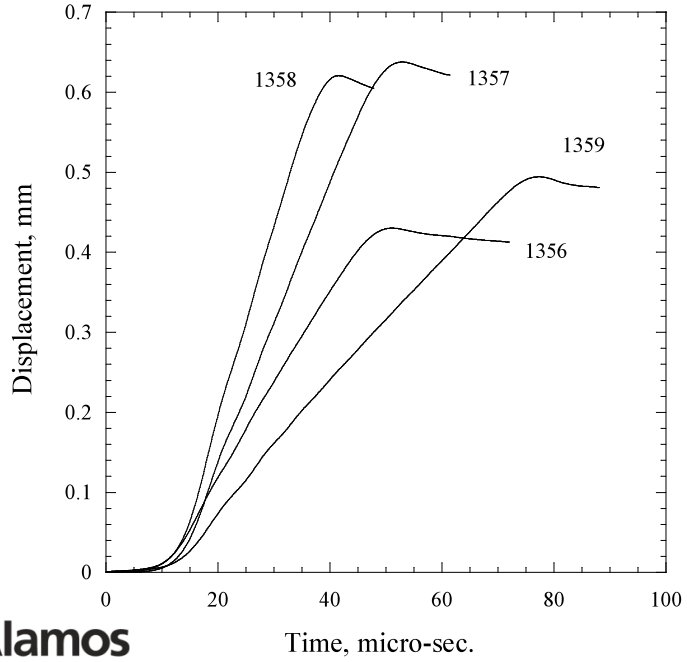

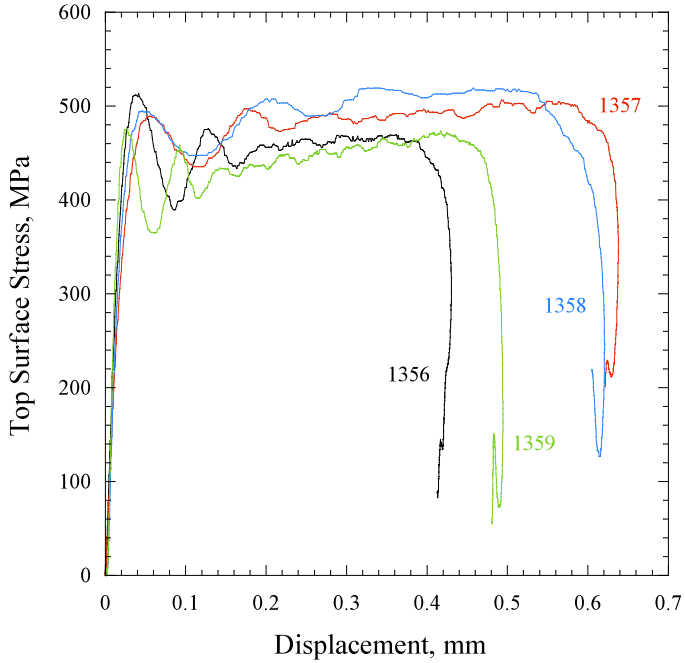

Numerical model with boundary conditions

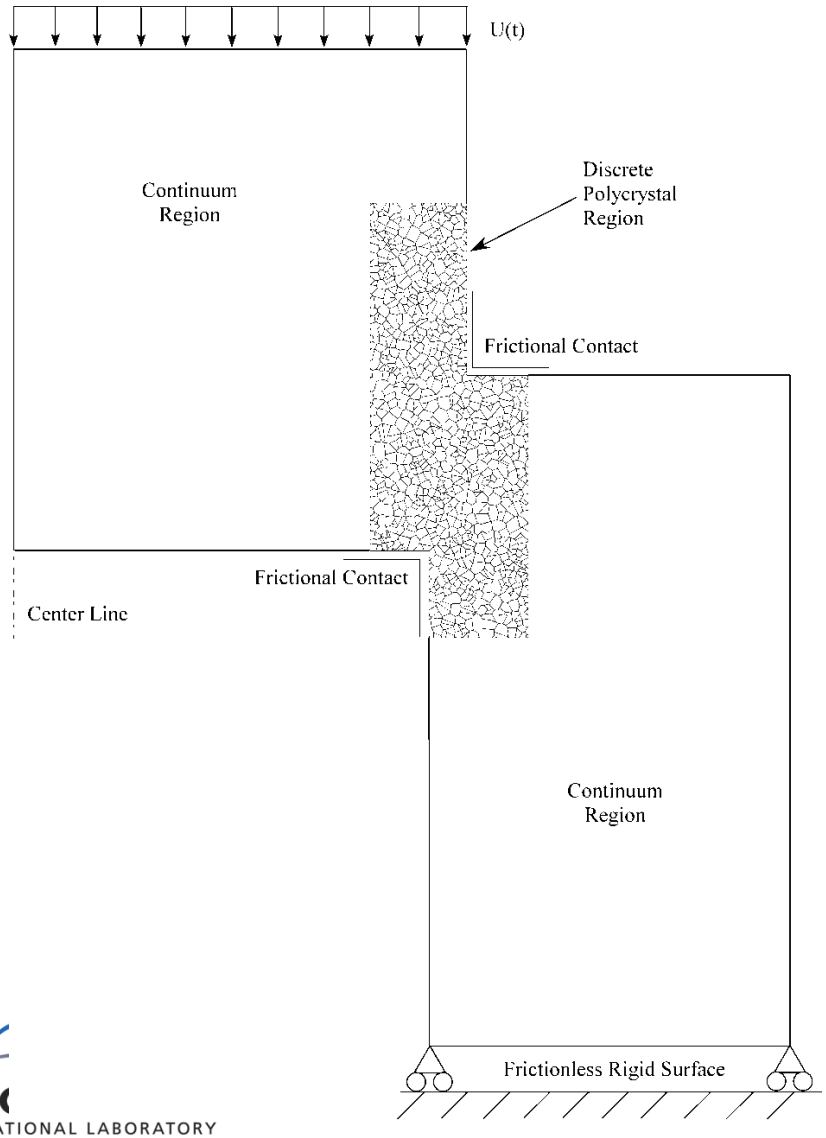

- Axisymmetric, 3 node linear elements for shear zone
- Adiabatic
- Embedded 1091 grain polycrystal region
- 40 μm grain size
- ~ 7 μm element size
- Rate-dependent isotropic continuum regions
- Frictionless contact surfaces at corners
- ABAQUS - implicit used but dynamic displacement rate applied
- 3 crystallographic realizations

Small strain continuum model for the inner and outer regions

Stress

$$\dot{\boldsymbol{\sigma}} = \underline{\mathbf{C}}\dot{\boldsymbol{\varepsilon}}^{e}$$

Strain

$$\dot{\boldsymbol{\varepsilon}} = \dot{\boldsymbol{\varepsilon}}^{e} + \dot{\boldsymbol{\varepsilon}}^{p}$$

Normality Flow

$$\dot{\boldsymbol{\varepsilon}}^{p} = \frac{3}{2}\dot{\bar{\varepsilon}}^{p}\frac{\boldsymbol{\sigma}'}{\bar{\sigma}}$$

Flow Surface

$$\bar{\sigma} - \sigma_{f}\left(\dot{\bar{\varepsilon}}^{p}, \theta\right) = 0$$

$$\bar{\sigma} = \sqrt{\tfrac{3}{2}\sigma' \cdot \sigma'}$$

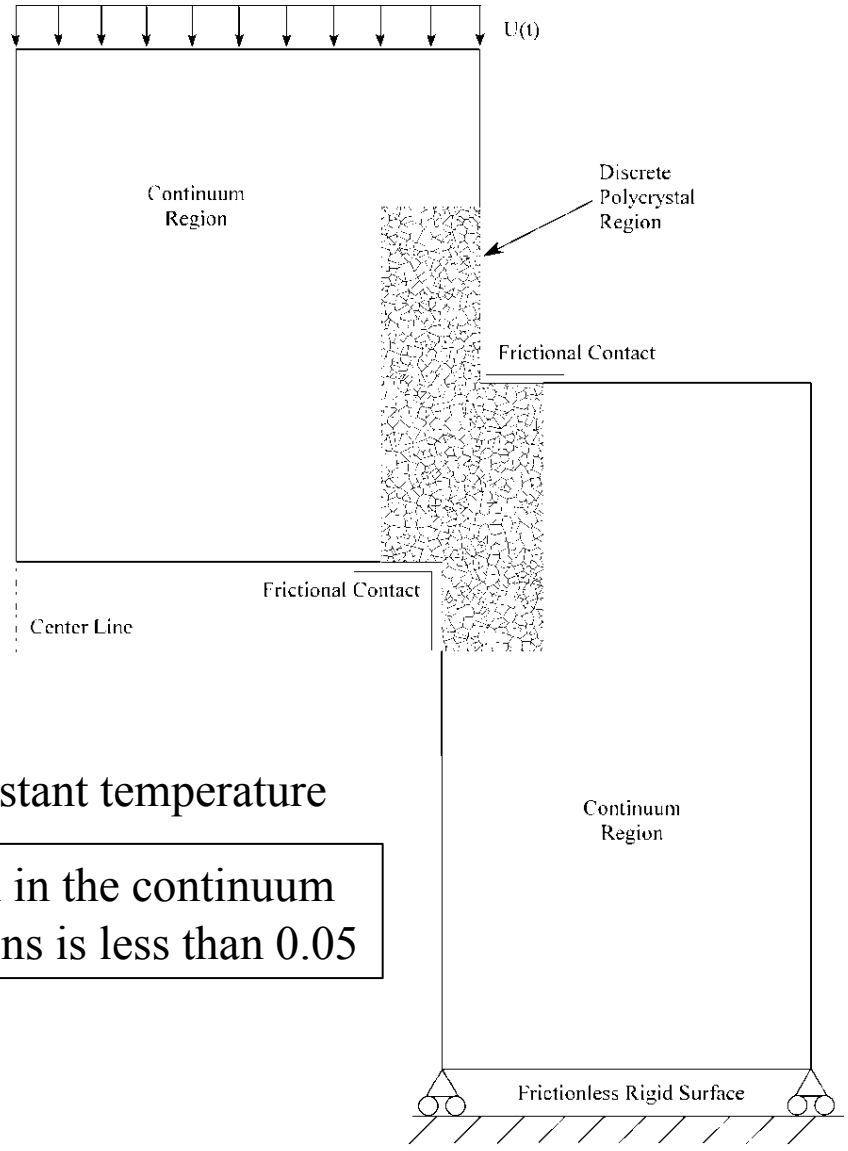

Constant temperature

Strain in the continuum Regions is less than 0.05

MTS model - continuum

Follansbee & Kocks, 1988; Chen & Gray, 1996; Maudlin et al., 1999

$$\sigma_f = \sigma_a + \frac{\mu}{\mu_0}\left(S_i\left(\dot{\varepsilon},\theta\right)\hat{\sigma}_i + S_\varepsilon\left(\dot{\varepsilon},\theta\right)\hat{\sigma}_\varepsilon\right)$$

$\sigma_a = 40$ MPa $\hat{\sigma}_i = 1203,\ 167$ MPa $\hat{\sigma}_\varepsilon = 0$

$$\mu = \mu_0 - \frac{D_0}{\exp\left(\frac{\theta_0}{\theta}\right) - 1}$$

$\mu_0 = 65.25$ GPa
$D_0 = 0.38$ GPa
$\theta_0 = 40$ °K

$$S_i\left(\dot{\varepsilon},\theta\right) = \left(1 - \left[\frac{k\theta}{\mu b^3 g_{0i}} \ln\left(\frac{\dot{\varepsilon}_{0i}}{\dot{\varepsilon}}\right)\right]^{1/q_i}\right)^{1/p_i}$$

$$S_\varepsilon\left(\dot{\varepsilon},\theta\right) = \left(1 - \left[\frac{k\theta}{\mu b^3 g_{0\varepsilon}} \ln\left(\frac{\dot{\varepsilon}_{0\varepsilon}}{\dot{\varepsilon}}\right)\right]^{1/q_\varepsilon}\right)^{1/p_\varepsilon}$$

$b = 2.863$ Å
$g_{0i} = 0.1236\ ,\ 5.1463$
$\dot{\varepsilon}_{0i} = \dot{\varepsilon}_{0\varepsilon} = 10^7\ \text{s}^{-1}$
$q_i = 3/2$
$p_i = 1/2$
$q_\varepsilon = 1$
$p_\varepsilon = 2/3$

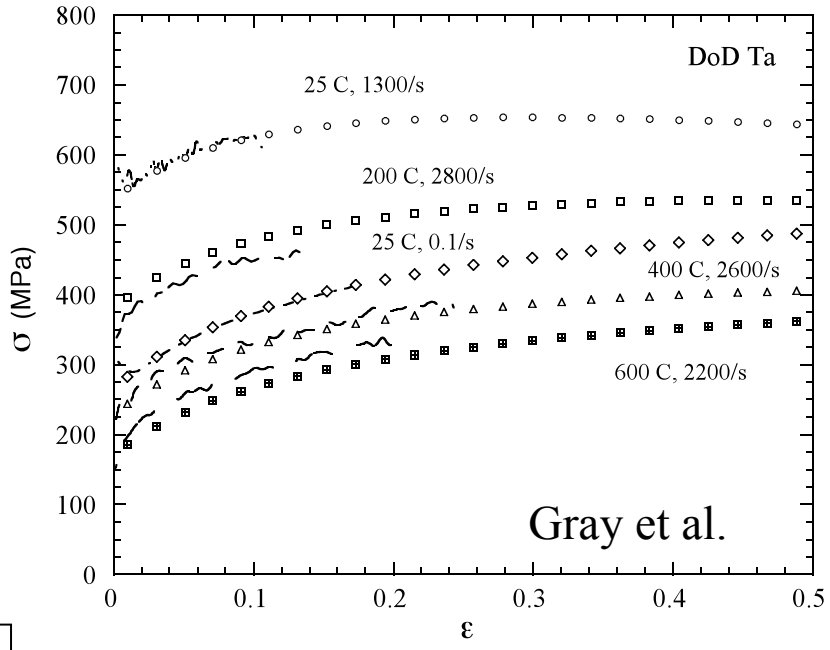

$$\frac{d\hat{\sigma}_\varepsilon}{d\varepsilon} = h_0\left(1 - \frac{\hat{\sigma}_\varepsilon}{\hat{\sigma}_{\varepsilon s}}\right)^\kappa$$

$$\frac{\hat{\sigma}_{\varepsilon s}}{\hat{\sigma}_{\varepsilon s_0}} = \left(\frac{\dot{\varepsilon}}{\dot{\varepsilon}_{0_{\varepsilon s}}}\right)^{\frac{kT}{\mu b^3 g_{0_{\varepsilon s}}}}$$

$h_0 = 2.0$ GPa
$\kappa = 3$
$\hat{\sigma}_{\varepsilon s_0} = 350$ MPa
$\dot{\varepsilon}_{0_{\varepsilon s}} = 10^7$
$g_{0_{ss}} = 1.6$

Shear zone single crystal model

Asaro & Rice (1977) , Acharya & Beaudoin (2000),
Kothari & Anand (1998), Busso et al. (2000), Kocks (1976)
Kalidindi et al. (1992), Bronkhorst et al. (1992), Anand (1998)

Stress

$$\mathbf{T}^* = \mathbb{L} \left[\mathbf{E}^* - \mathbf{A}\left(\theta - \theta_0\right) \right]$$

$$\mathbf{T}^* \equiv \mathbf{F}^{*-1}\left(\det \mathbf{F}^*\right)\mathbf{T}\mathbf{F}^{*-T}$$

$$\mathbf{E}^* \equiv \frac{1}{2}\left(\mathbf{F}^{*T}\mathbf{F}^* - \mathbf{1}\right)$$

$$\mathbf{F}^* = \mathbf{F}\mathbf{F}^{p^{-1}}$$

Texture

$$\mathbf{m}^\alpha = \mathbf{F}^* \mathbf{m}_0^\alpha$$

$$\mathbf{n}^\alpha = \mathbf{F}^{*-T} \mathbf{n}_0^\alpha$$

Hardening

$$\dot{s}^\alpha = \sum_\beta h^{\alpha\beta} \left| \dot{\gamma}^\beta \right| \qquad h^{\alpha\beta} = \left[r + \left(1 - r\right)\delta^{\alpha\beta} \right] h^\beta$$

$$h^\beta = h_o \left(\frac{s_s^\beta - s^\beta}{s_s^\beta - s_0^\beta} \right)$$

$$s_s^\beta = \hat{s}_s^\beta \left(\dot{\gamma}, \theta\right) = s_{s_0} \left(\frac{\dot{\gamma}^\beta}{\dot{\gamma}_0} \right)^{\frac{k\theta}{A}}$$

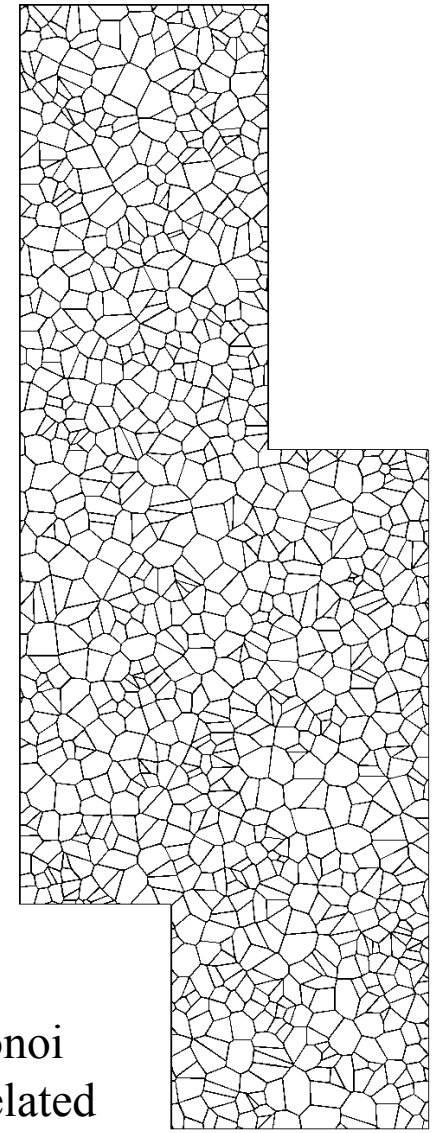

Voronoi tesselated

1091 grains

Shear zone single crystal model

Asaro & Rice (1977) , Acharya & Beaudoin (2000),
Kothari & Anand (1998), Busso et al. (2000), Kocks (1976)
Kalidindi et al. (1992), Bronkhorst et al. (1992), Anand (1998)

Flow Rule

$$\mathbf{L}^p = \dot{\mathbf{F}}^p \mathbf{F}^{p^{-1}} = \sum_\alpha \dot{\gamma}^p \mathbf{S}_0^\alpha \qquad \mathbf{S}_0^\alpha \equiv \mathbf{m}_0^\alpha \otimes \mathbf{n}_0^\alpha$$

$$\dot{\gamma}^\alpha = \dot{\gamma}_0 \exp\left[-\frac{F_0}{k\theta}\left\langle 1 - \left\langle \frac{\left|\tau^\alpha\right| - s^\alpha \dfrac{\mu}{\mu_0}}{s_l^\alpha \dfrac{\mu}{\mu_0}} \right\rangle^p \right\rangle^q\right] \operatorname{sgn}\left(\tau^\alpha\right)$$

$$\tau^\alpha \equiv \left(\mathbf{C}^* \mathbf{T}^*\right) \cdot \mathbf{S}_0^\alpha$$

$$\mathbf{C}^* = \mathbf{F}^{*^T} \mathbf{F}^*$$

$$\frac{\mu}{\mu_0} \cong \frac{C_{12}}{C_{12_0}} = 1 + \frac{m_{12}}{C_{12_0}}\theta$$

Adiabatic Heating

$$\dot{\theta} = \frac{\eta}{\rho c_p} \sum_\alpha \tau^\alpha \dot{\gamma}^\alpha$$

Simmons & Wang, 1971

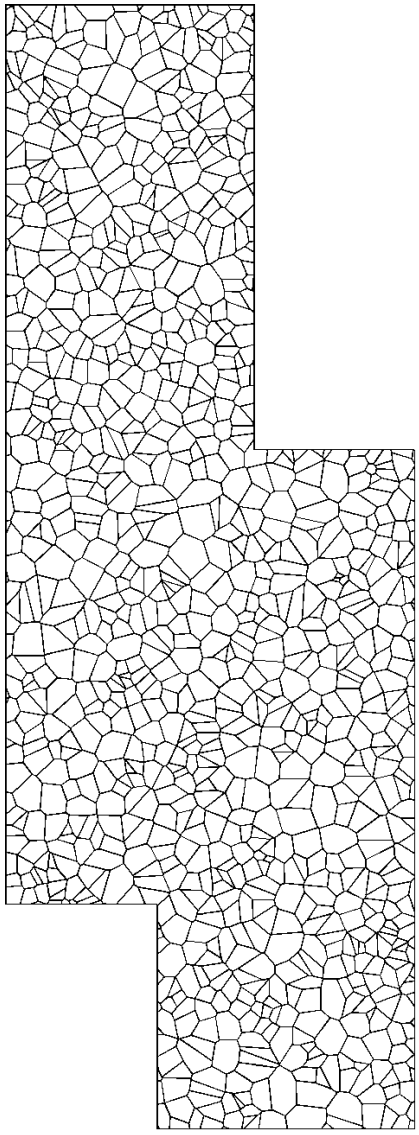

900 μm between corners

Single crystal model - Ta

Material Parameter Evaluation
512 Elements/Grains

Single Crystal Model

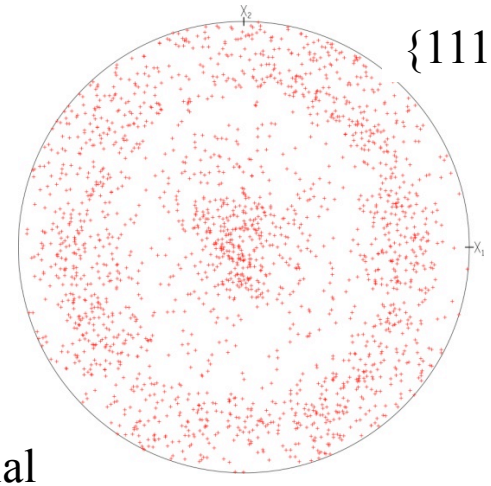

Initial Texture

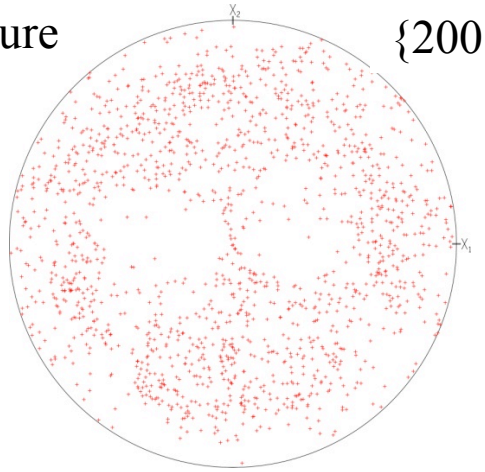

$\rho = 16640$ kg/m^3
$c_p = 150$ J/kg-K
$\alpha = 6.5$ μm/m-K
$\eta = 0.0, 0.95$
$m_{11} = -24.5$ MPa/K
$C_{11_0} = 268.5$ GPa
$m_{12} = -11.8$ MPa/K
$C_{12_0} = 159.9$ GPa
$m_{44} = -14.9$ MPa/K
$C_{44_0} = 87.1$ GPa
$r = 1.4$

$\dot{\gamma}_0 = 10^7$ sec^{-1}
$s_0 = 50$ MPa
$s_l = 550$ MPa
$F_0 = 2.1\times10^{-19}$ J
$p = 0.34$
$q = 1.66$
$s_{s_0} = 125$ MPa
$h_{s_0} = 300$ MPa
$A = 10^{-18}$ J

Ta - 24 BCC systems
{110}<111> , {112}<111>

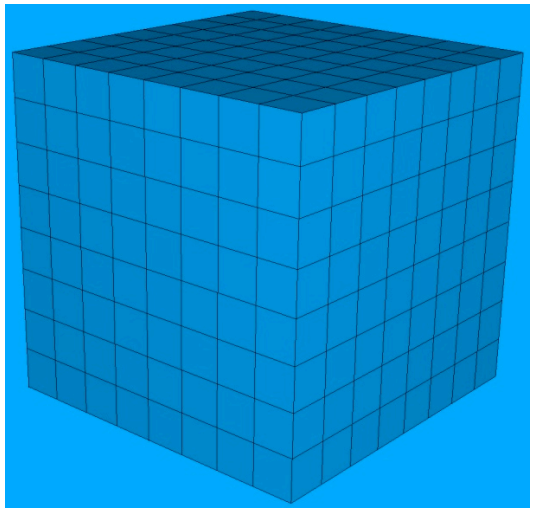

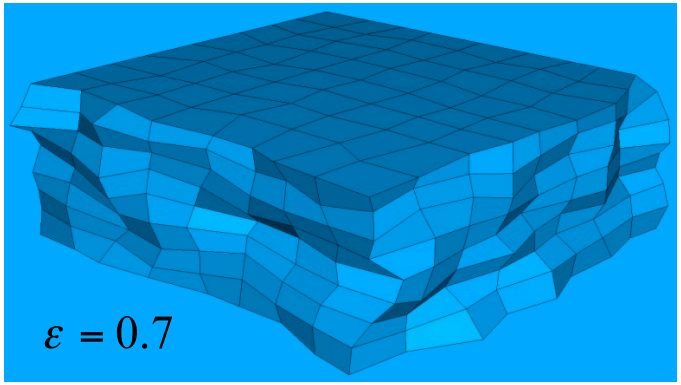

Single crystal model - Ta

Single Crystal Model

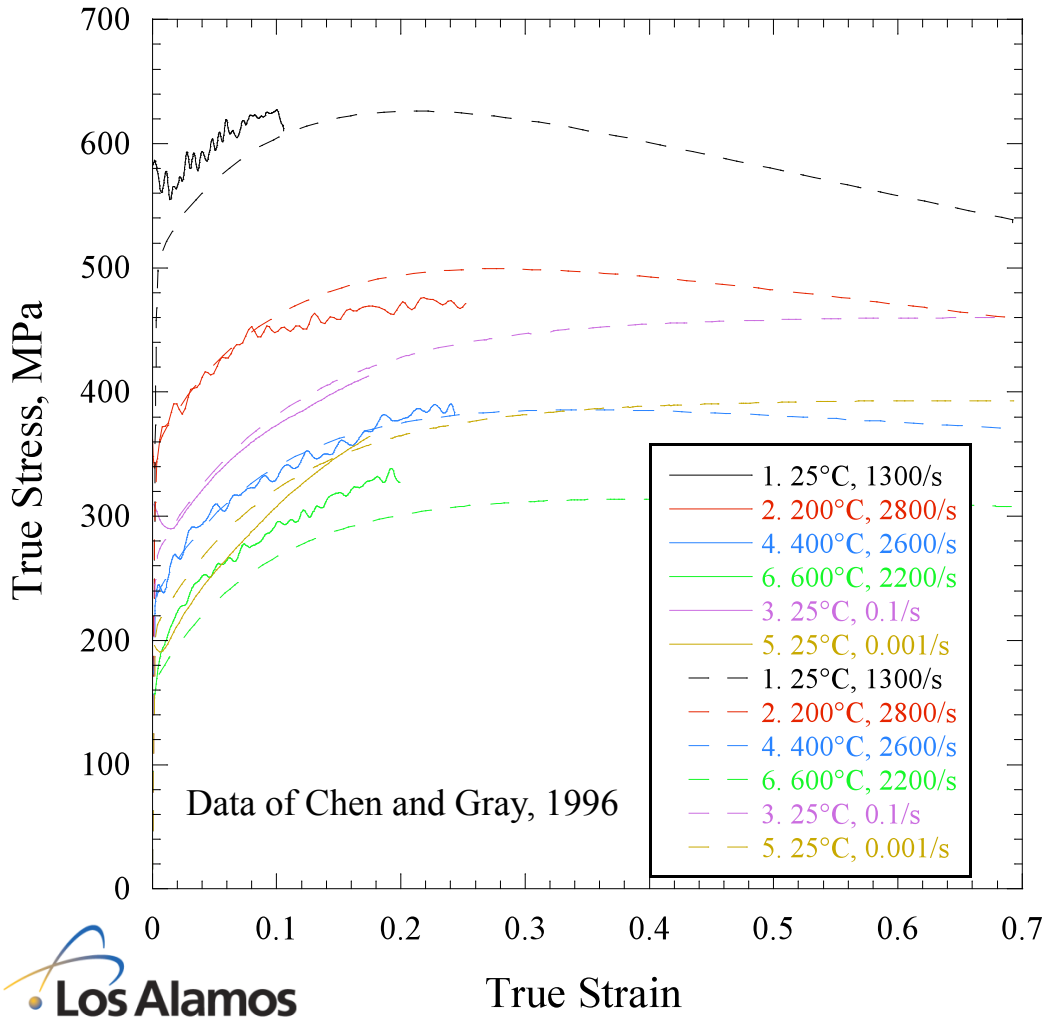

Material Parameter Evaluation

Ta - 24 BCC systems
{110}<111> , {112}<111>

$\rho = 16640$ kg/m^3
$c_p = 150$ J/kg-K
$\alpha = 6.5$ μm/m-K
$\eta = 0.0, 0.95$
$m_{11} = -24.5$ MPa/K
$C_{11_0} = 268.5$ GPa
$m_{12} = -11.8$ MPa/K
$C_{12_0} = 159.9$ GPa
$m_{44} = -14.9$ MPa/K
$C_{44_0} = 87.1$ GPa

$r = 1.4$
$\dot{\gamma}_0 = 10^7$ sec^{-1}
$s_0 = 50$ MPa
$s_l = 550$ MPa
$F_0 = 2.1\times10^{-19}$ J
$p = 0.34$
$q = 1.66$
$s_{s_0} = 125$ MPa
$h_{s_0} = 300$ MPa
$A = 10^{-18}$ J

Experimental load-displacement response is over-predicted

- Although the loading rate difference is described, overall the model over-predicts the magnitude of load required to deform the sample.
- This is believed to be caused primarily by 2D representation.
- The single crystal model could also be inadequate to well represent this level of detail.

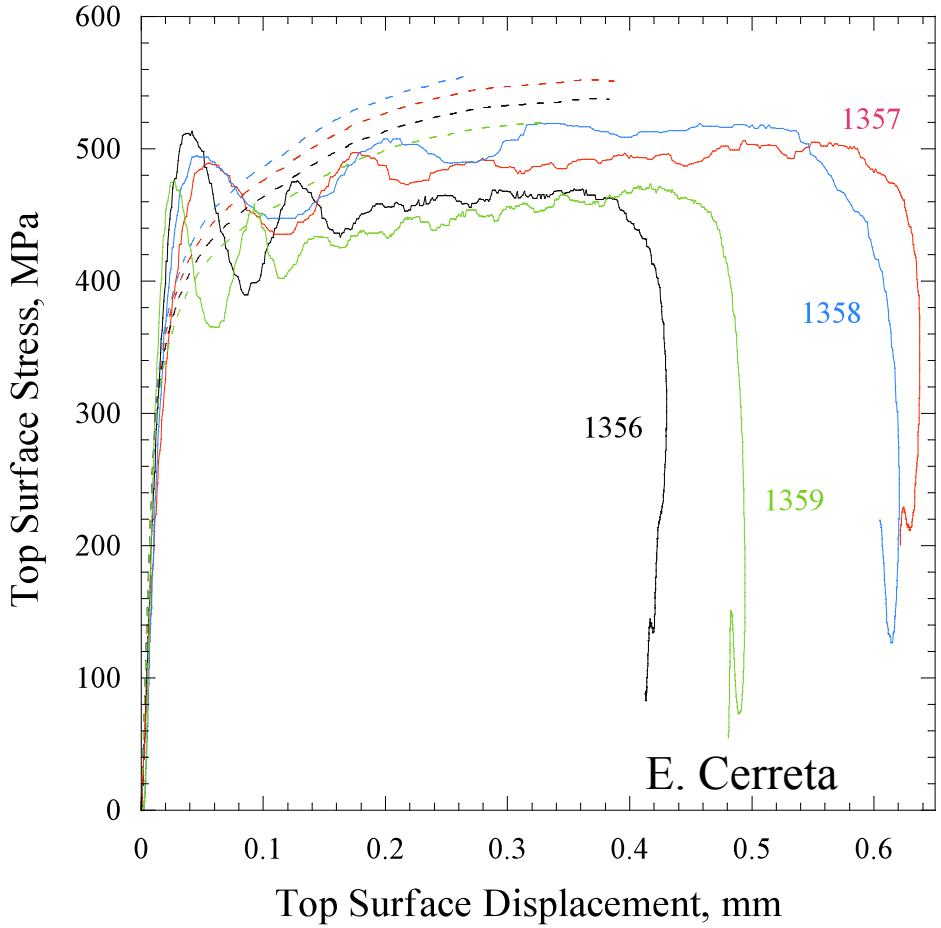

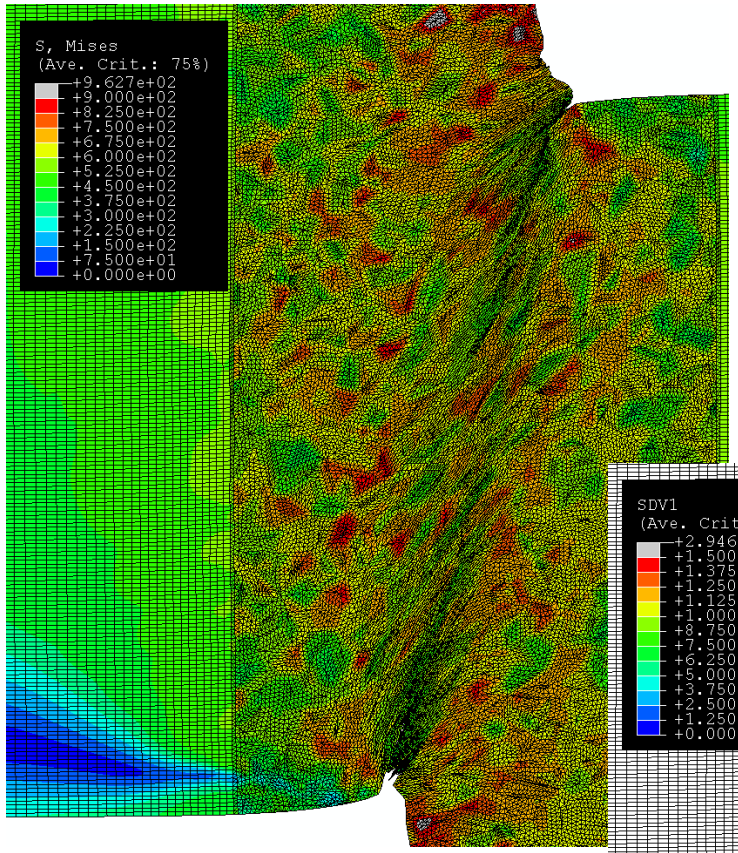

Realization 1

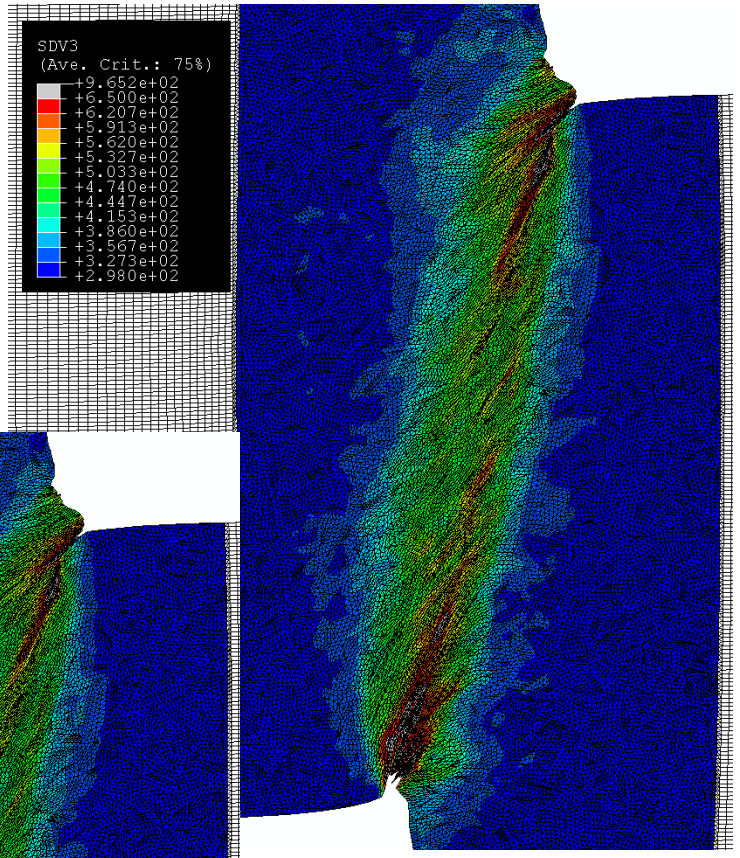

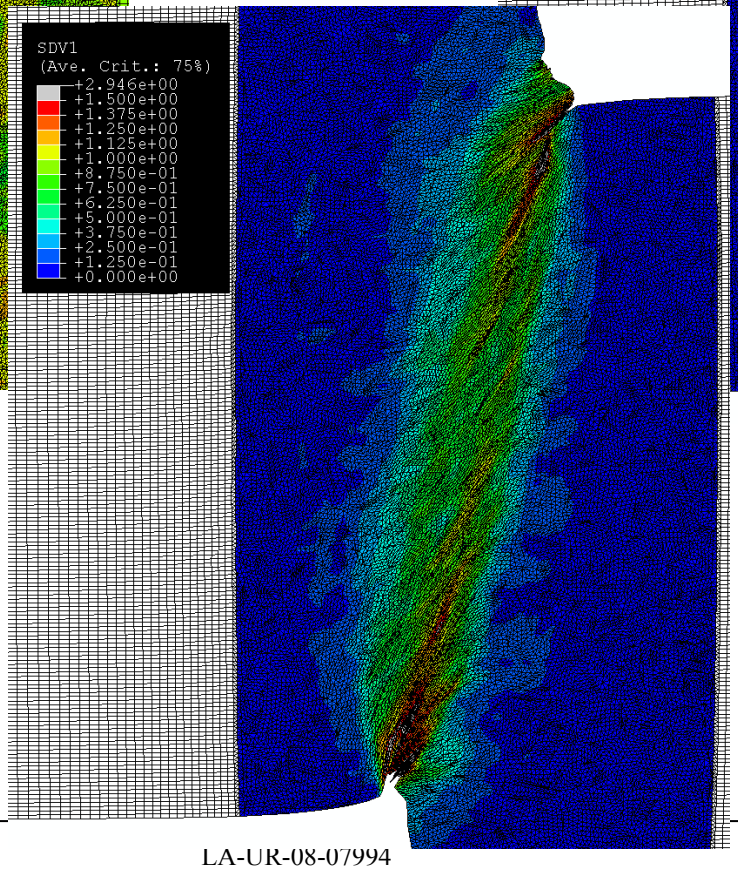

Mises Stress, MPa

Temp., K

Eq. Pl. Strain

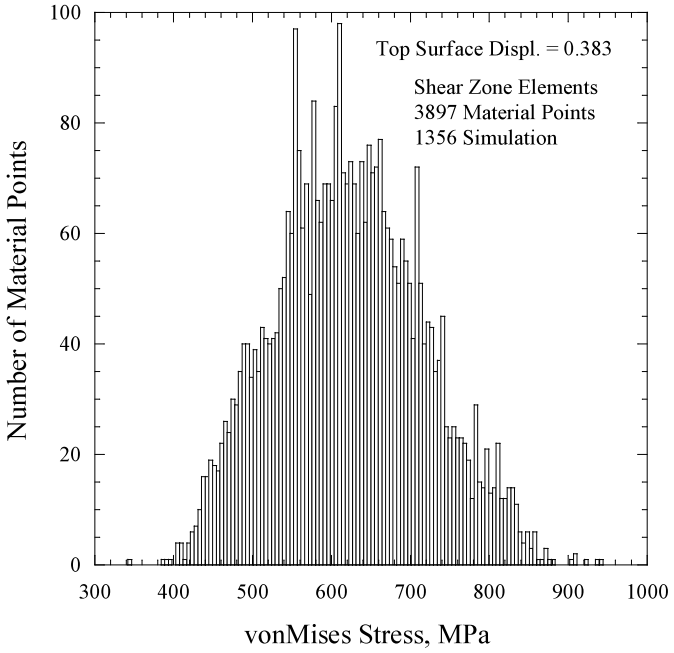

Realization 1

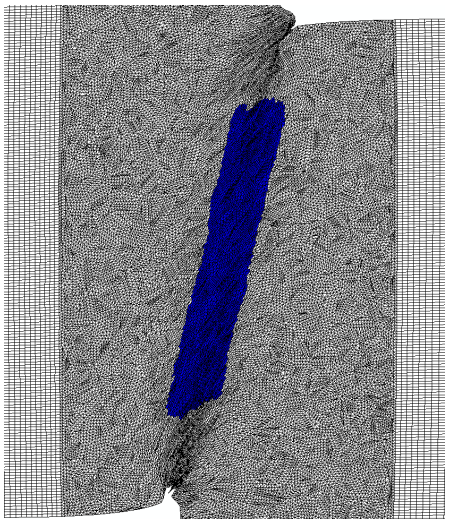

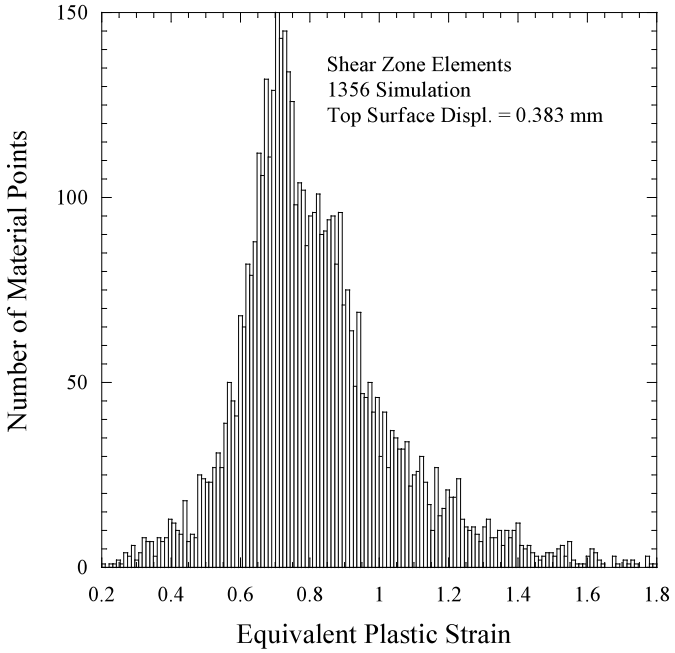

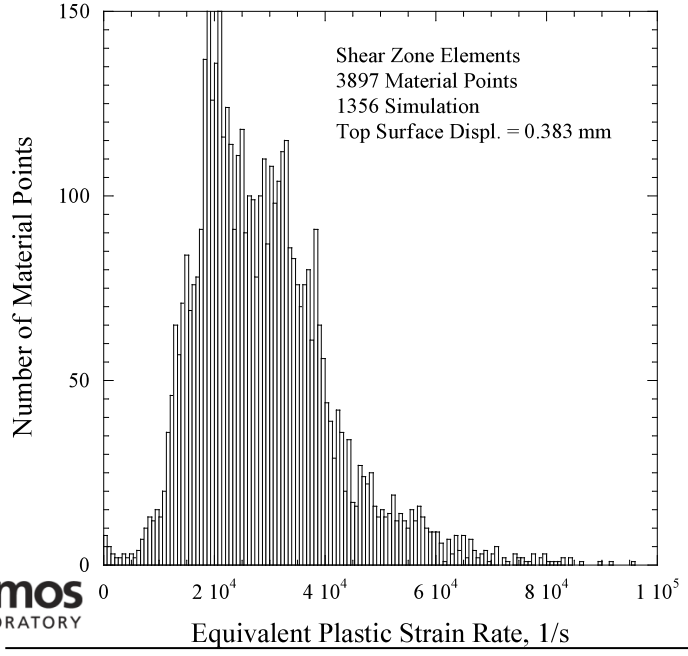

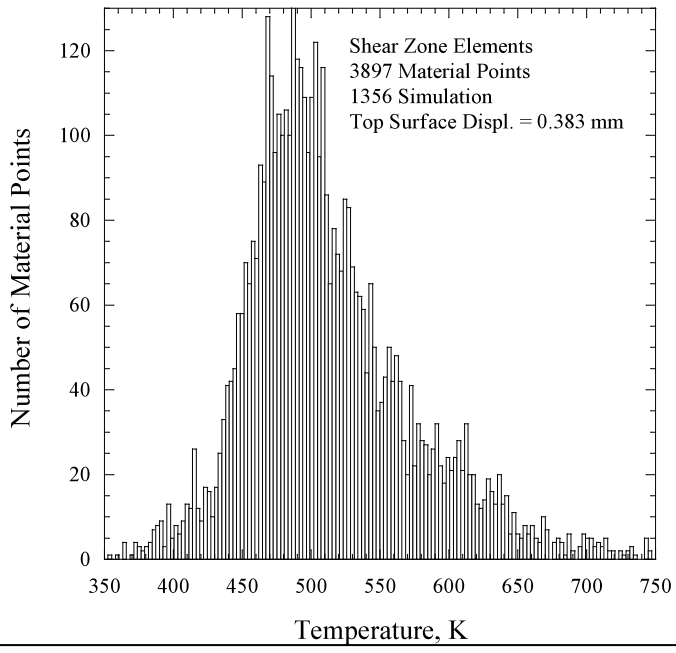

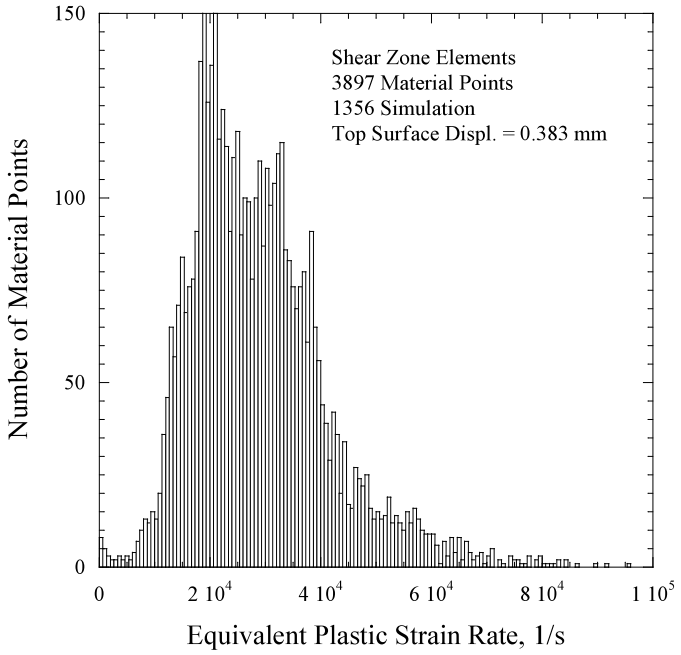

Realization 1

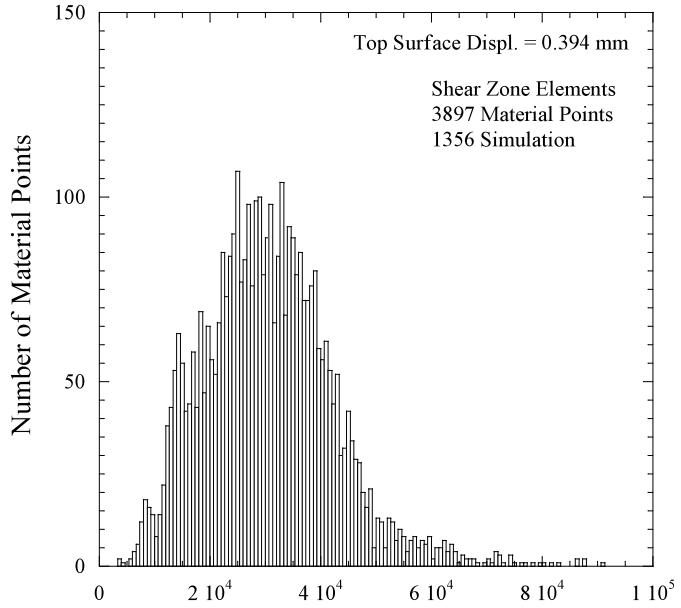

Realization 3

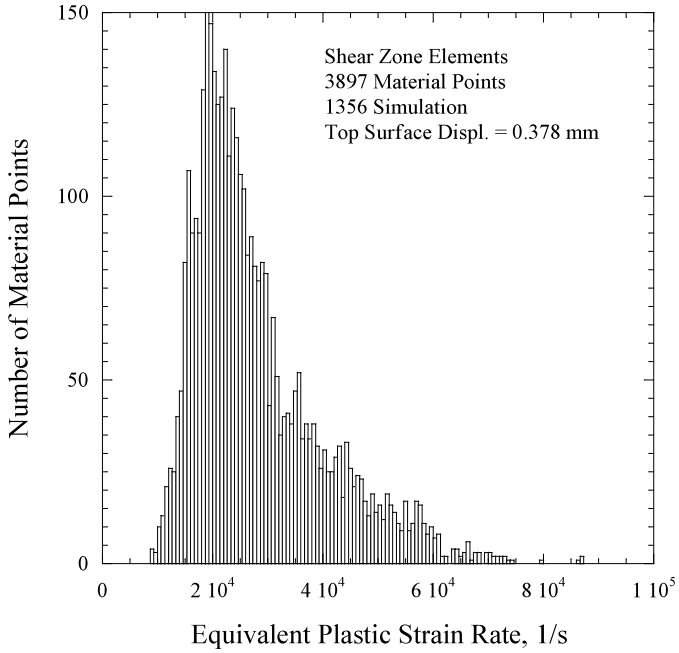

Realization 2

Realization 1

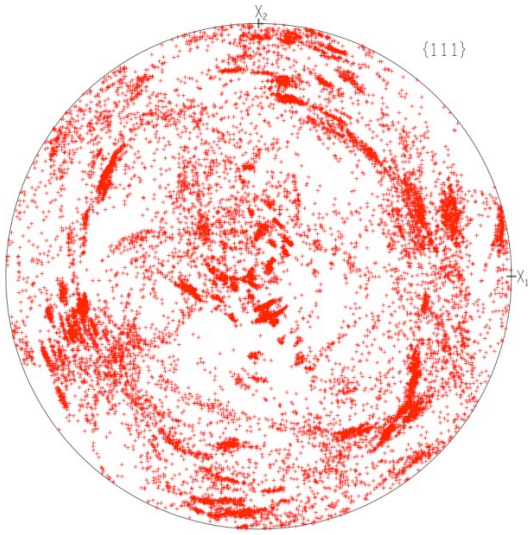

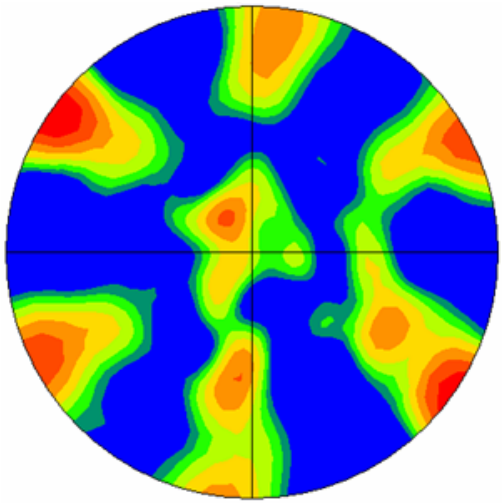

{111}

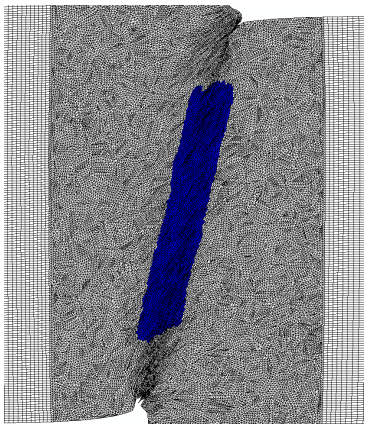

Experiment

{110}

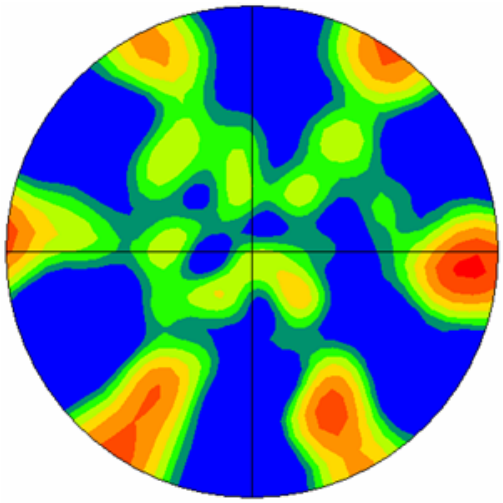

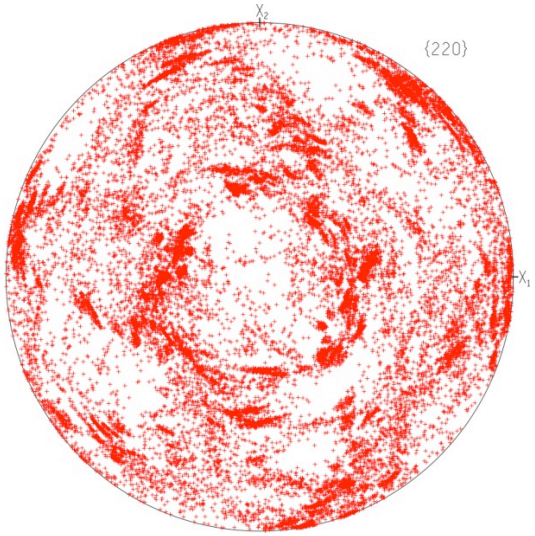

E. Cerreta, J. Bingert

Measurement of Granular Aspect Ratio

Ross

Grain morphology (aspect ratio) was measured along lines parallel to shear zone

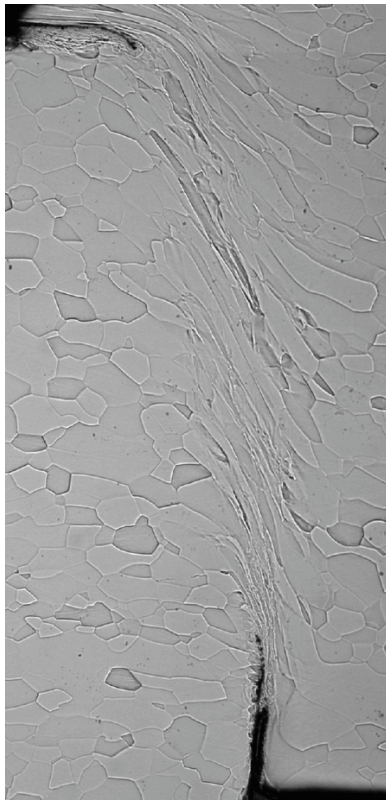

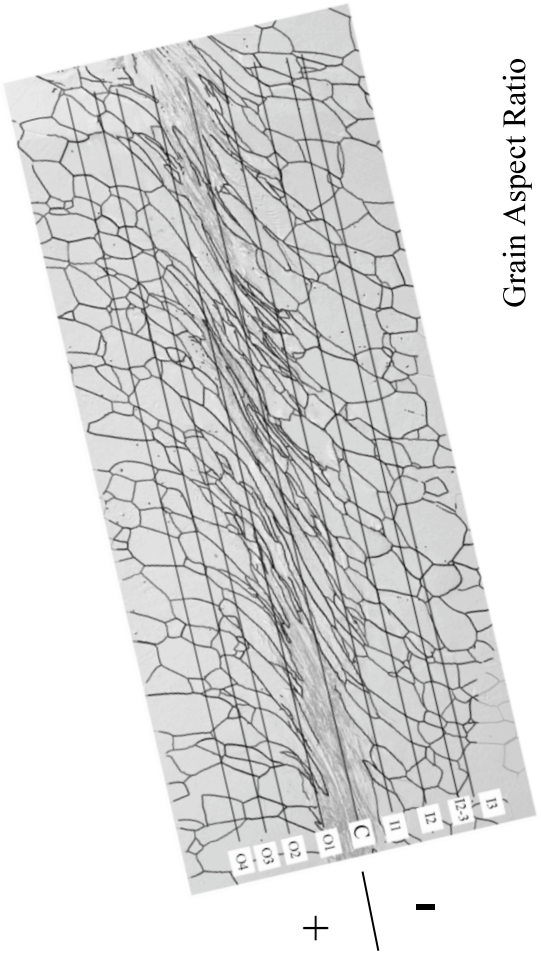

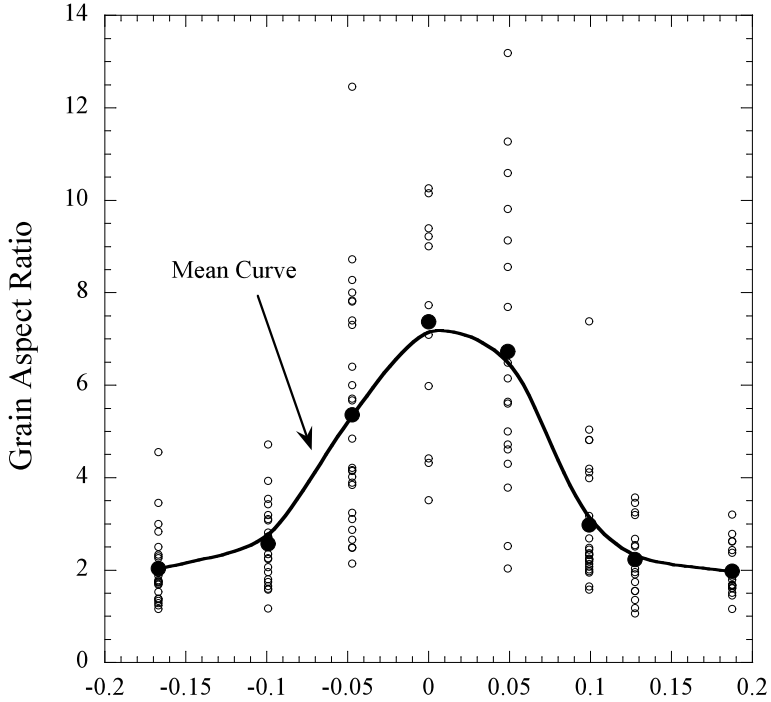

$$\varepsilon_l = \tfrac{2}{3}\ln\left(\frac{AR}{\overline{AR_0}}\right) \quad \text{Lower bound}$$

$$\varepsilon_u = \tfrac{2}{3}\ln\left(AR \cdot \overline{AR_0}\right) \quad \text{Upper bound}$$

$$\overline{AR_0} = 1.9$$

3 Differing Crystallographic Realizations

Realization 1 Realization 2 Realization 3

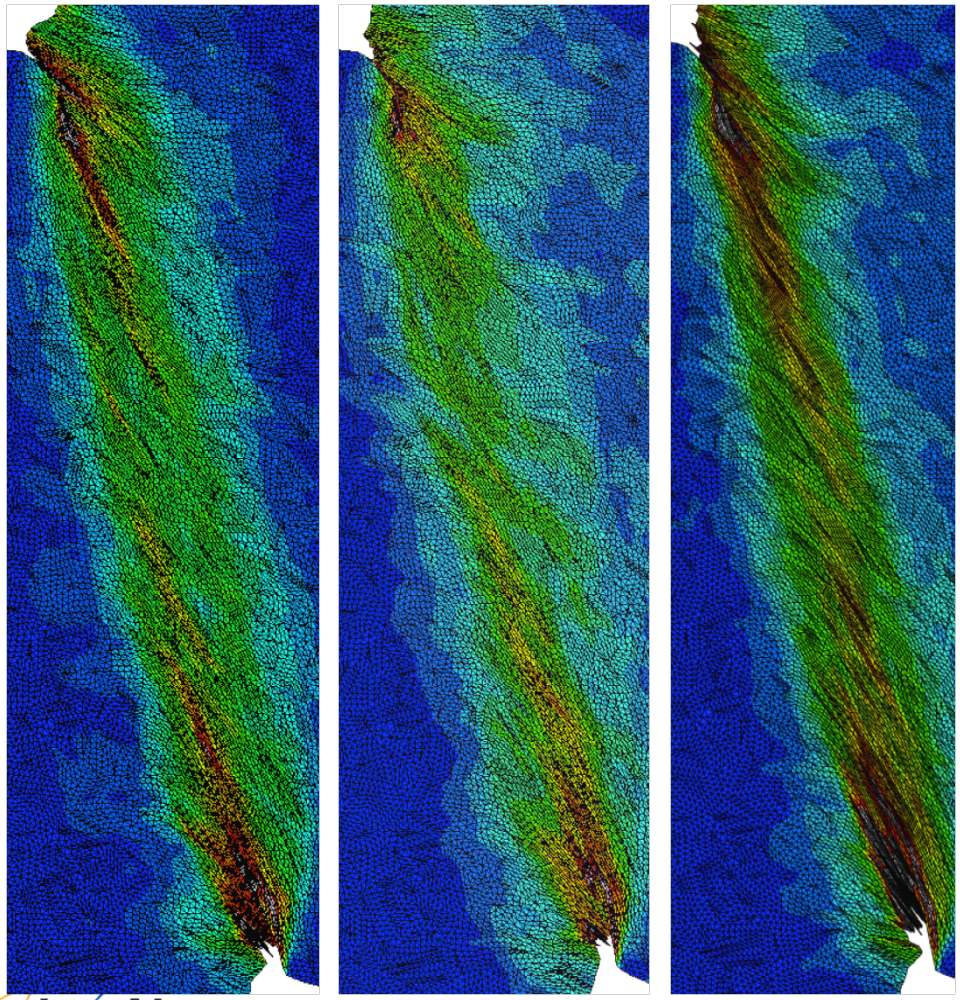

Region of equivalent plastic strain extraction

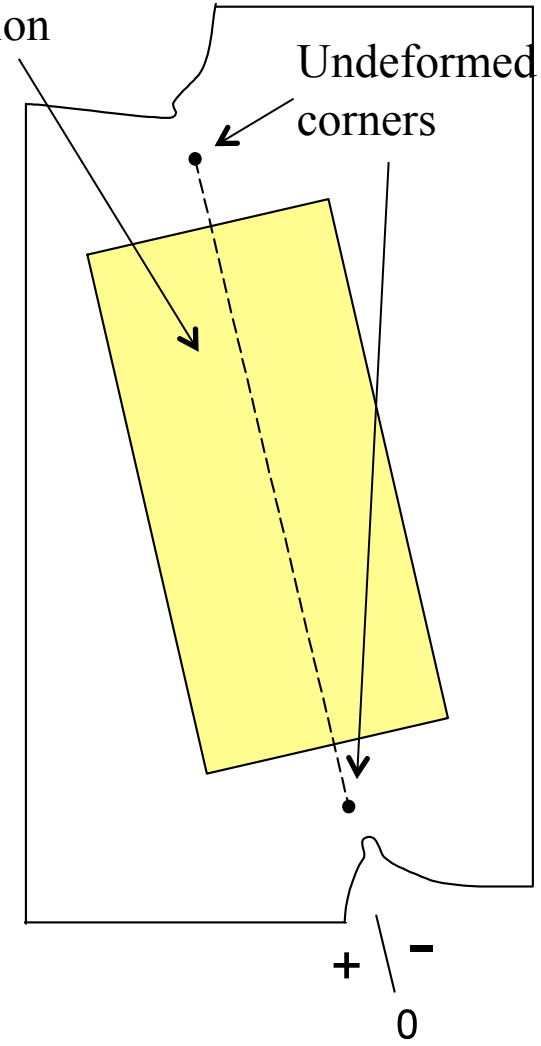

$\overline{\varepsilon}^{p}$

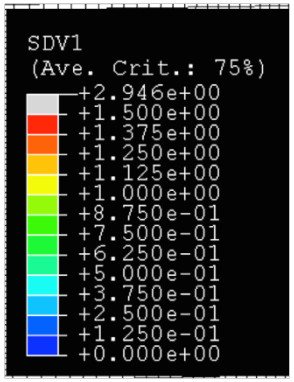

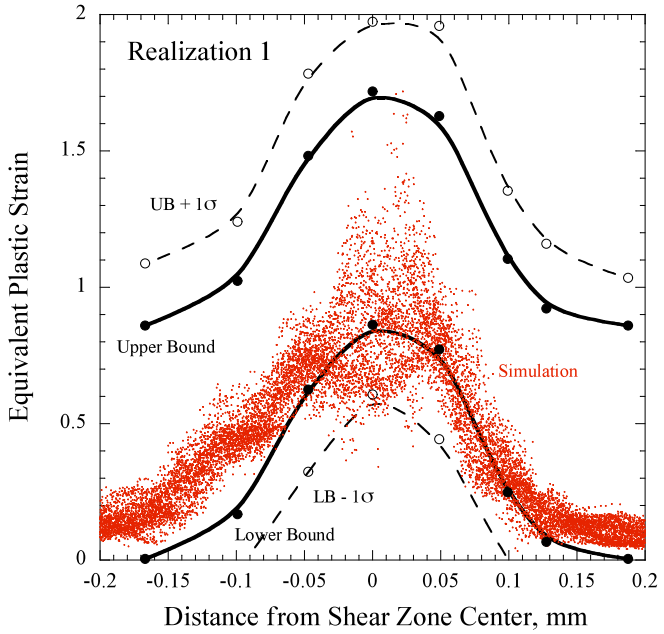
Realization 1
Equivalent Plastic Strain
Distance from Shear Zone Center, mm
UB + 1σ
Upper Bound
Simulation
LB - 1σ
Lower Bound
2
1.5
1
0.5
0
-0.2
-0.15
-0.1
-0.05
0
0.05
0.1
0.15
0.2

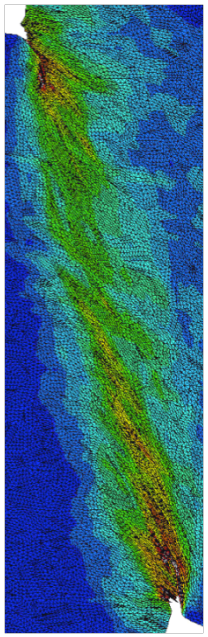

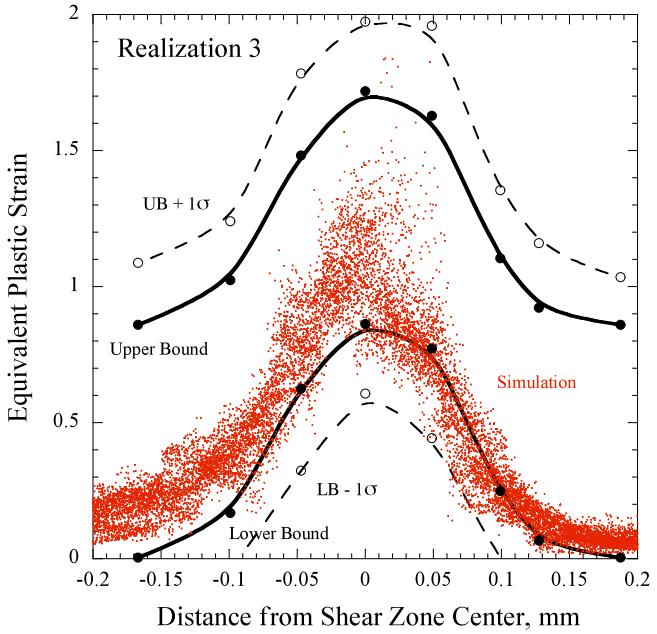
Realization 3
Equivalent Plastic Strain
Distance from Shear Zone Center, mm
UB + 1σ
Upper Bound
Simulation
LB - 1σ
Lower Bound
2
1.5
1
0.5
0
-0.2
-0.15
-0.1
-0.05
0
0.05
0.1
0.15
0.2

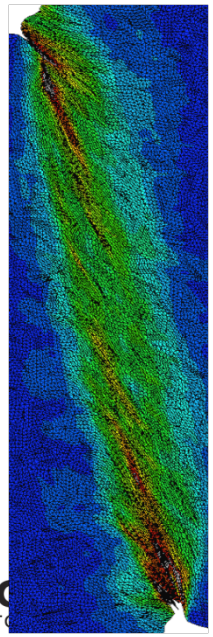

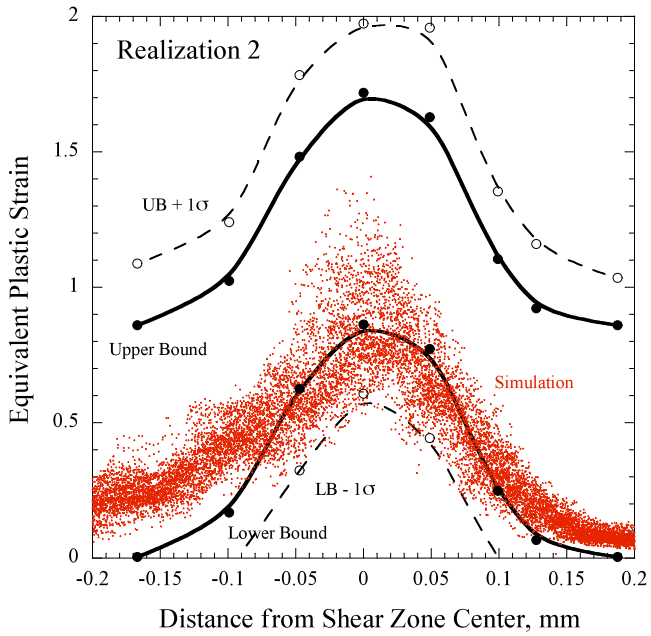
Realization 2
Equivalent Plastic Strain
Distance from Shear Zone Center, mm
UB + 1σ
Upper Bound
Simulation
LB - 1σ
Lower Bound
2
1.5
1
0.5
0
-0.2
-0.15
-0.1
-0.05
0
0.05
0.1
0.15
0.2

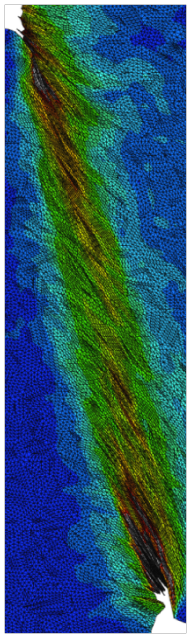

Summary & comments

- Damage and failure in polycrystalline metallic materials is strongly dependent upon microstructural details – modern lower length scale tools are necessary to assist in our learning about these complex physical processes. This can then properly motivate the development of physically based higher length scale models for use in applications.
- In general, we do not have the ability to adequately represent the topology of polycrystalline microstructures – this is especially true in 3D. Sub-granular initial state is also a concern – in ways similar to MD.
- The modeling results compare OK with experimental measurements. Comments are:
  - Stress response is consistently over-predicted.
  - Texture prediction clearly shows 2D deformation gradient.
  - Shear zone strain profile is well predicted.
  - Due to tessellation limitations, triangular elements were required.

Lawrence Livermore National Laboratory

This work performed under the auspices of the U.S. Department of Energy by Lawrence Livermore National Laboratory under Contract DE-AC52-07NA27344.

Multiscale Models for the Dynamic Strength of Ta and V

Tom Arsenlis

ASC PEM Constitutive Properties Team Leader

LLNL-PRES-425432

LLNL Team

- PLS
  - Dan Orlikowski
  - Per Soderlind
  - Meijie Tang
  - Lin Yang
  - Vasily Bulatov
  - Jaime Marian
- Engineering
  - Moono Rhee
  - Rich Becker
  - Dan Nikkel
- Comp
  - Gregg Hommes

Strategy for describing dynamic material strength is to build constitutive models that depend on microstructural observables

- Replace common (integrated) strength state variable with microstructural variables that can be investigated through sub-grid physics simulations
  - Material Phases and Crystal Structures, Dislocation Density, Grain Size, Twin Volume Fraction, etc.
  - Microstructural variables are experimentally accessible

- Task of building a strength model can be conceptually subdivided into two parts
  - Determining Microstructure-Strength Relationship
  - Determining Microstructural Evolution with Deformation

Microstructural variables allow results of sub-grid physics simulations to be incorporated in a straight forward manner

UCRL-PRES-236631

Tantalum and Vanadium are chosen as demonstrations for multiscale modeling architecture

- Information from simulations at multiple length scales is combined to build macroscopic constitutive models
  - Ab-initio Methods provide equation of state, pressure-temperature dependent elastic constants, and ideal strength limits
  - Molecular Statics/Dynamics provide dislocation mobility
  - Dislocation Dynamics provide dislocation structure-strength relationship, and dislocation density evolution
  - Continuum Methods provide homogenization methods for elastic/plastic response
- Strength models assume a dislocation glide mechanism for dynamic plastic relaxation
  - Twinning and shear induced phase transformation mechanisms are being considered for future model developments

Structure of the proposed constitutive model is informed by sub-grid physics simulations

- Dislocation density is the primary state variable

Orowan's Equation

$$\dot{\varepsilon}^{p} = \frac{\rho b v}{M^{T}}$$

Two dislocation velocity regimes

$$\tau_{dyn} = \sqrt[n]{\tau_{drag}^{n} + \tau_{therm}^{n}}$$

$$\tau_{drag}^{n} = B\left(\frac{v - v_0}{c_0}\right)\sqrt{1 - \left(\frac{v}{c_0}\right)^{2}}$$

$$\tau_{Therm}^{n} = a_0 \exp\left(\frac{\theta}{a_T}\right)\tau_p \left\{\exp\left[(\beta_0 + \beta_T\theta)\ln\left(\frac{v + v_T}{c_0}\right)\right] - \exp\left[(\beta_0 + \beta_T\theta)\ln\left(\frac{v_T}{c_0}\right)\right]\right\}$$

Dislocation-Structure Strength Relationship

$$\sigma^{e} = M^{T}\left[\tau_{dyn}(v) + \tau_{ath} + \tau_{disl}(\rho)\right]$$

- Material constants, microstructure strength relationship and evolution equations are determined from sub grid physics simulations

Ab initio methods are used to determine elastic constants as a fn(P,T)

$$C_{ij}(P,T) = C_{ij}^{0}(P) + \delta C_{ij}^{ion}(P,T) + \delta C_{ij}^{el}(P,T)$$

cold ion-thermal electron-thermal

T dependence at ambient P

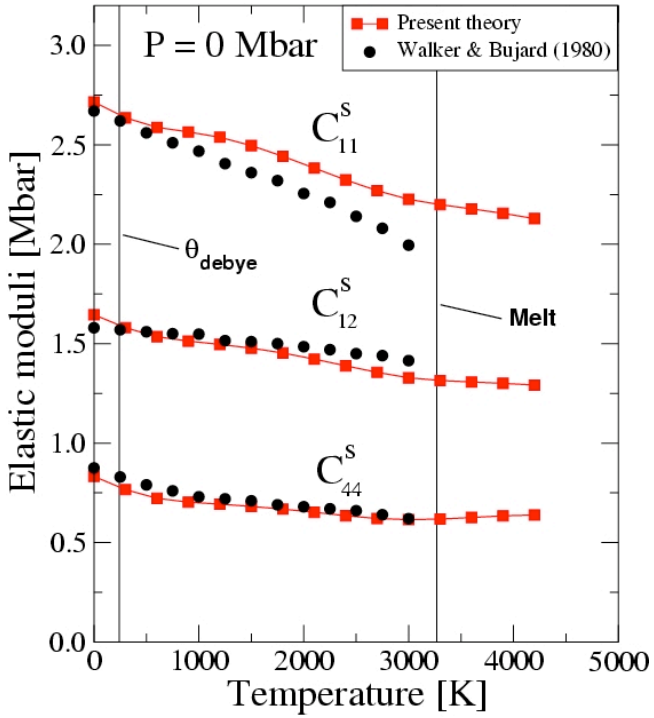

Cold: *Ab initio* DFT strains at T = 0

Ion-thermal: strain derivatives of MGPT phonons

Electron-thermal: *Ab initio* DFT strains at finite T

P dependence at 300 K

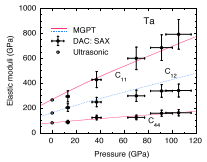

Simulations are validated against static experimental data

UCRL-PRES-236631

Finite element techniques are used to homogenize elastic constants

Random grain distribution in a finite element model

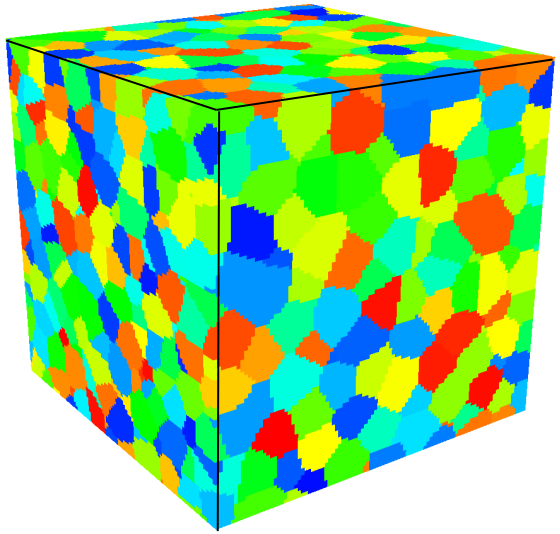

Bulk modulus taken directly from the EOS

Model exercised in six pure shear deformation modes and the results are averaged

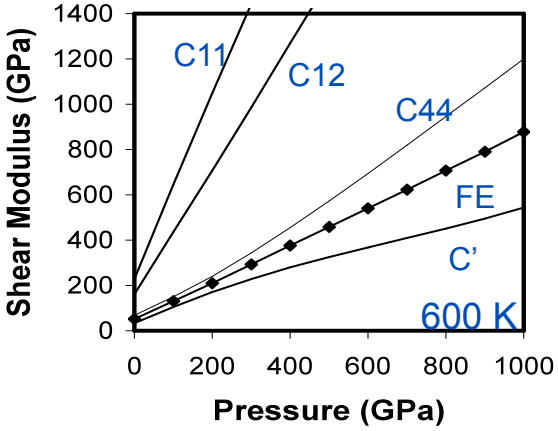

Comparison of homogenized modulus to anisotropic moduli

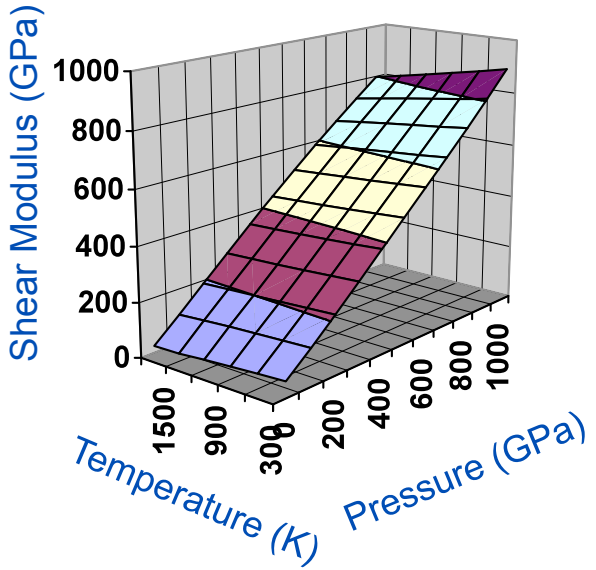

Pressure-Temperature dependence of homogenized shear modulus

Elasticity used to determine stress state from elastic strains

UCRL-PRES-236631

Well parameterized molecular dynamics/statics simulations are needed to simulate the physics of dislocations

- Ab initio methods are well suited for simulating the response of perfect crystals but limitations in simulation volumes prevent simulation of dislocations
- MGPT potentials have been developed that capture the essential atomic physics from ab-initio simulations for the range of pressures and temperature of interest

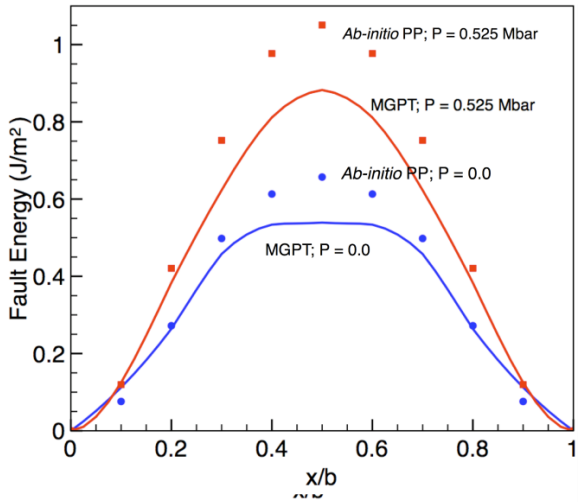

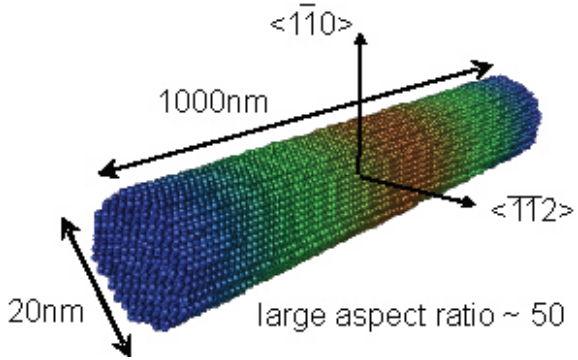

- Molecular Dynamics/Statics are appropriate for investigating the energetics and kinetics of isolated dislocation defects

Molecular statics simulations yield mobility information in the thermally-activated regime

The activation energy for screw dislocation motion is the barrier for kink nucleation

It is obtained from the molecular statics results at zero shear stress

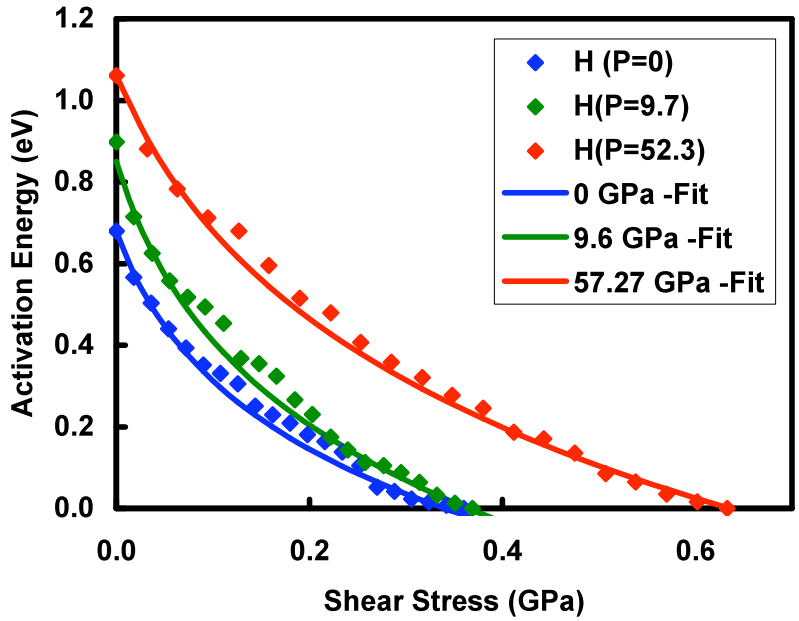

$$\tau_p^s = G_0\left[0.006939 + 0.0018786\left(\frac{P}{G_0}\right) + 0.003530\left(\frac{P}{G_0}\right)^2\right]$$

Exp: τ_P = 0.35±0.05 GPa at ambient conditions

Wang and Bainbridge, Metall. Trans. 3, 3161 (1972)

The Peierls stress is the stress required to move a dislocation in the absence of thermal activation

Complete mobility function is created by combining molecular statics and dynamics simulations – Screw dislocation

Velocity is smooth in the transition from thermally activated regime to drag regime

Molecular dynamics simulations able to simulate across the transition

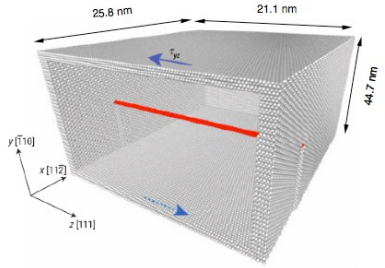

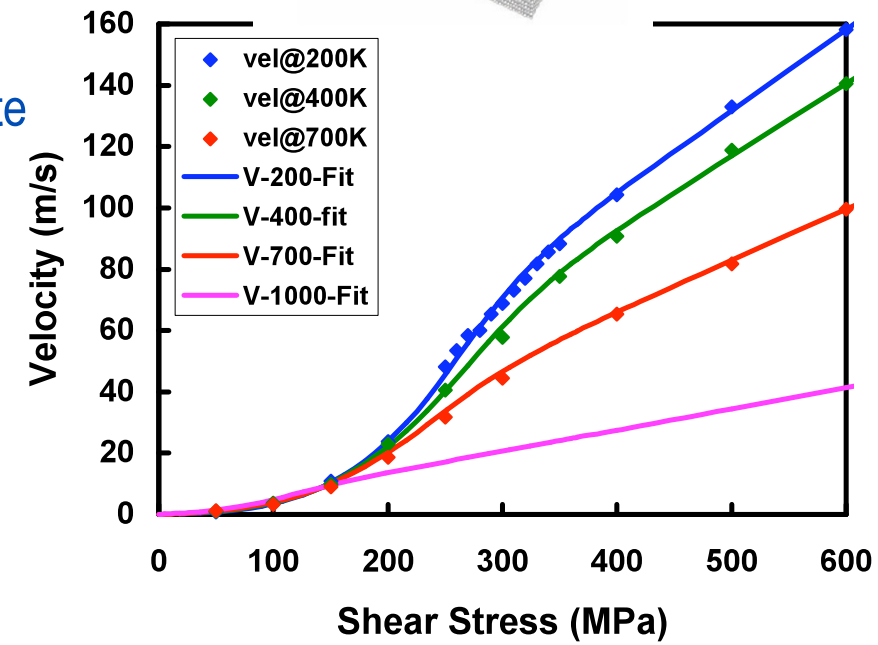

$$\tau_{dyn} = \sqrt[n]{\tau_{drag}^{n} + \tau_{therm}^{n}}$$

$$\tau_{drag}^{n} = B\left(\frac{v - v_0}{c_0}\right)\sqrt{1 - \left(\frac{v}{c_0}\right)^2}$$

$$\tau_{Therm}^{n} = a_0 \exp\left(\frac{\theta}{a_T}\right)\tau_p \left\{\exp\left[(\beta_0 + \beta_T\theta)\ln\left(\frac{v + v_T}{c_0}\right)\right] - \exp\left[(\beta_0 + \beta_T\theta)\ln\left(\frac{v_T}{c_0}\right)\right]\right\}$$

Function fit to molecular statics and dynamics data is used as input to dislocation dynamics and final continuum constitutive model.

LLNL-PRES-425452

UCRL-PRES-236631

ParaDiS code has been developed at LLNL to integrate the multiplication and interactions of dislocations for simulating evolution of strength

Dislocation network represented by interconnected line segments

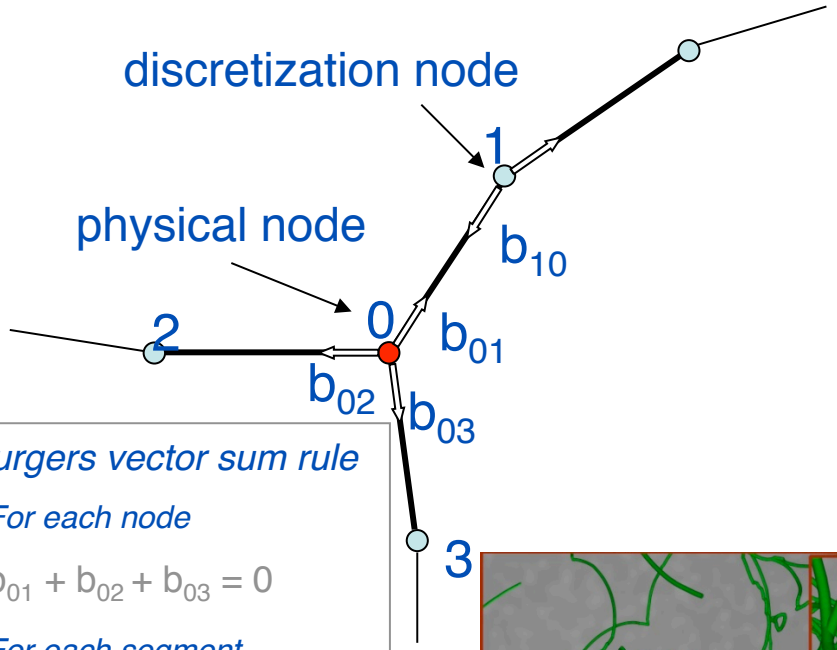

Burgers vector sum rule

- *For each node*

  $b_{01} + b_{02} + b_{03} = 0$

- *For each segment*

  $b_{01} + b_{10} = 0$

DD Algorithm

Node force

$$\vec{f}_{orce_i} = -\frac{\partial E_{nergy}(\{\vec{p}_{osition_i}\})}{\partial \vec{p}_{osition_i}}$$

Elasticity from ab initio

Node velocity

$$\vec{v}_{elocity_i} = M_{obility}(\vec{f}_{orce_i})$$

obtained from MD

Move nodes

$$\vec{p}_{osition_i} = \vec{p}_{osition_i} + \vec{v}_{elocity_i} \cdot \Delta t_{ime}$$

topology changes

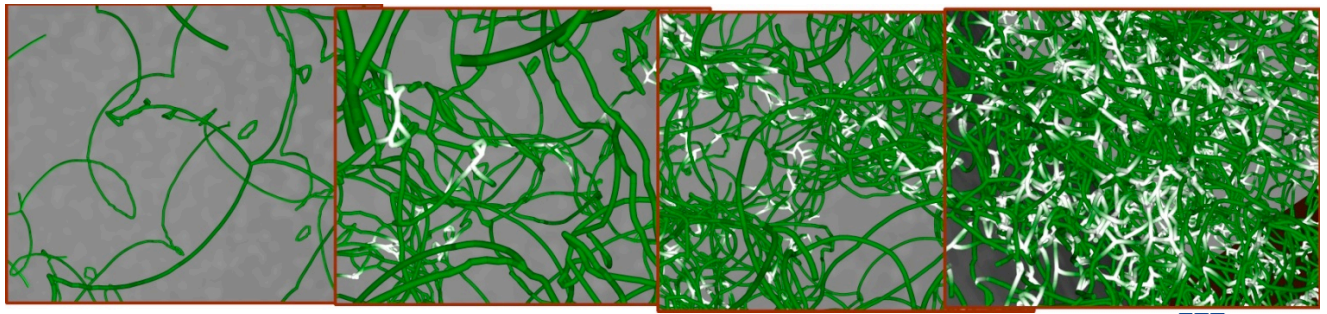

UCRL-PRES-236631

BG/L resource required to conduct ParaDiS simulations of dynamic strength

- Total 16 ParaDiS simulations carried out on BG/L
  - BG/L: 131,072 total CPUs (IBM PowerPC) with 500Mb memory/node(2CPUs)

- Degrees of Freedom in typical DD simulations > 1 million
  - -1/3 of Machine (up to 48K CPUs total) for ~ 3 months
  - Total CPU hours approximately 70 million hours
  - Each job requiring about 1-32K CPUs (#DOF dynamically changing)
  - Matrix of Conditions
    - Pressures 0 and 600 KBar
    - Orientations [001] and [111]
    - Strain rate 1.e3 and 1.e5
    - Temperature 400K and 1000K

Simulations typically reached 4-5% plastic strain

UCRL-PRES-236631

Data reduction from ParaDiS simulations

- Stress strain, dislocation density, and dislocation flux histories are taken as output from which to construct coarse model
- Current coarse grained model uses saturation densities as a functions of strain rate, pressure and temperature as well as a dislocation density-strength relation

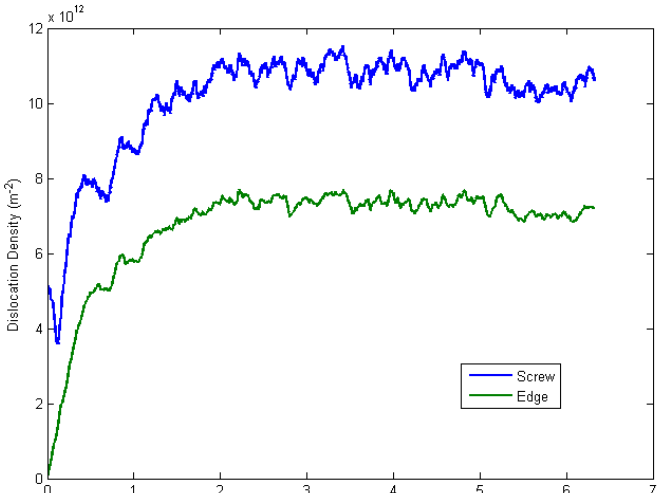

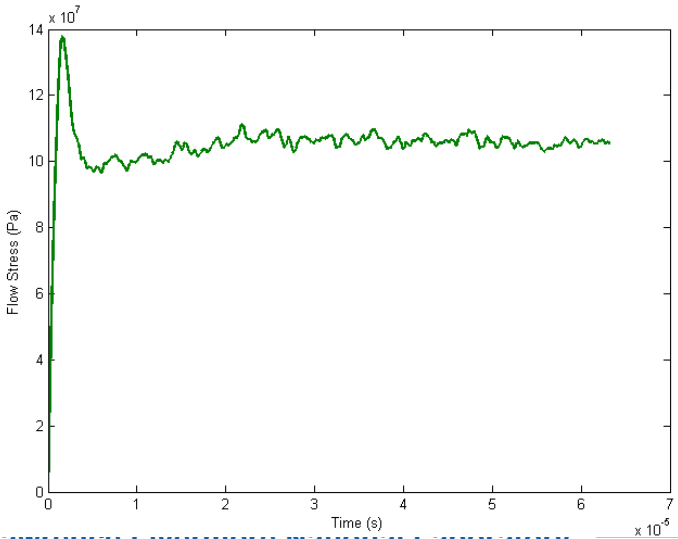

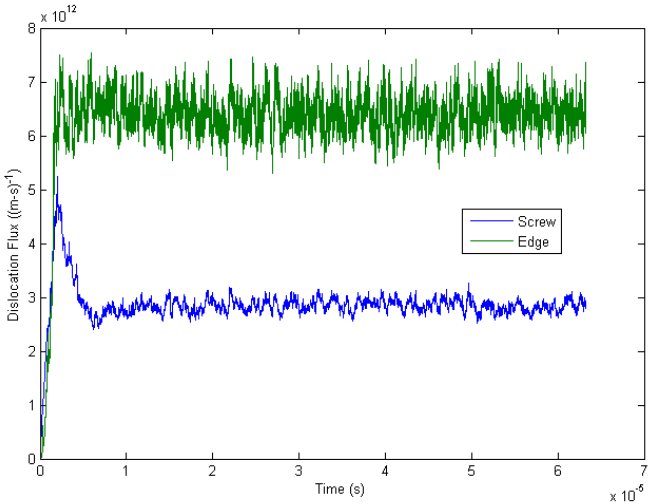

UCRL-PRES-236631

Comparison with Z and laser data evaluates yield strength at high strain rates

Stepped Ta target and drive

Bastea, et al

Pressure drive

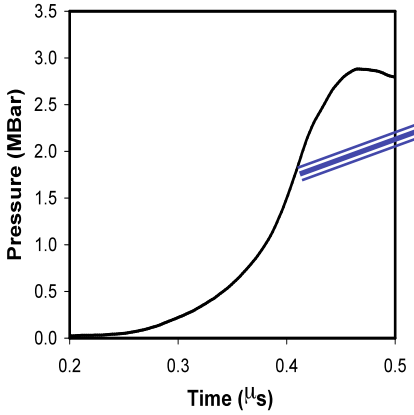

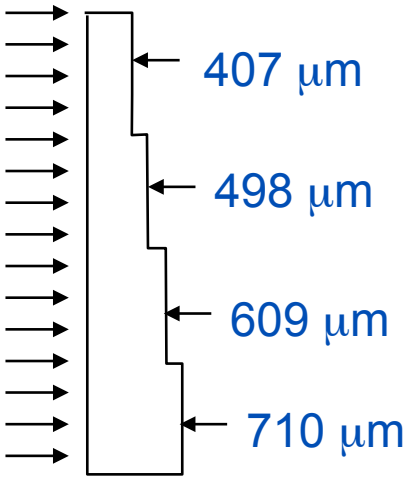

Velocity from steps

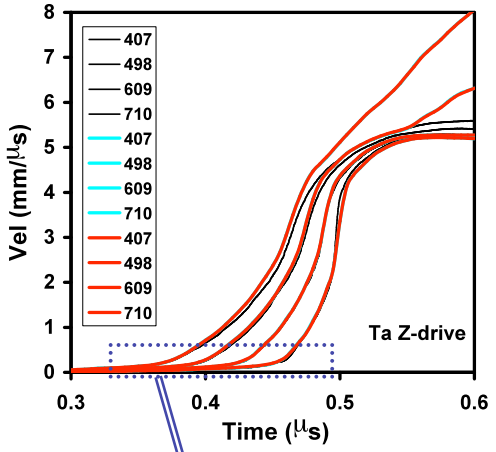

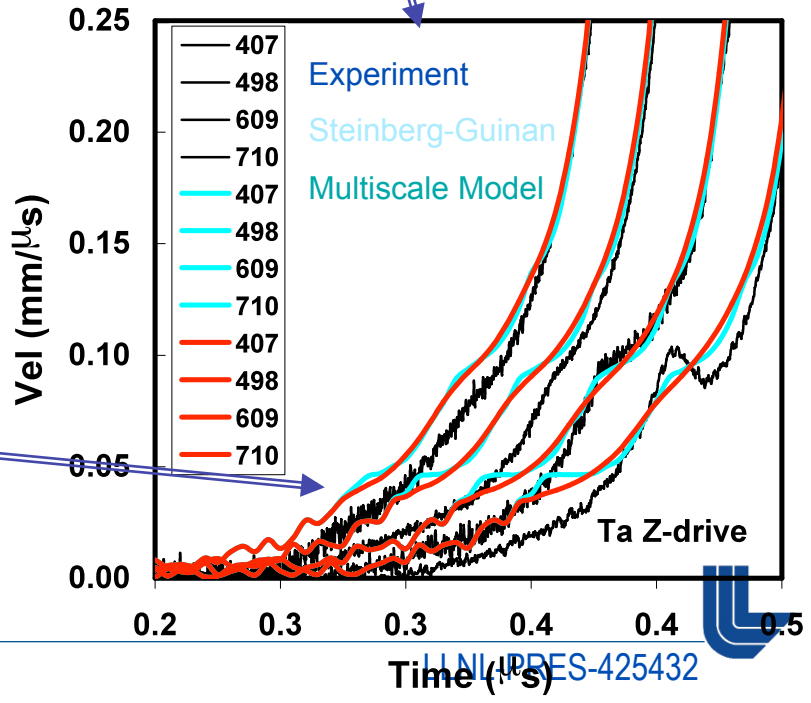

- Ramp pressure loading produces strain rates of 5×10^6 sec^{-1}
- Yield strength is evident as a step on the initial ramp of the velocity curve
- Strength predictions are significantly below what the experiments suggest

The pullback signal in a gas gun test probes yield behavior at pressure

Stepped gas gun target

Stölken et al

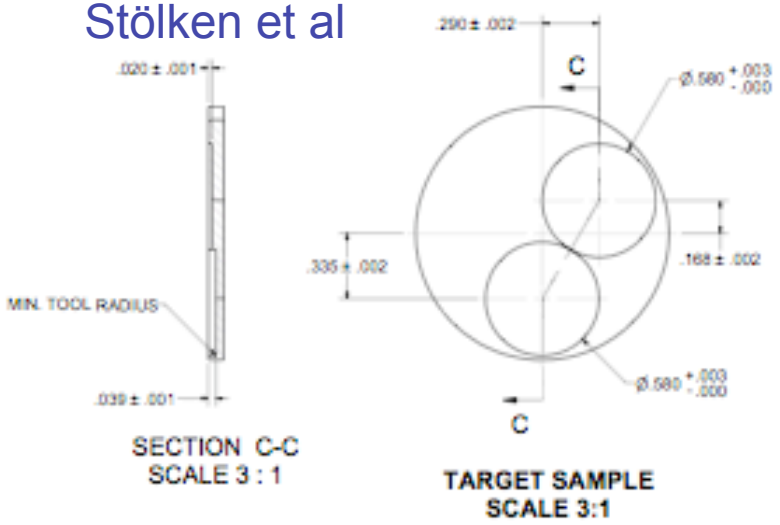

Strength estimated from best fit of hydro code MTS model fit with pull back data

Free surface velocity

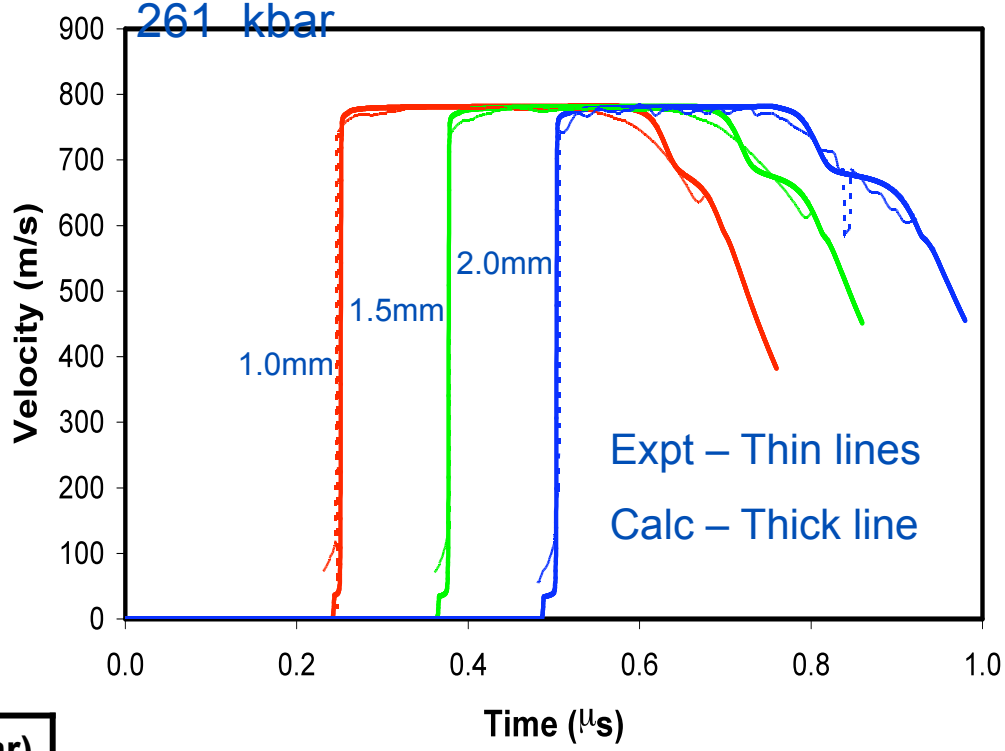

Pressure	MTS fit (kbar)	Prediction (kbar)
99	5.9	8.4
261	7.5	10.8
533	20.1	12.6

The simulations with the mutiscale model and others show considerably less dispersion than the experiments.

Model over predicts rate of instability growth but performs considerably better standard model

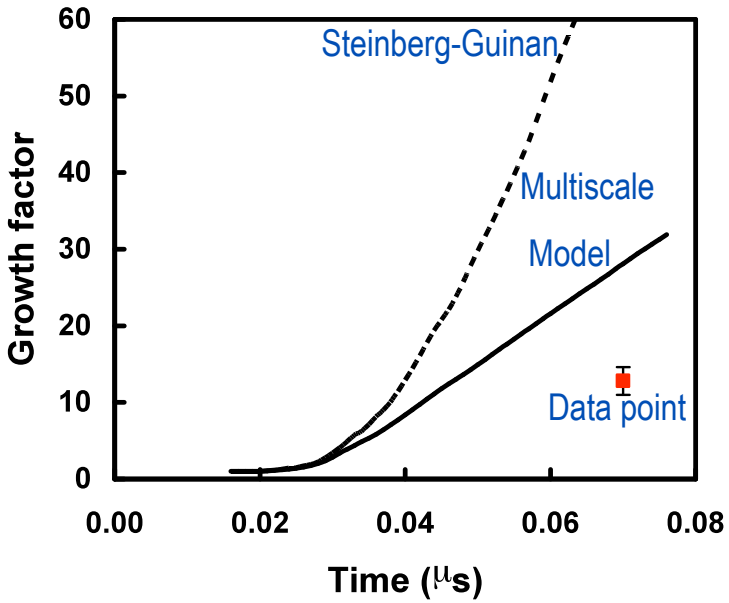

Initial

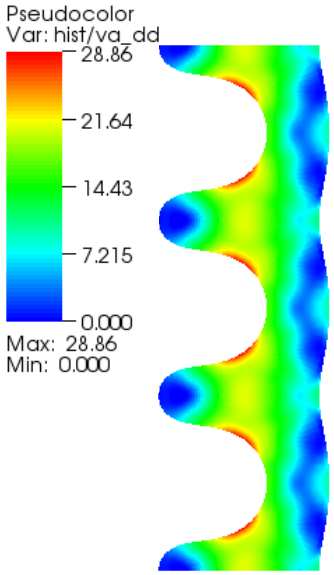

strain rate 1/μs

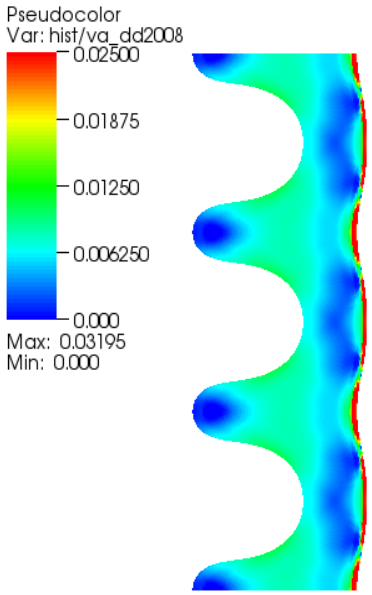

Edge dislocation velocity cm / μs

Model is significantly stiffer than “blue book” Steinberg-Guinan and comes much closer to experiment

Strength is due to dislocation velocity in the phonon drag range and increased dislocation density. Both will be diminished at lower rates

Conclusion

- The goal of the multiscale modeling project is to produce strength models in regimes where little or no experimental data exist
- Pass information across length scales from subatomic to engineered part
- The multiscale models appear to behave better than standard models under dynamic straining conditions
- Model details and parameters are available in several published LLNL reports
- Future models will include twinning and multiple phases

JOWOG 32MAT

January 29, 2010
Friday

LA-UR-

Approved for public release;
distribution is unlimited.

Title:	
Author(s):	
Intended for:	

Form 836 (7/06)

Phases, Microstructures, and Thermodynamic Properties of Ga Alloyed Plutonium

Franz Freibert

Acknowledgements:

T. Saleh, J. Mitchell, P. Crawford, and D. Schwartz (MST-16);

A. Migliori, J. Betts, Y. Suzuki, I. Mihut-Stroe (NHMFL)

Los Alamos National Laboratory

JOWOG 32 Focused Exchange Meeting

Lawrence Livermore National Laboratory

January 25 – 29, 2010

Los Alamos NATIONAL LABORATORY EST.1943

Casting Pu-Ga Alloys

PHYSICAL AND MECHANICAL METALLURGY STUDIES ON DELTA STABILIZED PLUTONIUM-GALLIUM ALLOYS

By
H. R. Gardner
Plutonium Metallurgy Development Unit
Metallurgy Development Section

BNWL-13
UC-25, Metals, Ceramics, and Materials (TID-4500, 38th Ed.)

April 1965

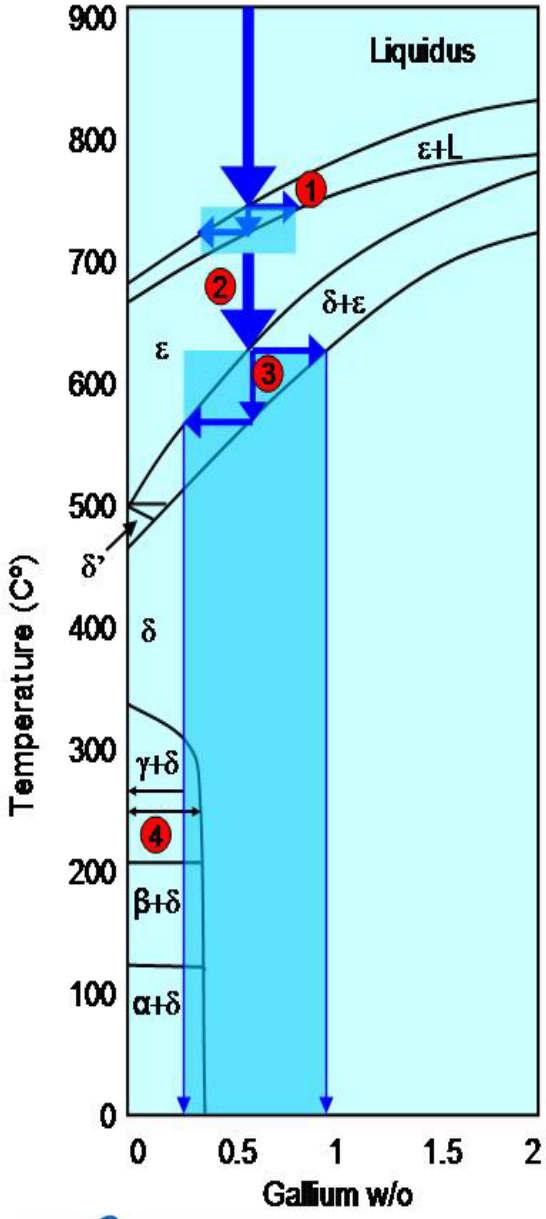

1

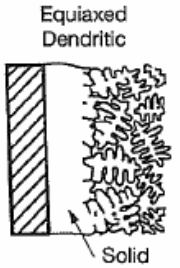

Solidification within ε+L phase field involves equiaxed dendrite formation initiated at the mold walls. Micro-segregation of Ga or "coring" occurs.

2 **Anisotropic negative thermal expansion and low yield strength in ε–phase results in plastic flow and dendrite breakage. Ga diffuses quickly due to high temperature and so reduces coring.**

Time in ε phase.

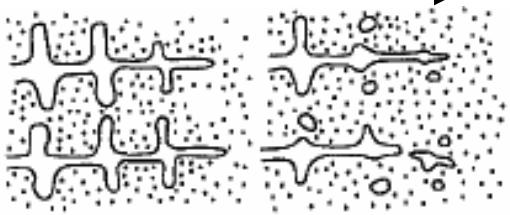

3

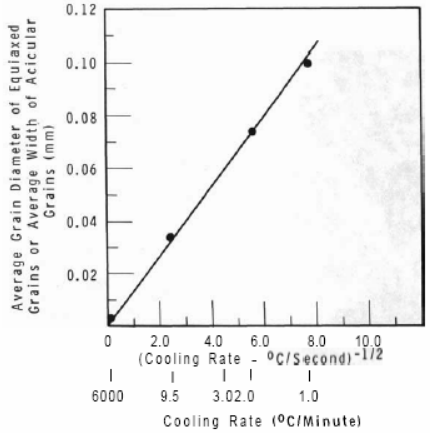

Micro-segregation of Ga or "coring" occurs once again with residual cores acting as nucleation points. Cooling rate through δ+ε phase field determines size of final cored grains.

4 **Phase segregation occurs in Pu rich regions. Upon cooling, α-phase regions contain soluble Ga. Both α-phase and δ–phase regions remain metastable and under extreme residual stress due to density and thermal expansion differences of phases.**

Los Alamos NATIONAL LABORATORY EST.1943

Microstructure of Phase Segregated Pu-Ga Alloys (Ga Coring & Phase Segregation)

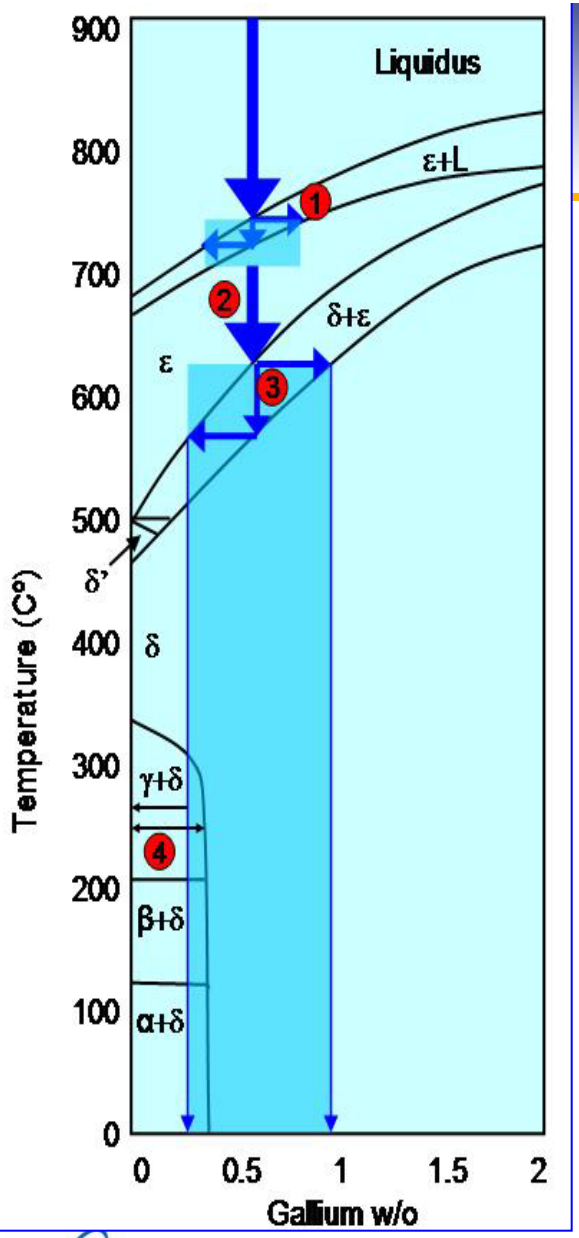

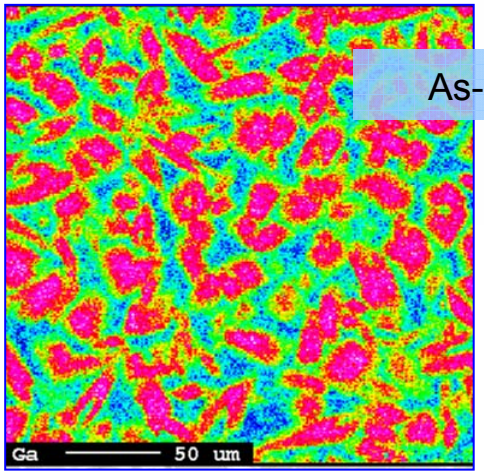

As-cast

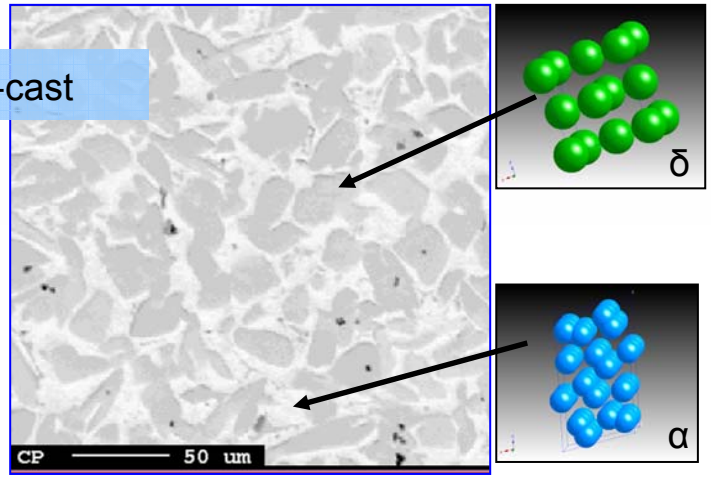

Average Ga Concentration: 1.61 +/- 1.0 at. %

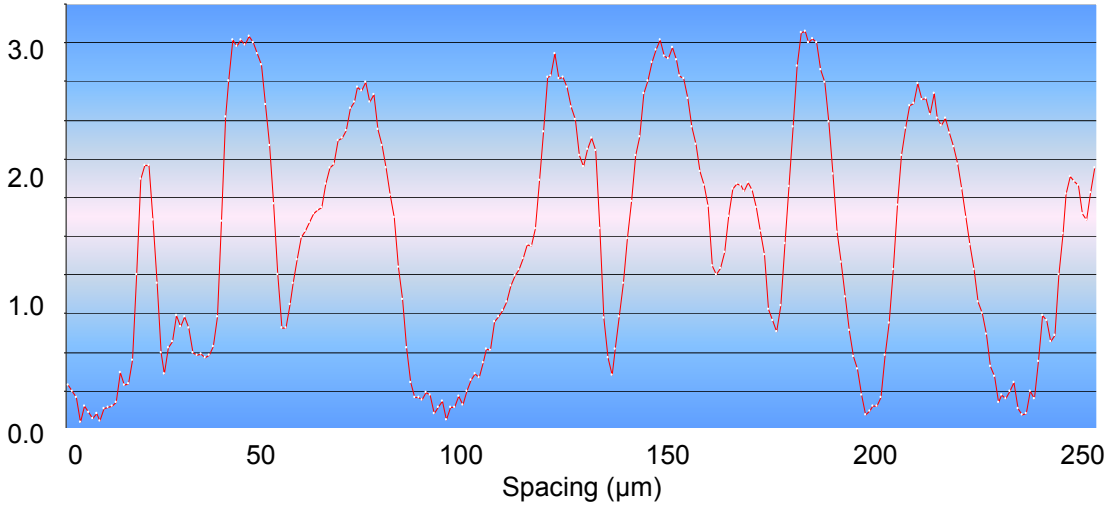

Los Alamos NATIONAL LABORATORY EST.1943

Ga Concentration and Microstructure Homogenization

Indicators of Homogeneity:

- Uniform Ga Distribution
- Single Phase (δ-phase)
- Uniform Dist. in Ga Conc. => Narrow Dist. of Lattice Const. => Narrow X-Ray Diffraction Peaks
- No evidence of phase transitions in thermal expansion.

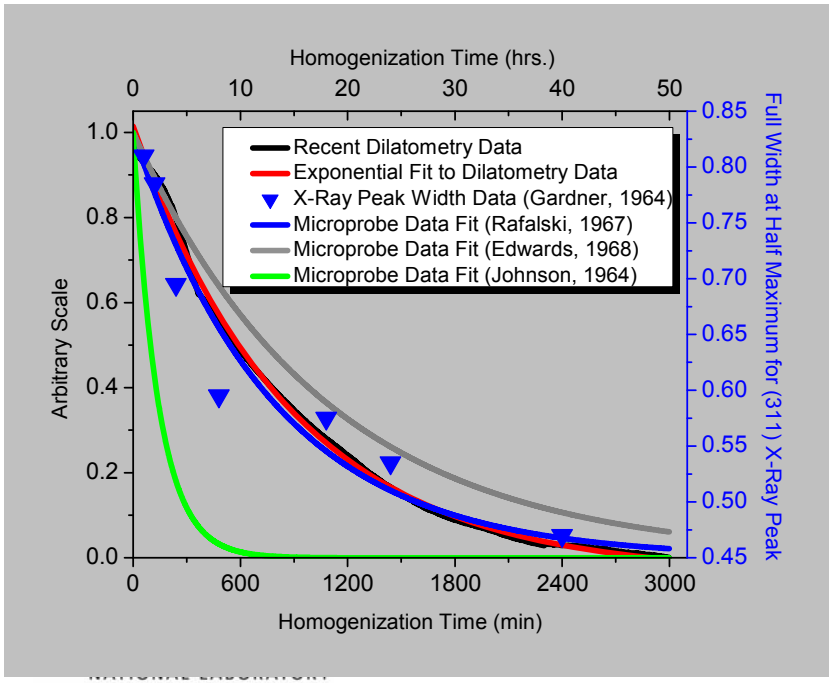

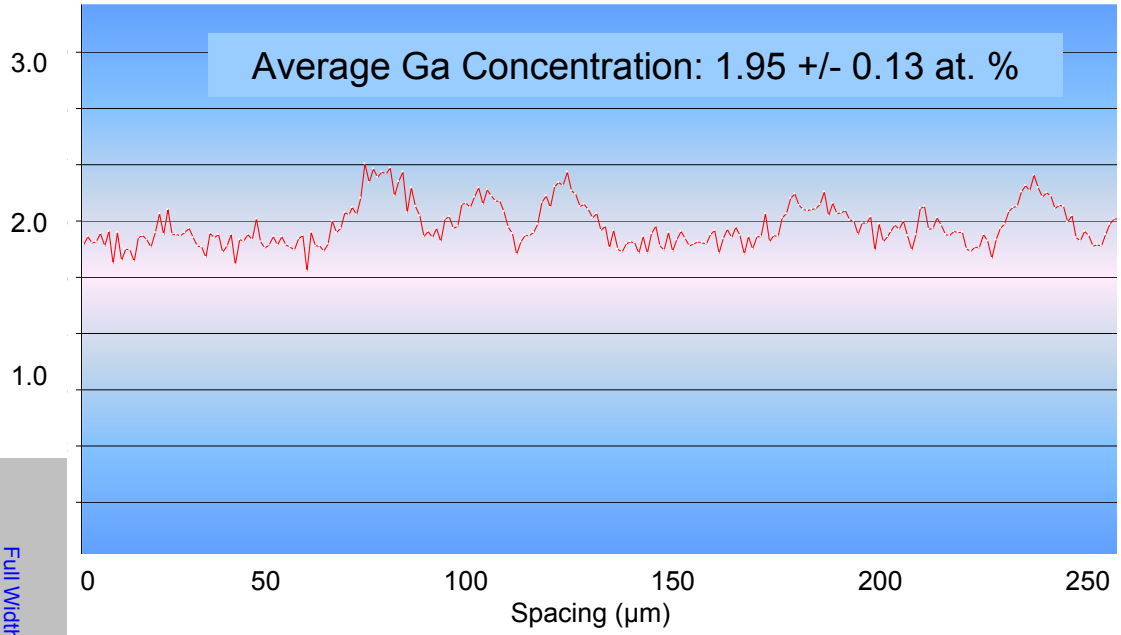

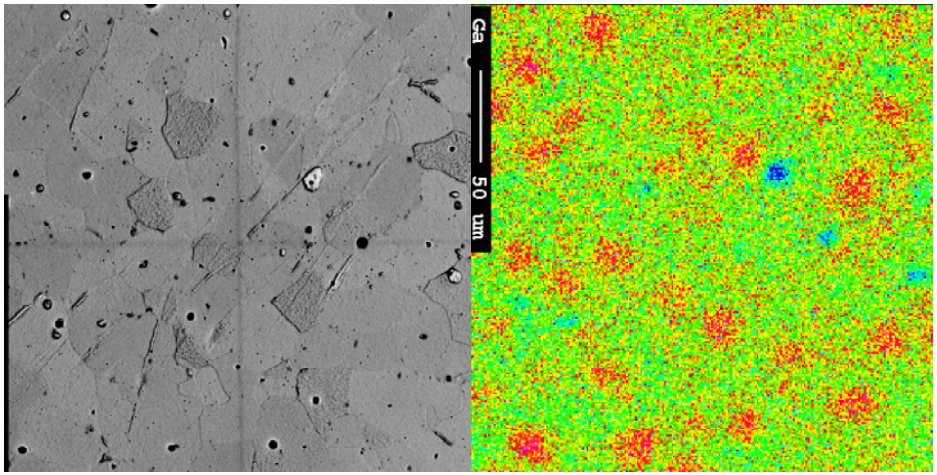

Pu-Ga Alloy Compositional Mapping and Hardness

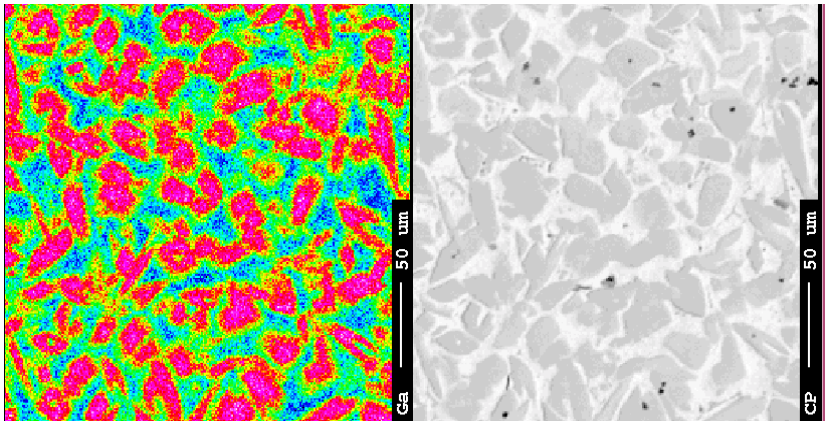

J.D. Montalvo, C. Davis, and A. Neumann, 2008

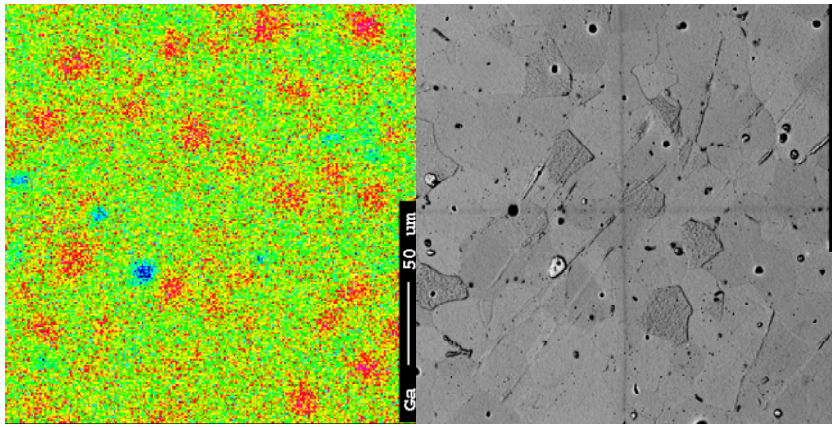

Local mechanical properties correlate with Ga heterogeneity and phase segregation. Directional thermal gradients experienced while cooling impact local phase properties.

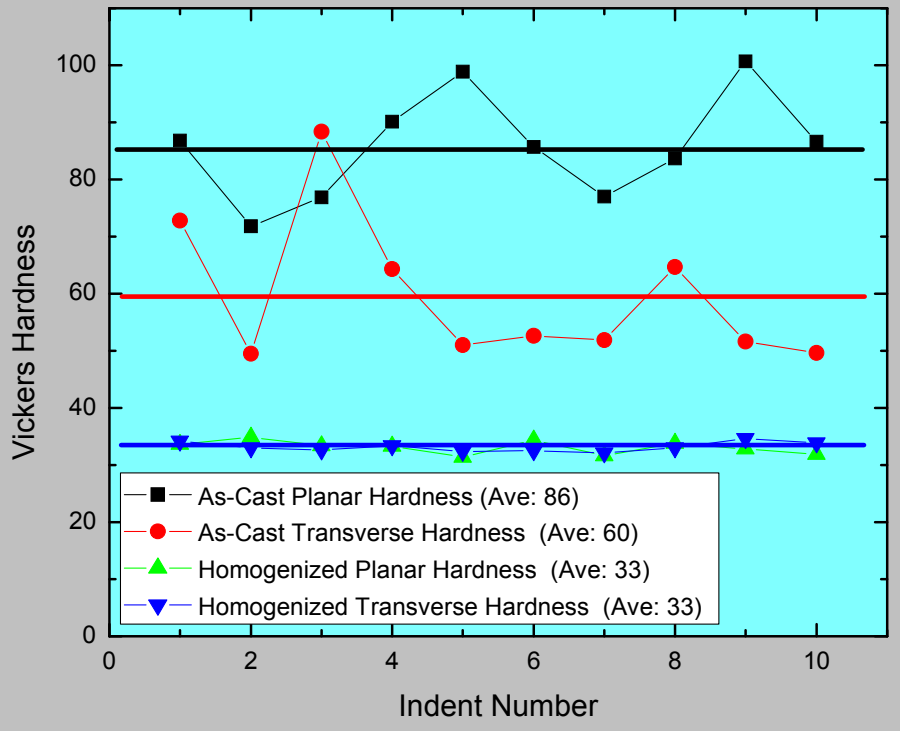

Los Alamos NATIONAL LABORATORY EST.1943

Microstructural Changes with Thermally Induced $\alpha' \leftrightarrow \delta$ Transformation

Martensite phase transformation in Pu-Ga δ-phase stable alloys at T<-100°C involves the formation of monoclinic α' platelets. Reversion occurs at T>50°C with little microstructural evidence of transformation, but becomes resistant after repeated cycling.

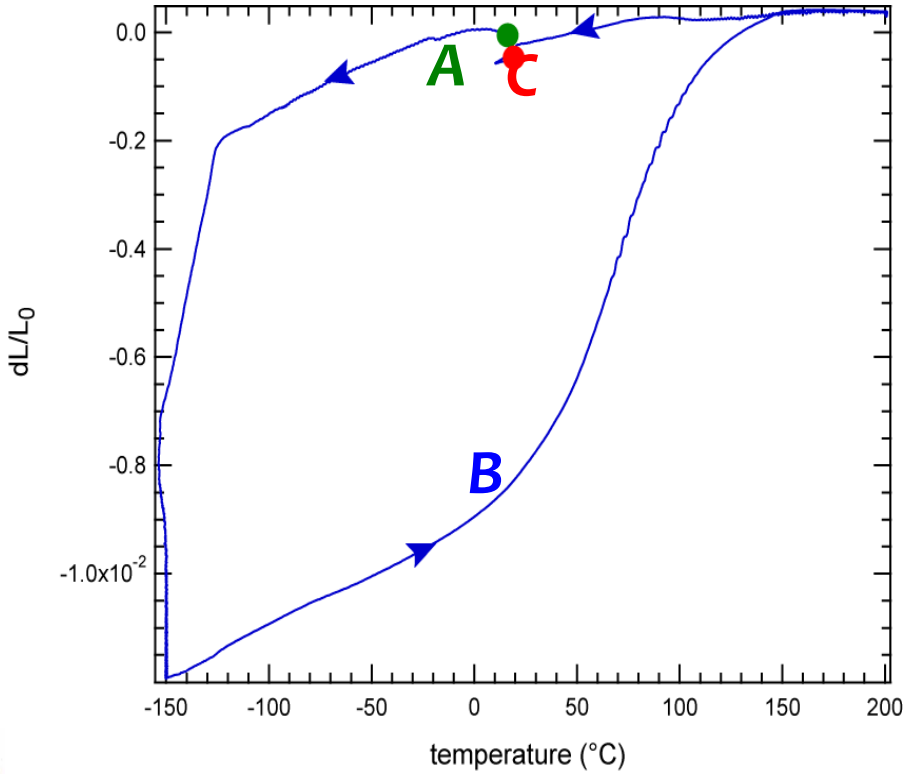

J.N. Mitchell, C.J. Boehlert, & F.J. Freibert (2009)

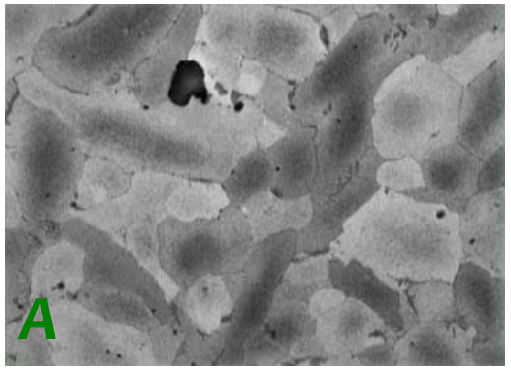

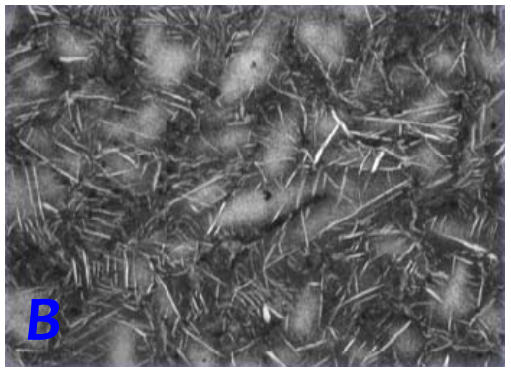

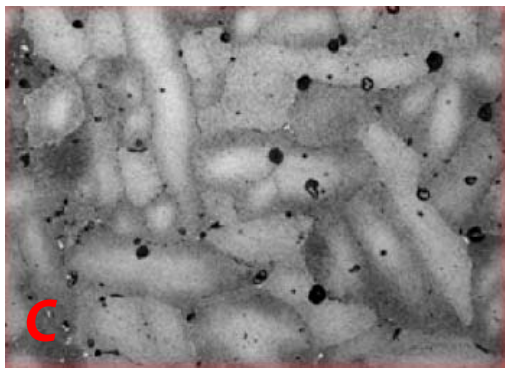

Microstructural Changes with Mechanically Induced $\alpha' \leftrightarrow \delta$ Transformation

40mm Gas Gun Pu Target Preparation and Residual Microstructure

The steps used to produce 40mm gas gun samples leave different quantities of residual α':
Edge Coring/Machining: 20μm
Hand Lapping:<5 μm

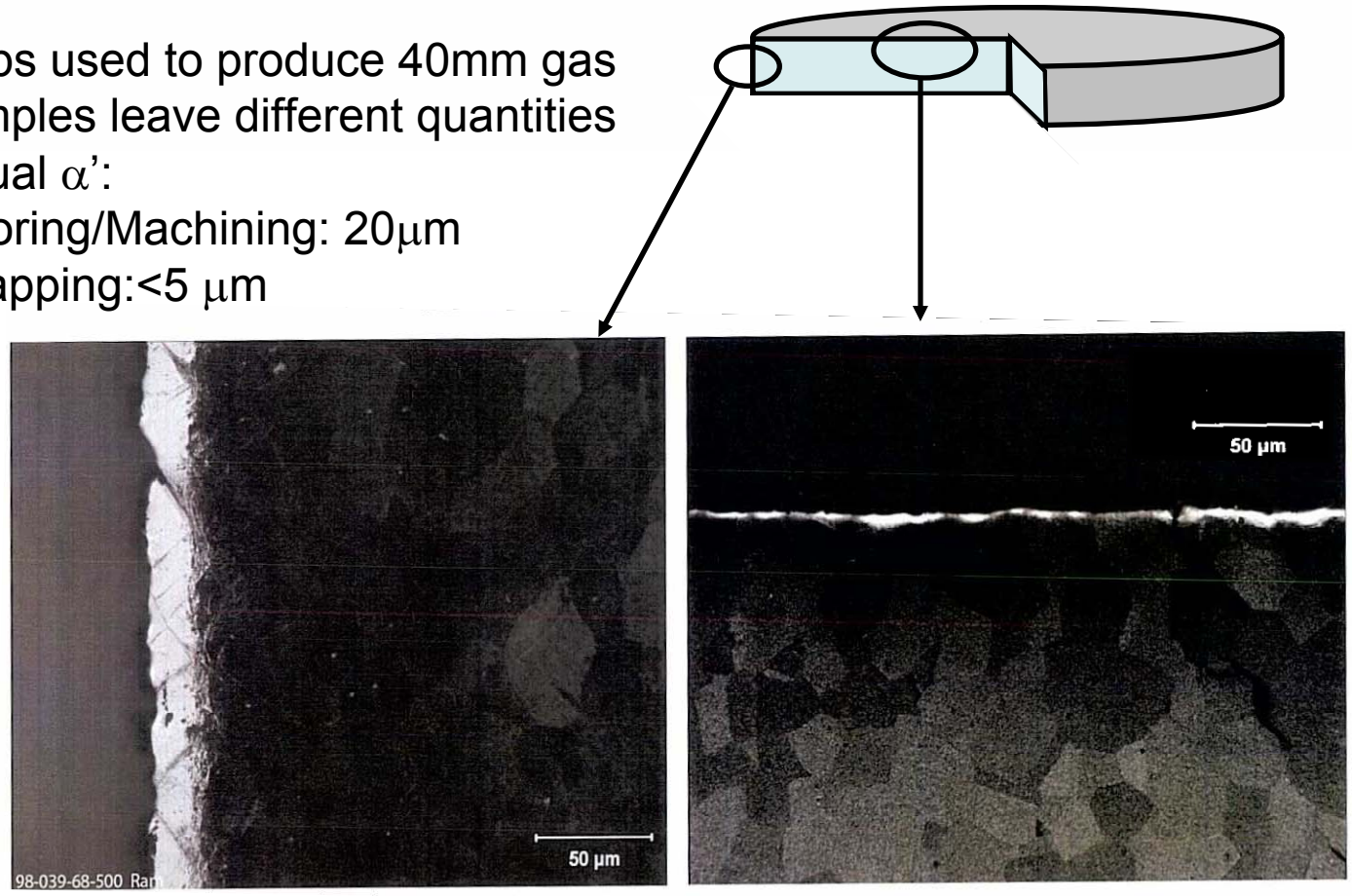

Thermophysical Properties: Density, Thermal Expansion and Resonant Ultrasound Spectrometry

The following body of work is explicitly dependent on the coupling of the thermophysical properties of density, thermal expansion and elastic moduli.

ρ_{To} → $\frac{\Delta L(T)}{L_{To}} = -\frac{\Delta\rho(T)}{3\rho_{To}}$ → $B(\rho, \upsilon_L, \upsilon_T)$ and $G(\rho, \upsilon_T)$

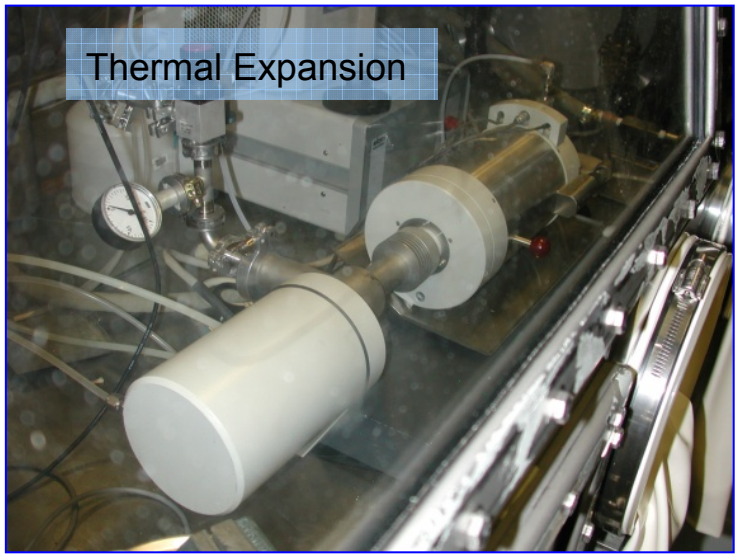

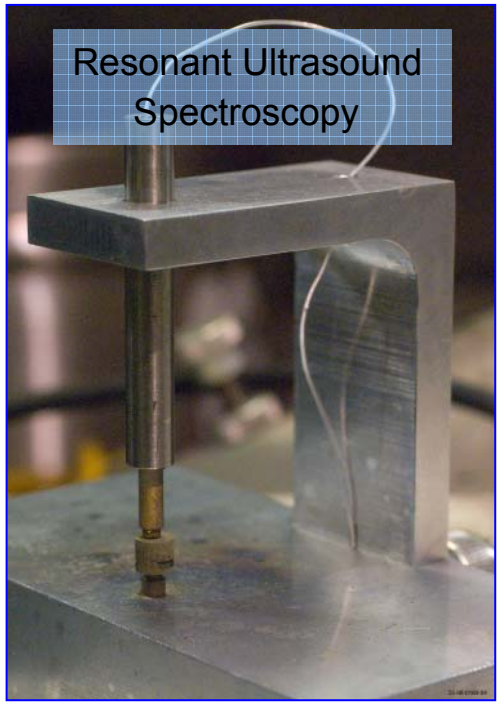

Los Alamos NATIONAL LABORATORY EST.1943

Resonant Ultrasound Spectrometry Basics

Samples are mounted between acoustic active and passive transducers.

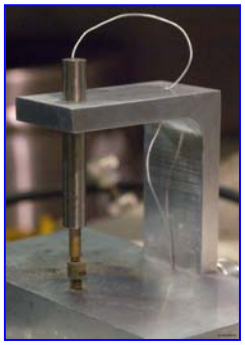

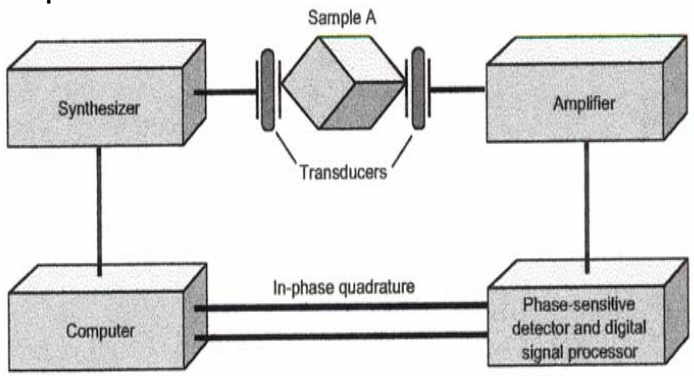

When driven acoustically to resonance, the samples vibrate in standing modes unique to the resonant frequency.

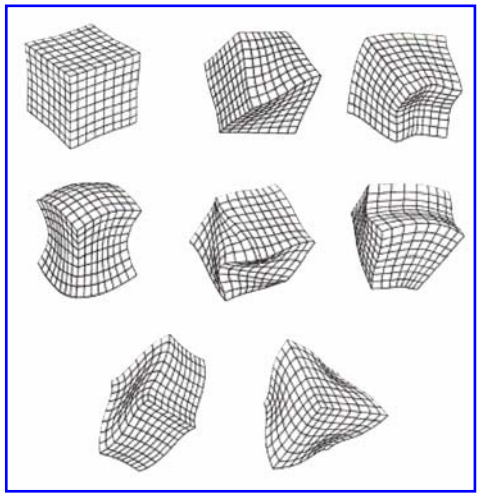

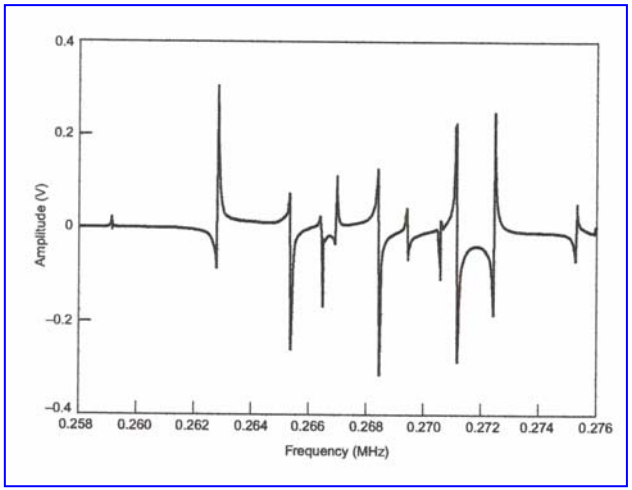

The response spectrum is dependent on geometry, density and elastic moduli. The moduli are determined by solving the inverse problem - the elastic response of an ideal elastic solid of identical geometry and density and crystalline structure.

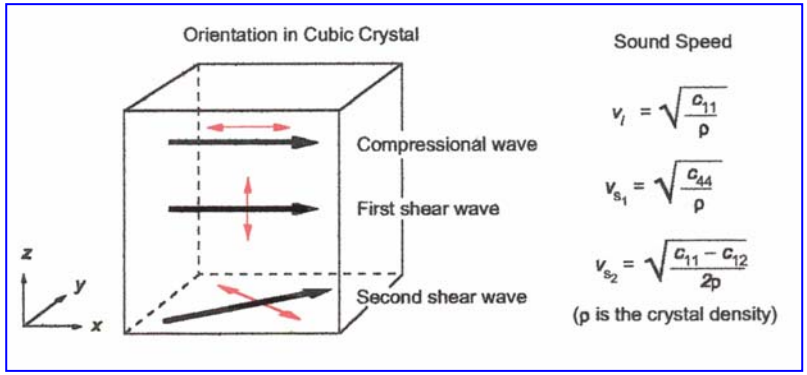

Los Alamos NATIONAL LABORATORY EST.1943

Detectability of Polycrystalline Inhomogeneity

For RUS an inhomogeneous material looks homogeneous to a propagating wave when the wavelength of the acoustic wave is much greater than the length scale of the features of inhomogeneity.

Conservative Estimate: for a one-dimensional elastic medium with free boundaries, the **resonance wavelength λ** of a standing wave is $\lambda=2l/n$, where l is the **length of the sample** and n is an **integer number of nodes in the standing wave**.

In utilizing RUS, the first ten resonance frequencies are sufficient to accurately determine two elastic constants. A sample may be considered homogeneous if the **maximum size of an inhomogeneity ε** is much much smaller than resonance wavelength of a standing wave in the smallest dimension of the sample or $\varepsilon << l_{min}/5$, where l_{min} is the **smallest dimension of the sample**.

For sample: 3mm x 3mm x 3mm $l_{min}/5$ = 600μm. Typical grains are 30μm.

Ulrich TJ, McCall KR, Guyer RA, *JASA* **111** 1667 (2002).
Freibert FJ, Mitchell JN, Saleh TA , Schwartz DS, *IOP Conf. Proc.: Actinides 2009.*

Age, Density and Elastic Moduli of Gallium Stabilized δ-Plutonium

Alloy and Phase	Age (dpa)	Density (g/cc)	Bulk Modulus (GPa)	Shear Modulus (GPa)	Fit RMS Error (%)
81% δ + 19% α (As-cast)	**0**	**16.5**	**33.0**	**19.0**	**3**
δ	0	15.8	27.3	15.8	0.5
δ	0	15.8	27.3	15.6	0.5
δ	2	15.7	29.6	15.6	1.2
δ	2	15.5	27.2	15.9	1.7
δ	2	15.7	31.2	15.3	1.1
δ	2	15.5	27.2	15.8	1.5
δ	2	15.5	27.7	16.0	1.2
δ	2.5	15.4	28.7	15.6	1.0
δ	2.5	15.2	28.9	15.6	0.6
δ	2.5	15.4	28.8	15.6	0.6
δ	2.5	15.3	29.4	15.0	0.9
δ	2.5	15.5	30.5	15.3	0.5
δ	3	15.7	28.5	15.7	1.3
δ	10	15.6	28.2	15.8	1.3
δ (Ave)	**2.5+/-2.3**	**15.5+/-0.18**	**28.6+/-1.3**	**15.6+/-0.27**	**1.0+/-0.4**

Thermal Expansion of Plutonium Unalloyed and Alloyed with Ga

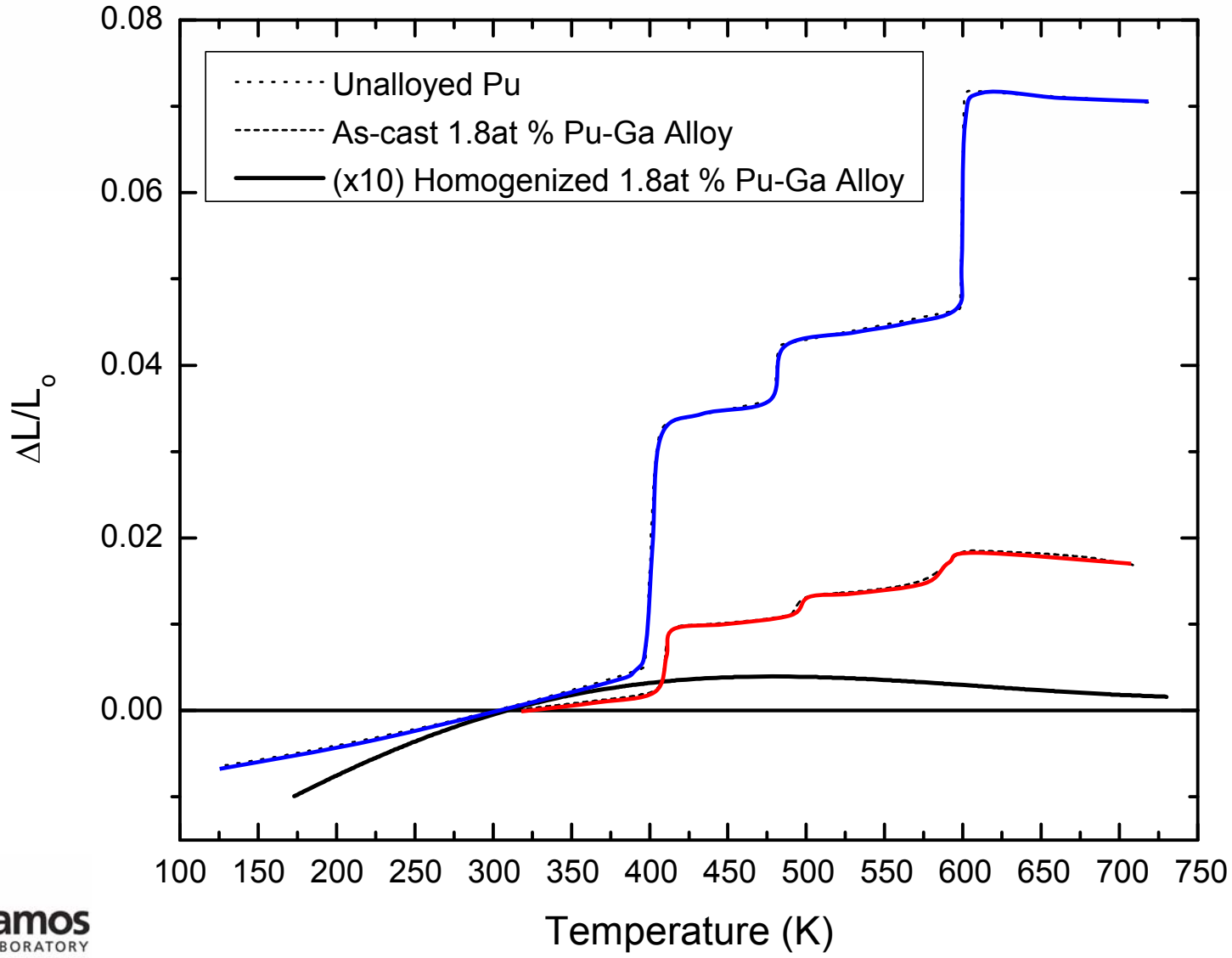

Thermodynamic Properties of Two-Phase Materials

Host Phase Volume Fraction: V_1

Solute Phase Volume Fraction: V_2

Composite Density: $\rho^* = \sum_i V_i \rho_i$

Ruess Composite Bulk Modulus:

$$K_R = K_1 + \frac{V_2}{1/(K_2 - K_1) + 3V_1/(3K_1 + 4G_1)}$$

Voight Composite Bulk Modulus:

$$K_V = K_2 + \frac{V_1}{1/(K_1 - K_2) + 3V_2/(3K_2 + 4G_1)}$$

Ruess Composite Shear Modulus:

$$G_R = G_1 + \frac{V_2}{1/(G_2 - G_1) + 6V_1(K_1 + 2G_1)/5G_1(3K_1 + 4G_1)}$$

Voight Composite Shear Modulus:

$$G_V = G_2 + \frac{V_1}{1/(G_1 - G_2) + 6V_2(K_2 + 2G_2)/5G_2(3K_2 + 4G_2)}$$

Voight-Ruess-Hill Composite Shear Modulus:

$$K^* = K_R + K_V, \quad G^* = G_R + G_V,$$

Single Phase and Composite Young's Modulus:

$$E_i = \frac{9K_iG_i}{(3K_i + iG_i)} \qquad E_L^* = \sum_i V_i E_i$$

Single Phase and Composite Poison's Ratio:

$$v_i = \frac{(3K_i - 2G_i)}{2(3K_i + G_i)} \qquad v_L^* = \sum_i V_i v_i$$

Isotropic Composite Thermal Expansion:

$$\alpha^* = \alpha_1 + \frac{(\alpha_1 - \alpha_2)(1/K^* - 1/K_1)}{(1/K_2 - 1/K_1)}$$

Fiber Composite Thermal Expansion:

$$\alpha_L^* = \alpha_1 + \frac{(\alpha_1 - \alpha_2)}{(1/K_2 - 1/K_1)}\left[\frac{3(1 - 2v_L^*)}{E_L^*} - \frac{1}{K_1}\right]$$

Hashin, Z. *J. Appl. Mech.-Trans. ASME* **50** 481 (1983)

Measured and Calculated Thermophysical Properties of Single and Two-phase Unalloyed and Ga Alloyed Pu (Freibert, 2010)

Phase Mix	Measured Density (g/cm^3)	Calculated Density (g/cm^3)	Measured Bulk Modulus (GPa)	Measured Shear Modulus (GPa)	Calculated Bulk Modulus (GPa)	Calculated Shear Modulus (GPa)	Measured Thermal Expansion Coefficient ($x10^{-6}$ K^{-1})	Calculated Thermal Expansion Coefficient ($x10^{-6}$ K^{-1})
α	19.6	-	48 to 82 [1]	40 to 60 [1]	-	-	40 to 60	-
β	17.7	-	34 [3]	17.5 [3]	-	-	36	-
γ	17.3	-	25 [2]	15 [2]	-	-	34	-
δ_{HT} [a]	15.9	-	-	-	-	-	-11	-
δ_{LT} [a]	15.8	-	23 to 37	12 to 20	-	-	8 to -1	-
$0.90\delta_{LT}+0.10\alpha'$	16.2	16.3	-	-	39.4	22.7	16	15.6
$0.81\delta_{LT}+0.19\alpha$	16.4	16.5	33	19	34.7	19.8	20	19.7
$0.81\delta_{LT}+0.19\beta$	16.0	16.1	-	-	27.3	15.4	10 to 40	11.9
$0.81\delta_{LT}+0.19\gamma$	15.9	16.0	-	-	24.4	13.5	12 to 80	12.4

[a] δ_{HT} and δ_{LT} stand for the high temperature stabilized δ-phase Pu and the low temperature Ga stabilized δ-phase Pu.

1. Migliori A, Pantea C, Ledbetter H, Stroe I, Betts JB, Mitchell JN, Ramos M, Freibert F, Dooley D, Harrington S, Mielke CH 2007, *JASA* **122** 1994
2. Stroe IR, Betts JB, Pantea C, Trugman A, Mitchell JN, Ramos M, Freibert F, Mielke CH, and Migliori A 2009, JASA. 125 2654
3. Migliori A, Suzuki Y 2009 unpublished data.

Interatomic Bonding in Plutonium

Materials Science and Engineering, 27 (1977) 133 - 136

Ratio of the Shear and Young's Moduli for Polycrystalline Metallic Elements*

H. M. LEDBETTER
Institute for Basic Standards, National Bureau of Standards, Boulder, CO 80302 (U.S.A.)
(Received in revised form August 17, 1976)

Elastic properties of single and mixed phase microstructures acts like a elastic solid with an central force interatomic potential, independent of density and crystal structure. ==>
Valid for homogeneous, quasi-isotropic materials having central forces between atoms.

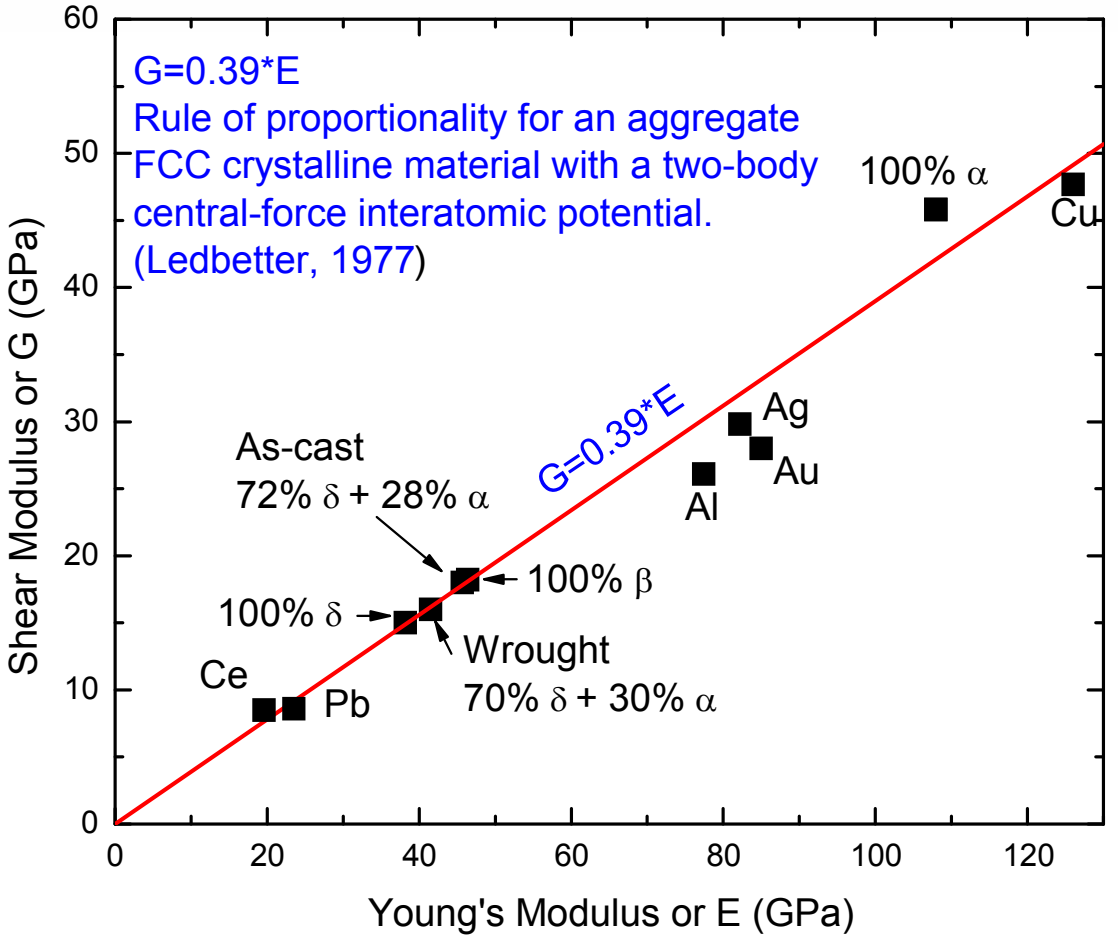

Thermodynamic Properties and Mie-Gruneisen EOS

Density: $\rho = 1/V$

Linear Thermal Expansion: α

Bulk Modulus: K

Specific Heat: C_P

$\longrightarrow$

Gruneisen Parameter:

$$\gamma = \frac{3\alpha K}{\rho C_P}$$

Fundamental EOS Quantity

Total Energy:

$$E = E_C + E_{TL} + E_{Te^-} + \cancel{E_{TLe^-}}$$ =0

Total Pressure:

$$P = P_C + P_{TL} + P_{Te^-} + \cancel{P_{TLe^-}}$$ =0

Mie-Gruneisen Equation of State for a Solid

$$P = P_C + \frac{\gamma E_{TL}}{V}$$

$$\gamma(V) = \frac{\gamma_C V}{V_C} + \frac{2}{3}\left(1 - \frac{V}{V_C}\right)$$

Pu Equilibrium and Kinetic Thermodynamic Properties

Method	α-Pu γ-values
Low Temperature Debye Solid $s=3k_B\theta_E\gamma(\gamma+1)/2V_a$	4.9
High Temperature Debye Solid $dB/dT=-3k_B\gamma(\gamma+1)/V_a$	5.1
Thermodynamic Temperature Dependence $\gamma=B\beta/C_p\rho$	2.5
Pressure Derivative of a Debye Solid $dB/dP=2\gamma+1$	7.0

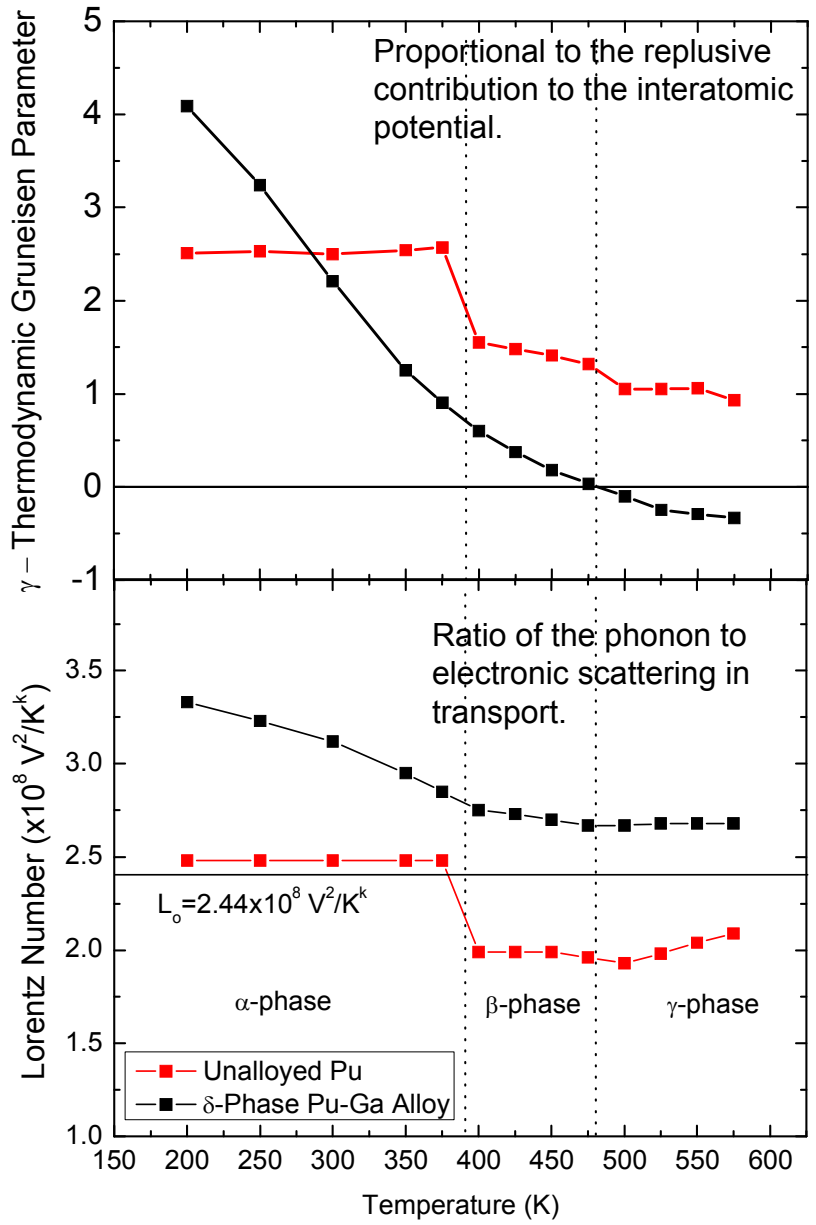

H. Ledbetter, PRB 71 (2005).

J. Andrews, Therm Conductivity 17 (1983).

Los Alamos NATIONAL LABORATORY EST.1943

Future Work

Short Term Goals

- Cast, fabricate and characterize microstructure of high density unalloyed Pu.
- Measure temperature dependence of thermal expansion, specific heat and elastic moduli.

Long Term Goals

- Examine thermodynamic properties (i.e., thermal expansion, specific heat and elastic moduli) at temperatures near phase transformations. Do phase transformations have electron (i.e., Schottky, etc.), phonon (i.e., phonon softening, etc.), and/or structural (i.e., martensite, etc.), characteristics?
- Explore thermodynamic properties of composite (i.e., mixed phase) materials correlating results with microstructures.

Investigations of dynamic friction at shocked interfaces: the FN8 vehicle

Stewart Stirk, Ron Winter, Peter Keightley
Tel. +44 1189 825294
Email. stewart.stirk@awe.co.uk

- Our interest is in simple experiments to investigate dynamic friction at dissimilar metal-metal interfaces.
- Contact pressures of many GPa and sliding velocities of many hundreds of metres per second.
- In particular, differential sliding generated by oblique shock is of interest.

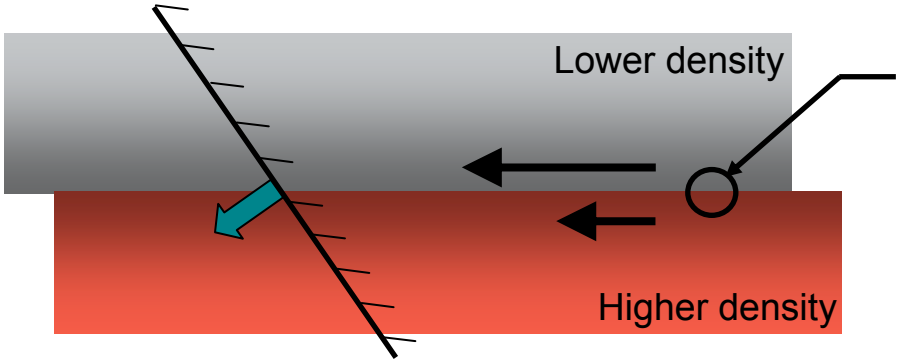

Differential motion generated by oblique shock

Pressures 5-100 GPa

- Motivation is to support development and validation of a physics-based friction (PBF) model. [G. J. Ball *et al*, AWE]

- Previous experiments designated the FN6 series achieved high velocity sliding at aluminium-steel interfaces driven by explosives.
- Qualitative information obtained by post-shock examination of the interfaces.

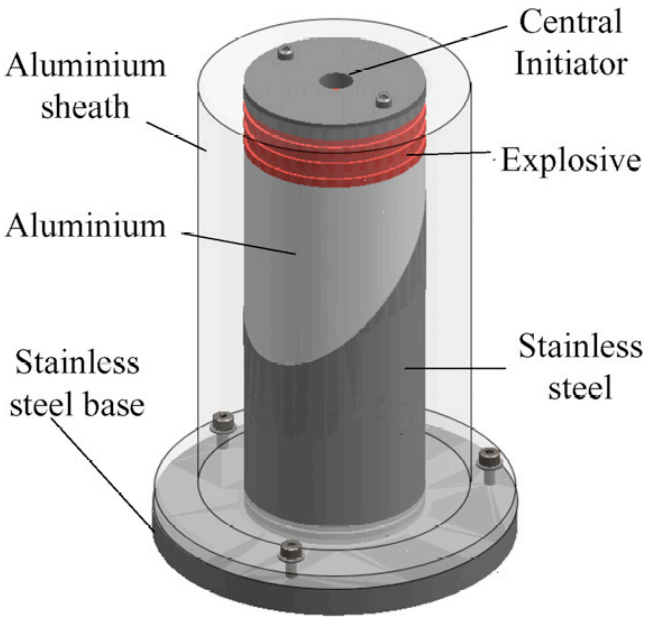

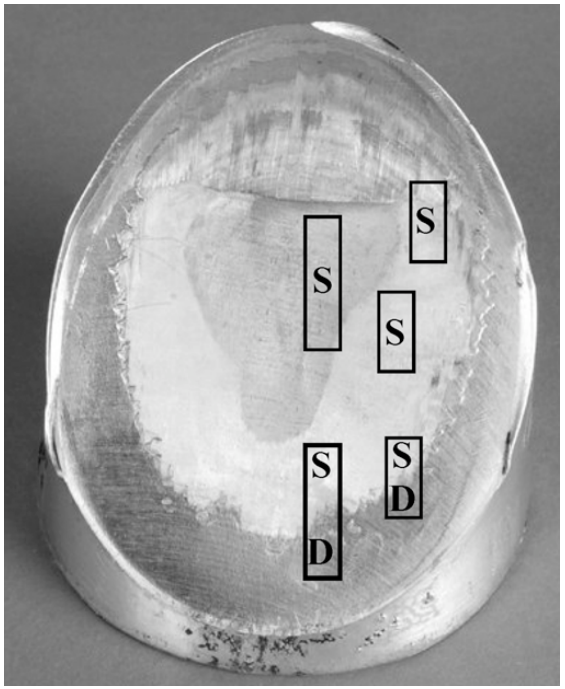

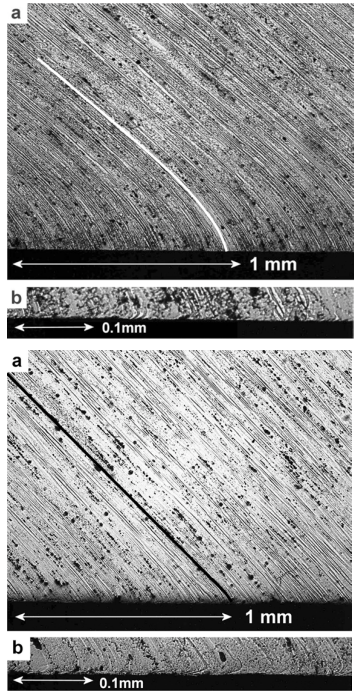

R. E. Winter, G. J. Ball, P. T. Keightley, J. Phys. D: Appl. Phys. **39**, 5043 (2006)

- One of the drawbacks of FN6 vehicle is that it is difficult to measure and quantify the sliding velocity at the interface.
- An alternative gas-gun vehicle designated FN8 can provide a quantitative measure of the sliding velocity which can be compared to model predictions:

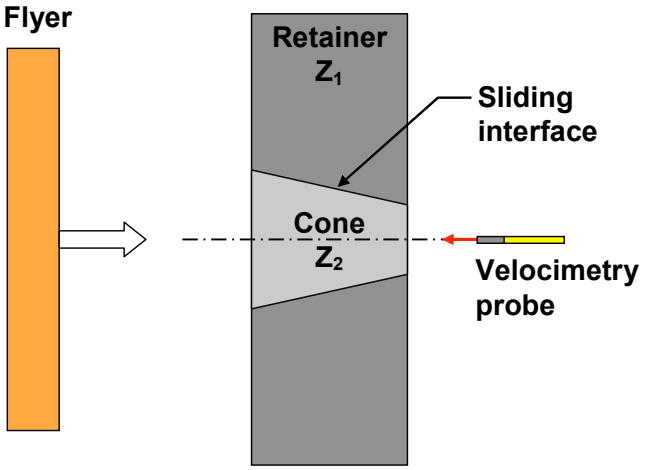

Modified version of Juanicotena's experiment (2005)

Pressures: Several GPa

Sliding velocity: Several 100's of m/s

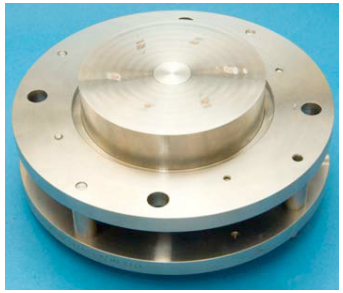

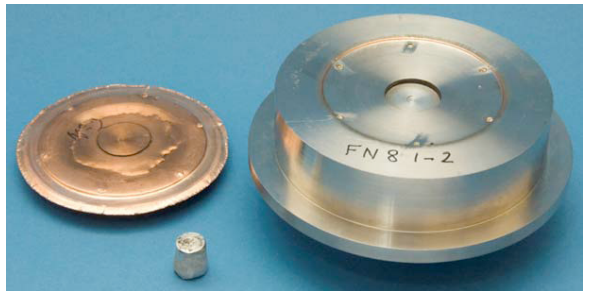

Planar gas-gun shock ⇨ **Lower impedance cone** / **Higher impedance retainer** ⇨ **Differential motion at the interface**

- 2D calculation shows the displaced cone which is sensed using rear surface velocimetry (HetV).

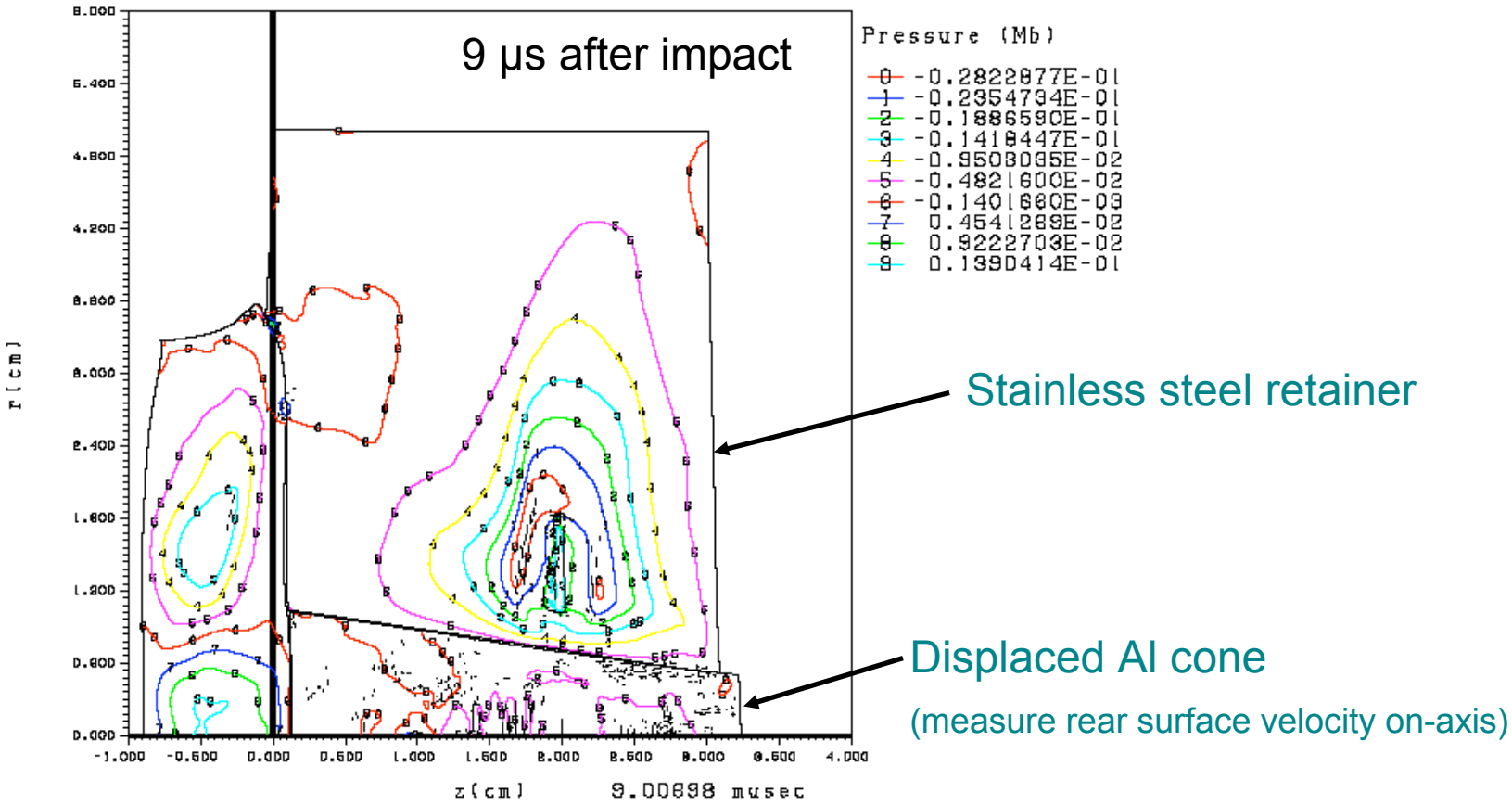

FN8 experimental data

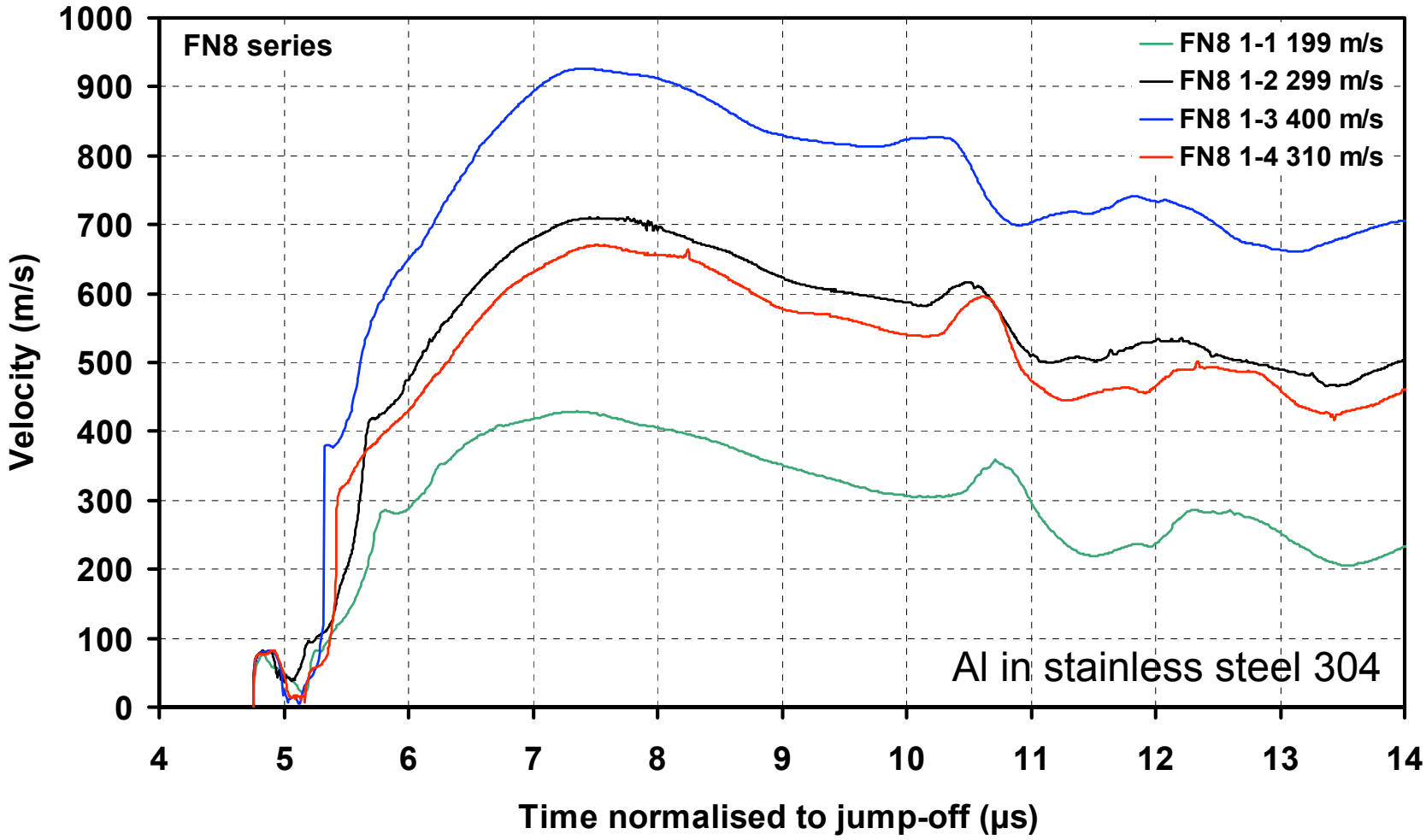

Poor repeatability between similar shots

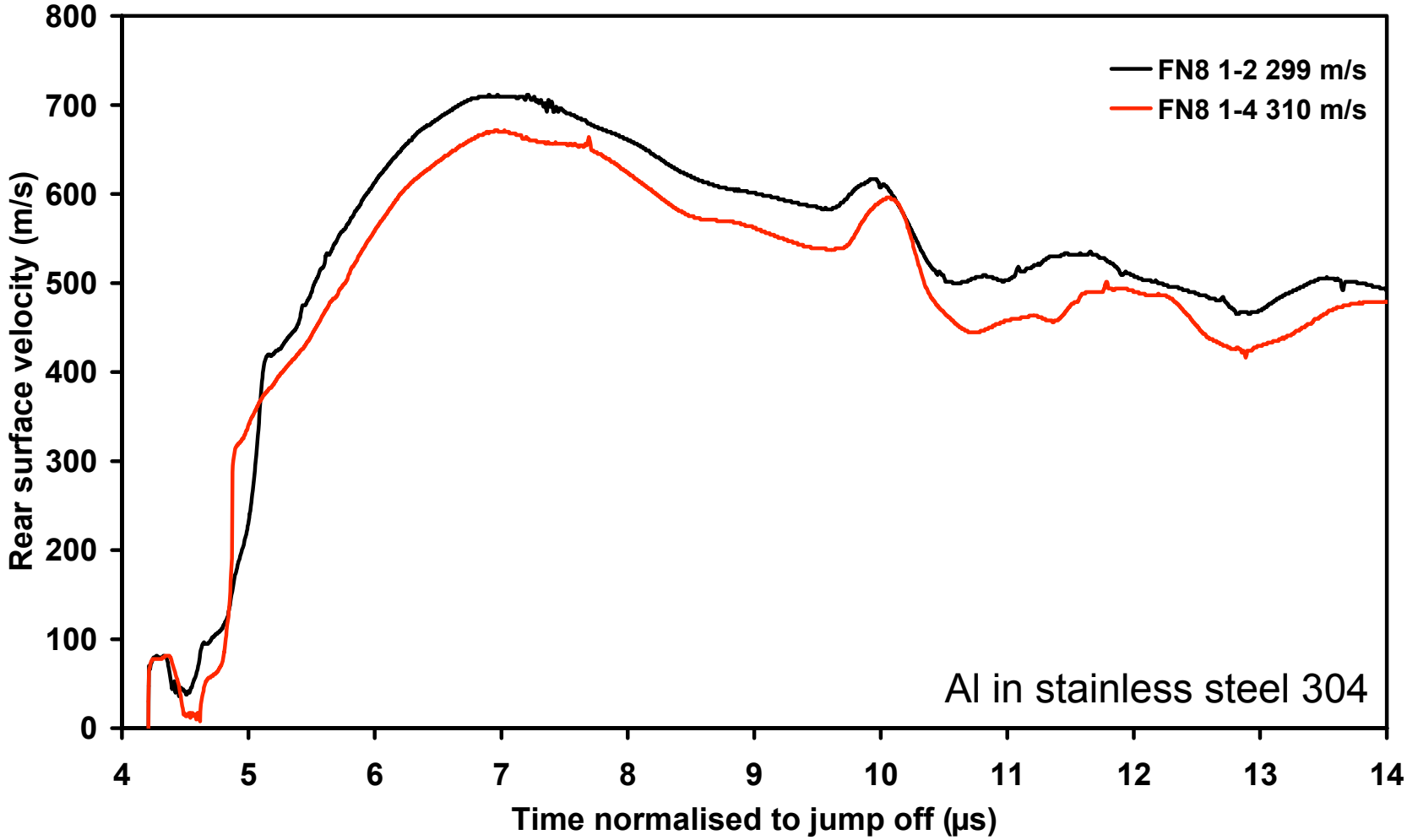

- A useful control measure is to fire an experiment with a larger central cone, such that the rear surface velocity is insensitive to friction before release.

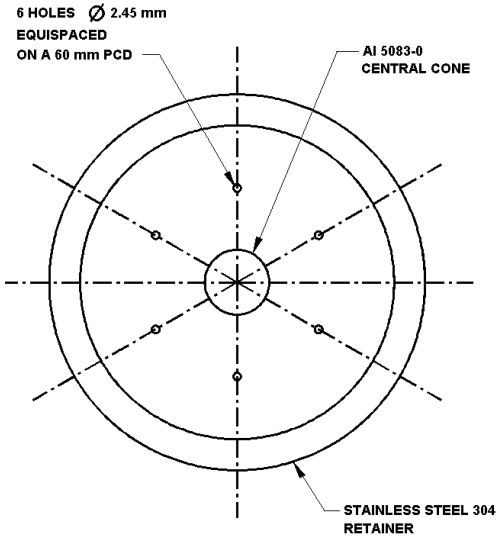

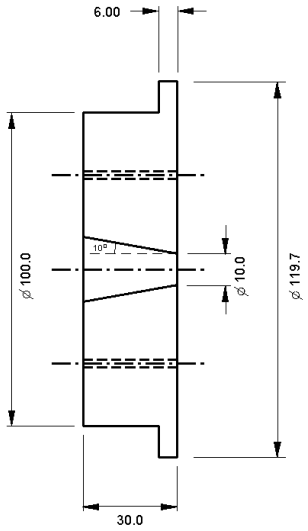

Friction test

Smaller central cone

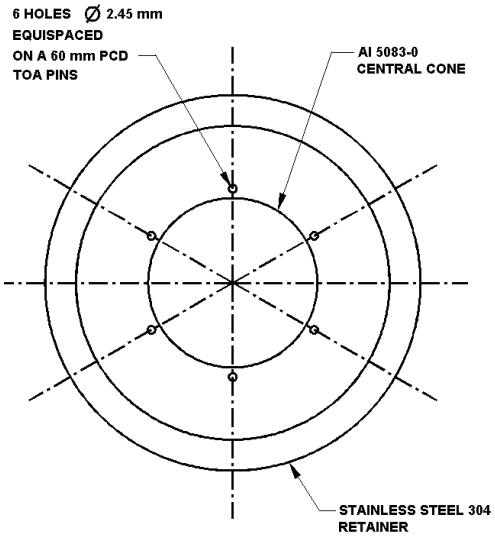

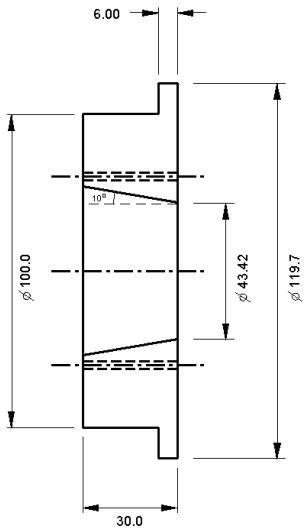

Control test

Larger central cone

Insensitive to friction – EoS experiment

Control experiments

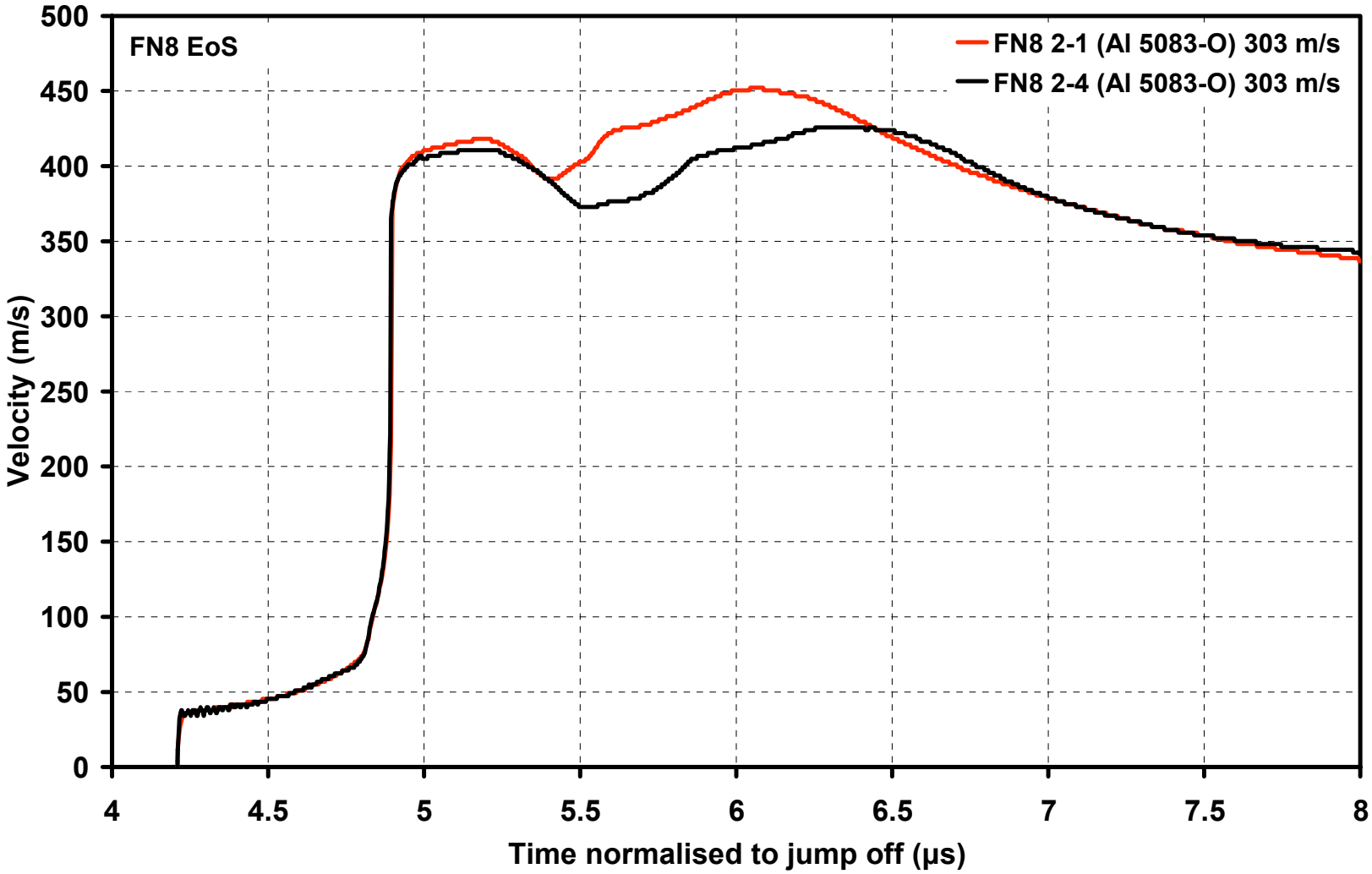

- The conclusions were that target build quality was to blame for the lack of experimental repeatability.
  - Machining tolerances and surface finishes.
  - Loading weight on the cone.
  - Presence of a gap at the interface?
  - Presence of machining oil and grease at the interface?
- Leads to a lack of ‘scientific’ confidence in the vehicle.
- A high quality build procedure is required to improve repeatability.

- FN8-HF series: A ‘high-fidelity’ target design:
  - Specify 0.8 µm surface finish at the interfaces.
  - Detailed metrology of all components prior to assembly.
  - Detailed assembly procedure:

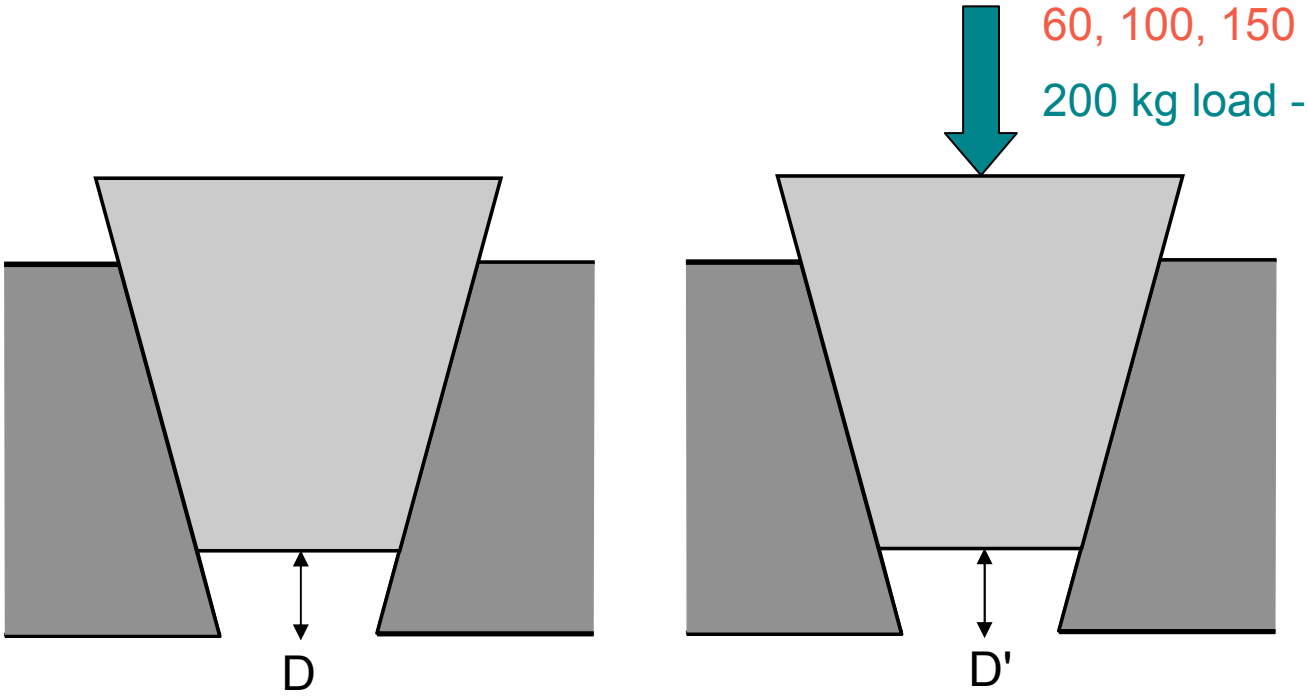

Loads applied continuously for 5 minutes.

Measure D pre and post assembly.

FN8-HF series; all at 300 m/s impact velocity

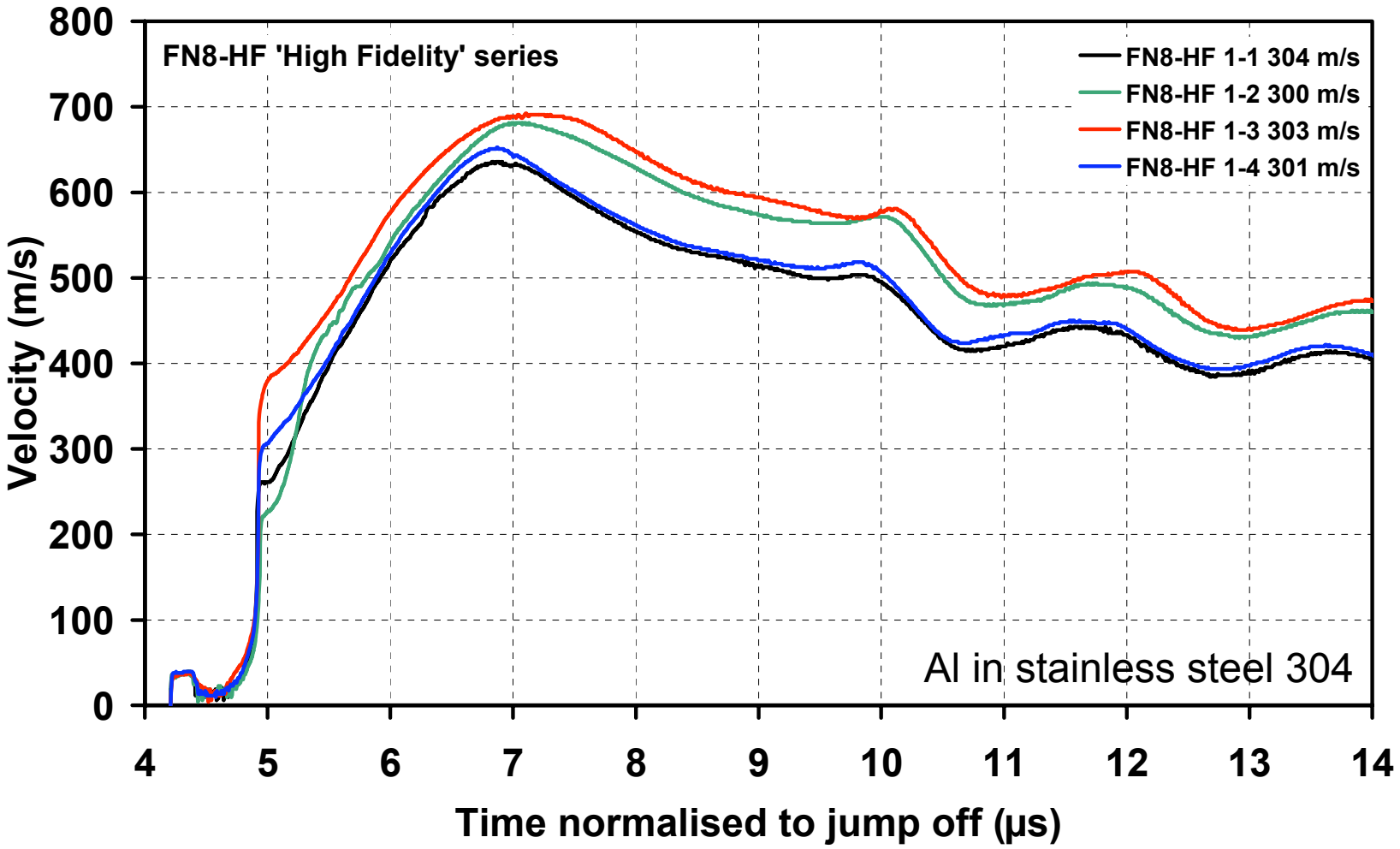

Comparison with original FN8 data

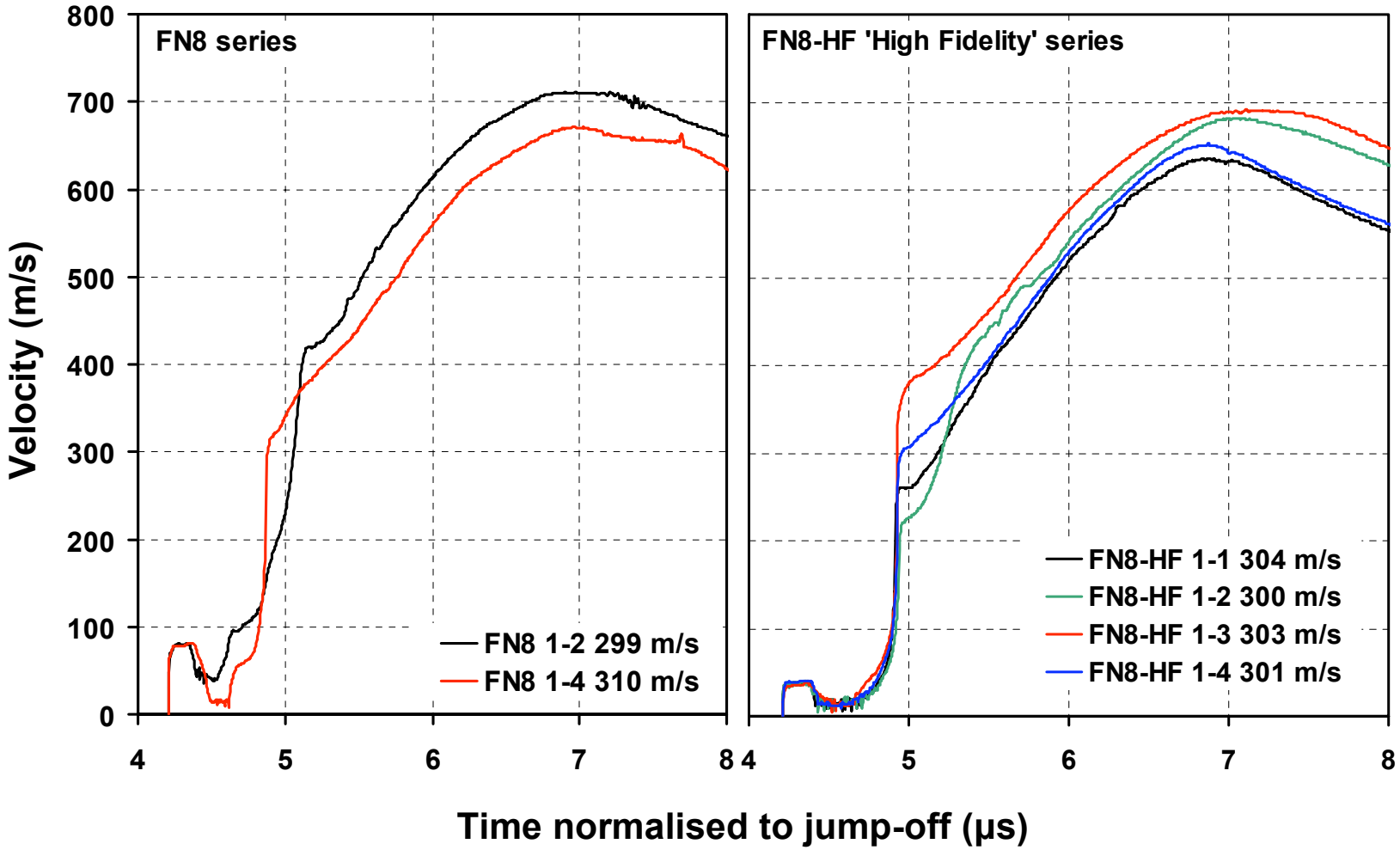

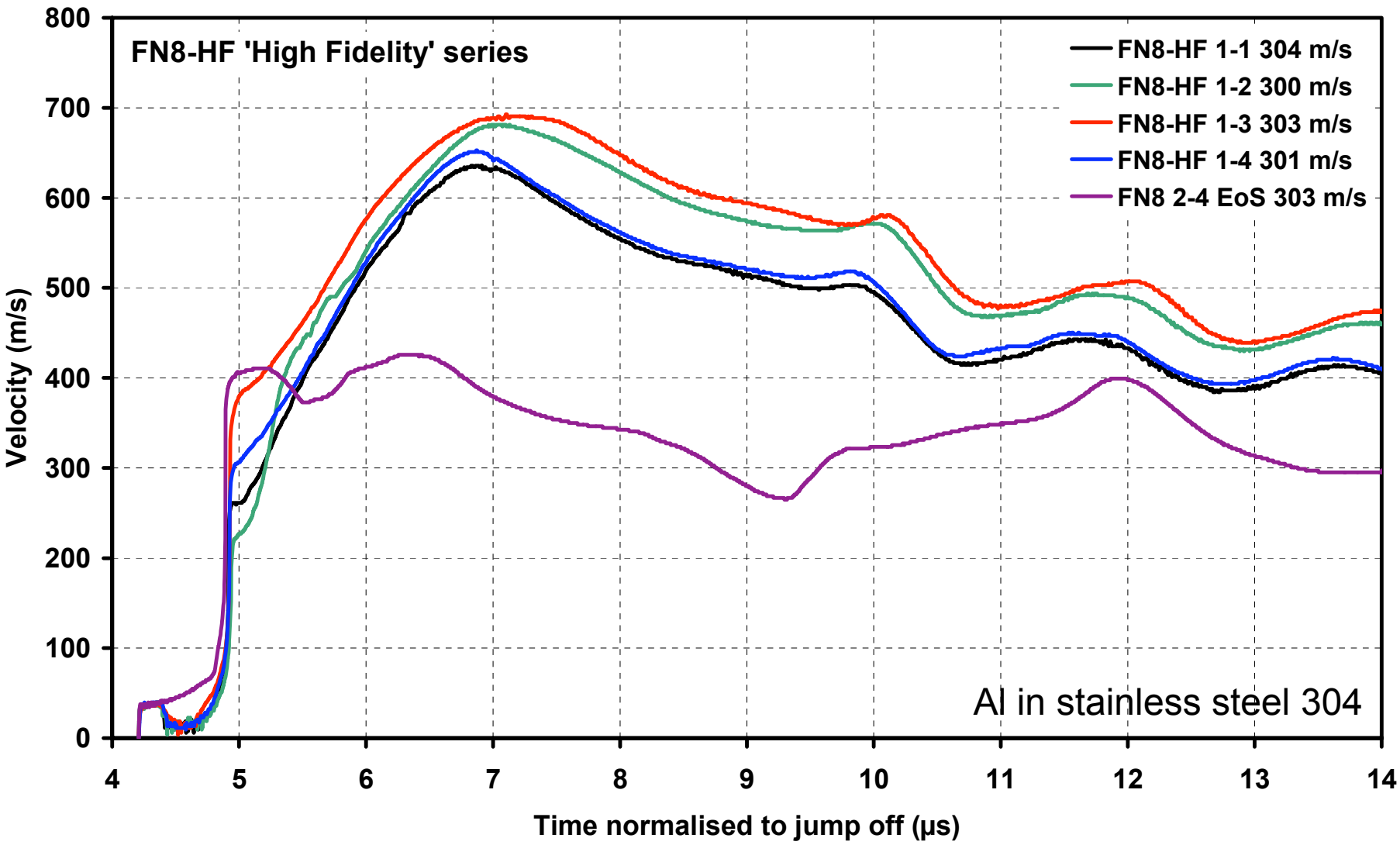
FN8-HF 'High Fidelity' series
FN8-HF 1-1 304 m/s
FN8-HF 1-2 300 m/s
FN8-HF 1-3 303 m/s
FN8-HF 1-4 301 m/s
FN8 2-4 EoS 303 m/s
Al in stainless steel 304
Velocity (m/s)
Time normalised to jump off (µs)
800
700
600
500
400
300
200
100
0
4
5
6
7
8
9
10
11
12
13
14

- Metrology information pre and post assembly allows further analysis of the target build.

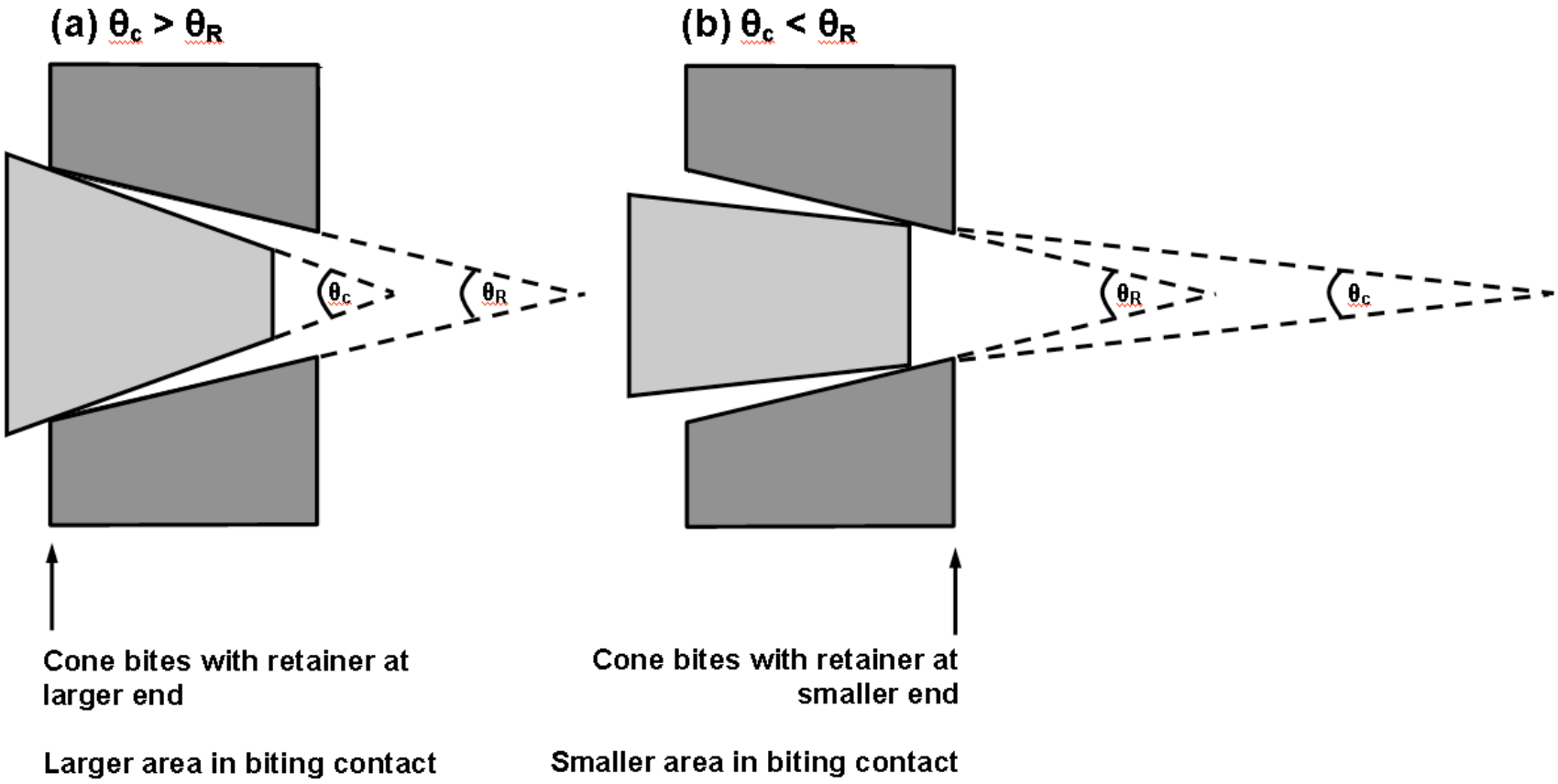

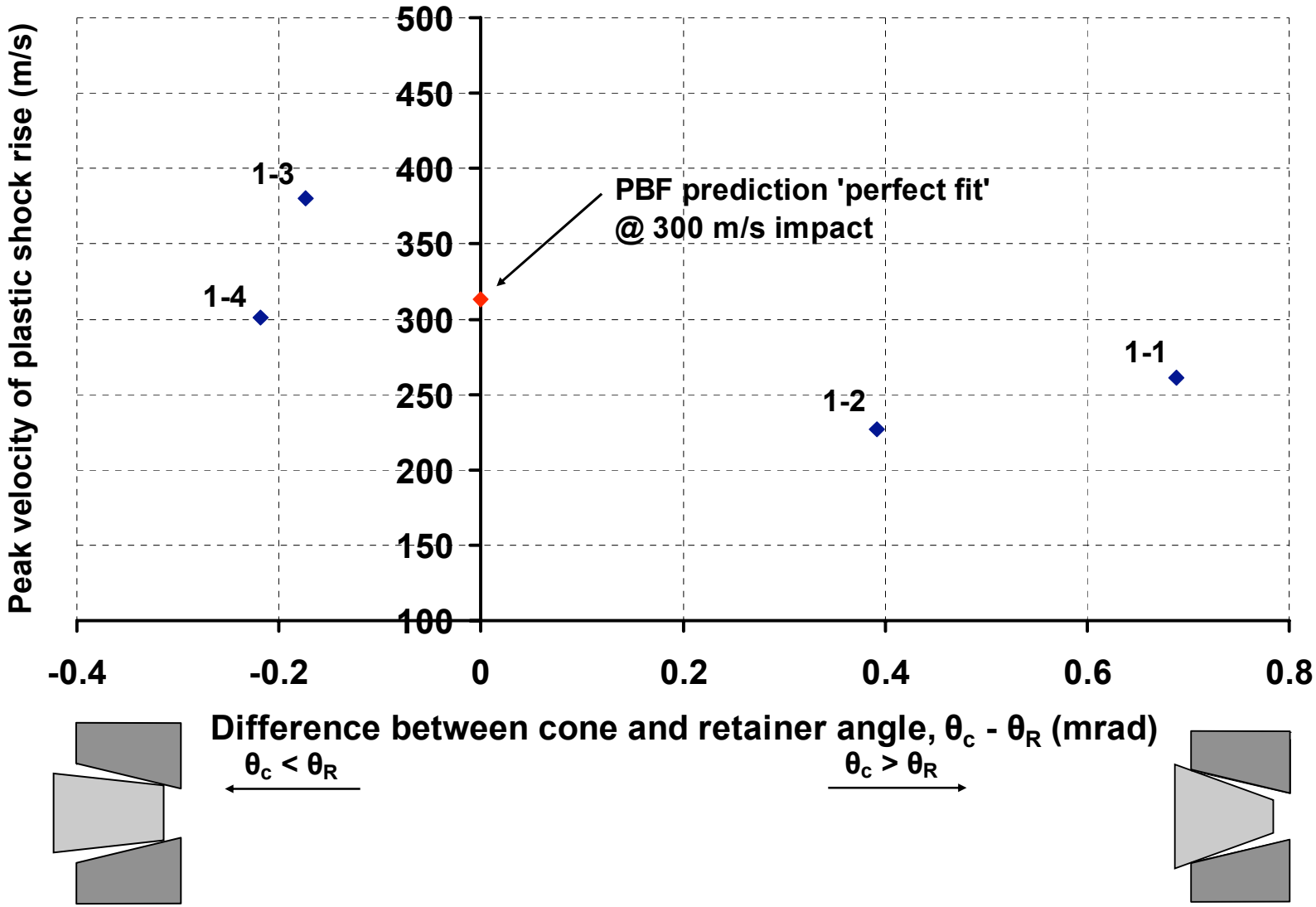
Peak velocity of plastic shock rise (m/s)
500
450
400
350
300
250
200
150
100
1-3
1-4
PBF prediction 'perfect fit'
@ 300 m/s impact
1-1
1-2
-0.4
-0.2
0
0.2
0.4
0.6
0.8
Difference between cone and retainer angle, θc - θR (mrad)
θc < θR
θc > θR

- Given that the displacement of the cone is measured after the load has been applied, the metrology information reveals where the components should theoretically meet.

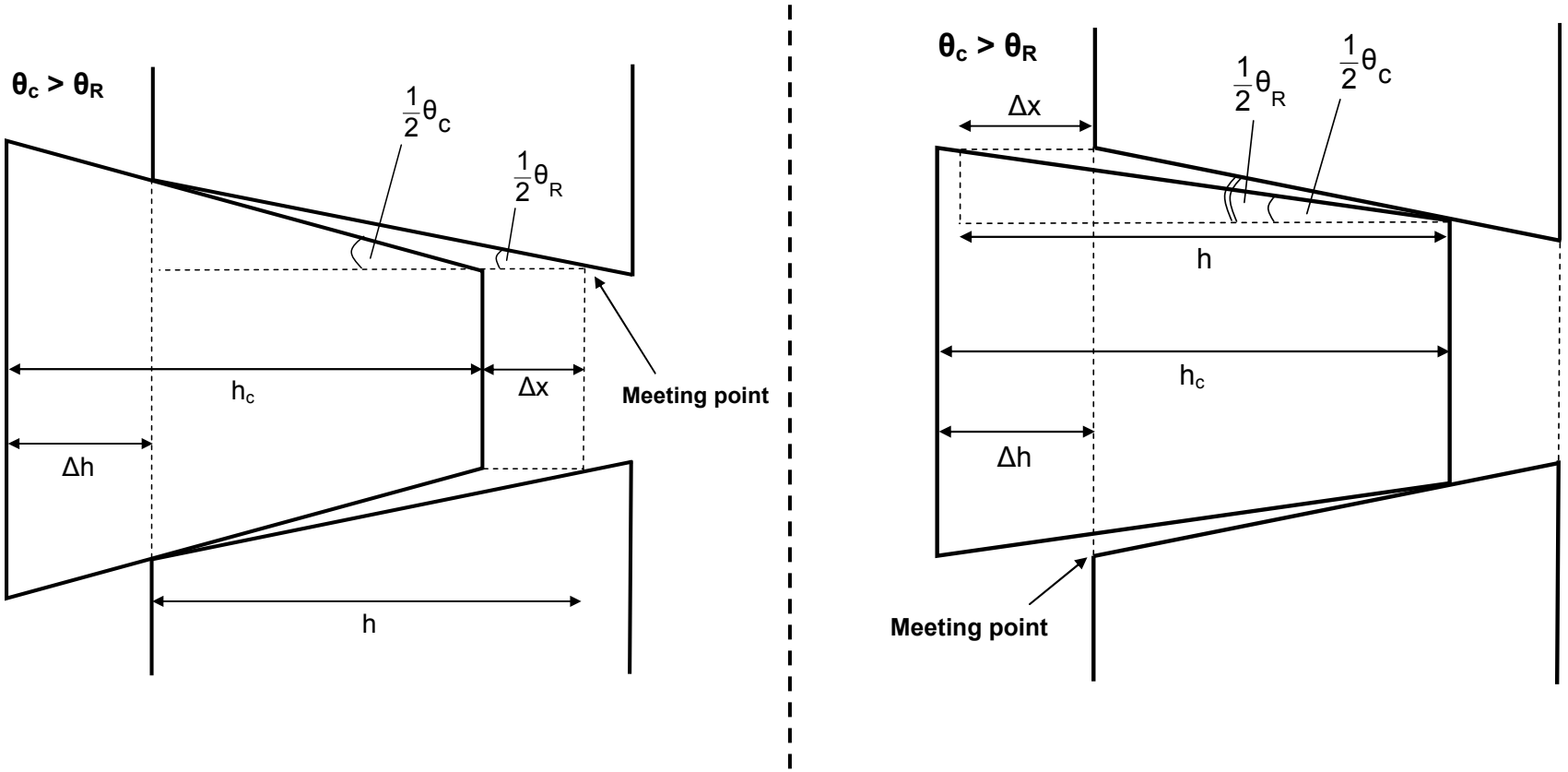

- Estimate of contact or gap at the specified measuring locations after loading:

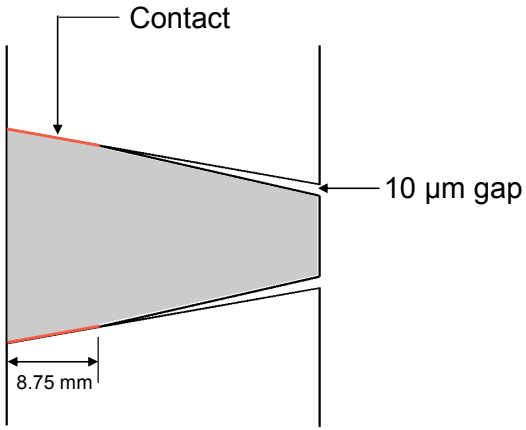

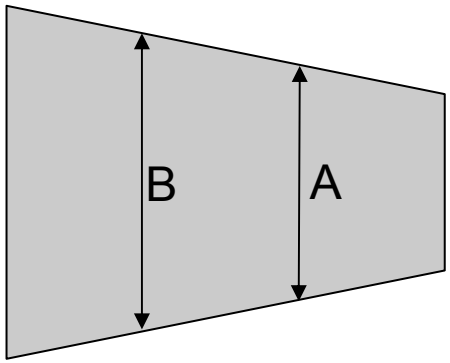

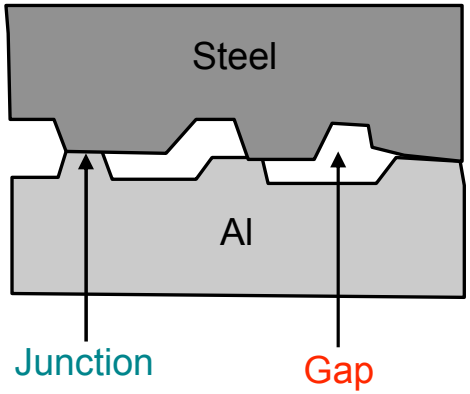

Shot label	δ_A (μm)	δ_B (μm)
FN8-HF 1-1	4 (gap)	-3 (interference)
FN8-HF 1-2	27 (gap)	23 (gap)
FN8-HF 1-3	-2 (interference)	0 (just contact)
FN8-HF 1-4	-15 (interference)	-13 (interference)

‘Best fitted’ tribo-pair compared with physics-based friction model.

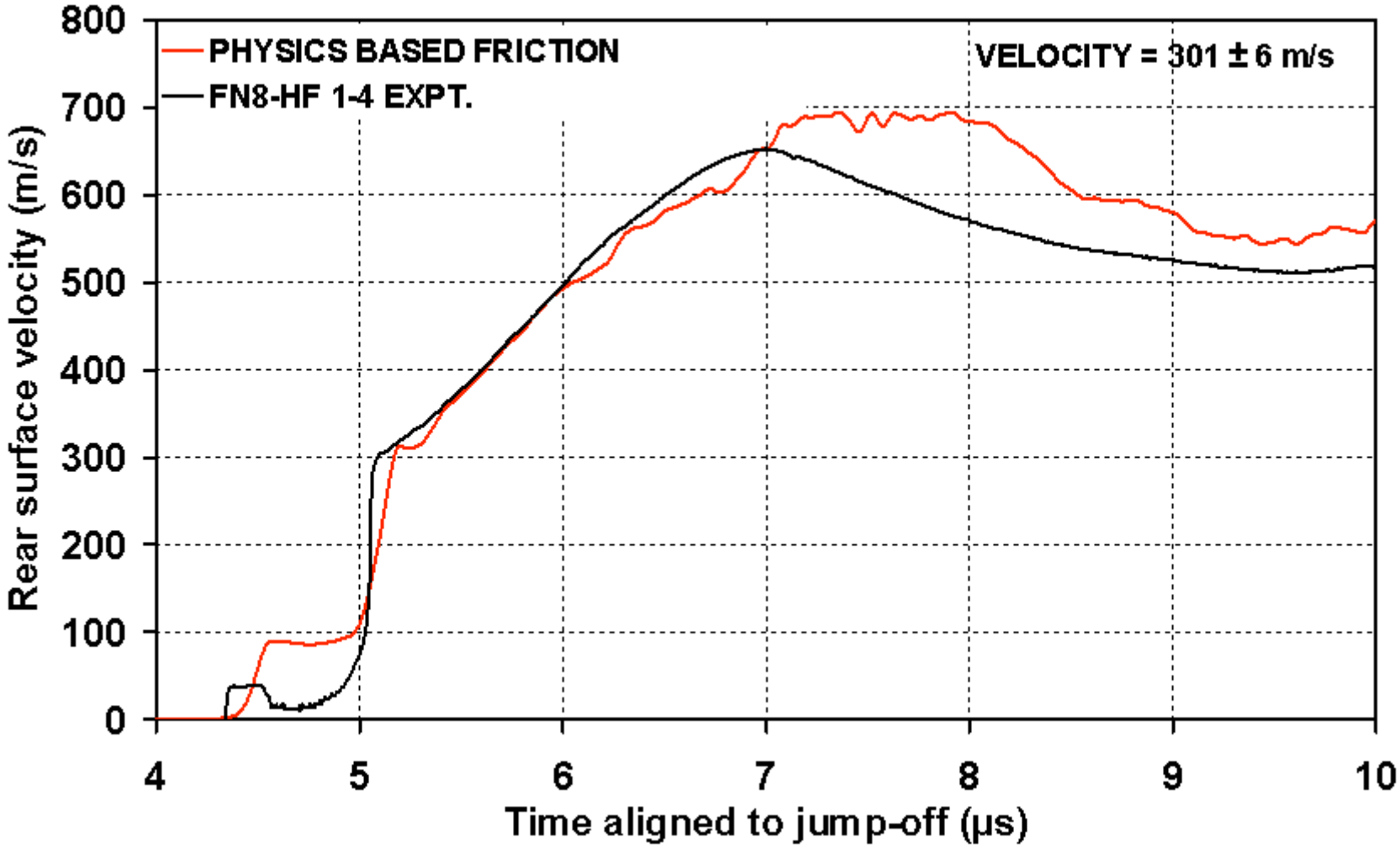

‘Worst fitted’ tribo-pair compared with physics-based friction model.

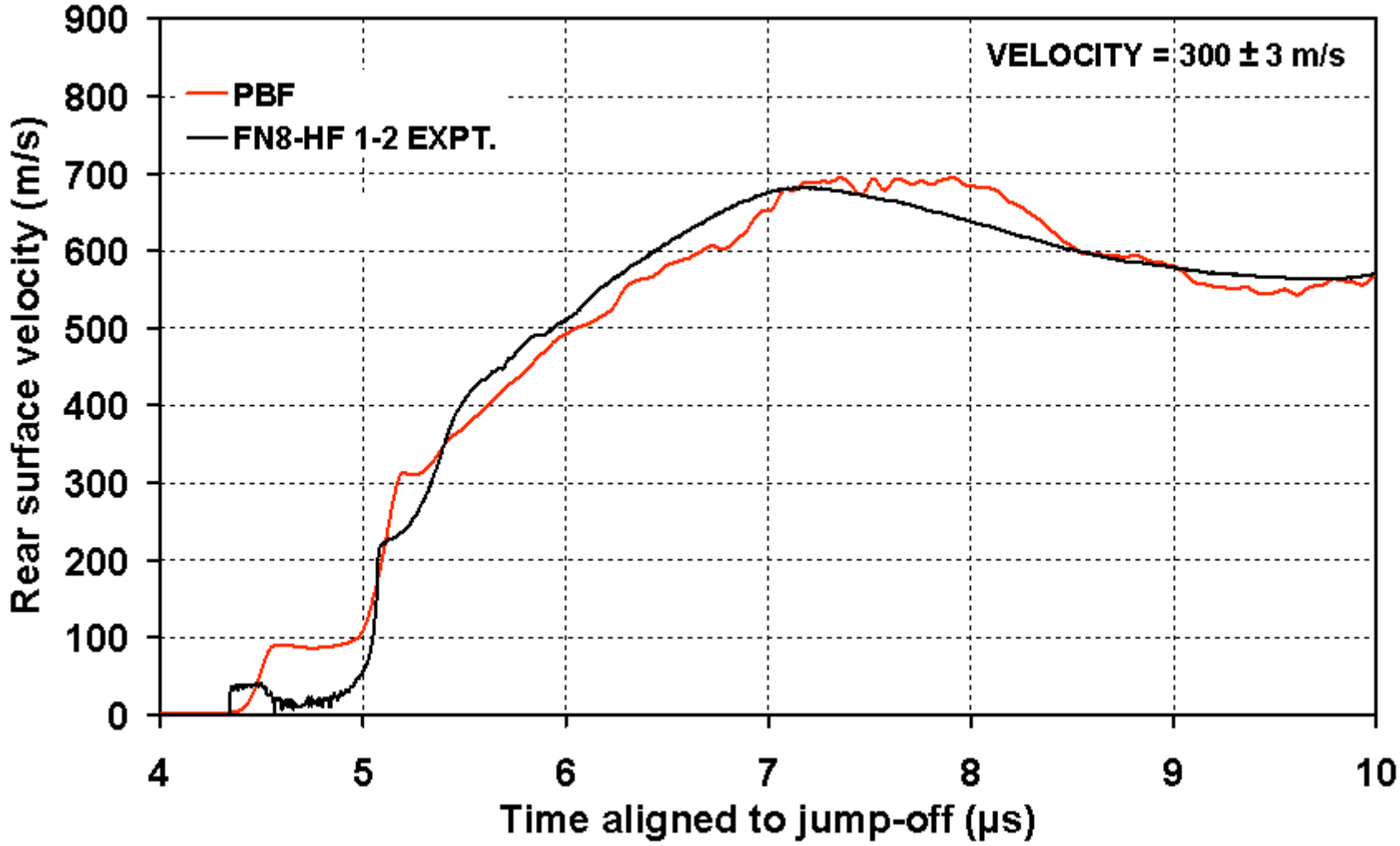

‘Worst fitted’ tribo-pair compared with physics-based friction model.

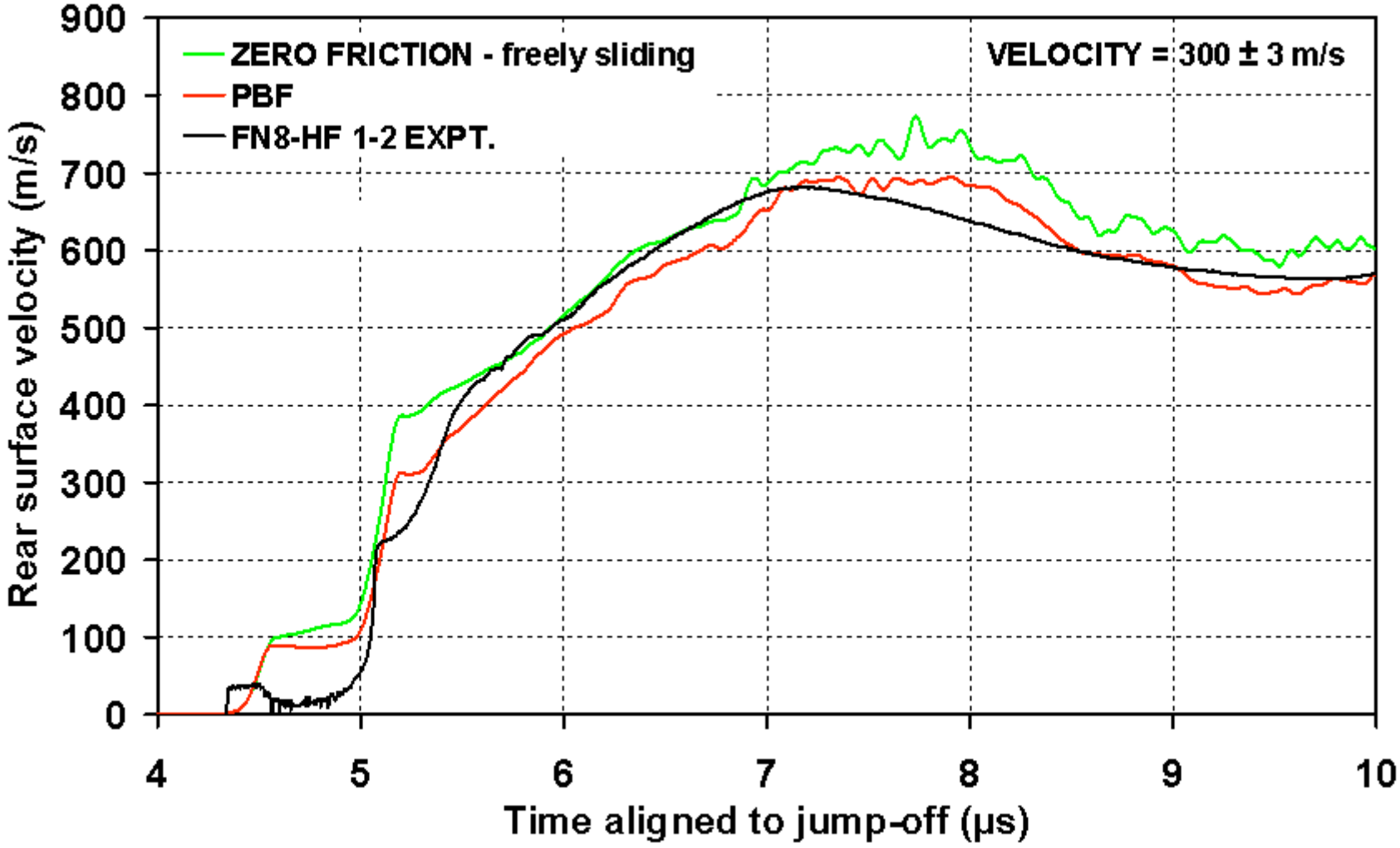

- The evidence is pointing towards unsatisfactory build quality again, despite these recent efforts.
- It appears the vehicle design at present is extremely sensitive to the interface quality.
- Possibility of “overloading” the cone during assembly.
- In the open literature, 60 kg loads are used but we needed 200 kg to make the cone ‘stick’.
- Possibility that variability is greater at lower velocities and that higher impact velocities may give better reproducibility
- To investigate other more-expensive tribo-pairs, the vehicle needs to be working in cheaper Al/SS pairs.
- Not yet confident enough in the experiment.

- Possible way forward to consider a double-angled cone with a shallower morse-taper fit at the larger end to allow a more controlled load prior to machining.